Theoretical Studies on the NO···H Interactions of Nitric Oxide, Organic Nitroxides, and Metal Nitrosyls in Selected Chemical Environments

Thesis Submitted to the **University of Calicut** for the Award of

Doctor of Philosophy in **Chemistry**

by

Thufail M Ismail

Under the supervision of

Dr. Sajith P. K.

DEPARTMENT OF CHEMISTRY

FAROOK COLLEGE (AUTONOMOUS), KOZHIKODE

KERALA, INDIA – 673632

December 2023

DECLARATION

I hereby declare that the thesis entitled "**Theoretical Studies on the NO···H Interactions of Nitric Oxide, Organic Nitroxides, and Metal Nitrosyls in Selected Chemical Environments**" is the bonafide report of the original work carried out by me under the supervision of Dr. Sajith P. K., assistant professor, department of chemistry, Farook college (autonomous), Calicut, Kerala for the award of the degree of Doctor of Philosophy in Chemistry under the Faculty of Sciences, University of Calicut, Kerala. The content of this thesis has not been submitted to any other Institute or University for the award of any degree or diploma, except where due acknowledgment has been made in the text.

Farook College
21-05-2024

Thufail M Ismail
U.O.No. 484/2019/Admn

CERTIFICATE

This is to certify that the work embodied in the thesis entitled **"Theoretical Studies on the NO···H Interactions of Nitric Oxide, Organic Nitroxides, and Metal Nitrosyls in Selected Chemical Environments"** submitted by Thufail M Ismail to the University of Calicut for the award of the degree of Doctorate of Philosophy in Chemistry under Faculty of Sciences, is an authentic record of precise research work carried out at the Department of Chemistry, Farook College (autonomous), Calicut, under my supervision and guidance. The contents of the thesis have been checked for plagiarism using the software 'DrillBit' and the similarity index falls under permissible limit of University of Calicut. I further certify that the contents of this thesis have not been submitted elsewhere for any degree or diploma. I also certify that the corrections/suggestions recommended by the adjudicators have been incorporated in the thesis.

Farook College
21-05-2024

Research Guide
Dr. Sajith P. K.

Dr. P.K. Sajith
Assistant Professor
Department of Chemistry
Farook College, Kozhikode - 673632

ACKNOWLEDGMENT

I am fortunate to have many individuals at my side and supporting me during this lengthy and arduous PhD journey. I am sure these words are incapable of conveying the help, guidance, support, and solace I have received from different corners. Yet, this is an attempt to thank them all; I apologize if I missed to mention anyone.

At this moment of accomplishment, I would like to express my sincere gratitude to my advisor, Dr. Sajith P.K., for his patience, motivation, enthusiasm and support. Despite his busy schedules, he managed to deal with this thesis work. His guidance as well as his professional approach to research helped me in completing this thesis.

I am grateful to Dr Ayisha Swapna K.A., the principal of the College, Dr Naseer K.M., former principal of the College, and Dr. Kavitha, head of the department, for providing me all necessary assistance for pursuing my research.

I am also gratefully acknowledging all the faculty members in the department of chemistry for their heartfelt advice and support in my research journey.

I take this opportunity to thank my Doctoral Committee members, Dr. N. K. Renuka, Dr. Mohamed Shahin T, and Dr. V. M. Abdul Mujeeb, for their valuable advice and comments for improving the research work.

I wish to place on record my gratitude to those who have helped in my work from outside the university. I thank Dr. Milind Deshmukh, Dr. Harisingh Gour Vishwavidyalaya, Madhya Pradesh, for his valuable suggestions and assistance while performing the MTA analysis. I also thank Rajadurai Vijay Solomon, Madras Christian College, Tamilnadu, for helping me to carry out EDA analysis.

I would like to express my gratitude to all the non-teaching staff in the department and the college for their kind help and support.

I gratefully acknowledge the financial assistance and the computational facility provided by the SERB, New Delhi, for pursuing my research.

As mentioned, throughout my PhD journey, I was blessed with some wonderful friends around me. My heartfelt gratitude is extended to my colleagues, especially Farhan, Hadiya, Ramya, Remya, Femina, Nizamudheen, Shanavas, Sumayya, Rejeena, and Athira. I

can never adequately thank them for all the memorable moments with fun we had, especially over tea in the last few years.

*Finally, I have no suitable words to express my gratitude to my family. My beloved parents, 'Umma' and 'Bapa', my dear spouse, Dr. Minna Basania, my lovely kids (*Amila and Alifa*), and my brother Adil, who are the real 'victims' of all troubles I come upon during my research work. Without their love and constant support this research would not have been possible. Also, I would like to dedicate my thesis to my family and close relatives. Words fail to express how grateful I am for all of the sacrifices that they've suffered for me. Their prayers sustained me so far. Thank God for everything…*

ABSTRACT

Nitric oxide (NO) and N–O bond bearing species have garnered significant attention due to their fundamental importance in diverse fields such as biology, medicine, environmental science, and chemistry. These compounds exhibit intermolecular NO···H hydrogen bonding interactions, which play a pivotal role in modulating various physicochemical properties, reaction pathways, kinetics, and many other practical applications. Our research aims to quantitatively analyze NO···H interactions exhibited by NO, nitroxyl (HNO), nitrous acid (HONO), nitroxides, and metal nitrosyls in different chemical environments using various quantum chemically derived descriptors within the framework of electronic structure methods. We have conducted a comparative analysis of environmentally and biologically relevant NO···H interactions within microhydrated networks of NO, HNO, and HONO, yielding valuable insights into the kinetics and mechanisms of water-mediated reactions involving these compounds. Additionally, we performed an extensive and quantitative theoretical assessment of NO···H bonding in nitroxide radicals, potentially contributing to the development of stable nitroxides with improved properties. Furthermore, we have also investigated the activation of NO radicals through interaction with Brønsted acid site in metal-loaded zeolites (ZSM-5), with the obtained results potentially applicable to catalytic NO decomposition reactions catalyzed by metal-loaded zeolites.

Keywords: Nitric oxide, Nitroxyl, Nitrous acid, Nitroxide radicals, Metal-loaded zeolites

സാരാംശം

ജീവശാസ്ത്രം, വൈദ്യശാസ്ത്രം, പരിസ്ഥിതി ശാസ്ത്രം, രസതന്ത്രം മേഖലകളിൽ അടുത്ത കാലത്തായി ശ്രദ്ധേയമായിരിക്കുകയാണ് N–O ബോണ്ടുള്ള നൈട്രിക് ഓക്സിഡ്. ഈ സംയുക്തങ്ങൾ ഇന്റർമോളിക്യുലാർ NO···H ഹൈഡ്രജൻ ബോണ്ടിംഗ് ഇന്ററാക്ഷനുകൾ പ്രദർശിപ്പിക്കുന്നു, വിവിധ ഫിസിക്കോകെമിക്കൽ പ്രോപ്പർട്ടികൾ, പ്രതികരണ പാതകൾ, ചലനാത്മകത, മറ്റ് പല പ്രായോഗിക പ്രയോഗങ്ങൾ എന്നിവ മോഡുലേറ്റ് ചെയ്യുന്നതിൽ ഇത് ഒരു പ്രധാന പങ്ക് വഹിക്കുന്നു. ക്വാണ്ടം രസതന്ത്ര സങ്കേതങ്ങൾ ഉപയോഗിച് NO, HNO, HONO, നൈട്രോസ്ക്വിഡ്സ്, മെറ്റൽ നൈട്രോസിൽ എന്നിവയിലെ വിവിധ രാസ പരിസരങ്ങളിലെ ഹൈഡ്രജൻ ബോണ്ടിങ്ങുകളുടെ അളവും വ്യാപ്തിയും വിശകലന വിധേയമാക്കുക എന്നതാണ് ഗവേഷണ ലക്ഷ്യം. പരിസ്ഥിതിക, ജീവശാസ്ത്ര മേഖലകളിൽ പ്രസക്തമായ NO, HNO, HONO എന്നിവയെ സൂക്ഷ്മ ജലാശയ ശൃംഖലകളിലെ NO···H ബന്ധങ്ങളെ താരതമ്യ പഠനത്തിന് വിധേയമാക്കുകയുണ്ടായി. നൈട്രോക്സൈഡ് റാഡിക്കലുകളിലെ NO···H ബോണ്ടിംഗിന്റെ വിപുലവും അളവ്പരവുമായ സൈദ്ധാന്തിക വിലയിരുത്തൽ ഞങ്ങൾ നടത്തി, മെച്ചപ്പെട്ട ഗുണങ്ങളുള്ള നൈട്രോക്സൈഡുകളുടെ വികസനത്തിന് സംഭാവന നൽകാം. കൂടാതെ, മെറ്റൽ-ലോഡഡ് സിയോലൈറ്റുകളിൽ (ZSM-5) ബ്രോൺസ്റ്റഡ് ആസിഡ് സൈറ്റുമായുള്ള രാസപ്രവർത്തനത്തിലൂടെ NO റാഡിക്കലുകളെ വിഘടിപ്പിക്കുന്നതിനെക്കുറിച്ചും ഞങ്ങൾ അന്വേഷിച്ചു, ലഭിച്ച ഫലങ്ങൾ മെറ്റൽ-ലോഡഡ് സിയോലൈറ്റുകളാൽ ഉത്തേജിപ്പിക്കപ്പെടുന്ന കാറ്റലിറ്റിക് NO ഡീകംപോസിഷൻ രാസപ്രവർത്തനങ്ങൾക്ക് ബാധകമാകാൻ സാധ്യതയുണ്ട്.

TABLE OF CONTENTS

LIST OF ABBREVIATIONS

BAS	Brønsted Acid Sites
BSSE	Basis Set Superposition Error
CC	Coupled Cluster
CI	Configuration Interaction
DCD	Direct Catalytic Decomposition
DFT	Density Functional Theory
ECP	Effective Core Potential
EDA	Energy Decomposition Analysis
EDNMR	Electron-Electron Double Resonance Detected Nuclear Magnetic Resonance
EPR	Electron Paramagnetic Resonance
GTO	Gaussian-Type orbitals
HF	Hartree-Fock
IR	Infrared
IUPAC	International Union of Pure and Applied Chemistry
LCAO-MO	Linear Combination of Atomic Orbitals- Molecular Orbitals
MESP	Molecular Electrostatic Potential
MP2	Second Order Møller-Plesset perturbation theory
MRI	Magnetic Resonance Imaging
MTA	Molecular Tailoring Approach
NBO	Natural Bond Orbital
NMR	Nuclear Magnetic Resonance
NOCV	Natural Orbitals for Chemical Valence
NOR	Nitric Oxide Reductase
NPF	New Particle Formation
QM/MM	Quantum Mechanics/Molecular Mechanics
QTAIM	Quantum Theory of Atoms in Molecules
RHF	Restricted Hartree-Fock
ROHF	Restricted Open-Shell Hartree–Fock
SAPT	Symmetry-Adapted Perturbation Theory
SCR	Selective Catalytic Reduction

STO	Slater-Type orbitals
UHF	Unrestricted Hartree-Fock
XRD	X-Ray Diffraction
ZSM-5	Zeolite Socony Mobil-5

PREFACE

Nitric oxide (NO) and N–O bond bearing species play vital roles in various atmospheric and biological events. Understanding their hydrogen bonding interactions in various chemical environments is crucial for explaining the different chemical reactions that occur during these events. In this thesis work, we investigate the hydrogen bonding interactions by NO functionality (NO···H interactions) of NO, nitroxyl (HNO), nitrous acid (HONO), nitroxides, and metal nitrosyls in selected chemical environments using electronic structure methods.

This thesis includes seven chapters. **Chapter 1** provides a general overview of the aforementioned N–O bond-bearing species and the importance of their intermolecular hydrogen bonding interactions in various chemical environments. This chapter also provides a brief overview of the theoretical approaches employed in this thesis.

Chapter 2 investigates the noncovalent interactions present between NO and water using molecular electrostatic potential (MESP), quantum theory of atoms in molecules (QTAIM), and natural bond orbital (NBO) analyses. NO forms hydrogen bonding (HB) and pnicogen bonding (PB) interactions with water. Further, the energies and cooperativity of all individual HBs and PBs in the microhydrated networks (up to four water molecules) of NO (i.e., $NO(H_2O)_{n=1-4}$) is estimated with the help of molecular tailoring approach (MTA) based calculations. Finally, the energies of HBs and PBs in NO…water interactions, as well as the total energies of NO…water and water…water interactions in $NO(H_2O)_{n=1-4}$ complexes, are compared.

Chapter 3 explores the HBs in the microhydrated networks (up to four water molecules, n = 1 – 4) of reduced forms of NO, such as NO^- and HNO. Herein, the energetic and cooperativity details of HBs demonstrate the difference in the HBs formed by anionic NO and N–O of HNO.

Similarly, **Chapter 4** discusses the difference in the strength of NO···H HBs and other HBs formed by HONO in their microhydrated networks (n = 1 – 4). The acidity of HONO and electron-withdrawing -OH bound NO functionality of HONO play major roles in influencing the strength of HBs present in $HONO(H_2O)_{n=1-4}$ complexes.

Chapter 5 discusses the intermolecular hydrogen bonding (NO···H) interactions between nitroxide radicals and HB donors such as HF, H_2O, and CH_4 molecules. The hydrogen bonding ability of nitroxides is measured using molecular electrostatic potential

(MESP) minimum (V_{min}) located around the O atom of NO functionality. Various substitutions on nitroxide radicals (X = H, CH_3, and F) influence the NO···H interaction strength. In addition, these electronic effects on the nitroxide framework reflect on values of MESP parameter V_{min} and interaction energy (E_{int}), and a good correlation is obtained between these two parameters. Thus, V_{min} values can be used as a key descriptor to infer the hydrogen bond strength of nitroxides. Additionally, the redistribution of Mulliken spin density on NO moiety caused by NO···H interactions would have significance in their spin labeling applications. Furthermore, the strength and nature of NO···H interactions with varying substitution and HB donors are assessed using QTAIM analysis. Finally, the symmetry-adapted perturbation theory (SAPT) calculations revealed the contributions of different energy components *viz.* electrostatic, exchange, induction, and dispersion to the interaction energies.

Chapter 6 describes the role of NO···H interaction between adsorbed NO and Brønsted acid sites (BAS) in the adsorption of NO on various metal-loaded ZSM-5 zeolites (M-ZSM-5). The N–O bond activation caused by NO···H interaction in H···(ON)–M-ZSM-5 complexes is measured using Mayer bond order and QTAIM parameters. The larger adsorption energy (E_{ads}) values obtained for H···(ON)–M-ZSM-5 complexes compared to (ON)–M-ZSM-5 quantifies the hydrogen bonding stabilization in H···(ON)–M-ZSM-5 complexes. Further, the hydrogen bonding ability of adsorbed NO is assessed with molecular electrostatic potential (MESP) value at the O atom (V_O) of NO in (ON)–M-ZSM-5 complexes. Interestingly, a good correlation obtained between V_O and HB distance suggests that V_O is a valid descriptor for assessing the hydrogen bond strength in H···(ON)–M-ZSM-5 complexes. Furthermore, the energy decomposition analysis (EDA) quantifies the intermolecular interactions in terms of Pauli's repulsion (E_{Pauli}), electrostatic (E_{ES}), and orbital interactions (E_{Orb}) energies.

Chapter 7 presents the major conclusions of previous chapters, and **Chapter 8** presents the future outlook of work (referred as recommendations).

Chapter 1

Introduction

Part A: Nitric Oxide (NO) and Other N–O Bearing Species

&

Part B: Overview of Computational Methods

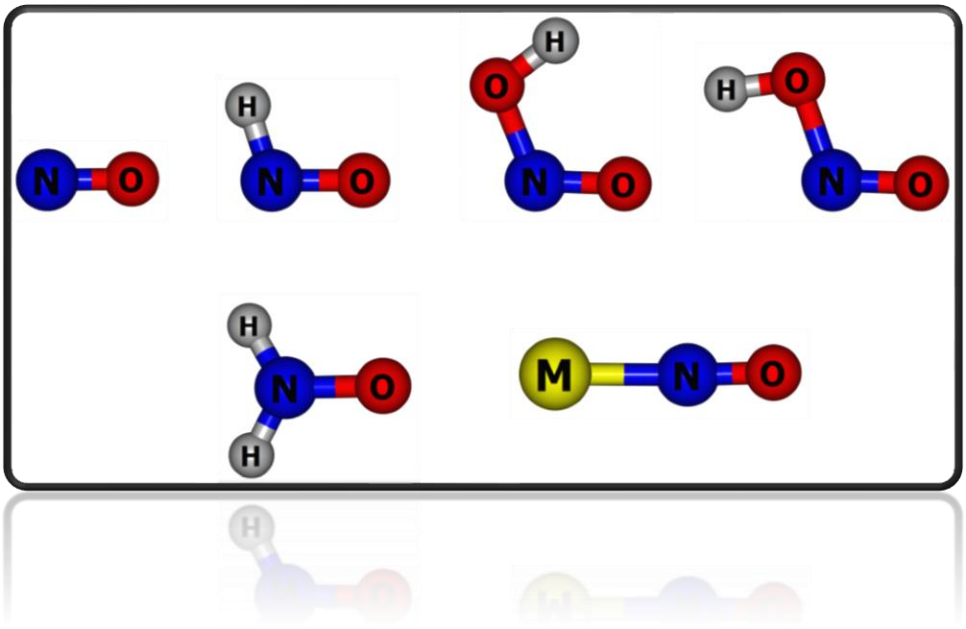

1.1 Abstract

The nitric oxide (NO) molecule and species bearing N–O bonds such as nitroxyl ion (NO^-), nitrosonium ion (NO^+), nitroxyl (HNO), nitrous acid (HONO), nitroxides, and metal nitrosyls have received enormous attention from a wide range of research communities over the last decades. Their unparalleled efforts unveiled the potential applications of these species in a variety of fields, including atmospheric chemistry, therapeutics, magnetism, molecular probes, polymer chemistry, and so on. It is intriguing to mention that the influence of noncovalent interactions in their applications is indisputable. Noncovalent interaction research has grown rapidly in recent decades. The identification, interpretation, and prediction of different types of noncovalent interactions are challenging in this field. It is due to the fuzzy character of noncovalent interaction with diverse electron donor-acceptor possibilities with short to long contact limits. Part A of this chapter discusses the significance of NO, reduced (NO^- and HNO), and oxidized species (NO^+ and HONO) of NO, nitroxide radicals, and metal nitrosyls (including NO adsorbed metal-loaded zeolites) in various fields of chemistry including atmospheric and biological chemistry, among others. Furthermore, it sheds light on the presence and relevance of NO···H hydrogen bonding interactions, within NO-water cluster systems, NO^-/HNO/HONO-water cluster systems, nitroxide-solvent systems, and NO adsorbed metal-loaded zeolites. The NO···H hydrogen bonding interactions in these systems can be investigated using various quantum mechanical methods. Part B of this chapter provides a brief introduction to the theoretical background of the computational techniques employed in this thesis. Electronic structure methods such as *ab initio*, semiempirical, and density functional theory are briefly explained. Also, briefly elucidated key theoretical analyses such as molecular electrostatic potential (MESP), quantum theory of atoms in molecules (QTAIM), natural bond orbital (NBO), energy decomposition (EDA), and molecular tailoring approach (MTA).

Part A: Nitric Oxide (NO) and Other N–O Bearing Species

1.2 Nitric oxide

Nitric oxide (NO) is a free radical molecule that has paramount importance in the field of atmospheric and biological sciences.[1,2] Therefore, the chemistry of NO primarily focuses on (i) studies aimed at controlling or sequestering NO released into the atmosphere through various anthropogenic sources, and (ii) understanding its role in critical biological processes.[3] It is well known that increased NO emissions into the atmosphere lead to the formation of photochemical smog, tropospheric ozone production, and acid rain, among other consequences.[4] On the contrary, the physiological significance of NO was not recognized until the late twentieth century. The role of NO in the relaxation of smooth muscle cells (vasodilation) and the inhibition of platelet aggregation was identified first.[5,6] These pioneering findings in medical science led to NO being celebrated as the "Molecule of the Year" by the journal Science in 1992.[7] Subsequently, in 1998, Robert F. Furchgott, Louis J. Ignarro, and Ferid Murad shared the Nobel Prize in medicine for their discoveries concerning "the role of NO as a signaling molecule in cardiovascular systems".[8] Similarly, numerous biological activities of NO as depicted in Figure 1.1 have been uncovered over the last two decades, including its involvement in immune response, neurotransmission, and angiogenesis, among others.[5]

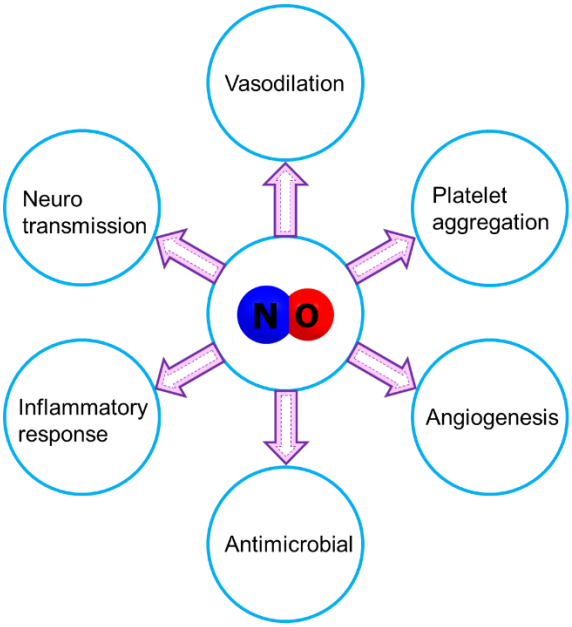

Figure 1.1 Roles of nitric oxide (NO) in biological systems.

1.3 Reduced and oxidised forms of nitric oxide

Research into the reduced forms (such as NO^- and HNO) and oxidized forms (such as NO^+ and HONO) of NO has also gained attention in recent decades.[9–12] Within the field of atmospheric chemistry, these species are commonly recognized as intermediates in the atmospheric reactions of nitrogen oxides (NO_x), and they are also linked to the nitrogen cycle, contributing to atmospheric pollution and other atmospheric phenomena.[13] It has been reported that the redox congeners of NO *viz.* NO^- and NO^+ have unique chemistry in biological systems compared to NO.[14]

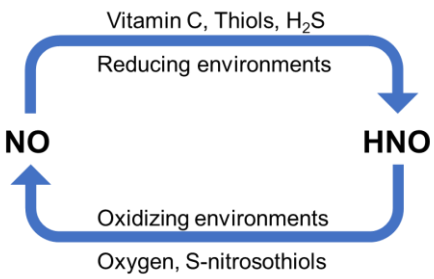

Figure 1.2 NO/HNO interconversion under physiological conditions.[10]

Besides, HNO is gaining recognition as a substantial participant in physiological and pharmacological processes following the NO species (Figure 1.2).[10,15] Certain studies propose that HNO could viably act as a substitute for NO in specific pharmacological contexts.[16] This potential for substitution encompasses various activities, including vasodilation, neurological signaling, and the regulation of enzyme activity, among others.[10] HNO exhibits the capability to exert both direct and indirect effects on diverse physiological conditions, despite its chemistry diverging from that of NO. This distinctive chemical behavior designates HNO as an innovative class of vasodilators, thus rendering it particularly advantageous for addressing heart failure.[17] Additionally, it offers a promising avenue for bettering neuronal damage linked to strokes.[18] Moreover, the reactivity of HNO with different thiols contributes to the inhibition of several thiol-containing enzymes.[19] On the other hand, the HONO molecule is a subject of interest in atmospheric chemistry. The photolysis of HONO stands out as a significant focal point in atmospheric chemistry due to its pivotal role in generating the hydroxyl radical alongside the NO radical.[20] Studies have indicated that the photolysis of HONO contributes to as much as 30% of the hydroxyl radicals produced during daylight hours.[21] Owing to its rapid photolytic decomposition, the lifetime of HONO is exceedingly

low during daytime hours.[12] During the nighttime, these photolytic processes come to a halt, leading to the accumulation of HONO in the atmosphere.[22]

1.4 Nitroxide radicals

Nitroxides are organic free radicals (with a general formula $R_2N–O•$ wherein R = alkyl group), and their molecular properties are primarily determined by the NO moiety.[23] Many studies indicate that $H_2NO•$ (the prototype of nitroxides) can form through the reaction between NO and H_2, as well as HNO and H species; these reactions are well-documented in the context of combustion chemistry involving nitrogen species.[24,25] Nitroxides hold a significant position in chemical research due to their versatile applications.[26–30] In the field of magnetism, nitroxide radicals serve as fundamental building blocks for organic magnetic materials.[28] Within the domain of EPR spectroscopy, they function as spin labels, facilitating investigations into the local environment of large biomolecules.[30–34] Moreover, their utility extends to medicinal applications, where they act as antioxidant drugs to manage oxidative stress and as contrast agents to enhance the relaxation rates of solvent protons in MRI scans.[35,36] Furthermore, their potential roles as hydrogen abstractors and radical scavengers in organic and polymerization reactions, respectively, have sparked keen interest among chemical researchers.[26] Notably, nitroxides like PROXYL ((2,2,5,5-tetramethylpyrrolidine-1-yl)oxidanyl), TEMPO (2,2,6,6-tetramethylpiperidin-N-oxyl), and others find extensive use in this field owing to their specificity and selectivity (Figure 1.3).[37–39]

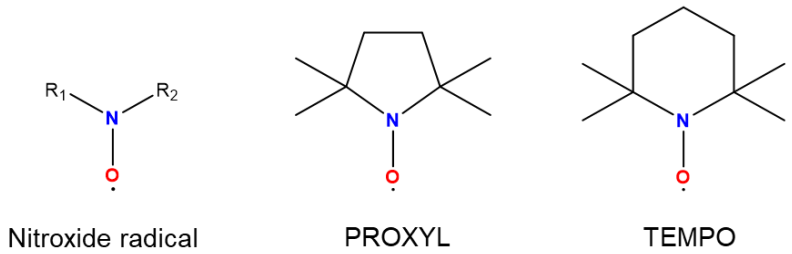

Figure 1.3 General formula of nitroxide radicals (R = alkyl group) and two examples *viz.*, PROXYL ((2,2,5,5-tetramethylpyrrolidine-1-yl)oxidanyl) and TEMPO (2,2,6,6-tetramethylpiperidin-*N*-oxyl).

1.5 NO adsorbed on metal-loaded zeolites

The escalating environmental consequences of increasing NO emissions require effective strategies to eliminate them. Several techniques have been developed to promptly mitigate NO.[40,41] Among them, direct catalytic decomposition (DCD) and selective catalytic reduction

(SCR) stand out as extensively employed methods for NO decomposition.[40,41] In the SCR technique, NO undergoes reduction using reductants such as H_2, NH_3, urea, hydrocarbons, etc., resulting in the production of N_2 and H_2O, whereas DCD yields N_2 and O_2. Various catalysts come into play for both DCD and SCR techniques, encompassing noble metals, metal oxides, perovskites, zeolite-based materials, metal-organic frameworks, etc. (Figure 1.4). Among these catalysts, metal-loaded zeolites are promising due to their distinct activity and thermal stability.[40–43] Zeolites exhibit unique pore structures, confinement effects, and tunable acidity, making them particularly interesting.[44,45] When combined with metals, these features culminate in metal-loaded zeolites with exceptional catalytic performance.[46,47] Notably, Cu(I) and other transition metals (such as Fe, Co, Ni, Pd, Ag, Au, etc.) ion-exchanged zeolites (Figure 1.5), especially ZSM-5, which have been extensively employed in both experimental and theoretical investigations pertaining to NO decomposition.[48–53]

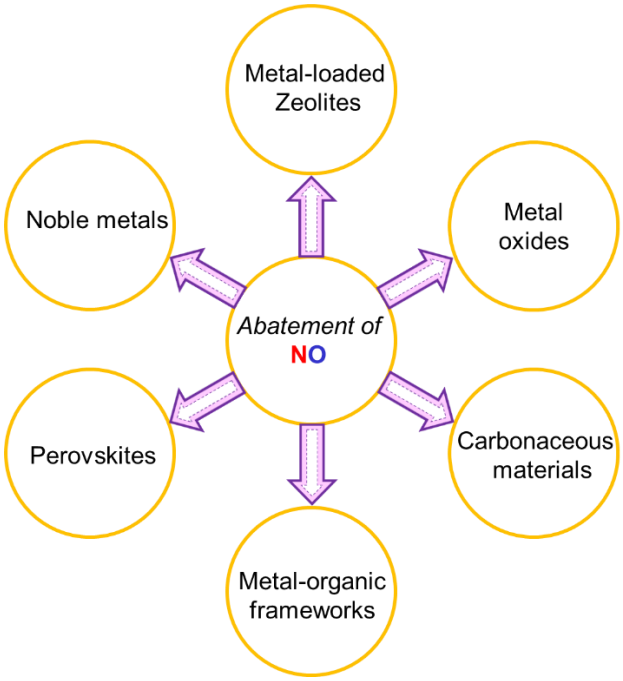

Figure 1.4 Various catalysts used for NO abatement processes.

Copper-loaded ZSM-5 zeolites (Cu-ZSM-5) have played a pivotal role as catalysts in this field since Iwamoto and colleagues unveiled their remarkable activity towards NO decomposition in 1984.[54] The debate concerning whether the copper within Cu-ZSM-5 exists as single or dimer entities persists.[55–57] Nonetheless, a multitude of experimental and theoretical studies have shed light on the NO decomposition pathway on Cu-ZSM-5, indicating the formation of Cu(I)–NO and Cu(I)–$(NO)_2$ species.[58,59] The presence of Cu(I)–NO species in Cu-ZSM-5 adsorbed with NO was identified by employing EPR

spectroscopy.[60] Their findings unveiled a bent Cu(I)–NO adduct and the spin density primarily confined with NO moiety. In an investigation of NO reduction facilitated by Cu- and Fe-loaded zeolites, Rudolph and Jacob revealed that NO exhibits stronger binding to Fe centers within the zeolite framework than to Cu.[61] Similarly, Stepniewski et al. probed the Co–NO bonding within Co-ZSM-5 utilizing DFT methods, and elucidated the charge transfer between Co and NO along with the activation of the N–O bond upon coordination to Co.[62] Apart from the nature of metals and their respective sites within zeolite matrices, the presence of Brønsted acid sites (BAS) within zeolites (See Figure 1.6) has profound implications for catalytic applications.[63,64] Zeolite-based BAS are known to catalyze numerous organic reactions.[65–67] These acid sites originate from the presence of Si–(OH)–Al units within the zeolite framework.[68,69] This is one reason for their categorization as solid acid catalysts.[70,71]

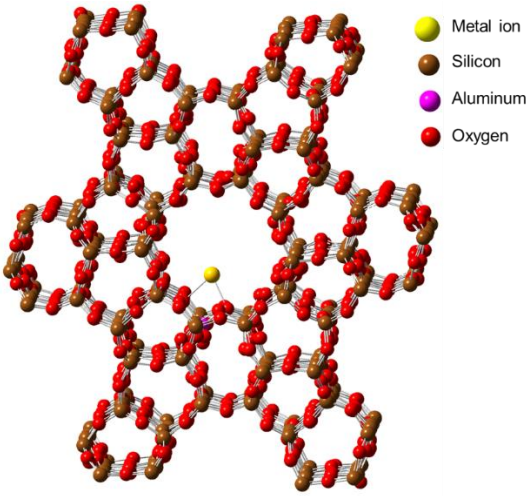

Figure 1.5 Structure of metal-loaded ZSM-5 zeolite framework. Color codes of atoms are listed in the top right corner.

1.6 Hydrogen bonding: a general perspective

It is important to highlight that hydrogen bonding plays a significant role in the unique properties of water, often referred to as "the elixir of life," as well as in the structure of DNA, which holds the fundamental secrets of life. Despite its importance, the term "hydrogen bond" only entered literary usage a little over a century ago.[72] In fact, a universally accepted definition for hydrogen bonding interactions did not emerge until the modern definition recommended by IUPAC in 2011.[73] According to the modern IUPAC definition, a hydrogen bond represents “an attractive interaction between a hydrogen atom from a molecule or molecular fragment X–H in which X is more electronegative than H, and an atom or a group of atoms in the same or different molecule, in which there is evidence of bond formation”.[73]

Various experimental and theoretical methods are employed to investigate the evidence of hydrogen bond formation. Spectroscopic techniques such as infrared (IR), nuclear magnetic resonance (NMR), microwave, Raman, and X-ray diffraction (XRD) are widely utilized for the experimental characterization of hydrogen bonds.[74] On a theoretical level, several analyses are commonly employed in the study of hydrogen bonding. These include the molecular electrostatic potential (MESP),[75] quantum theory of atoms in molecules (QTAIM),[76] natural bond orbital (NBO),[77] and energy decomposition analyses (EDA).[78] A concise overview of these theoretical analyses is presented in the second part (Part B) of this chapter.

Hydrogen bonding studies have unquestionably captivated researchers across diverse fields for over a century. Still, many details regarding hydrogen bonding interactions within various chemical systems remain to be unveiled. In this thesis, we investigate the NO···H hydrogen bonding interactions present in NO-water cluster systems, a few reduced and oxidized forms of NO-water cluster systems, nitroxide-solvent systems, and NO-adsorbed metal-loaded zeolites. A concise review of the relevant literature on these subjects is provided below.

1.7 NO-water clusters

Studies show that the formation of weakly bound molecular complexes of small atmospheric molecules with water clusters affects their molecular behavior.[79] Water molecules catalyze numerous atmospheric reactions, leading to the creation of aerosols, smog, and other significant environmental threats.[80–82] Evidence from numerous experimental studies highlights water as a medium for a wide range of photochemical reactions involving nitrogen oxides. These reactions lead to interconversions of nitrogen oxide species and the formation of their hydroxide forms.[83–86] In a review by Mack and Bolton on NO formation reactions, it was observed that the less stable nitrogen oxides, such as NO_3^- and NO_2^-, readily undergo photolysis, resulting in the production of NO in the presence of water.[87] This photoproduction of NO over sea surfaces is a significant focus in ocean science research due to its impact on the marine environment and aquatic species metabolism.[88–92] The steady-state concentration of NO in seawater plays a critical role in regulating NO levels in the atmosphere, making the ocean a potential reservoir of NO. [89,92,93] Hence, the hydration of NO emerges as a crucial process in both atmospheric and biological systems, making the interactions between water molecules and NO a focal point of interest within this field.

Due to the radical nature of NO, the study of its molecular interactions presents challenges. It even serves as a benchmark molecule for investigating the weak interactions of open-shell molecules.[94,95] Numerous theoretical investigations have been conducted to comprehend the interactions involved in microhydration processes of various atmospheric and biologically important molecules at the molecular level.[96–100] However, the microhydration of NO has not been explored at the molecular level. Previously, several research groups employed techniques such as infrared and mass spectrometry, along with laser ionization, to confirm hydrogen bond interactions between neutral NO and H_2O.[101–103] Using *ab initio* methods, Myszkiewicz and Sadlej were the first to report the potential energy surface of the NO(H_2O) complex.[104] They primarily identified three types of interactions between NO and water: interaction between the N-atom of NO and the O-atom of water, hydrogen bond through the N-atom, and hydrogen bond through the O-atom of NO. In addition, various theoretical analyses, including molecular electrostatic potential (MESP), quantum theory of atoms in molecules (QTAIM), and natural bond orbital (NBO), were employed to study the interaction between NO and water in NO-(H_2O) complexes.[105,106] Orenha et al. applied these analyses to the most stable structure of the NO-(H_2O) complex and compared it with ionic forms of NO-water complexes.[101] Their results indicate that the interaction between NO and water in NO-(H_2O) is significantly weaker than those in ionic forms of NO-water complexes.

1.8 Nitroxyl anion-, nitrosonium ion-, nitroxyl-, and nitrous acid-water clusters

As mentioned, the interconversions between NO and its redox species (NO^- and NO^+) are integral parts of enormous atmospheric and biological processes.[9] On top of this, the reaction chemistry of hydrated systems of NO ions is discussed in many experimental and theoretical studies.[107–109] Eaton et al. recorded the photoelectron spectrum of $NO^-(H_2O)_2$ complexes.[107] In addition, the formation of cyclic hydrogen bond networks in $NO^-(H_2O)_n$ complexes has been reported in several studies.[108] Besides, many studies have been devoted to studying the reaction between NO^- and water and the concomitant formation of intracluster nitroxyl (HNO) and OH^-.[110] Similarly, Relph et al. explored the reaction between NO^+ and a set of water molecules that form nitrous acid (HONO) with the help of isomer-specific vibrational spectroscopy and *ab initio* calculations.[109] Hammam et al. provided theoretical insight for the same reaction and established the importance of the number of water molecules and its effect on the hydration process of NO^+.[111] Similarly, there are some successful attempts to study the intracluster reaction of $NO^+(H_2O)_n$ systems.[112,113]

The hydration reactions of NO ions (NO^- and NO^+) often result in the formation of HNO and HONO, respectively. Like NO, the complexes formed by nitroxyl (HNO) and nitrous acid (HONO) with water molecules have significance in both atmospheric and biological chemistry. HNO's atmospheric and biological chemistry revolves around its reactivity in dimerization.[114] Numerous experimental and theoretical investigations have concurred that the rate of this dimerization process experiences a noteworthy enhancement in aqueous solutions.[115–117] A case in point is the work of Fehling and Friedrichs, who explored the variables influencing the rate of dimerization in solution, presenting a mechanism based on DFT calculations utilizing both implicit and explicit solvation models of water.[117] Their findings indicated a marked reduction in the activation barrier through the presence of explicit water molecules, attributed to the stabilizing effect of hydrogen bonding on the transition state. A comparable water-mediated mechanism for the dimerization of HNO is also postulated by Zhang and Thynell, employing theoretical methods such as DFT and ab initio, in conjunction with kinetic simulations.[116] On the other hand, Zhao and Du conducted an exploration of complexes formed by HONO with dimethylamine and water molecules using DFT calculations.[22] They predicted the potential for these complexes to initiate new particle formation (NPF), a process with significant importance in atmospheric aerosol chemistry. Zhao et al. probed the molecular complexes of HONO with HCl and water molecules, proposing a mechanism for ClNO formation through the reaction between HONO and HCl, facilitated by water molecules.[118] Nitrosyl chloride (ClNO), a toxic gas and a contributor of Cl radicals to the atmosphere, emerges as a result of this process. Furthermore, it is hypothesized that molecular complexes of HONO with water clusters could serve as sites for water condensation.[119]

1.9 Hydrogen bonding interactions of nitroxide radicals

The hydrogen bonding interactions of nitroxide radicals play crucial roles in the various applications mentioned above.[120] These interactions markedly contribute to the stabilization of macromolecules and crystals.[37,121] Many spin labeling studies have reported on the hydrogen bonding interactions between nitroxide-based spin probes and solvent molecules.[120,122–126] These studies employ site-directed spin-labeling EPR spectroscopy to gather insights into the structure and dynamics of biomolecules. The sensitivity of nitroxide EPR parameters to the polarity of solvent molecules is a focal point of extensive research within this domain.[23] Smirnova et al. demonstrated that the high-frequency EPR spectra are responsive to hydrogen bonds formed between a nitroxide-based lipid bilayer spin probe and

polar solvent molecules.[127] Their investigations into the biophysical properties of the lipid bilayer environment in cell membranes underscore the significance of these interactions.

Ikryannikova et al. explored the hydration effects on the NO moiety of nitroxides through DFT methods; they observed a redistribution of spin densities on the NO moiety induced by the presence of surrounding water molecules.[125,126] Owenius et al. employed solvents with varying dielectric constants to investigate the alterations in EPR parameters resulting from hydrogen bonds formed between nitroxide probes and solvent molecules ($R_2NO\cdots H$).[123] Their DFT findings harmoniously align with the shifts in EPR parameters attributed to these $R_2NO\cdots H$ hydrogen bonds. Similarly, Nalepa et al. detailed the impact of $R_2NO\cdots H$ hydrogen bonding configurations between nitroxides and diverse polar protic solvents on the magnetic parameters of nitroxide-based spin probes. They accomplished this through high-field EPR and EDNMR spectroscopy techniques.[124]

Recently, Chestnut et al. effectively employed this sensitivity of nitroxide spin label magnetic parameters on $R_2NO\cdots H$ interactions with water molecules, to create profiles of water concentration across the membranes of lipid bilayers.[128] They employed the hyperfine sublevel correlation (HYSCORE) spectroscopy technique, which enables the measurement of water concentrations by detecting the hydrogen bonds formed by the paramagnetic center on nitroxides. The implications of $R_2NO\cdots H$ interactions are also important in organic reaction mechanisms due to the hydrogen abstraction capability of nitroxides.[29,38,39] Specifically, derivatives like TEMPO and PROXYL find application in abstracting hydrogen atoms from weak hydrogen bonds, including metal hydrides, phenols, thiols, and allylic positions.[23,38,39] In the case of organic radical scavenging by nitroxides, the $R_2NO\cdots H$ hydrogen bond interactions result in a reduction of the scavenging reaction rate.[129] Furthermore, Romero et al. reported the potential for the transmission of ferromagnetic interaction through $R_2NO\cdots H$ interactions in alkyl-substituted nitroxide radicals.[130]

1.10 NO and Brønsted acid sites in zeolites

Several studies have revealed the pivotal role played by Brønsted acid sites (BAS) in the catalytic activity of ZSM-5 and other zeolites across a range of chemical reactions.[63,131–133] Similar to the investigation of metal adsorption within metal-loaded zeolites, there has been a substantial body of research documenting the binding of adsorbates to BAS in zeolites.[134–136] For instance, Wang et al. investigated the adsorption of several nitrogen oxides on BAS and Fe^{3+} in H-BEA (a beta zeolite containing BAS) and Fe-BEA, respectively, utilizing FT-IR

spectroscopy.[134] Experimental and theoretical studies demonstrate the formation of hydrogen bonds between nitrogen oxides and BAS within BAS-containing zeolites.[137,138] In a theoretical study, Sajith et al. investigated the role of Brønsted acidic protons in the mechanism of direct NO decomposition over the dimeric Cu active center in Cu-ZSM-5, employing the quantum-mechanics/molecular-mechanics (QM/MM) method.[139] Their findings highlight that protonation significantly reduces the activation barrier of key steps in the NO decomposition pathway. This conclusion aligns with the observations of Kawakami and Ogura, who arrived at a similar deduction in their investigations of the NO decomposition reaction on Fe-loaded zeolites with proton sites.[140]

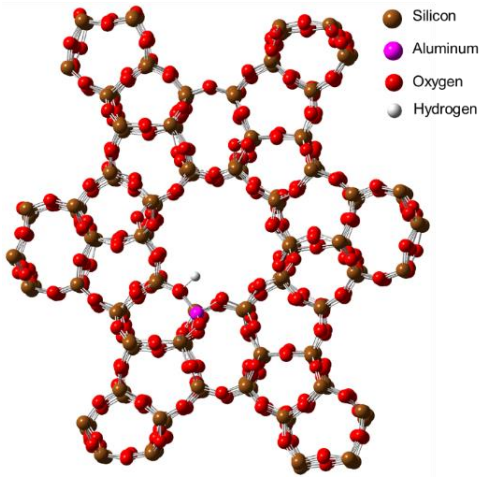

Figure 1.6 ZSM-5 framework with Brønsted acid site (BAS). Color codes of atoms are listed in the top right corner.

It is interesting to observe that the impact of hydrogen bonding interactions on the stabilization of nitrogen oxide adsorption and the cleavage of N–O bonds has been extensively documented within various biological systems.[141–143] In a DFT study concerning the Cu-containing N_2O reductase reaction, Solomon and his colleagues computed the stabilization energy resulting from the hydrogen bond between the O-atom of N_2O and the lysine residue of the reductase, revealing a range of 3 – 5 kcal/mol.[141] Furthermore, they noted a reduction in the activation barrier for N–O bond cleavage during the N_2O reductase reaction when the transition state engaged in hydrogen bonding interactions with neighboring water or formic acid molecules. Similarly, Lu et al. investigated NO reduction on the flavo-diiron nitric oxide reductase (NOR), utilizing a combined approach of QM/MM and ^{57}Fe Mössbauer spectroscopy.[142] They elucidated the presence of a hydrogen bond between the NO molecule bound to Fe and a tyrosine proton of the flavo-diiron protein in an intermediate formed during the NO reduction reaction. This interaction led to a reduction in the reaction

barrier for N–O bond cleavage. In a parallel to the biological NOR reactions, numerous biomimetic models involving heme/non-heme coordination with metals, particularly Cu, Fe, and Co, have been employed to explore the catalytic reduction of NO with the aid of hydrogen bonding.[143,144] Recently, Wijerante et al. highlighted the pivotal role of hydrogen bonding interactions involving ligands or solvent water molecules with NO in a copper complex undergoing the NOR reaction.[145] They proposed a mechanism wherein the hydrogen bonding and protonation capabilities of ligands and the adjacent water molecule govern the process of NO reduction.

Part B: Overview of Computational Methods

1.11 Computational chemistry

Computational chemistry uses computational modelling and simulations to solve chemical problems. In recent decades, rapid advancements in computing technologies have resulted in tremendous progress within computational chemistry. This progress in computational chemistry is attributed to the development of robust theoretical methods in conjunction with fast algorithms. The primary goal of computational chemistry studies is to integrate various theoretical methods to achieve synergy between experimental and theoretical results. For instance, the advanced spectroscopic data enables better theoretical modeling, while the theoretical results serve to validate the experimental findings or vice versa. As a result, the experimental and theoretical analyses are in tandem. Fundamentally, the computational chemistry methods are based on two approaches, i.e., classical mechanics and quantum mechanics. The computational methods developed from quantum mechanics are known to be electronic structure methods, and it is further divided into *ab-initio* methods, semi-empirical methods, and density functional theory (DFT). For this thesis work, electronic structure methods are used and the descriptions of those methods are briefly given in the following section.

1.12 *Ab initio* methods

The word '*ab-initio*' itself means 'from the beginning'. For solving the Schrödinger equation, this method uses charge and mass of nuclei and electrons, speed of light, Plank's constant,

etc. Though these calculations generate more accurate results for any chemical system, they are very time-consuming and require a huge amount of computational power.

1.12.1 The Schrödinger equation

Schrödinger equation describes the state of any chemical system in terms of wave function (Ψ). The Ψ is a function of position and time. In this thesis, our computational methods are based on time-independent version of Schrödinger equation, the simplest form of this equation is as follows (Eq. 1),

$$\hat{H}\Psi = E\Psi \qquad \text{(Eq. 1.1)}$$

Here, $\hat{H}$ is Hamiltonian operator, which is made up of kinetic and potential energy operators for all the nuclei and electrons of a system, and E is the total energy for the corresponding system. The $\hat{H}$ operator consider nuclear-nuclear, nuclear-electron, and electron-electron interactions; it is written as below (Eq. 1.2) for a system containing N-numbers of electrons and M-numbers of nuclei.

$$\hat{H} = -\frac{\hbar^2}{2m_\alpha}\sum_{\alpha=1}^{M}\nabla_\alpha^2 - \frac{\hbar^2}{2m_i}\sum_{i=1}^{N}\nabla_i^2 + \sum_{\alpha=1}^{M}\sum_{\beta>\alpha}^{M}\frac{Z_\alpha Z_\beta e^2}{r_{\alpha\beta}} - \sum_{\alpha=1}^{M}\sum_{i=1}^{N}\frac{Z_\alpha e^2}{r_{i\alpha}} + \sum_{i=1}^{N}\sum_{j>i}^{N}\frac{e^2}{r_{ij}}$$

(Eq. 1.2)

In Eq. 1.2, the m_i and m_α represent mass of electron and nuclei, respectively, e is electronic charge, Z is atomic number, i and j refer to electrons, α and β refer to nuclei, $\hbar$ is Plank's constant (h) divided by 2π, ∇^2 denotes the Laplacian operator, and r is the position vector. Note that, the first and second terms represent the kinetic energy operators for electrons and nuclei, respectively, and the remaining terms are of potential energy operators corresponding to nuclear-electron, nuclear-nuclear, and electron-electron interactions (3rd, 4th, and 5th terms, respectively). The exact solution of Schrödinger equation is only obtained for hydrogen-like atoms because electron-electron repulsion is absent therein. For many electron systems, many approximations are made to solve the Schrödinger equation. Among that, a few important approximations/methods, such as Born-Oppenheimer, LCAO-MO, Hartree-Fock, and electron correlation, are briefly explained below.

1.12.2 Born-Oppenheimer approximation

On considering the motion of the nucleus and electron, the speed of the nucleus can be approximated to zero as relative to the speed of the electron. It is because a nucleus is much

heavier (more than 1000 times) than an electron. Based on these facts, Born and Oppenheimer approximated the kinetic energy of the nucleus to be zero and the nuclear-nuclear repulsion to be a constant value for a chemical system. As a result, the Schrödinger equation is simplified as follows,

$$\left(\hat{H}_{el} + \hat{V}_{NN}\right)\Psi_{el} = (E_{el} + V_{NN})\Psi_{el} \qquad \text{(Eq. 1.3)}$$

$$\hat{H}_{el} = -\frac{\hbar^2}{2m_e}\sum_{i=1}^{N}\nabla_i^2 - \sum_{\alpha=1}^{M}\sum_{i=1}^{N}\frac{Z_\alpha e^2}{r_{i\alpha}} + \sum_{j=1}^{N}\sum_{i>j}^{N}\frac{e^2}{r_{ij}} \qquad \text{(Eq. 1.4)}$$

$$\hat{V}_{NN} = \sum_{\alpha=1}^{M}\sum_{\beta>\alpha}^{M}\frac{Z_\alpha Z_\beta e^2}{r_{\alpha\beta}} \qquad \text{(Eq. 1.5)}$$

Here, $\hat{V}_{NN}$ is the potential energy term for nuclear-nuclear repulsion, this has a constant value for a particular system. Hence, the Schrödinger equation for electronic motion can be written as follows,

$$\hat{H}_{el}\Psi_{el} = E_{el}\Psi_{el} \qquad \text{(Eq. 1.6)}$$

Further, the total energy of a system can be calculated by adding the E_{el} with $\hat{V}_{NN}$, i.e.,

$$E_{total} = E_{el} + \hat{V}_{NN} \qquad \text{(Eq. 1.7)}$$

1.12.3 Variation theorem

According to the variation theorem, an approximate (trial) wave function is taken for determining the energy of a system with the help of a known Hamiltonian. The calculated value of energy is known as the expectation value of energy (<E>), which is always greater than or equal to the ground state energy (E_0) of the particular system.

$$<E> = \frac{\int \Psi_{trial}{}^{*}\hat{H}\Psi_{trial}d\tau}{\int \Psi_{trial}{}^{*}\Psi_{trial}d\tau} \geq E_0 \qquad \text{(Eq. 1.8)}$$

In general, the trial wave function is designed with one or more variables that can be varied in order to obtain a minimum value for E (i.e., a closer value to E_0).

1.12.4 LCAO-MO approximation

The trial wave function is often constructed by the method of linear combination of atomic orbitals (LCAO). For an electron in a molecular orbital (MO) of a molecule, the trial wave function (Ψ) can be formed with a linear combination of atomic orbitals (Φ) with respective coefficients (C).

$$\Psi = \sum_{i=1}^{n} C_i \Phi_i \qquad \text{(Eq. 1.9)}$$

The coefficient (C_i) expresses the contribution of an atomic orbital (Φ_i) in MO. The values of coefficients that minimize the energy for the Ψ can be calculated using the variational principle.

1.12.5 Hartree-Fock method

Hartree and Fock developed a method to tackle the difficulty of the electron-electron repulsion term when solving the Schrödinger equation for many-electron systems. It is also known as Hartree-Fock self-consistent field theorem.

According to Hartree's approximation, an electron is moving in a static field created by all nuclei and an average field of all other electrons. Hence, the Hamiltonian for an electron is,

$$\widehat{H}_{el} = -\frac{\hbar^2}{2m_i} \sum_i^N \nabla_i^2 - \sum_\alpha^M \sum_i^N \frac{Z_\alpha e^2}{r_{i\alpha}} + V_i \qquad \text{(Eq. 1.10)}$$

Here, the first term represents the kinetic energy operator for electrons and the second term refers to the potential energy operator for all nucleus-electron interactions. The V_i term refers to the potential energy operator for an electron (say i^{th}) due to the average field of other electrons ($\neq i$). Thus, V_i is determined by the summation of potential energies on i^{th} electron due to all other electrons ($j \neq i$) with a wave function Φ_j. This can be expressed as,

$$V_i = \sum_{j \neq i}^{N} \int \Phi_j^2 \frac{e^2 d\tau_j}{r_{ij}} \qquad \text{(Eq. 1.11)}$$

The total wave function (Ψ) of this many electrons system can be expressed as the product of 'N' hydrogen-like orbitals (Φ),

$$\Psi = \Phi_1(1)\Phi_2(2) \ldots \ldots \Phi_n(n) \qquad \text{(Eq. 1.12)}$$

In Hartree's approximation, an iterative procedure is followed to solve the Schrödinger equation. Firstly, the $\widehat{H}_{el}$ operator is applied for an electron (i^{th}) to generate an improved one-electron wave function Φ_i'. Then, this procedure is repeated for all other electrons, and finally, an improved total wave function Ψ will be obtained. Next, the improved Φ_i' is used to solve the one-electron Schrödinger equation which results in a more improved one-electron wave function. Accordingly, the iterative procedure can be repeated

until the V_i obtained is so close to the earlier V_i. This final potential is called 'self-consistent field (SCF)' and the associated orbitals are called self-consistent field orbitals.

The major drawback of Hartree's approximation is the effect of the interchange of electrons. To solve this problem, Fock incorporated antisymmetrized wave function (see Eq. 1.13) as in a determinant form into Hartree's method. Now, it is known as the Hartree-Fock method. The determinant employed herein is the Slater determinant.

The Slater determinant is constructed by the spin orbitals. The general form of Slater determinant for an N-electron system is,

$$\Psi = \frac{1}{\sqrt{N!}} \begin{vmatrix} \chi_i(x_1) & \chi_j(x_1) & \dots\dots & \chi_k(x_1) \\ \chi_i(x_2) & \chi_j(x_2) & \dots\dots & \chi_k(x_2) \\ \vdots & \vdots & \vdots & \vdots \\ \vdots & \vdots & \vdots & \vdots \\ \chi_i(x_N) & \chi_j(x_N) & \dots\dots & \chi_k(x_N) \end{vmatrix} \qquad \text{(Eq. 1.13)}$$

where N electrons occupy N spin orbitals $(\chi_i, \chi_j, \dots\dots \chi_k)$. $\frac{1}{\sqrt{N!}}$ is the normalization constant.

A short-hand notation of the Slater determinant (single Slater determinant) is shown below, in which the diagonal elements of the determinant are only present.

$$\Psi\ (x_1, x_2, \dots\dots\ x_N) = |\chi_i \chi_j \dots\dots\ \chi_k\rangle \qquad \text{(Eq. 1.14)}$$

The operator used by Fock (Fock operator, $\hat{F}(i)$) to solve this antisymmetrized wave function is,

$$\hat{F}(i) = -\frac{\hbar^2}{2m_e}\sum_i^N \nabla_i^2 - \sum_\alpha^M \sum_i^N \frac{Z_\alpha e^2}{r_{i\alpha}} + \sum_{i=1}^{N/2}\sum_{j=1}^{N/2}(2\hat{J}_{ij} - \hat{K}_{ij}) \qquad \text{(Eq. 1.15)}$$

$$\hat{F}(i) = \hat{H}_i^{core} + \sum_{i=1}^{N/2}\sum_{j=1}^{N/2}(2\hat{J}_{ij} - \hat{K}_{ij}) \qquad \text{(Eq. 1.16)}$$

Here, the $\hat{J}_{ij}$ and $\hat{K}_{ij}$ are Coulomb operator (see Eq 1.17) and exchange operator (see Eq. 1.18) respectively. The Coulomb operator $(\hat{J}_{ij})$ refers to the electrostatic interaction of electrons in the χ_i and χ_j orbitals, while the exchange operator $(\hat{K}_{ij})$ refers to the exchange energies of electrons in the χ_i and χ_j orbitals. The $\hat{H}_i^{core}$ represents the Hamiltonian of an electron in a hydrogen-like atom.

$$\hat{J}_{ij} = \int\int \chi_i(x_1)^* \chi_j(x_2)^* \left[\frac{1}{r_{12}}\right] \chi_i(x_1)\chi_j(x_2) d\tau_1 d\tau_2 \qquad \text{(Eq. 1.17)}$$

$$\widehat{K}_{ij} = \int\int \chi_i(x_1)^* \chi_j(x_2)^* \left[\frac{1}{r_{12}}\right] \chi_i(x_2)\chi_j(x_1) d\tau_1 d\tau_2 \qquad \text{(Eq. 1.18)}$$

The energy of an electron (i^{th}) is calculated by,

$$\hat{F}(i)\Psi = \varepsilon_i \Psi \qquad \text{(Eq. 1.19)}$$

The ε_i energy (orbital energy) is in the form of,

$$\varepsilon_i = \varepsilon_i^0 + \sum_{i=1}^{N/2} \sum_{j=1}^{N/2} (2\hat{J}_{ij} - \widehat{K}_{ij}) \qquad \text{(Eq. 1.20)}$$

where ε_i^0 denotes the one-electron energy calculated in the absence of other electrons. The remaining term in the equation refers to the sum of electrostatic and exchange energies for the interaction of an electron (i^{th}) with all other electrons ($i \neq j$).

1.12.6 RHF, UHF, and ROHF methods

The restricted Hartree-Fock (RHF) method is applied to molecules with singlet spin. In RHF calculation, each pair of electrons in an orbital is constrained to have the same spatial wave function for both α and β spin functions. This type of molecular system is called a closed-shell singlet (css) system.

The restriction applied in the RHF method is relaxed in the unrestricted Hartree-Fock (UHF) method. In UHF calculations, different orbital spatial wave functions are allowed for electrons with different spins. This method is applied to molecular systems with unpaired electrons.

Restricted Open Hartree-Fock (ROHF) method can also be used for a molecular system with unpaired electrons. Herein, the paired electrons in an orbital have the same spatial functions, hence RHF principle is treated therein. But the spatial function of orbital with unpaired electron can have either the spin α or β.

The molecular systems with unpaired electron are called open-shell systems. In this thesis, the chemical systems with nitric oxide molecules, nitroxides, and most of the metal nitrosyls are open-shell systems.

1.12.7 Roothaan-Hall equation

The HF equation is further modified by Roothaan and Hall. They used the trial wave function as a linear combination of a complete set of known orthonormal functions. These functions are called basis functions, it is represented as,

$$\Psi = \sum_{i=1}^{k} C_{ia}\, \chi_i \qquad \text{(Eq. 1.21)}$$

where C_{ia} is expansion coefficient, χ_i is the basis function and k is the number of basis functions.

Substitution of this Ψ in the above Hartree-Fock equation (Eq. 1.19), followed by multiplication of both sides by another basis function χ_j^* and integrating over the entire space will lead to a set of k linear equations called the Roothaan-Hall equation. A compact expression of the Roothaan-Hall equation in the form of a single matrix is,

$$FC = SCE \qquad \text{(Eq. 1.22)}$$

where F is the Fock operator in the matrix, S is the overlap matrix integral, C is the matrix for expansion coefficient and E is the diagonal matrix for orbital energies ε_i.

1.12.8 Methods for treating electron correlation

The main limitation of the HF method is that electron-electron interaction is not considered explicitly; rather, they approximate that an electron is moving in an average field of other electrons. Hence, the difference in HF calculated energy and ground state minimum energy of a system is regarded as the electron correlation energy. This electron correlation energy is considered in a few methods, *viz*., Møller-Plesset Perturbation, Configuration Interaction, and Coupled Cluster methods. These methods are generally called post-HF methods or higher *ab initio* methods. Of course, these methods produce very accurate results for a system, but the computational expenses for performing these calculations are enormous. Hence, these methods are applicable only for systems containing a small number of atoms with a reasonable computational cost.

1.12.8.1 Møller-Plesset perturbation theory

In Møller-Plesset perturbation theory, the electron-electron correlation is treated by a perturbation term to a known Hamiltonian (eigenfunctions and eigenvalues are known). The sum of known Hamiltonian ($\hat{H}_0$) and the perturbation term $\hat{V}$ will give the actual Hamiltonian ($\hat{H}$). The eigenfunctions and eigenvalues of $\hat{H}_0$ are solved by the HF iterative method. The eigenfunctions and eigenvalues of $\hat{V}$ is obtained by perturbative procedure with various orders. Hence, this is a correction to energy obtained by HF. The actual Hamiltonian ($\hat{H}$) is represented as,

$$\hat{H} = \hat{H}_0 + \lambda\hat{V}$$

$$\hat{H}|\Psi_i\rangle = \left(\hat{H}_0 + \lambda\hat{V}\right)|\Psi_i\rangle = \varepsilon_i|\Psi_i\rangle \qquad \text{(Eq. 1.23)}$$

The eigenfunctions and eigenvalues of $\hat{H}_0$ can be represented as $\left|\Phi_i^{(0)}\right\rangle$ and $E_i^{(0)}$ (HF-energy). Expansion of perturbed ε_i and $|\Psi_i\rangle$ can be represented as a power series in λ,

$$\varepsilon_i = E_i^{(0)} + \lambda E_i^{(1)} + \lambda^2 E_i^{(2)} + \cdots \qquad \text{(Eq. 1.24)}$$

$$|\Psi_i\rangle = \left|\Phi_i^{(0)}\right\rangle + \lambda\left|\Phi_i^{(1)}\right\rangle + \lambda^2\left|\Phi_i^{(2)}\right\rangle + \cdots \qquad \text{(Eq. 1.25)}$$

If this power series is truncated at second order, then it is known as Møller-Plesset second order perturbation (MP2) theory. This MP2 theory is widely used as a post-HF method. The energy expression for a MP2 method is,

$$E_i^{(0)} = \langle\Phi_i^{(0)}|\hat{H}_0|\Phi_i^{(0)}\rangle, \qquad E_i^{(1)} = \langle\Phi_i^{(0)}|\hat{V}|\Phi_i^{(0)}\rangle, \qquad E_i^{(2)} = \langle\Phi_i^{(0)}|\hat{V}|\Phi_i^{(1)}\rangle \quad \text{(Eq. 1.26)}$$

1.12.8.2 Coupled cluster methods

In coupled cluster (CC) method, the many electrons wave function is constructed by using excitation operators to calculate the electron-electron correlation. This method considered as a good mathematically refined technique for obtaining electron-electron correlation energy. The wave function can be represented as,

$$|\Psi\rangle = e^{\hat{T}}|\Psi_0\rangle \qquad \text{(Eq. 1.27)}$$

Here, the $|\Psi_0\rangle$ is a Slater determinant obtained in the HF method. The $\hat{T}$ is an excitation operator, which is expressed as a sum of operators of a single $(\hat{T}_1)$, double $(\hat{T}_2)$, triple $(\hat{T}_3)$, etc. excitations.

$$\hat{T} = \hat{T}_1 + \hat{T}_2 + \hat{T}_3 + \cdots \qquad \text{(Eq. 1.28)}$$

The variations in the CC method are based on the highest number of excitations considered in $\hat{T}$. One of the popular CC methods, i.e., the CCSD method includes single $(\hat{T}_1)$ and double $(\hat{T}_2)$ excitations in $\hat{T}$ (i.e., $\hat{T} = \hat{T}_1 + \hat{T}_2$). Herein, the $|\Psi_0\rangle$ function is a linear combination of singly and doubly excited slater determinants. These calculations require a very huge computational cost. Further, the next variants of CC methods such as CCSDT (with single,

double, and triple excitations operator) and CCSDQ (with single, double, triple, and quadruple excitations operator) are more expensive than CCSD method. The CCSD(T) method (T in bracket indicates that perturbative triples) is considered to be the gold-standard calculation in quantum chemistry.

1.12.8.3 Configuration interaction

In the configuration interaction (CI) method, the excited states are also included for the electronic state calculations. The complete CI wave function is a linear combination of Slater determinants with all the possible electronic configurations. If only one electron has moved from each determinant, then the CI method is known as CIS (configuration interaction single-excitation). The CIS calculations do not correct ground state energy, but it will give an idea about excited states. The CISD (configuration interaction single and double excitation) calculations give correlation corrected ground state energy. The CISDT (configuration interaction single, double, and triple excitation) and CISDTQ (configuration interaction single, double, triple, and quadruple excitation) calculations are computationally expensive, hence this is performed only for very highly accurate results required cases. In principle, the full CI calculations using an infinitely large basis set will provide exact quantum mechanical results.

1.12.9 Basis sets

All the electronic structure calculations are based on the trial wave function designed for a system. Choosing a trial wave function is the starting point for solving the Schrödinger equation for a system. In this regard, the basis set is the set of mathematical functions that can be used to construct a trial wave function. There are two types of mathematical basis functions extensively used in computational chemistry calculations, i.e., Slater-type orbitals (STOs; χ^{STO}) and Gaussian-type orbitals (GTOs; χ^{GTO}). The mathematical forms of STOs and GTOs are described below (Eq. 29 and Eq. 30, respectively),

$$\chi^{STO}(r,\varphi,\phi) = Nr^{n-1}e^{(-\xi r)}Y_m^l(\varphi,\phi) \qquad \text{(Eq. 1.29)}$$

$$\chi^{GTO}(r,\varphi,\phi) = Nr^{2n-2-l}e^{(-\xi r^2)}Y_m^l(\varphi,\phi) \qquad \text{(Eq. 1.30)}$$

where N is the normalization constant, r is the distance from the nucleus, n, l, and m refers to principal, azimuthal, and magnetic quantum numbers, ξ is orbital exponent, and $Y_m^l(\varphi,\phi)$ term represent the angular part of the wave function. The STOs have very similar hydrogen-like atomic orbitals, thus, these basis functions are most efficient in representing

the electronic configurations of atoms. The demerit of STOs is their computational cost, STOs used in calculations are highly expensive, especially for large systems. To overcome this problem, Boys proposed GTOs in 1950. Actually, the linear combination of three or more GTOs can mimic the behavior of a STO. An orbital is represented by combinations of GTOs, which is known as a contracted Gaussian type orbital, wherein each GTOs is known to be a primitive GTO.

Basis sets are further classified into minimal, double zeta, triple zeta, etc., based on the number of basis functions used to represent an atomic orbital.

1.12.9.1 Minimal basis set

The minimal basis set consists of one basis function for each atomic orbital.
For example: Hydrogen atom, 1s orbital = one basis function

Fluorine atom, 1s + 2s + $2p_x$ + $2p_y$ + $2p_z$ orbitals = five basis functions.

STO-3G is generally used minimal basis set in which the basis function consists of three primitive Gaussians. This basis set is good for speedy and rough calculations, but has poor accuracy in results.

1.12.9.2 Multi zeta basis sets

The double zeta and triple zeta basis sets consist of two and three basis functions, respectively, for each atomic orbital. For example: there will be ten and fifteen basis functions for fluorine atoms according to double zeta and triple zeta basis sets, respectively.

1.12.9.3 Split valence basis sets

Pople developed split valence basis sets to increase the basis functions only for valence orbitals since the valence orbitals are involved in chemical bonding. In such basis sets, a minimal basis set is used for core orbitals, whereas double zeta or triple zeta basis sets are for valence orbitals.

For example: the 6-31G basis set for fluorine atom: 1s orbital (core) is described by one basis function (minimal basis set) consisting of six primitive Gaussian functions. 2s, $2p_x$, $2p_y$, and $2p_z$ (valence) orbitals are described by two types of basis functions (double zeta), in which one type consists of 3 primitive Gaussian functions and the other type consists of 1 primitive Gaussian function. Therefore, total 9 (1 + 4 + 4) basis functions and 22 (6 + 12 + 4) primitive functions.

6-311G basis set for fluorine atom: 1s orbital (core) is described by one basis function (minimal basis set) consisting of six primitive Gaussian functions. 2s, $2p_x$, $2p_y$, and $2p_z$ (valence) orbitals are described by three types of basis functions (triple zeta), in which one type consists of 3 primitive Gaussian functions and the other two types consist of 1 primitive Gaussian function. Therefore, total 13 (1 + 4 + 4 + 4) basis functions and 26 (6 + 12 + 4 + 4) primitive functions.

1.12.9.4 Polarization and diffuse functions

The polarization and diffuse functions can be incorporated into basis sets. This is done by adding functions of higher angular momentum for polarized basis sets, whereas, adding functions that have a small exponent to describe the electron density away from the nucleus is called diffused basis sets. Generally, p-type functions are used to polarize electrons of hydrogen atoms, whereas, d-type functions for other main group atoms, and f-type functions for transition metals. The notation used for polarized functions of *p* and *d* is (d,p) or **, i.e., 6-31G(d,p) or 6-31G**. The notation used for the diffuse function is ++. For example, 6-31G++ is used for diffuse on hydrogen atoms and heavy atoms.

In this work, we have extensively used these polarization and diffuse functions in our split valence basis sets, i.e., 6-311G++(d,p). Besides, Dunning's correlation-consistent basis set viz. aug-cc-pVTZ is used for better energetics in small cluster calculations,[146] and Ahlrichs and coworkers developed (later modified by Weigend) def2-SVP and def2-TZVP basis sets were used for metal complexes.[147] Herein, the def2-SVP and def2-TZVP basis sets are double zeta and triple zeta, respectively, they contain polarization functions. The aug-cc-pVTZ basis set is a triple zeta basis set that contains polarization and diffuse functions.

1.12.9.5 Effective core potential

For heavy atoms, many basis functions are required to represent the atomic orbitals, hence the computational cost will be huge in this case. This problem can be overcome by introducing an effective potential for chemically insignificant core orbitals. The effective core potential (ECP) is known as pseudopotential, e.g., LANL2DZ and def2-TZVP are ECP-enabled basis set.[147,148]

1.12.10 Basis set superposition error (BSSE)

When two monomers (A and B) approach each other, their basis sets are going to overlap. In this situation, each monomer borrows a basis set of others, this creates a basis set

superposition error (BSSE) in their dimer energy calculations.[149,150] Boys and Bernardi proposed a counterpoise correction (CP) to tackle BSSE.[151]

The general equation for the interaction energy of a dimer AB is,

$$E_{int}(AB) = E_{AB}^{AB}(AB) - E_{A}^{A}(A) - E_{B}^{B}(B) \qquad \text{(Eq. 1.31)}$$

where the superscripts represent the basis set used and subscripts refer to geometry. Therefore, $E_{AB}^{AB}(AB)$ is the energy of dimer AB calculated using the dimer basis set (i.e., union of basis sets on A and B monomers) and dimer geometry. The CP equation is given below,

$$E_{int}^{CP} = E_{AB}^{AB} - E_{A}^{AB} - E_{B}^{AB} \qquad \text{(Eq. 1.32)}$$

where superscript AB means the basis set of AB dimer. That means basis sets of dimer is used to calculate the energies of monomers.

1.13 Semi-empirical methods

The huge requirements of computational power for performing *ab initio* calculations on larger chemical systems are tackled by semi-empirical methods. This is done by making several approximations during solving the Schrödinger equation. In semi-empirical calculations, the experimentally derived parameters or high-level calculation data are used to simplify the calculations. Since this method employs more approximations in calculations, the results obtained are less accurate.

A few examples of semi-empirical methods are MNDO, AM1, PM3, etc.

1.14 Density functional theory

One of the major disadvantages of HF calculations is the complexity of wave function, especially in the case of larger chemical systems. In HF calculations, the total wave function depends on the 3N spatial coordinates and N spin coordinates for an N-number of the electron system. This makes computation extremely difficult for large molecular systems with larger basis sets used. In density functional theory (DFT), calculations are based on electron density, not the wave function. The electron density depends on 3 coordinates only. Hence, the 3N coordinate problem will reduce to a 3 coordinate problem in the DFT method as compared to the HF method.

1.14.1 Hohenberg-Kohn theorem

Hohenberg and Kohn proposed two fundamental theorems about DFT, these are known as foundations of DFT. According to their first theorem, the ground state energy of a system (E^0) is a functional of electron density (ρ).

$$E^0 = E[\rho_0(r)] \qquad \text{(Eq. 1.33)}$$

Here, the ρ_0 should satisfy the condition when N is the total number of electrons.

$$N = \int \rho_0(r) d^3r \qquad \text{(Eq. 1.34)}$$

The second Hohenberg-Kohn theorem states that "the electron density that minimizes the energy of the overall functional is the true electron density corresponding to the full solution of the Schrödinger equation". The variational principle is applied in DFT too. For a trial electron density ($\rho(r)$), the energy calculated (E) is always greater than or equal to the ground state energy of the system (E^0).

$$E[\rho(r)] > E[\rho_0(r)] \geq E^0 \qquad \text{(Eq. 1.35)}$$

Note that, the true functional that relates the electron density to the ground state remains unknown. Hence, the DFT calculations use approximate functionals.

1.14.2 Kohn-Sham approach

Kohn and Sham (K-S) proposed a formalism to calculate the ground state electron density, which is regarded as the foundation of current molecular DFT calculations. According to K-S formalism, it starts with an assumption that many electrons in a system are a system of non-interacting electrons. The DFT energy $E[\rho(r)]$ calculated by a trial density $\rho(r)$ can be written as,

$$E[\rho(r)] = T_s[\rho(r)] + E_{ne}[\rho(r)] + J[\rho(r)] + E_{XC}[\rho(r)] \qquad \text{(Eq. 1.36)}$$

where, T_s is kinetic energy functional for non-interacting electrons, E_{ne} and J is the potential energy functional for nuclear-electron interaction and classical electron-electron repulsion respectively. E_{XC} is exchange-correlation functional, which includes corrections for all non-classical electron-electron interactions.

1.14.3 Exchange-correlation functional

The exchange-correlation functional E_{XC}, can be expressed as,

$$E_{XC}[\rho(r)] = \Delta T[\rho(r)] + \Delta V[\rho(r)] \qquad \text{(Eq. 1.37)}$$

$\Delta T[\rho(r)]$ represents the kinetic correlation energy and $\Delta V[\rho(r)]$ refers to the potential correlation energy and exchange energy. These exchange-correlation energies are the corrections due to electron-electron interactions as compared to the actual system. Note that, the accuracy of K-S method relied upon the quality of $E_{XC}[\rho(r)]$ term.

The exact solution for $E_{XC}[\rho(r)]$ term is unknown because the explicit functional form of exchange-correlation potential energy for a real system is not known. Hence, several approximations are used for obtaining an approximate exchange-correlation functionals.

1.14.3.1 Local density approximation

The local density approximation (LDA) uses a functional of uniform electron density as an initial guess for $E_{XC}[\rho(r)]$ functional. This approximation is based on the notion that exchange-correlation functional for a hypothetical system of uniform electron gas can be derived exactly. The $E_{XC}[\rho(r)]$ term according to LDA can be expressed as follows,

$$E_{XC}^{LDA}(r) = E_{XC}^{electron\ gas}[\rho(r)] \qquad \text{(Eq. 1.38)}$$

For a uniform electron gas system, the electron density remains the same at all points but in the real system, it is not the same. Therefore, the LDA method is not good for calculating the various properties of a real system, but it is widely employed in band structure calculations in the solid state. The Perdew and Wang (PW), Wilk and Nusair (VWN), etc. are examples of LDA functionals.[152]

1.14.3.2 Generalized gradient approximation

According to Generalized Gradient Approximation (GGA), a gradient of electron density is added to the LDA functional. Hence, this method depends upon both general electron density ($\rho(r)$) and electron density gradient ($\nabla\rho(r)$). The $E_{XC}[\rho(r)]$ term according to GGA can be expressed as follows,

$$E_{XC}^{GGA}(r) = E_{XC}[\rho(r), \nabla\rho(r)] \qquad \text{(Eq. 1.39)}$$

The Becke functional (B88)[153] and Lee, Yang, and Parr functional (LYP)[154] are the popular GGA exchange and correlation functionals, respectively.

1.14.3.3 Meta-generalized gradient approximation

According to meta-generalized gradient approximation (meta-GGA), a Laplacian of electron density ($\nabla^2\rho(r)$) the term is added to GGA functionals. This is expressed as follows,

$$E_{XC}^{meta-GGA}(r) = E_{XC}[\rho(r), \nabla\rho(r), \nabla^2\rho(r)] \qquad \text{(Eq. 1.40)}$$

Minnesota functionals (M06)[155] and Tao-Perdew-Staroverov-Scuseria (TPSS)[156] functionals are popular examples of meta-GGA functionals. The exchange energy for M06-L is expressed as,

$$E_X^{M06-L} = \sum_\sigma \int dr\, [F_{X\sigma}^{PBE}(\rho_\sigma, \nabla\rho_\sigma) f(\omega_\sigma) + \varepsilon_{X\sigma}^{LSDA} h_X(x_\sigma, z_\sigma)] \qquad \text{(Eq. 1.41)}$$

where $F_{X\sigma}^{PBE}(\rho_\sigma, \nabla\rho_\sigma)$ is exchange energy density of the PBE, $\varepsilon_{X\sigma}^{LSDA}$ is local spin density approximation for exchange. The correlation energy for M06-L is expressed as,

$$E_C^{\alpha\beta} = \int e_{\alpha\beta}^{UEG}\left[g_{\alpha\beta}(x_\alpha, x_\beta) + h_{\alpha\beta}(x_{\alpha\beta}, z_{\alpha\beta})\right] dr \qquad \text{(Eq. 1.42)}$$

1.14.3.4 Hybrid-functionals

The hybrid functionals include some percentage of exchange energies obtained from the HF method (E_X^{HF}) along with exchange and correlation functionals of DFT (E_{XC}^{DFT}) to improve the quality of E_{XC} term. The E_X^{HF} is the certain percentage of exchange energy from HF theory, whereas E_{XC}^{DFT} is the exchange and correlation energy obtained from LDA, GGA, or other DFT formalism. This can be expressed as follows,

$$E_{XC} = E_X^{HF} + E_{XC}^{DFT} \qquad \text{(Eq. 1.43)}$$

B3LYP and PBE0 are popular examples of hybrid functionals. In B3LYP, Becke 3-term correlation functional (B3) and Lee, Yang, and Parr exchange functional (LYP) are incorporated.[154,157]

$$E_{XC}^{B3LYP} = (E_X^{LSDA} + E_C^{VWN3}) + a_0(E_X^{HF} - E_X^{LSDA}) + a_X \Delta E_X^{B88} + a_C(E_C^{LYP} - E_C^{VWN3}) \qquad \text{(Eq. 1.44)}$$

where Becke specified the semi-empirical parameters $a_0 = 0.20$, $a_X = 0.72$, and $a_C = 0.81$. These parameters are calculated by using total atomic energies, ionization potentials, fitting

atomization energies, and proton affinities. The $LSDA$ is local spin density approximated functional, the $VWN3$ is a LDA functional, and $B88$ and LYP are GGA functionals.

1.14.4 Dispersion correction in DFT

Sometimes DFT calculations fail to effectively describe the dispersion interactions such as Van der Waals and hydrogen bonding.[158] This leads to inaccurate results in particular systems where dispersion effects dominate over other effects. The limitations of standard DFT methods can be tackled by adding dispersion correction into the functionals. Grimme proposed a dispersion correction known as DFT-D3 in 2011, which is widely recognized in this field.[159]

1.15 Theoretical analyses

There are many theoretical analyses available for providing useful chemical information about the atoms and bonding properties of any molecular system based on computational solutions of the Schrödinger equation. In this thesis, analyses such as molecular electrostatic potential, quantum theory of atoms in molecules, natural bond orbital, energy decomposition, and molecular tailoring-based approach are used. Those analyses are briefly described below.

1.15.1 Molecular electrostatic potential (MESP) analysis

The molecular electrostatic potential of a molecule is a physically observable quantity. It can be detected by experimentally using diffraction methods.[160] Theoretically, it is calculated rigorously based on the distribution of electron density ($\rho(r)$) using equation (Eq. 1.45) given below.[160]

$$V(r) = \sum_A^N \frac{Z_A}{|r-R_A|} - \int \rho\,(r')\,\frac{d^3r'}{|r-r'|} \qquad \text{(Eq. 1.45)}$$

The $V(r)$ is the potential at any point with a position vector 'r' in a three-dimensional space of a molecule. The Z_A and R_A represents the nuclear charge and radius vector of atom A, and $\rho\,(r')$ is the electron density near r. In Eq. 1.45, the first term refers to the nuclear potential and the second term refers to the electronic contributions. Hence, the combination of these two terms expresses the effect of nuclei and electrons in a particular region of molecular systems. For a neutral molecule, the $V(r)$ is positive at the nucleus and negative values at electron-rich sites. The most positive potential value in a region is termed V_{max}, which indicates the electron-deficient site, while the more negative potential (V_{min}) reflects

the electron-rich site. Therefore, MESP analysis on a molecular system is an effective tool to figure out the features of lone pairs, π-bonds, electrophilic sites, nucleophilic sites, noncovalent interactions, etc.[161–165] Thus, MESP analysis on chemical entities would connect their chemical features with physical properties. MESP plot of a representative example, i.e., electron density distribution on an isodensity (ρ = 0.001 au) surface of water molecule calculated at MP2/aug-cc-pVTZ//MP2/6-311++G(d,p) level is illustrated in Figure 1.7. The V_{min} site appears around the oxygen atom with a value of −32.2 kcal/mol, and V_{max} sites are near the hydrogen atom with a value of 44.4 kcal/mol.

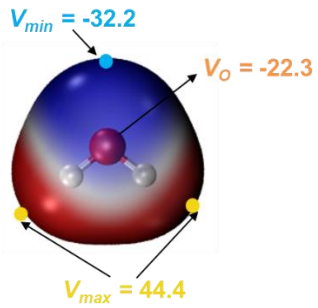

Figure 1.7 Electrostatic potential mapped on isodensity molecular surface (ρ = 0.001 au) of water calculated at the MP2/aug-cc-pVTZ//MP2/6-311++G(d,p) level. The positions of V_{max} and V_{min} sites are represented by golden and cyan spheres respectively. The values of V_{max} and V_{min} are given in kcal/mol and V_O (MESP on oxygen atom of water) in au. The color ranges: Blue for negative potential and Red for positive potential.

Further, MESP analysis can also calculate the potential at the nucleus of an atom. In Figure 1.7, the potential at the oxygen atom of water (V_O) is shown in orange color.

$$V_B = \sum_{A \neq B}^{N} \frac{Z_A}{|R_B - R_A|} - \int \frac{\rho\,(r')d^3r'}{|R_B - r'|} \qquad \text{(Eq. 1.46)}$$

Eq. 1.46 defines the potential (V_B) at a particular atom's (say B) nucleus with a radius vector r = R_B located in a three-dimensional space of a molecular system, where Z_A and R_A represent the nuclear charge and radius vector of atom A (A ≠ B), and r' is a point near to R_B.

1.15.2 Quantum theory of atoms in molecules (QTAIM) analysis

Bader's QTAIM analysis generates the topology of electron density ($\rho(r)$) on a chemical system. The $\rho(r)$ distribution in a chemical system is characterized by critical points. On these critical points, the first derivative of $\rho(r)$ vanishes and these points are the sites of electron density extrema (minima, maxima, and saddle points). There are four types of

critical points, *viz.*, (3, -3), (3, -1), (3, +1), and (3, +3). The critical points are labeled by the ω (number of nonzero eigenvalues of the Hessian matrix of $\rho(r)$) and σ (algebraic sum of signs of eigenvalues) parameters (i.e., (ω, σ)). Here, the (3, -3) critical point is the nuclear critical point, the (3, -1) is called as bond critical point, the (3, +1) is a ring critical point, and the (3, +3) is a cage critical point. Since the nuclei are attractors of the gradient field of $\rho(r)$, the region surrounded to nuclei has a certain charge distribution and these regions in a molecular system is called basins or atomic basins. The bond critical point (bcp) is present on the boundary of the basins of two neighboring atoms. Hence, the presence of bcp between two atoms indicates a linkage between electronic charge densities accumulated on those two particular atoms. This linkage (a gradient field line) between two atoms in a molecular graph is known as a bond path. The molecular graph of a chemical system is the pictorial representation of critical points and the network of bond paths.

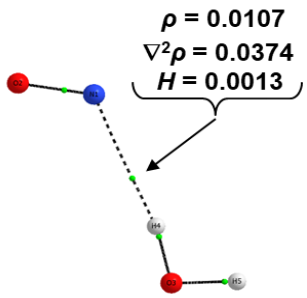

Figure 1.8 QTAIM molecular graph of NO(H_2O) interacted system (hydrogen bond through N-atom of NO) calculated at the MP2/aug-cc-pVTZ//MP2/6-311++G(d,p) level. The connectivity between atoms are the bond paths, and the green sphere on each bond path is the bond critical point.

In this thesis, the bcp is extensively used to account for the noncovalent interactions in our chemical systems. QTAIM parameter $\rho(r)$ at the bcp provides valuable information about the associated chemical bond. This $\rho(r)$ value reflects the strength of a bond. In general, the $\rho(r)$ value greater than 0.20 au is regarded as a covalent bond, while $\rho(r)$ less than 0.10 au is considered as closed-shell interaction (ionic, hydrogen, dihydrogen bonding, etc.).[166] The sign of Laplacian of $\rho(r)$ ($\nabla^2\rho(r)$) at bcp signals to the type of bonding present between two atoms.[167] The values of $\nabla^2\rho(r)$ less than zero is found for covalent bonding, whereas $\nabla^2\rho(r)$ greater than zero is observed in the case of closed-shell interactions. The electron energy densities such as potential ($V(r)$), kinetic ($G(r)$), and total ($H(r)$) are another parameters of QTAIM that can give ideas about the nature of bonding interactions.[168] The

negative values of total electron energy density ($H(r) = G(r) + V(r)$) at the bcp of a noncovalent interaction reveals its shared (covalent) nature, whereas, positive values of $H(r)$ indicate the closed-shell type interactions. QTAIM parameters calculated at MP2/aug-cc-pVTZ//MP2/6-311++G(d,p) level for bcp on the hydrogen bond present between a nitric oxide and water molecule is demonstrated in Figure 1.8.

1.15.3 Natural bond orbital (NBO) analysis

NBO analysis is a technique for investigating the hybridization and covalency of atoms in a polyatomic wave function.[77] NBO provides a picture of localized orbitals that are involved in bonding, bearing lone pairs, etc. NBO analysis treats a set of effective valence atomic orbitals as natural atomic orbitals (i.e., NAOs) based on the details in the wave function of an optimized molecular structure. The basic requirement for a NAO is the orthonormality and maximum occupancy. Hence, these NAOs are compatible for describing the atomic and bonding properties of a molecular system. In NBO calculations, the NAOs form natural hybrid orbitals (NHOs), and the linear combination of orthonormal NHOs forms a bond. For example, the σ-bond present between A and B atoms, i.e., σ_{AB} forms by the linear combination of orthonormal hybrid orbitals such as h_A and h_B (see Eq. 1.47).

$$\sigma_{AB} = c_A h_A + c_B h_B \qquad \text{(Eq. 1.47)}$$

$$\sigma^*_{AB} = c_A h_A - c_B h_B \qquad \text{(Eq. 1.48)}$$

Similarly, the antibonding σ^*_{AB} are formed by the same NHOs, but which represent the unused atomic valence space by covalent bond formation (see Eq. 1.48).
Overall, the sequence followed by the NBO analysis is,

$$input\ basis\ set \rightarrow NAOs \rightarrow NHOs \rightarrow NBOs$$

Natural population analysis (NPA): This gives the natural charge on atoms. The NPA charge ($q_i^{(A)}$) on NAO of an atom A is the diagonal density matrix element in the NAO basis.

$$q_i^{(A)} = \langle \phi i^{(A)} | \acute{\Gamma} | \phi i^{(A)} \rangle \qquad \text{(Eq. 1.49)}$$

The NPA charge is in good agreement with the other theoretical and experimental estimations of charges, hence, this charge is extensively used in various chemical systems to measure the charge transfer.[169]

Stabilization energy of donor-acceptor orbitals in a chemical bonding: the stabilization energy ($E^{(2)}$) of the interaction between donor(i)-acceptor(j) orbitals can be calculated based on second-order perturbation theory in NBO analysis.[170] The $E^{(2)}$ associated with this interaction can be estimated as,

$$E^{(2)} = q_i \, F(i,j)^2/(\varepsilon_j - \varepsilon_i) \qquad \text{(Eq. 1.50)}$$

Here, q_i is the electron occupancy in the donor orbital, ε_i and ε_j are the energies (diagonal elements) of donor and acceptor orbitals, and $F(i,j)$ are the off-diagonal elements of the NBO matrix.

1.15.4 Energy decomposition analysis (EDA)

Energy decomposition analysis is a technique to investigate the energy components of a chemical bonding. This is developed basically from the theories put forward by Morokuma and Jeziorski.[171] Morokuma's theory is based on a variational approach and is commonly called EDA,[172] while Jeziorski et al. followed a perturbative approach known as symmetry-adapted perturbation theory (SAPT).[173] Both of these methods give insight into the physical nature of bonding interactions, and thus provide an idea of the attractive and repulsive forces involved in a chemical interaction.

It is reported that a combination of SAPT with HF and DFT calculation is applicable for small to large molecular systems.[174] It has been reported that SAPT-HF (i.e., SAPT0) calculated interaction energies for radical systems are in reasonable agreement with experimental results, and these calculations require less computational cost.[175] Hence, the SAPT0 method attracts much interest in open-shell SAPT calculations. Similarly, the EDA is also extensively used in a variety of molecular systems, especially metal complexes, proteins, and so on.[176]

In this work, we have used both SAPT0 and EDA methods appropriately based on the nature of chemical systems supported by the literature data. A brief description of these methods is given below.

SAPT0: The zeroth-order SAPT (SAPT0) is the simplest form of wave function-based SAPT methods. According to SAPT calculation of interactions energy (E_{int}^{SAPT}), it is the sum of the physically distinct components,[173] such as electrostatic, exchange, induction, and dispersion (i.e., E_{elst}, E_{exch}, E_{ind} , and E_{disp}, respectively).

It can be expressed as follows,

$$E_{int}^{SAPT} = E_{elst} + E_{exch} + E_{ind} + E_{disp} \quad \text{(Eq. 1.51)}$$

$$E_{elst} = E^{10}{}_{elst} + E^{12}{}_{elst} + E^{13}{}_{elst} \quad \text{(Eq. 1.52)}$$

$$E_{exch} = E^{10}{}_{exch} + E^{11}{}_{exch} + E^{12}{}_{exch} \quad \text{(Eq. 1.53)}$$

$$E_{ind} = E^{20}{}_{ind} + E^{20}{}_{exch-ind} \quad \text{(Eq. 1.54)}$$

$$E_{disp} = E^{20}{}_{disp} + E^{20}{}_{exch-disp} + E^{21}{}_{disp} + E^{22}{}_{disp} \quad \text{(Eq. 1.55)}$$

where, superscripts n and l of E^{nl} denote the order of perturbation corrections. E_{elst} (Eq. 1.52) accounts for the electrostatic interactions of uncorrelated and correlated electric multipole moments of monomers. E_{exch} (Eq. 1.53) the term can be interpreted as the effect due to the quantum mechanical tunneling of electrons between monomers in an interacted system and also the effect of intramonomer correlation on exchange. E_{ind} (Eq. 1.54) accounts for the damped interactions between various multipole (permanent and induced) moments of monomers and also the additional repulsion because of the coupling of electron exchange and the induction interaction. E_{disp} (Eq. 1.55) accounts the interactions of instantaneous electric multipole moments of monomers in an interacted system as well as the intramonomer correlation corrections, and also the additional repulsion because of the coupling of electron exchange and the dispersion interactions. Additionally, $\delta E^2{}_{HF}$ the term is added to E_{int}^{SAPT}, which accounts for the approximate third and higher-order exchange and induction effects via HF calculation and this will improve the E_{int}^{SAPT} value.

In SAPT0 calculations, it avoids all the intramonomer correlation terms, which speeds up the computation.[177] Therefore, components of interaction energy calculated by SAPT0 can be expressed as follows,

$$E_{int}^{SAPT0} = E^{10}{}_{elst} + E^{10}{}_{exch} + E^{20}{}_{ind} + E^{20}{}_{exch-ind} + E^{20}{}_{disp} + E^{20}{}_{exch-disp} + \delta E^2{}_{HF}$$

(Eq. 1.56)

On the other hand, the main energy components contributed to the energy of a chemical bond is calculated by EDA is as follows. [172]

$$E_{int}^{EDA} = E_{elst} + E_{pauli} + E_{orb} \quad \text{(Eq. 1.57)}$$

The electrostatic term E_{elst} is usually attractive, Pauli's term E_{pauli} is always repulsive and the E_{orb} is always attractive. Here, the E_{elst} accounts for the energy of classical electrostatic interaction between the fragments in a molecular system. The E_{pauli} originates from the electron exchange repulsion between fragments based on Pauli's antisymmetry principle. Thus, these two energy component terms are complementary to the E_{elst} and E_{exch} terms described in the SAPT method. Besides, the E_{orb} results from the orbital mixing of fragments. The E_{orb} can be further decomposed into different contributions from orbitals, which are various irreducible representations Γ of the point group of the molecule.

$$E_{orb} = \sum_{\Gamma} \Delta E_{\Gamma} \qquad \text{(Eq. 1.58)}$$

1.15.5 Molecular tailoring approach (MTA)

MTA is a fragmentation-based method for estimating the energies of individual noncovalent interactions in chemical systems.[178] This method is proposed by Gadre and co-workers by applying the cardinality principle.[79] The concept of MTA is how a tailor cuts a large cloth into pieces and stitches them together by overlapping the cuts. In MTA, a molecular system is divided into different manageable sets of overlapping fragments, on which the calculations can be easily performed at any level of theory. Initially, this method was successfully used to estimate the intramolecular hydrogen bonding interactions in various molecules.[179,180] It is now widely used to estimate the energies and cooperativity contribution of individual intermolecular interactions in various molecular systems.[181–183] These studies show the advantages of MTA in estimating the interaction energies in terms of accuracy and computational cost. Energetics of individual interactions reveal the binding affinity between molecules in their assembly and stabilize the intermediate and transition state during chemical reactions. All the individual solute-water interactions are important to understand the water-mediated reactions. Besides, cooperativity details are crucial in molecular cluster studies for understanding how individual intermolecular interactions affect the characteristics of molecular clusters collectively.[79] These effects may influence the physical and chemical characteristics of clusters. For instance, in hydrogen bonding, the cooperativity can result in changes in bond lengths, angles, bond energy and overall molecular conformation.[184–186] Furthermore, these effects are also observed in many biopolymers, including proteins and nucleic acids, affecting a large range of biochemical and physiological processes.[178]

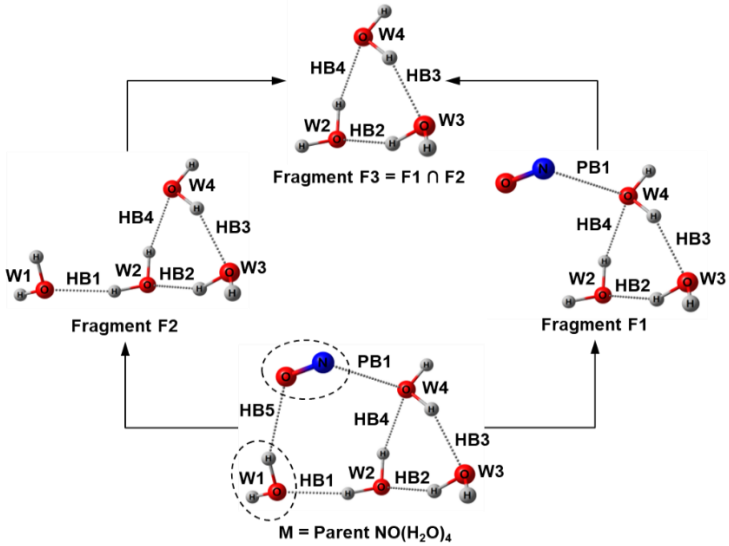

Scheme 1.1 Fragmentation scheme for the estimation of energy of hydrogen bond HB5 in a representative $NO(H_2O)_4$ complex (denoted as M).

The fragmentation procedure followed in MTA to calculate an individual hydrogen bond energy of a representative complex $NO(H_2O)_4$ is illustrated in Scheme 1. Herein, four water molecules are indicated as W1, W2, W3, and W4. The hydrogen bond denoted by HB5 is formed by the interaction between the O atom of NO and the H atom of W1. By removing W1 and NO from parent $NO(H_2O)_4$, respectively, the two primary fragments, F1 and F2, are generated. If we virtually place the fragments F1 and F2 together, the geometry of parent $NO(H_2O)_4$ may be restored. Such virtual geometry of $NO(H_2O)_4$ loses out on two things, *viz.*, (i) the N− O…H interaction corresponding to HB5 is lost and (ii) the structural part corresponding to water trimer (containing W2, W3, and W4), common to both primary fragments F1 and F2 is counted twice. In Scheme 1, this common water trimer is represented as a secondary fragment F3 (i.e., F1∩F2). Accordingly, the energy of the parent complex (M) may be obtained by subtracting the single-point energy of F3 from the sum of the single-point energies of F1 and F2. However, this energy of $NO(H_2O)_4$ does not include the energy of HB5. Therefore, the energy of HB5 is obtained as $E_{HB5} = (E_{F1} + E_{F2} - E_{F3}) - E_M$, where E_M is the energy of $NO(H_2O)_4$. Furthermore, if we isolate the dimer W1…NO containing HB5 bond from the $NO(H_2O)_4$, then this dimer lacks cooperativity contribution of other HBs/PBs that are present in $NO(H_2O)_4$. Note that the geometry of this dimer is the same as that in the $NO(H_2O)_4$. The interaction energy of such dimer is obtained within the supermolecular approach as, $E_{HB5}^{dimer} = (E_{W1} + E_{NO}) - E_{W1...NO}^{dimer}$, where E_{W1}, E_{NO}, and $E_{W1...NO}^{dimer}$ are the energies of W1, NO, and dimer respectively. The difference between E_{HB5} and E_{HB5}^{dimer} is the cooperativity contribution towards the HB5. From the formalism of the

MTA-based method, the positive energy values indicate the stability of a particular interaction. The negative values of cooperativity, which is knowns as anti-cooperativity, indicating the energy of an interaction in the complex is lower than that of the corresponding dimer (isolated from the complex).

1.16 Conclusions

In Part A of this chapter, a brief overview was presented, emphasizing the significance of various forms of NO - ranging from reduced (NO^- and HNO) to oxidized species (NO^+ and HONO) - in both atmospheric and biological chemistry. This section also discussed the applications of nitroxides and NO-adsorbed metal-loaded zeolites. Furthermore, it sheds light on hydrogen bonding (NO···H) interactions, examining their presence and relevance within NO-water cluster systems, NO^-/HNO/HONO-water cluster systems, nitroxide radical-solvent systems, and NO-adsorbed metal-loaded zeolites. Notably, diverse applications of NO···H interactions were discussed. A deeper investigation into the strength, nature, and influencing factors of these NO···H interactions is warranted for a comprehensive understanding of their applications. In this work, we concentrated on comprehending the strength, nature, and influencing factors of NO···H interactions within selected chemical systems.

Part B of this chapter offered a brief introduction to the theoretical foundations of the computational techniques employed in this thesis. It provides a concise account of electronic structure methods, including *ab initio*, semiempirical, and density functional theory. Furthermore, it briefly elucidated key theoretical analyses such as molecular electrostatic potential (MESP), quantum theory of atoms in molecules (QTAIM), natural bond orbital (NBO), energy decomposition (EDA), and molecular tailoring approach (MTA)-based.

Chapter 2

Quantitative Assessment of Noncovalent Interactions in $NO(H_2O)_{n=1-4}$ Complexes

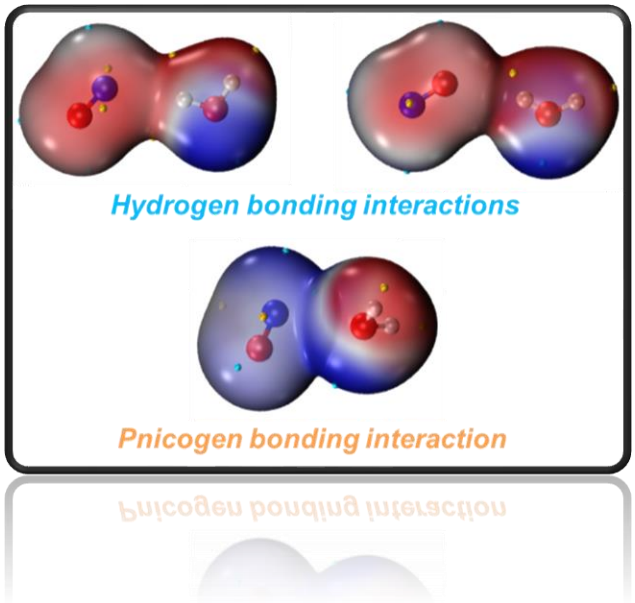

2.1 Abstract

Nitric oxide (NO) plays a vital role in various atmospheric and biological events. Hydration of NO is inevitable to describe different reactions that occur during these events. The present study is an attempt to investigate the noncovalent interactions in microhydrated networks (up to four water molecules) of NO (i.e., $NO(H_2O)_{n=1-4}$) using the MP2/aug-cc-pVTZ//MP2/6-311++G(d,p) level of theory. The interactions between NO and water have been probed by molecular electrostatic potential (MESP), quantum theory of atoms in molecules (QTAIM), and natural bond orbital (NBO) analyses. The NO can form hydrogen bonds (HBs; via N- and O-atoms of NO, designated as (NO)···H interactions) and pnicogen bonds (PBs) with water depending on the orientation. The individual energy and cooperativity contributions of HBs and PBs present in $NO(H_2O)_{n=1-4}$ complexes are estimated with the help of a molecular tailoring approach (MTA) based calculations. The MTA-based analysis revealed that the water…water interactions are the strongest in $NO(H_2O)_n$ complexes, whereas HBs and PBs in NO…water interactions are the weakest. Among (NO)···H interactions, the HBs formed by N- atom (with energies ranging from 0.35 to 2.10 kcal/mol) is stronger than the HBs by O-atom (energies ranging from −0.10 to 1.09 kcal/mol). The present study quantifies the energetics of HBs and PBs and their interplay in microhydrated networks of NO.

2.2 Introduction

Nitric oxide (NO) is a fascinating molecule that regulates numerous atmospheric, biological, and physiological events.[1,2] The interactions of NO with water clusters are highly relevant since the hydration of NO is an indispensable process in atmospheric and biological systems. Microhydration studies can provide a better understanding of intermolecular interactions in hydrated systems at the molecular level.[187,188] However, microhydration of NO is not yet reported in the literature. It remains a challenge for researchers to conceptually understand the interaction of NO with other molecular systems due to its radical character, and often NO is considered as a benchmark system for studying the weak interactions shown by open-shell species.[95,189] Previous studies have addressed the interaction between NO and water within the context of hydrogen bonding interactions.[106,190] On the other hand, the interaction of NO via the N-atom with the O-atom of a water molecule is reported as an electron donor-acceptor interaction.[105,190] It is obvious that noncovalent interactions other than HBs are present in $NO(H_2O)$ complexes. Energies and cooperativity details of interactions present between NO

and water clusters are beneficial to figuring out the different water-mediated reactions of NO.[79]

In this study, we aim to investigate the features of interactions between NO and water in $NO(H_2O)$ complexes with the help of molecular electrostatic potential (MESP), quantum theory of atoms in molecules (QTAIM), and natural bond orbital (NBO) analyses. In addition, molecular tailoring approach (MTA) based calculations are employed to estimate the energies and cooperativity of these noncovalent interactions individually. For the microhydration of NO, a stepwise increase in water cluster size (up to 4 water molecules, i.e., n = 1–4) is followed because the gradual accumulation of solvent molecules bridges the gap between the effect of microsolvation and bulk solvation.[191]

2.3 Computational methods

The structures of all $NO(H_2O)_{n=1-4}$ complexes and their monomers are simulated using the MP2/6-311++G(d,p) level of theory with the Gaussian 16 program package.[192] For optimization, initial structures were modeled according to existing literature data of similar molecules and chemical intuitions. A bottom-up approach is also applied for larger clusters, e.g., the $NO(H_2O)_3$ is modeled by adding one H_2O to $NO(H_2O)_2$ through different sides.[191] Similarly, the top-down approach also aided in finding any missed configurations of a $NO(H_2O)_n$ complex. In order to achieve the objectives of the study, we have focused on configurations having maximum interactions between NO and water. The optimized geometries were confirmed as local minima by frequency analysis and noted the absence of imaginary frequencies. The Gibbs free energy change (ΔG) associated with the formation of the most stable structures of $NO(H_2O)_{n=1-4}$ at 298 K and 1 atm is calculated.

For improved energetics, single-point calculations are carried out at the MP2 method by employing the aug-cc-pVTZ basis set for estimating the binding energy as well as MTA-based noncovalent interaction energies in all complexes. The MESP, QTAIM, and NBO analyses were also performed at the MP2/aug-cc-pVTZ//MP2/6-311++G(d,p) level of theory. AIMAll software is used for QTAIM analysis.[193] MESP analysis is carried out using Multiwfn software,[194] and visualized using VMD software.[195] NBO analysis is carried out using NBO version 3.1 implemented in Gaussian 16 software,[196] and the results are visualized using Chemcraft software.[197]

The binding energy (E_{BE}) of all $NO(H_2O)_n$ complexes is calculated by supermolecular approach using Eq. 2.1, wherein $E_{NO(H_2O)_n}$, E_{NO}, and nE_{H_2O} are the energy of $NO(H_2O)_n$

complex, the energy of NO molecule, and the energy of a water molecule multiplied by the number of water molecules (n) present in that particular complex.

$$E_{BE} = E_{NO(H_2O)_n} - (E_{NO} + nE_{H_2O}) \quad \text{(Eq. 2.1)}$$

2.4 Results and discussion

2.4.1 MESP analysis

The molecular electrostatic potential (MESP) analysis examines the anisotropy in the electron density distribution on molecules by mapping the electrostatic potential on an isodensity surface of molecules.[198–201] Thus, MESP features can be employed to understand the interaction sites of molecules.[202,203] The electrostatic potential on molecular surfaces (at an isodensity value of 0.001 au) of NO and water is shown in Figure 2.1(a). The location of the MESP minima (V_{min}) and the MESP maxima (V_{max}) of monomers can be used to recognize the nucleophilic and electrophilic regions, respectively.[204] The positions of V_{min} and V_{max} are marked in Figure 2.1. During the complex formation between NO and H_2O, there is a change in corresponding MESP maxima and minima, and the magnitude of these MESP changes are designated as ΔV_{max} and ΔV_{min}, respectively.[205,206] Thus, $\Delta V_{max} = V_{max\_iso} - V_{max\_com}$, where V_{max_iso} and V_{max_com} are V_{max} located on a particular site of isolated species and its interacted complex, respectively. Similarly, we can define ΔV_{min}, and its magnitude is a rough estimate of the change in the electron density during the complex formation.

In the case of H_2O, the V_{min} values appear around the oxygen atom at −32.2 kcal/mol. For NO, the V_{min} values are −9.2 and −1.1 kcal/mol observed near the N and O atoms, respectively. The electron-rich nature of the oxygen atom of H_2O than that of NO is evident from the more negative V_{min}. MESP topography of NO further reveals that the electron-deficient regions around the N–O bond axis and are more localized over the N-atom with V_{max} values of 16.3 kcal/mol. The molecular electrostatic potential surfaces corresponding to three possible modes of NO…water interactions are also portrayed in Figure 2.1(b).

The hydrogen bonding (HB) interactions of NO ((NO)···H), through N- (O–N…H) and O-atoms (N–O…H) as electron donors with water, are illustrated in Figure 2.1(b). Upon complexation with water through N-atom and O-atom, the V_{min} values at the interacting sites are found to be −2.4 and 3.6 kcal/mol, respectively. The calculated ΔV_{min} of interacting atoms N and O are 6.8 and 4.7 kcal/mol, respectively. Similarly, for these O–N…H and N–O…H interactions, ΔV_{max} values on the H atoms of water are 22.0 and 8.7 kcal/mol, respectively.

Based on the changes in MESP values, it can be assessed that the HB through the N-atom is slightly more stable than through the O-atom. The corresponding E_{BE} values indicate the same, which are found to be −1.72 and −0.87 kcal/mol, respectively, for O–N…H and N–O…H interactions. Previously, Salmi et al. interpreted this with molecular orbitals, the greater strength of O–N…H interaction than N–O…H is mainly attributed to the dominant contribution of the N-atom to the highest occupied molecular orbital (HOMO) of the NO monomer.[190]

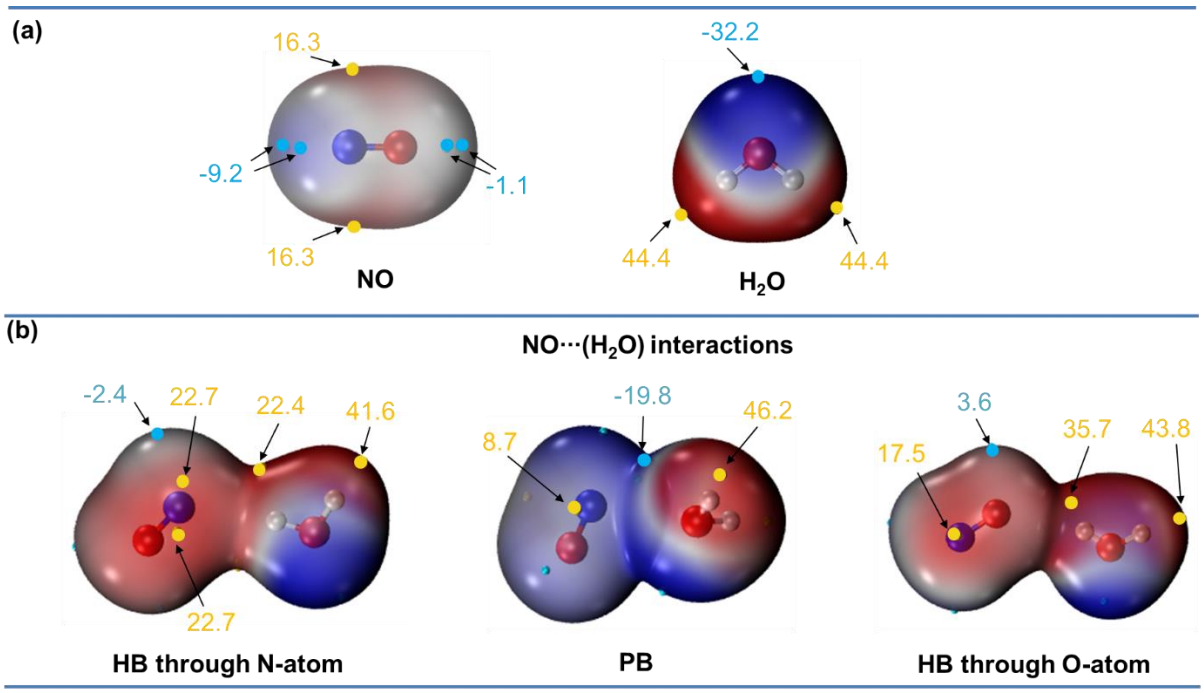

Figure 2.1 Electrostatic potential mapped on isodensity molecular surface (ρ = 0.001 au) of (a) monomers, and (b) dimers. The positions of V_{min} and V_{max} at interacting sites are represented by cyan and golden spheres, respectively, and the corresponding values are shown in kcal/mol. The color ranges: Blue for negative potential and Red for positive potential.

Besides, the interaction associated with the electron-deficient (V_{max}) region on the N-atom and electron-dense region of water is called a pnicogen bond (PB).[207,208] During the formation of PB, the V_{max} value of 16.3 kcal/mol on the N atom of isolated NO is changed into 8.7 kcal/mol; the calculated ΔV_{max} value is 7.6 kcal/mol, which is accompanied by a change in V_{min} on the oxygen atom of H_2O from −32.2 to −19.8 kcal/mol (ΔV_{min} = 12.4 kcal/mol). These ΔV_{max} and ΔV_{min} values associated with NO and water indicate a PB interaction between NO and water, and the corresponding binding energy (E_{BE}) is −1.39 kcal/mol.

2.4.2 QTAIM analysis

QTAIM plots of NO-water dimer complexes are displayed in Figure 2.2. The values of QTAIM parameters *viz.* electron density ($\rho(r)$), Laplacian of electron density ($\nabla^2\rho(r)$), and the total electron energy density ($H(r)$) at the bond critical point (bcp) in NO…water interactions are shown in Figure 2.2. The $\rho(r)$ value (0.0107 au) for HB through N-atom is greater than the $\rho(r)$ value (0.0073 au) of HB through O-atom. This again confirms the greater strength of HB formed via N-atom than the O-atom of NO with water. Besides, the bond path connecting the N-atom of NO and the O-atom of water is evidence for PB interaction between NO and water, with a $\rho(r)$ value of 0.0083 au at the bcp of PB. In general, the positive values for $\nabla^2\rho(r)$ and $H(r)$ parameters for all these noncovalent bonds in NO(H_2O) complexes suggest that they all are typical closed-shell interactions.

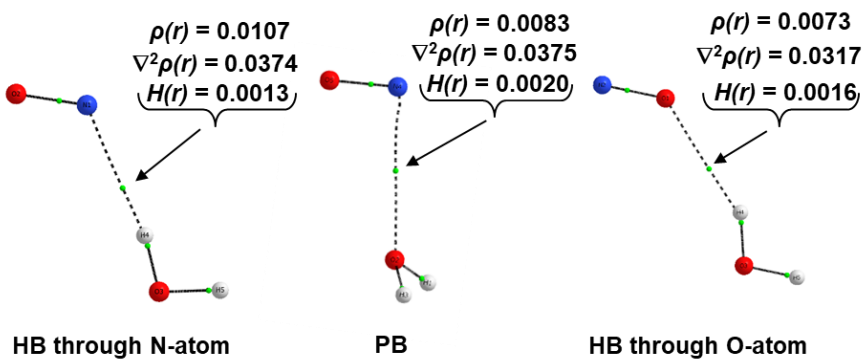

Figure 2.2 The QTAIM molecular graph of NO(H_2O) complexes. The QTAIM parameters at the bcp (which are shown as small green spheres on each bond path) of intermolecular interactions are given in au.

2.4.3 NBO analysis

An NBO view of donor-acceptor orbitals involved in the HB/PB interactions of NO(H_2O) dimers and their stabilization energies ($E^{(2)}$; values greater than 0.1 kcal/mol are considered) are displayed in Figure 2.3. For HB interactions via N- and O-atoms of NO, the lone pairs of N- (lp(N)) and O-atoms (lp(O)) of NO respectively, interact with the O–H antibonding orbital (σ^*_{O-H}) of water, wherein the total $E^{(2)}$ energy is calculated to be 1.23 and 0.13 kcal/mol respectively. Based on total $E^{(2)}$ energy values, the HB through the N-atom of NO is stronger than HB through the O-atom. The interaction associated with lone pairs of oxygen atom of water and antibonding (π^*_{N-O}) orbital of the N–O bond has a total stabilization ($E^{(2)}$) energy of 0.67 kcal/mol, which again confirms the PB interaction.

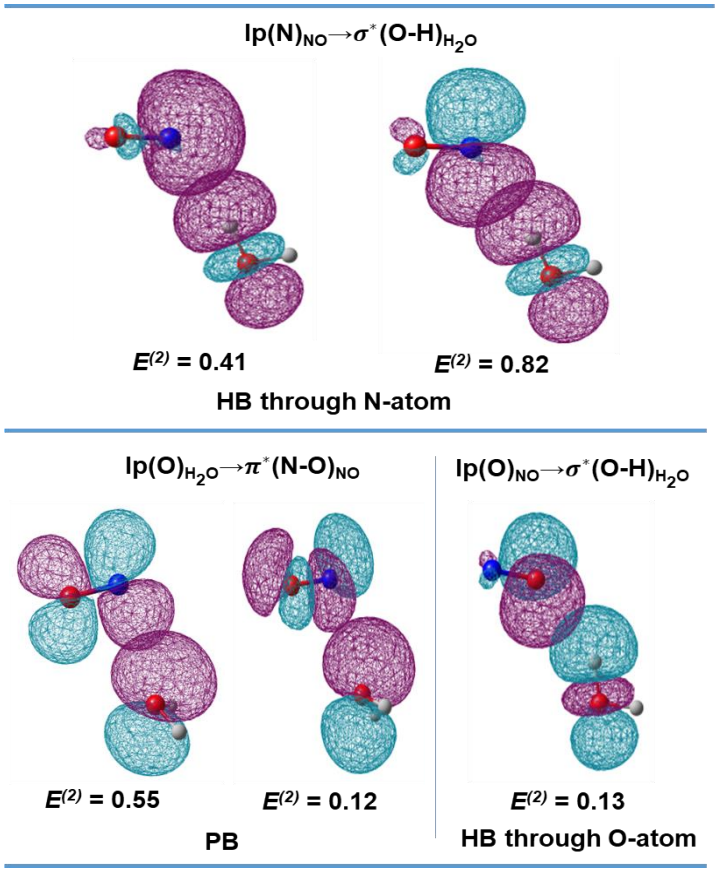

Figure 2.3 The donor-acceptor orbitals (isovalue = 0.03 au) involved in hydrogen bonding (HB) (via N- and O-atoms of NO) and pnicogen bonding (PB) interactions in $NO(H_2O)$ complexes. The $E^{(2)}$ energy (in kcal/mol) for these interactions is estimated based on second-order perturbation theory in NBO analysis.

2.4.4 Microhydrated complexes of NO ($NO(H_2O)_{n=1-4}$)

After addressing the possible interactions between NO and H_2O in their $NO(H_2O)$ dimer complexes, we further investigated the microhydration of NO up to four water molecules. The $NO(H_2O)_{n=1-4}$ complexes with different isomers are designated according to their cluster size (n-value) and the order of stability. The binding energy (E_{BE}) values determine the stability order (see Table 2.1); the most stable isomer is indicated with **A**. The other isomers are named **B**, **C**, **D**, etc., based on the decreasing magnitude of E_{BE}. For instance, three isomers are present for the $NO(H_2O)_2$ complex; the most stable isomer is **2A**, followed by **2B** and **2C**, wherein **2C** is the least stable isomer. It should be emphasized that we optimized several possible configurations of $NO(H_2O)_n$ complexes; however, a configurational sampling of these water complexes was not attempted. In fact, this is not the primary objective of our study, and the structures presented here are sufficient to differentiate and

quantify the possible noncovalent interactions between NO and water in $NO(H_2O)_{n=1-4}$ complexes.

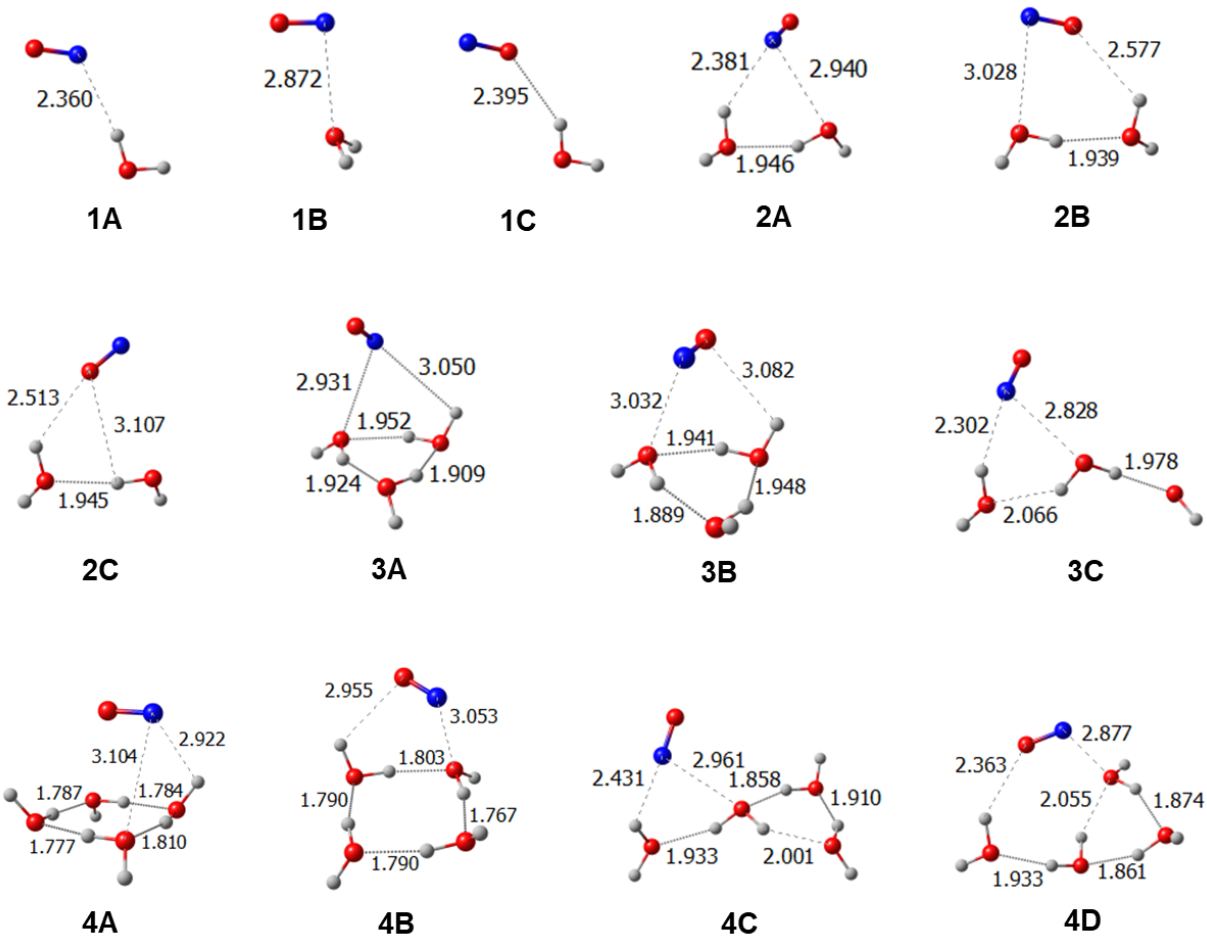

Figure 2.4 Optimized geometries of $NO(H_2O)_{n=1-4}$ complexes. The relevant distance of noncovalent interactions is given in Å unit.

The optimized geometries of various isomers of $NO(H_2O)_n$ complexes for each cluster size (n = 1 to 4) are presented in Figure 2.4. The (NO)···H HBs (via N- and O-atom of NO) and PBs are seen in the complexes with varying cluster sizes. The distances of all the HBs and PBs formed by NO are in the range of 2.302 – 3.107 Å and 2.828 – 3.104 Å, respectively. In $NO(H_2O)$ complexes, the HB through the N-atom of NO with water is the most stable isomer (**1A**), the next stable isomer **1B** is interacted with by PB, and the HB through the O-atom of NO with water is the least stable isomer. This is in line with the strength of intermolecular interactions assessed using QTAIM and NBO analyses. It is worth noting that PB and HB via N-atom of NO is observed in all the most stable isomers in each category of $NO(H_2O)_{n=2-4}$, i.e., in **2A**, **3A**, and **4A**. This suggests that the N-atom of NO is

involved in the noncovalent interactions of energetically preferred configurations of $NO(H_2O)_n$ complexes. Besides, it is worth mentioning that water molecules form a ring (self-association) in the most stable isomers of $NO(H_2O)_n$ complexes with cluster sizes three and four. Thus, the complexes with self-association of water clusters are the energetically preferred configuration in $NO(H_2O)_{n=3\text{-}4}$ categories.

2.4.5 Energetics of noncovalent interactions in $NO(H_2O)_{n=1\text{-}4}$ complexes

As mentioned above, the E_{BE} for various noncovalent bonding, *viz*. HB through N-atom (**1A**), PB (**1B**), and HB through O-atom (**1C**) present in $NO(H_2O)_1$ complex are −1.72, −1.39, and −0.87 kcal/mol, respectively. We further employed the molecular tailoring approach (MTA)-based method to estimate the energies of all individual noncovalent interactions in $NO(H_2O)_{n=1\text{-}4}$ complexes. All these values are displayed in Figure 2.5. In addition, the sum of MTA-based energies of all individual noncovalent interactions shown by NO with water (designated as $\sum E_{NO\ldots H_2O}$) and the sum of energies of all the individual water…water interactions (designated as $\sum E_{H_2O\ldots H_2O}$) in $NO(H_2O)_n$ complexes are presented in Table 2.1 along with E_{BE} values.

In dihydrate NO complexes (i.e., $NO(H_2O)_2$), three monomers interacted to form a cyclic structure, and the E_{BE} values obtained fall in the range of −6.76 to −8.17 kcal/mol. In the most stable isomer **2A**, the N-atom of NO participates in both HB and PB; the $\sum E_{NO\ldots H_2O}$ for these interactions is calculated as 3.76 kcal/mol. Similarly, the $\sum E_{NO\ldots H_2O}$ of **2B** is calculated as 2.31 kcal/mol, wherein the interactions of PB and HB through the O-atom of NO are observed. Further, **2C** shows two HBs through O-atom of NO with a $\sum E_{NO\ldots H_2O}$ of 1.82 kcal/mol. This again suggests that the energies of HBs through the O-atom of NO are weaker than HBs and PBs through the N-atom of NO. The $\sum E_{H_2O\ldots H_2O}$ values of **2A**, **2B**, and **2C** are in a range of 5.21 – 5.33 kcal/mol; this is much higher than that of $\sum E_{NO\ldots H_2O}$ values.

Among trihydrate NO complexes, i.e., $NO(H_2O)_3$, the water cluster forms a cyclic trimer in **3A** and **3B**, whereas a linear form of water trimer is present in **3C**. The estimated $\sum E_{H_2O\ldots H_2O}$ values around 21 kcal/mol in the cases of **3A** and **3B** reveal the exceptional stability of cyclic water form compared to the linear form of water (**3C**), where the $\sum E_{H_2O\ldots H_2O}$ is 9.14 kcal/mol. In contrast to this, the calculated $\sum E_{NO\ldots H_2O}$ values in **3A** (1.69 kcal/mol) and **3B** (1.22 kcal/mol) are much lower than that obtained for **3C** (4.01 kcal/mol). This is attributed to the weaker water…water interactions in linear water trimer that make

NO…water interactions much stronger in **3C** than other isomers (**3A** and **3B**). Nonetheless, the **3C** isomer is the least stable among other isomers; the E_{BE} value of **3C** (−12.39 kcal/mol) is lower by around 6 kcal/mol than **3A** (E_{BE} = −18.28 kcal/mol) and **3B** (E_{BE} = −18.04 kcal/mol).

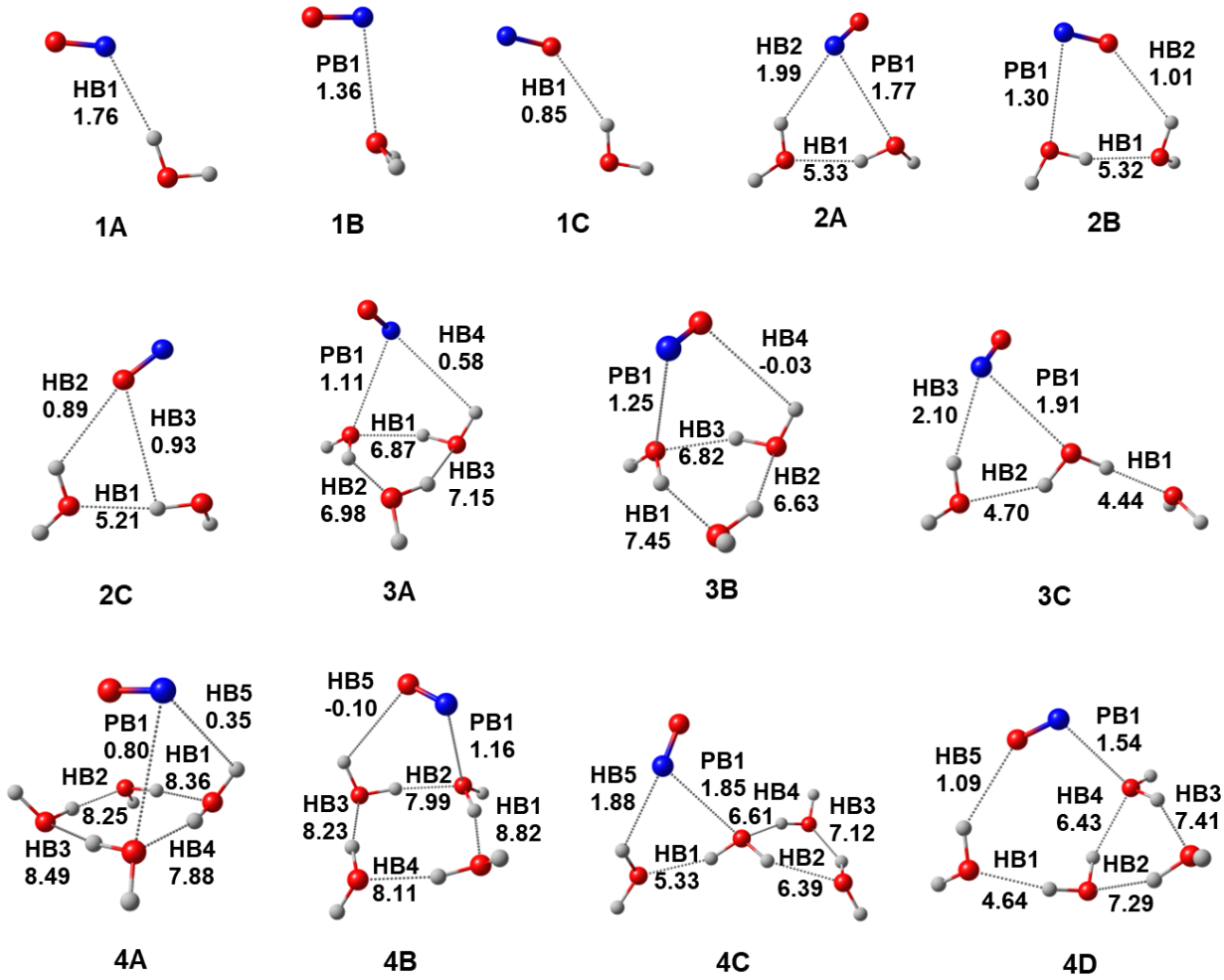

Figure 2.5 Values of all individual interaction energies (in kcal/mol) in $NO(H_2O)_{n=1-4}$ complexes *viz*. pnicogen and hydrogen bonding (PB and HB), estimated by MTA.

In the case of tetrahydrate NO complexes, the water molecules of **4A** and **4B** form a tetrameric cyclic ring structure. NO interacts with this cyclic ring via HB and PB. The **4A** and **4B** are the most stable, with close E_{BE} values, −30.69 and −30.43 kcal/mol, respectively. In **4C** and **4D** complexes, the water molecules form a three-membered ring. The NO interacts with the three-membered ring via PB and the fourth water molecule through HB. Note that the **4C** and **4D** isomers are less stable, and calculated E_{BE} values are −24.38 and −24.16 kcal/mol, respectively. This is mainly due to the reason that the cyclic tetramer form of water clusters (in **4A** and **4B**) are more stable ($\sum E_{H_2O\ldots H_2O}$ values in the order of 32 – 33 kcal/mol)

compared to that of **4C** and **4D** ($\sum E_{H_2O\ldots H_2O}$ values in the order of 25 – 26 kcal/mol). Considering the NO…water interactions in **4A** and **4B**, the $\sum E_{NO\ldots H_2O}$ is quantified as 1.15 and 1.06 kcal/mol, respectively, whereas these values in **4C** and **4D** are calculated to be 3.73 and 2.64 kcal/mol, respectively. This again suggests that the complexes (**4C** and **4D**) with weaker water…water interactions have comparatively stronger NO…water interactions than the complexes (**4A** and **4B**) with stronger water…water interactions.

Table 2.1 Values of binding energies (E_{BE}) calculated by supermolecular approach, and the sum of energies of relevant individual interactions estimated by MTA in $NO(H_2O)_{n=1-4}$ complexes. All energy values are in kcal/mol.

Structure	E_{BE}	sum of individual interaction energies from MTA calculations	
		$\sum E_{NO\ldots H_2O}$	$\sum E_{H_2O\ldots H_2O}$
1A	−1.72	1.76	-
1B	−1.39	1.36	-
1C	−0.87	0.85	-
2A	−8.17	3.76	5.33
2B	−7.13	2.31	5.32
2C	−6.76	1.82	5.21
3A	−18.28	1.69	21.00
3B	−18.04	1.22	20.90
3C	−12.39	4.01	9.14
4A	−30.69	1.15	32.98
4B	−30.43	1.06	33.15
4C	−24.38	3.73	25.45
4D	−24.16	2.64	25.77

In general, the lower range of $\sum E_{NO\ldots H_2O}$ values (from 0.85 to 4.01 kcal/mol) as compared to $\sum E_{H_2O\ldots H_2O}$ values (range from 5.21 to 33.15 kcal/mol) suggest that the energies of NO…water interactions have little contribution towards the stabilization of $NO(H_2O)_n$ complexes. Also, water molecules form cyclic structures mainly by themselves (self-association), and NO is located on any one side of these rings when the cluster size increases. Similar structures of weakly bound complexes can be seen in previous studies of $CO(H_2O)_n$,

$OCS(H_2O)_n$, and $CO_2(H_2O)_n$.[209–211] For example, the most stable structures reported for the $CO(H_2O)_{n=1-5}$ complexes have a similar configuration to the microhydrated network of $NO(H_2O)_{n=1-4}$ described here.[211]

2.4.6 Cooperativity contributions in $NO(H_2O)_{n=2-4}$ complexes

The values of cooperativity contributions (E^{Coop}) along with the energies of all individual interactions (E_{Int}^{MTA}) in $NO(H_2O)_{n=2-4}$ complexes are presented in Table 2.2. The energies of individual interactions calculated in the respective dimers (E^{Dimer}) isolated from the complex are also presented in Table 2.2. The cooperativity contribution is the difference between these two energies, i.e., E_{Int}^{MTA} and E^{Dimer}, because the E^{Dimer} lacks the cooperativity contribution of other neighboring molecular interactions.

From Figure 2.5 and Table 2.2, the energies of (NO)···H HBs through the N-atom of NO with H_2O (O–N…H) calculated by MTA-based method fall in the range between 0.35 and 2.10 kcal/mol, while the corresponding HB energies in the respective isolated dimers fall between 0.63 and 1.64 kcal/mol. Hence, the cooperativity contributions towards this O–N…H interactions range from −0.27 to 0.46 kcal/mol. Similarly, a lower range of energy values is found for N–O…H interactions, i.e., from −0.10 to 1.09 kcal/mol; the interaction energies in the respective dimers isolated from complexes fall in a range of 0.50 to 0.84 kcal/mol. Consequently, the cooperativity contributions towards N–O…H interactions fall between −0.66 and 0.26 kcal/mol. On the other hand, the energies of PBs present in $NO(H_2O)_{n=2-4}$ complexes range between 0.80 and 1.91 kcal/mol, while the corresponding energies in the respective dimers isolated from the complex are slightly lower in range (from 1.03 to 1.43 kcal/mol). The slight difference in the range of these energy values is attributed to the modulation in the PB energies by the cooperative network of other HBs present in each complex. Accordingly, the cooperativity contributions towards PB range from −0.23 to 0.59 kcal/mol. The negative values of cooperativity (i.e., anti-cooperativity) indicate that the energy of a PB calculated in the complex is lower than that of the corresponding dimer (isolated from the complex). In the case of water…water interactions, the individual interaction energies obtained by the MTA-based method fall between 4.44 and 8.82 kcal/mol. The interaction energy calculated for isolated water…water dimers ranges from 4.21 to 5.06 kcal/mol. This imparts cooperativity contributions in the range between −0.20 and 3.98 kcal/mol towards water…water interactions.

It is evident from the above discussion that the cooperativity contributions toward water networks (water…water interactions) are significant in $NO(H_2O)_{n=2-4}$ complexes, whereas the contributions of cooperativity towards interactions of NO with water are comparatively less. But more importantly, this is one of the reasons for the lower values of $\sum E_{NO\ldots H_2O}$ found in $NO(H_2O)_n$ complexes, as discussed in the previous section.

Table 2.2 The relevant structural parameters *viz.* distance (in Å) and bond angle (in degree), energy in complex (E_{Int}^{MTA}), energy in the dimer (E^{Dimer}), and cooperativity contribution (E^{Coop}) of all individual interactions in $NO(H_2O)_{n=1-4}$ complexes. All energy values are in kcal/mol.

Complex	Interaction Labels	Distance of interaction	Bond angle	E_{Int}^{MTA}	E^{Dimer}	E^{Coop}
1A	HB1	2.360	171	-	1.76	-
1B	PB1	2.872	94	-	1.36	-
1C	HB1	2.395	134	-	0.85	-
2A	HB1	1.946	154	5.33	4.89	0.45
	HB2	2.381	141	1.99	1.54	0.45
	PB1	2.940	99	1.77	1.32	0.45
2B	HB1	1.939	165	5.32	5.06	0.26
	HB2	2.577	125	1.01	0.75	0.26
	PB1	3.028	84	1.30	1.04	0.26
2C	HB1	1.945	170	5.21	5.06	0.15
	HB2	2.513	127	0.89	0.74	0.15
	HB3	3.107	100	0.93	0.79	0.15
3A	HB1	1.952	148	6.87	4.78	2.09
	HB2	1.924	147	6.98	4.49	2.49
	HB3	1.909	150	7.15	4.84	2.32
	HB4	3.050	104	0.58	0.78	-0.19
	PB1	2.931	97	1.11	1.13	-0.02
3B	HB1	1.889	150	7.45	4.84	2.61
	HB2	1.948	147	6.63	4.44	2.19
	HB3	1.941	148	6.82	4.81	2.01
	HB4	3.082	102	-0.03	0.50	-0.53
	PB1	3.032	88	1.25	1.36	-0.12
3C	HB1	1.978	179	4.44	4.64	-0.20
	HB2	2.066	141	4.70	4.59	0.11
	HB3	2.302	156	2.10	1.64	0.46
	PB1	2.828	99	1.91	1.32	0.59
4A	HB1	1.784	166	8.36	4.88	3.48
	HB2	1.787	165	8.25	4.84	3.41

	HB3	1.777	166	8.49	4.86	3.63
	HB4	1.810	165	7.88	4.88	3.01
	HB5	2.922	110	0.35	0.63	-0.27
	PB1	3.104	84	0.80	1.03	-0.23
4B	HB1	1.767	167	8.82	4.84	3.98
	HB2	1.803	165	7.99	4.89	3.10
	HB3	1.790	166	8.23	4.90	3.33
	HB4	1.790	166	8.11	4.84	3.27
	HB5	2.955	108	-0.10	0.56	-0.66
	PB1	3.053	89	1.16	1.34	-0.19
4C	HB1	1.933	158	5.33	4.55	0.78
	HB2	2.001	145	6.39	4.46	1.93
	HB3	1.910	151	7.12	4.83	2.29
	HB4	1.858	153	6.61	4.80	1.81
	HB5	2.431	134	1.88	1.50	0.38
	PB1	2.961	97	1.85	1.39	0.46
4D	HB1	1.933	170	4.64	4.21	0.43
	HB2	1.861	152	7.29	4.35	2.94
	HB3	1.874	153	7.41	4.82	2.59
	HB4	2.055	143	6.43	4.62	1.81
	HB5	2.363	142	1.09	0.84	0.25
	PB1	2.877	96	1.54	1.43	0.10

2.4.7 Comparison between (NO)···H HBs and PBs in $NO(H_2O)_{n=1-4}$ complexes

When comparing the (NO)···H HBs (formed via N-atom of NO) and PBs in $NO(H_2O)$ dimer complexes, the (NO)···H HB has slightly higher energy (1.76 kcal/mol) than PB (1.36 kcal/mol), whereas (NO)···H HB formed via O-atom of NO has the lowest energy (0.85 kcal/mol). Further, Figure 2.6 describes the energies and cooperativity contributions of (NO)···H HBs and PBs in $NO(H_2O)_{n=2-4}$ complexes. Since (NO)···H HBs are formed by N- and O-atoms of NO, a broader range of energies (from −0.10 to 2.10 kcal/mol) are observed for (NO)···H HB interactions in Figure 2.6. Herein HBs formed via O-atom have lower range of energies (from −0.10 to 1.09 kcal/mol) than the HBs via N-atom of NO (from 0.35 to 2.10 kcal/mol). In the case of PBs, comparatively shorter range of energies (from 0.80 to 1.91 kcal/mol) is obtained in $NO(H_2O)_{n=2-4}$ complexes. It is also to be noted that the upper range of energy values of HBs and PBs are comparable in $NO(H_2O)_{n=2-4}$ complexes. The cooperativity contributions (E^{Coop}) towards (NO)···H HBs and PBs range from −0.66 to 0.46 kcal/mol and from −0.23 to 0.59 kcal/mol, respectively, also show the same trend.

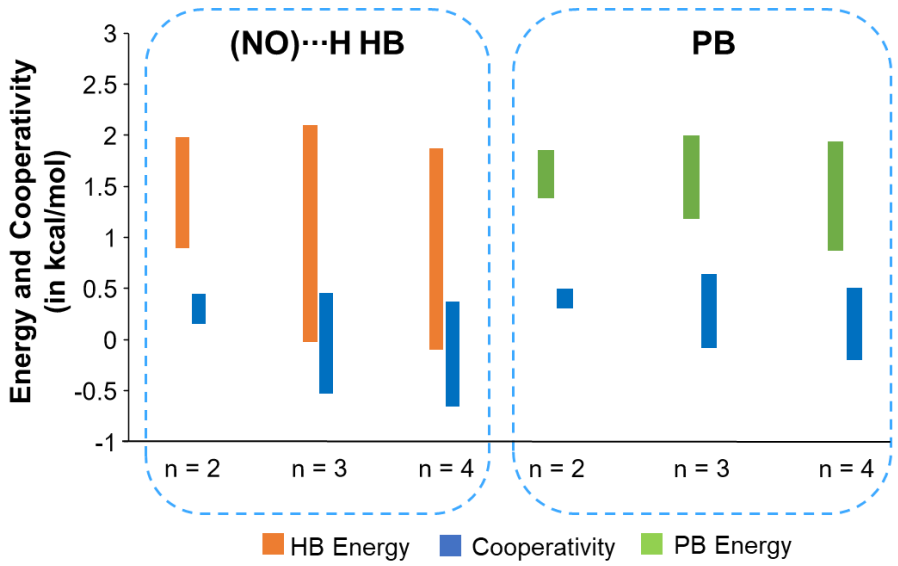

Figure 2.6 Comparison between energies and cooperativity contribution of (NO)···H HBs and PBs in $NO(H_2O)_{n=2-4}$ complexes.

2.4.8 Free energy of $NO(H_2O)_n$ complex formation

The free energy of formation (ΔG) is a useful parameter for predicting the thermodynamic stability of $NO(H_2O)_n$ complexes. Table 2.3 provides the ΔG values (calculated at 298 K and 1 atm) of the $NO(H_2O)_{n=1-4}$ complexes. It can be seen that $NO(H_2O)_{n=1-4}$ complexes have positive ΔG values ranging from 3.37 to 12.07 kcal/mol. This implies that $NO(H_2O)_n$ complexes are stable only at very low temperatures and pressure, and thus occur in the upper atmosphere.[4,212] Similar findings were reported for weakly bound complexes like $CO_2(H_2O)_n$ and $OCS(H_2O)_n$.[209,210] In addition, previous studies have shown that the astronomically relevant molecules including NO are adsorbed into dust grains coated with water ice in the interstellar medium at low temperature (10 K).[213]

Table 2.3 ΔG values (in kcal/mol; at 298 K and 1 atm) of $NO(H_2O)_{n=1-4}$ complexes.

Complex	ΔG
1A	3.92
1B	3.37
1C	4.20
2A	7.96
2B	6.71
2C	7.50

3A	7.97
3B	8.42
3C	11.33
4A	7.19
4B	7.19
4C	12.07
4D	11.60

2.5 Conclusions

In this study, we examined various noncovalent interactions present in $NO(H_2O)_{n=1-4}$ complexes at the MP2/aug-cc-pVTZ//MP2/6-311++G(d,p) level of theory. The MESP analysis revealed the location of the electron-rich and electron-deficient regions of NO. Based on this, the (NO)···H hydrogen bonding (HB; formed via N- and O-atom of NO) and the pnicogen bonding (PB) interactions are discussed in $NO(H_2O)$ complexes. Further, QTAIM analysis confirmed the HB and PB interactions between NO and water, and NBO analysis rendered the orbitals involved in the HB and PB interactions.

Besides, we applied the MTA-based method to estimate the individual (NO)···H HBs and PBs in NO…water interactions as well as water…water interactions in $NO(H_2O)_{n=1-4}$ complexes. The HB formed via N-atom of NO is the strongest interaction between NO and water (with an HB energy of 1.76 kcal/mol), followed by PB interaction (1.36 kcal/mol), and HB via O-atom of NO (0.85 kcal/mol) is the weakest interaction in $NO(H_2O)$ dimer complexes. In $NO(H_2O)_{n=2-4}$ complexes, the coexistence of (NO)···H HBs and PBs is noted. Herein, the energies of (NO)···H HBs range between −0.10 and 2.10 kcal/mol, while the energies of PBs range between 0.80 and 1.91 kcal/mol. The broader range of (NO)···H HB energies is owing to the lower energy values of HBs formed via the O-atom of NO (range from −0.10 to 1.09 kcal/mol) as compared to the N-atom of NO (range from 0.35 to 2.10 kcal/mol). Interestingly, the highest HB (2.10 kcal/mol) and PB (1.91 kcal/mol) energies are noted in the **3C** complex, where NO interacts with a linear water trimer. The weaker water…water interactions in the linear form of the water cluster compared to the cyclic form might account for the comparatively stronger NO…water interactions (sum of individual energies, i.e., $\sum E_{NO\ldots H_2O}$ = 4.01 kcal/mol) observed in **3C**. However, in $NO(H_2O)_{n=2-4}$

complexes, the energies estimated for the sum of all the NO…water interactions ($\sum E_{NO\ldots H_2O}$ range from 1.06 to 4.01 kcal/mol) show a weaker strength as compared to the sum of all the water…water interactions ($\sum E_{H_2O\ldots H_2O}$ between 5.21 and 33.15 kcal/mol). Comparatively lower values of cooperativity contribution found for NO…water (from −0.66 to 0.59 kcal/mol) than for water…water (between −0.20 and 3.98 kcal/mol) interactions also reveal the same. This may be the reason for the ring formation of water clusters (self-association) in the most stable isomers of $NO(H_2O)_{n=3\text{-}4}$ complexes. Thus, the self-association of water molecules is the energetically preferred configuration in $NO(H_2O)_n$ complexes with cluster sizes above three.

In summary, the present study brings out the interplay of intermolecular hydrogen-, and pnicogen-bonding in terms of energetics of these individual interactions present in the microhydrated NO complexes. The MTA-based method is indeed useful for this purpose. This encourages one to employ the present MTA-based method to understand the intermolecular interaction present in the microhydrated structure of other related species.

Publication based on this chapter:

Thufail M. Ismail; Patkar, D.; Sajith, P. K.; Deshmukh, M. M. Interplay of Hydrogen, Pnicogen, and Chalcogen Bonding in $X(H_2O)_{n=1\text{-}5}$ (X = NO, NO^+, and NO^-) Complexes: Energetics Insights via Molecular Tailoring Approach. *The Journal of Physical Chemistry A* **2023**, 127, 10360–10374.

Chapter 3

Energetics of Hydrogen Bonding Interactions in $NO^{-}(H_2O)_{n=1-4}$ and $HNO(H_2O)_{n=1-4}$ Complexes

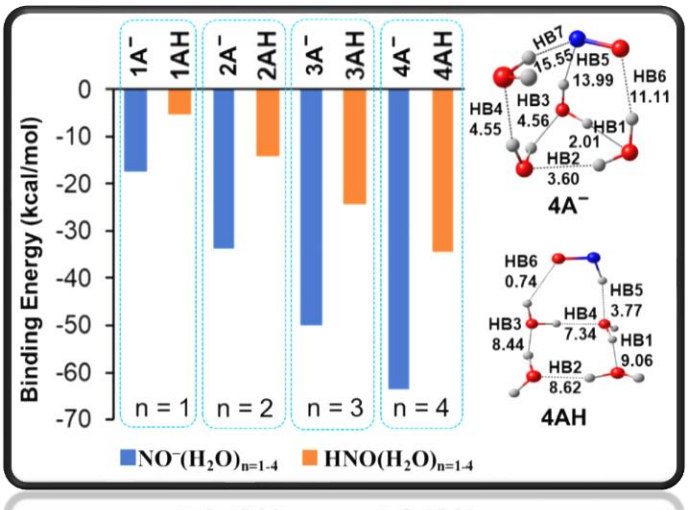

3.1 Abstract:

Hydration of NO^- and HNO (reduced species of NO) play important roles in various atmospheric and biological events. In this study, we investigate the microhydration of NO^- and HNO (up to four water molecules, n = 1–4) using *ab initio* method at the MP2/6-311++G(d,p) level. Molecular electrostatic potential (MESP), quantum theory of atoms in molecules (QTAIM), and natural bond orbital (NBO) analyses are used to explore the hydrogen bonding (HB) in NO^-…water and HNO…water interactions. The energies and cooperativity contribution of individual HBs present in the microhydrated clusters of NO^- and HNO, i.e., $NO^-(H_2O)_{n=1-4}$ and $HNO(H_2O)_{n=1-4}$, are examined with the help of molecular tailoring approach-based (MTA-based) method. In the case of $NO^-(H_2O)$ dimer complexes, the strength of HB interactions via both N- and O-atoms of NO^- with water is comparable (~ 18 kcal/mol). The addition of water molecules increases the NO^-…water interactions in $NO^-(H_2O)_n$ complexes, thus increasing the total energies of individual HB interactions ($\sum E_{NO^-\ldots H_2O}$) in the order of 30 – 52 kcal/mol is noted with cluster size from two to four. Herein, the individual energies of HBs formed via N- and O-atoms are comparable, with energies ranging from 11.34 to 16.56 kcal/mol and from 11.11 to 16.39 kcal/mol, respectively. The strength of water…water HB interactions is also seen to increase with the increase in the cluster size ($\sum E_{H_2O\ldots H_2O}$ values range from 0.18 to 25.64 kcal/mol for n = 2 to 4), which could be explained by the positive values of cooperativity contribution for these HBs. On the other hand, HNO can form HB interactions through three of its atoms (H-, N-, and O-) with water in their $HNO(H_2O)$ dimer complexes. The energies of these HBs are in the order of 2 – 5 kcal/mol in their dimers. In $HNO(H_2O)_{n=2-4}$ complexes, the strength of HNO…water interactions increased with the increase in cluster size; the total energies of individual HB interactions ($\sum E_{HNO\ldots H_2O}$) increases up to 18.19 kcal/mol with n=4. Herein, the individual energies of HBs formed by N- and O-atoms are in the range of 0.20 – 6.55 kcal/mol and 0.26 – 5.19 kcal/mol, respectively. Whereas, a slightly higher range of individual energy values (ranging from 3.11 to 7.24 kcal/mol) are obtained for HBs via H-atom of HNO. In the case of water…water interactions in $HNO(H_2O)_{n=2-4}$ complexes, which is also increased as the cluster size grew. The larger positive values of cooperativity contribution (range from −0.70 to 4.38 kcal/mol) obtained for HBs in $HNO(H_2O)_{n=2-4}$ complexes also reveal the same. On comparing the HBs (formed via N- and O-atoms, i.e., (NO)···H interactions) of $NO^-(H_2O)_n$ and $HNO(H_2O)_n$ complexes, the HBs in NO^-…water interactions are much stronger than the HBs in HNO…water interactions. This implies that

NO^- is a stronger HB acceptor than the -N=O functionality of HNO, which is attributed to the additional charge on NO. The higher binding energy values of $NO^-(H_2O)_n$ complexes than $HNO(H_2O)_n$ complexes also reveal the same. Further, the strong NO^-…water interactions result in cross-associated HB networks in most stable complexes of $NO^-(H_2O)_{n=2-4}$. On the other hand, cross-associated HB networks is energetically preferred for $HNO(H_2O)_n$ complexes with n = 2 and 3, but self-association of water molecules is energetically more favored with n = 4.

3.2 Introduction

Hydrated systems of reduced species of NO (*viz.* NO^- and HNO) have been a subject of interest in many atmospheric and biological events. Microhydration studies could provide vital information about hydrated systems at the molecular level.[187,188] Also, the solute-water clusters in the gas phase provide a fundamental model for studying the features of various intermolecular interactions of bulk-water systems.[214] Both NO^- and HNO can form hydrogen bonding (HB) interactions with water, as evidenced by many experimental and theoretical studies.[108,215] From a fundamental point of view, Eaton et al. recorded the photoelectron spectrum of $NO^-(H_2O)_2$ clusters.[107] Inspired by this, several studies have reported the formation of an interconnected cyclic network of HBs in $NO^-(H_2O)_n$ complexes with n values varying from one to three.[108] Similarly, Solimannejad et al. theoretically investigated the $HNO(H_2O)_n$ complexes (n = 1–4) by using *ab initio* methods.[215] They primarily focussed on understanding the blue shift of NH...O interactions in nitroxyl-water clusters. However, no systematic investigation of the energies and cooperativity contribution of HBs in NO^-…water and HNO…water interactions in their microhydrated clusters are reported in the literature.

Insight into the strength and the cooperativity effect of individual HBs in microhydrated networks of a solute is indispensable for understanding the water-mediated reactions.[79] The present study is an attempt to estimate the energies and cooperativity of HBs present in the microhydrated complexes of NO^- and HNO with the help of molecular tailoring approach (MTA) based calculations. This work also investigates the features of HBs in NO^-…water and HNO…water interactions using molecular electrostatic potential (MESP), quantum theory of atoms in molecules (QTAIM), and natural bond orbital (NBO) analyses. Furthermore, an energetic comparison between the HBs formed by charged NO^- with water clusters and neutral HNO with water clusters is also included in this study.

3.3 Computational methods

The structures of all $NO^-(H_2O)_{n=1-4}$ and $HNO(H_2O)_{n=1-4}$ complexes were simulated using MP2/6-311++G(d,p) level of theory with Gaussian 16 program package.[192] For optimization, initial structures were modeled according to existing literature data of similar molecules and chemical intuitions. For larger clusters, a bottom-up approach is also applied, e.g. the $NO^-(H_2O)_3$ is modeled by adding one H_2O to $NO^-(H_2O)_2$ through different sides. Similarly, the top-down approach also aided in finding any missed configurations of complexes. The optimized geometries were confirmed as local minima by frequency analysis due to the absence of imaginary frequencies. Further, the Gibbs free energy change (ΔG) associated with the formation of the most stable structures of $NO^-(H_2O)_{n=1-4}$ and $HNO(H_2O)_{n=1-4}$ at 298 K and 1 atm pressure is calculated.

For improved energetics, single-point calculations are carried out at the MP2 method by employing the aug-cc-pVTZ basis set for estimating the binding energy and MTA-based HB energies of all complexes. The MESP, QTAIM, and NBO analyses were also performed at the MP2/aug-cc-pVTZ//MP2/6-311++G(d,p) level of theory. AIMAll software is used for QTAIM analysis.[193] MESP analysis is carried out using Multiwfn software,[194] and visualized using VMD software.[195] NBO analysis is carried out using NBO version 3.1 implemented in Gaussian 16 software,[196] and the results are visualized using Chemcraft software.[197]

The binding energy (E_{BE}) of $NO^-(H_2O)_n$ and $HNO(H_2O)_n$ clusters is calculated by the supermolecular approach using Eq. 3.1.[202,216]

$$E_{BE} = E_{cluster} - (E_{NO^-/HNO} + nE_{H_2O}) \qquad \text{(Eq. 3.1)}$$

In Eq. 3.1, the terms $E_{cluster}$, $E_{NO^-/HNO}$, and E_{H_2O} denote the total energy of the $NO^-(H_2O)_n$ or $HNO(H_2O)_n$ cluster, the energy of the NO^- or HNO monomers, and the energy of a water monomer multiplied by the number of water molecules (n) in a given cluster under consideration.

3.4 Results and discussions

As mentioned in previous studies, both NO^- and HNO interact with water through hydrogen bonds (HBs). The following sections discuss the various HBs present in the monohydrate complexes of NO^- and HNO (i.e., $NO^-(H_2O)_1$ and $HNO(H_2O)_1$, respectively) based on MESP, QTAIM, and NBO analyses. Further, the energies and cooperativity contribution of

all individual HBs in the microhydrated complexes of NO^- and HNO are discussed (i.e., $NO^-(H_2O)_n$ and $HNO(H_2O)_n$ with n = 1 to 4) in the later sections. A comparison of HBs in these microhydrated complexes of NO^- and HNO are offered in the final section.

For the sake of simplicity, the $NO^-(H_2O)_n$ complexes with different isomers are designated according to their cluster size (n-value) and the order of stability. The E_{BE} values determine the stability order; the most stable isomer is indicated with **A**$^-$. The other isomers are named **B**$^-$, **C**$^-$, **D**$^-$, etc., based on the decreasing magnitude of E_{BE} (see Table 3.1). For instance, the most stable isomer of $NO^-(H_2O)_2$ complex is named as **2A**$^-$, and other isomers are **2B**$^-$, **2C**$^-$, etc., depending on their decreasing stability. Similarly, the $HNO(H_2O)_n$ complexes with different isomers are designated according to their cluster size (n-value) and the order of stability. The most stable isomer is indicated with **AH** and the other isomers are named **BH**, **CH**, **DH**, etc., based on the decreasing magnitude of E_{BE} (see Table 3.3). For instance, the most stable isomer of the $HNO(H_2O)_2$ complex is named **2AH**, and other isomers are **2BH**, **2CH**, **2DH**, etc., depending on their decreasing stability.

3.4.1 MESP analysis

MESP features can be employed to understand the interaction sites of molecules.[202,203] The electrostatic potential on molecular surfaces (at an isodensity value of 0.001 au) of NO^-, HNO and water is shown in Figure 3.1(a). The V_{min} sites are located as a cylindrical belt around the π-bond of N–O, and the corresponding value is −147.9 kcal/mol. The two other V_{min} sites are along the N–O bond axis near N (−143.9 kcal/mol) and O-atoms (−137.8 kcal/mol). In the case of HNO, V_{min} sites are located near N- and O-atoms and a V_{max} site is located near the H-atom, implying that HNO can act as both HB acceptor and donor, respectively.

In $NO^-(H_2O)$ complexes (see Figure 3.1(b)), a reduction in these V_{min} values is noted when NO^- interacts with H_2O. The V_{min} site near the O-atom disappears when NO^- interacts via O-atom with H_2O in **1A**$^-$, concomitantly the V_{min} value around the N–O bond is reduced from −147.9 to −131.8 kcal/mol. In **1B**$^-$, the HB formed through the N-atom of NO^- reduces the V_{min} value near the N-atom from −143.9 to −132.5 kcal/mol.

For $HNO(H_2O)$ complexes (see Figure 3.1(c)), a reduction in V_{max} value near the H-atom of HNO is observed (from 32.5 to 19.1 kcal/mol) due to HB interaction with water in **1AH**, implying that HNO acts as HB donor in this interaction. On the other hand, V_{min} sites

near N- and O-atoms of HNO disappear when these atoms interact with water in **1BH** and **1CH**, respectively, indicating that HNO acts as HB acceptor in these complexes.

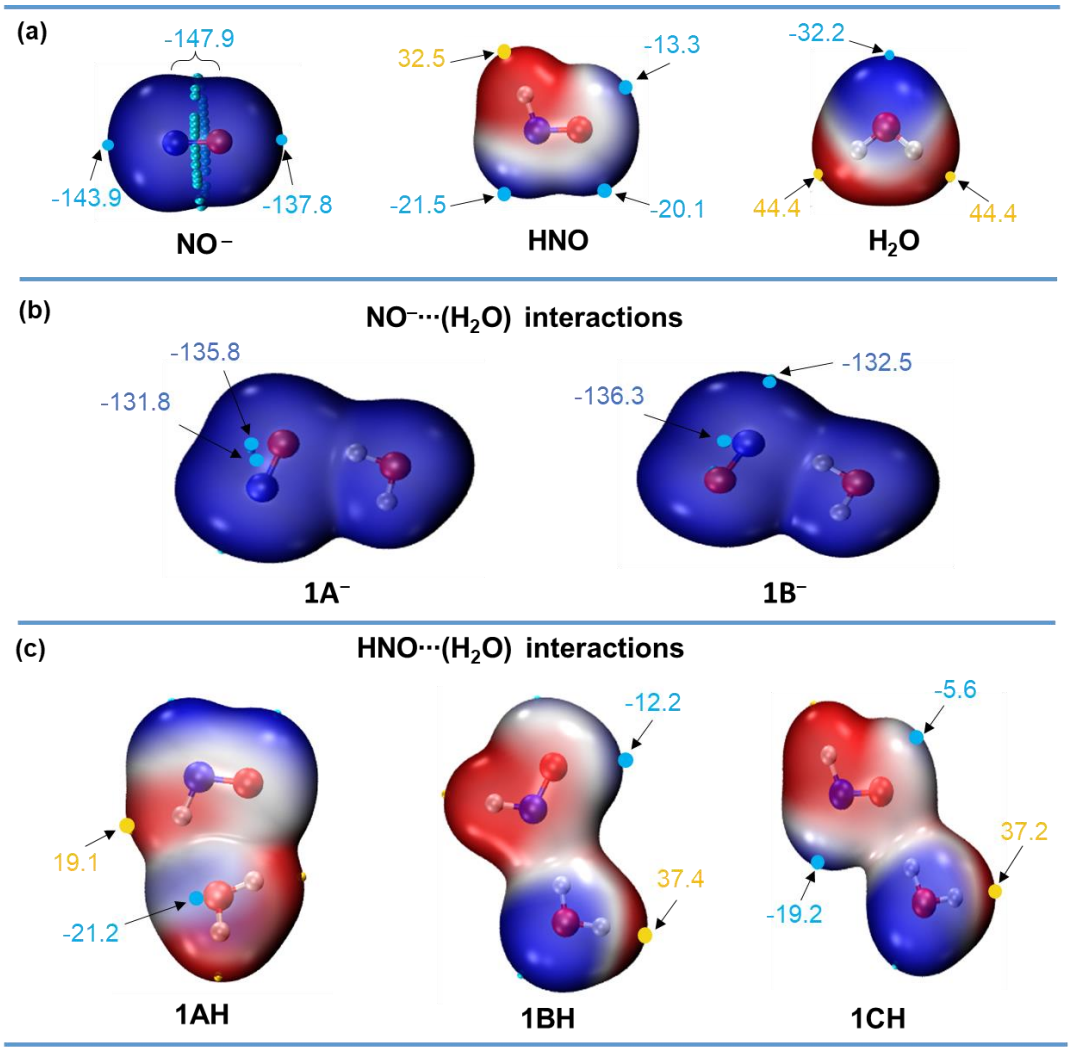

Figure 3.1 Electrostatic potential mapped on isodensity molecular surface (at 0.001 au) of monomers and dimers. (a) monomers, (b) $NO^-(H_2O)$ dimers, and (c) $HNO(H_2O)$ dimers. The positions of V_{min} and V_{max} at interacting sites are represented by cyan and golden spheres, respectively, and the corresponding values are shown in kcal/mol. The color ranges: blue for negative potential and red for positive potential.

3.4.2 QTAIM analysis

QTAIM plots of $NO^-(H_2O)$ and $HNO(H_2O)$dimer complexes are displayed in Figure 3.2. In $NO^-(H_2O)$ complexes, the electron density ($\rho(r)$) value at the bcp (0.0399 au) of HB formed via O-atom of NO^- with water (in **1A**$^-$) is comparable to that of $\rho(r)$ (0.0396 au) value at bcp of HB formed via N-atom of NO^- (in **1B**$^-$). Further, the positive Laplacian of electron density ($\nabla^2\rho(r)$) values and negative total electron energy density ($H(r)$) values for these HBs in

$NO^-(H_2O)$ complexes suggest that they show a mix of closed-shell and shared type interactions.

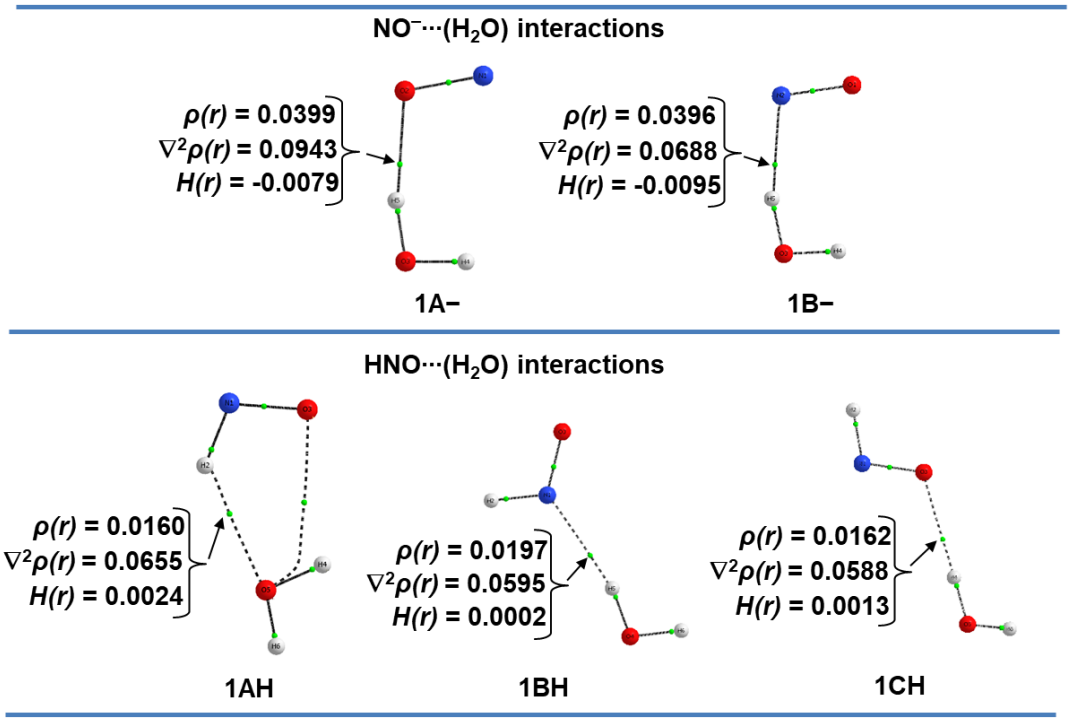

Figure 3.2 The QTAIM molecular graphs of $NO^-(H_2O)$ and $HNO(H_2O)$ complexes. The QTAIM parameters at bcp (which is shown as small green spheres on each bond path) of intermolecular interactions are given in au.

For $HNO(H_2O)$ dimer **1AH**, two bond paths are present between HNO and water, one is the H-atom of HNO with the O-atom of water, and the other one via the O-atom of HNO with the O-atom of water. However, the latter bond path is misleading in the context of shortest intermolecular contacts, because an HB interaction is expected for the O-atom of HNO with the H-atom of water. Similar, misleading bond paths are reported in the literature for QTAIM studies.[217,218] The $\rho(r)$ value obtained at the bcp of HB formed via H-atom of HNO is 0.0160 au. In **1BH** and **1CH**, the corresponding bond path for HBs formed via N- and O-atoms of HNO with water, respectively, is shown. Herein, comparatively a higher $\rho(r)$ value is obtained at bcp of HB via N-atom (0.0197 au) than HB via O-atom of HNO (0.0162 au). This reveals that the HB formed via the N-atom is stronger than HB via the O-atom of HNO. In addition, the positive values for $\nabla^2\rho(r)$ and $H(r)$ parameters for all of these HBs between HNO and water suggest that they are all typical closed-shell interactions.

3.4.3 NBO analysis

An NBO view of donor-acceptor orbitals involved in the HBs of $NO^{-}(H_2O)$ dimers and their stabilization energies ($E^{(2)}$; values greater than 0.1 kcal/mol are considered) are displayed in Figure 3.3. In **1A**$^{-}$ and **1B**$^{-}$, the lone pairs of O- (lp(O)) and N-atoms (lp(N)) of NO^{-} respectively, interact with the O–H antibonding orbital (σ^{*}_{O-H}) of water. In addition, the N–O bonding orbitals (π_{N-O} & σ_{N-O}) also interact with O–H antibonding orbital (σ^{*}_{O-H}) of water. For these interactions, the total $E^{(2)}$ energy is calculated to be 20.73 and 23.83 kcal/mol, for HB formed via O- and N-atoms of NO^{-}, respectively.

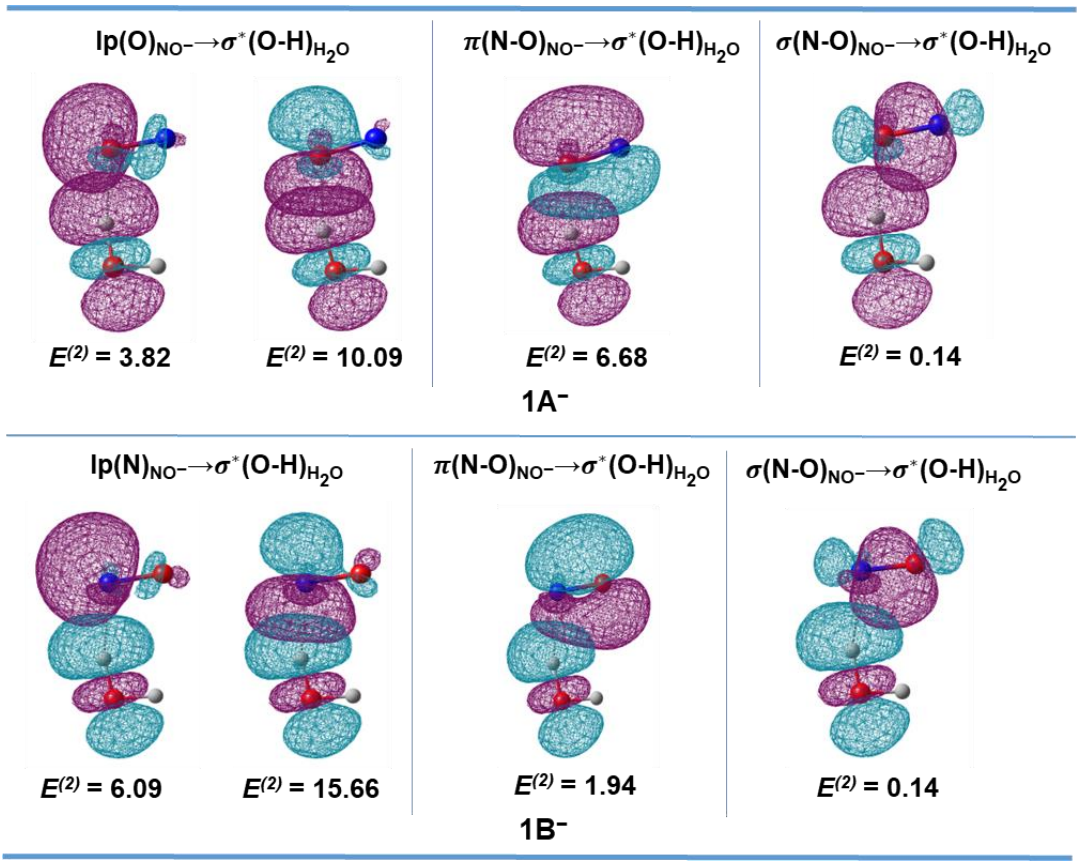

Figure 3.3 The donor-acceptor orbitals (isovalue = 0.03 au) involved in HB interactions via O- (**1A**$^{-}$) and N-atoms (**1B**$^{-}$) of NO^{-} in $NO^{-}(H_2O)$ complexes. The $E^{(2)}$ energy (in kcal/mol) for these interactions is estimated based on second-order perturbation theory in NBO analysis.

Figure 3.4 depicts the donor-acceptor orbitals involved in the HBs in $HNO(H_2O)$ dimers, as well as the corresponding stabilization energies ($E^{(2)}$; values greater than 0.1 kcal/mol are considered). For **1AH**, the interaction of lone pairs of O-atom (lp(O)) of water with the antibonding orbital of the N–H bond (σ^{*}_{N-H}) of HNO is the primary interaction with a total $E^{(2)}$ energy of 2.16 kcal/mol. Besides, an overlap of lone pairs of O-atom of HNO with

the antibonding orbital (σ^*_{O-H}) of water is obtained with a total $E^{(2)}$ value of 0.36 kcal/mol, and the N–H bonding orbitals (σ_{N-H}) also interact with the O–H antibonding orbital (σ^*_{O-H}) of water with an $E^{(2)}$ value of 0.26 kcal/mol. Hence, these orbital interactions signify that HNO acts as both HB acceptor and donor in **1AH**. On the other hand, in **1BH** and **1CH**, the lone pairs of N- and O-atoms of HNO, respectively, interact with antibonding orbital (σ^*_{O-H}) of water (with a total $E^{(2)}$ value of 4.36 and 2.82 kcal/mol, respectively). In addition, the N–H bonding orbitals (σ_{N-H}) also interact with the O–H antibonding orbital (σ^*_{O-H}) of water with an $E^{(2)}$ value of 0.12 kcal/mol in **1BH**. Therefore, the NBO results show that HNO acts as only HB acceptor (electron donor) in **1BH** and **1CH** complexes.

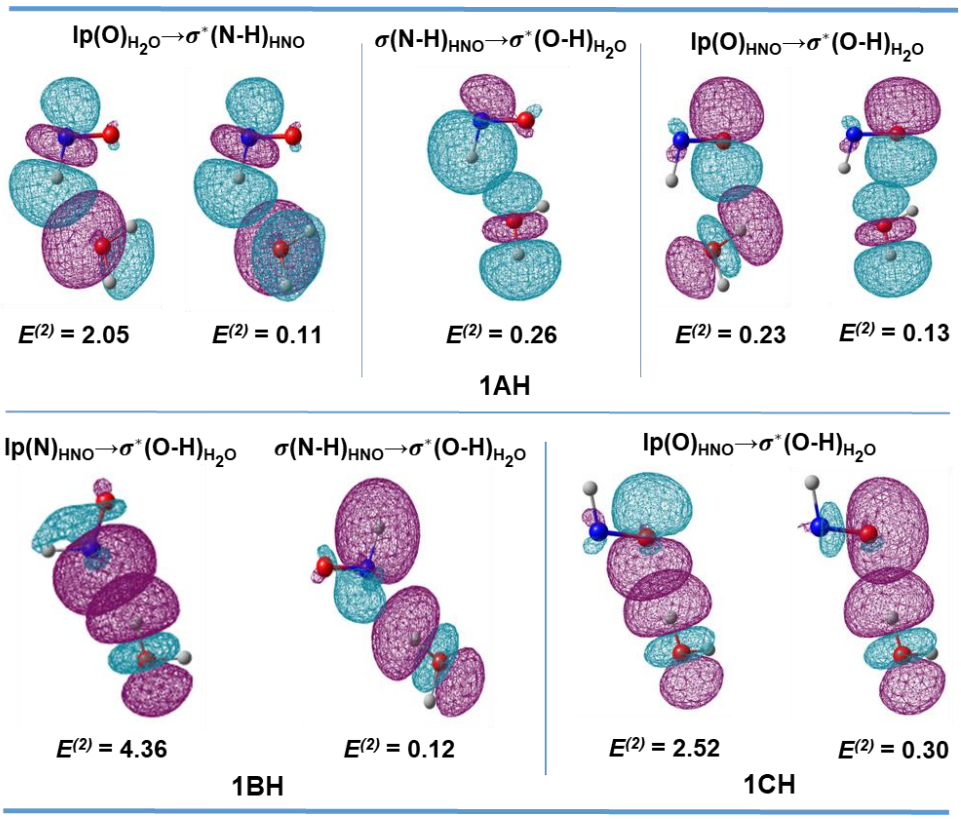

Figure 3.4 The donor-acceptor orbitals (isovalue = 0.03 au) involved in hydrogen bonding (HB) interactions via H-, N- and O-atoms of HNO in HNO(H_2O) complexes (**1AH**, **1BH**, and **1CH**). The total $E^{(2)}$ energy for these interactions is estimated based on second-order perturbation theory in NBO analysis.

3.4.4 Energetics of individual HBs in $NO^-(H_2O)_{n=1-4}$ complexes

The optimized geometries of isomers of each $NO^-(H_2O)_{n=1-4}$ categories are given in Figure 3.5. Herein, NO^- forms HBs with water molecules via both N- and O-atoms. The relevant structural parameters of these HBs are listed in Table 3.2. The HBs distances in NO^-…water

and water…water interactions are in the range of 1.676 – 2.150 Å and 1.732 – 2.357 Å, respectively. A previous study already reported the structures of $NO^{-}(H_2O)_n$ complexes (where n = 1 to 3).[108] Figure 3.5 also depicts the energies of all individual HB interactions (calculated by MTA) in each $NO^{-}(H_2O)_{n=1\text{-}4}$ complex. The total energies of these HBs present between NO^{-} and water ($\sum E_{NO^{-}\ldots H_2O}$) and in water…water interactions ($\sum E_{H_2O\ldots H_2O}$) obtained from MTA calculations are reported in Table 3.1. As mentioned, E_{BE} calculated by supermolecular approach are also given in Table 3.1.

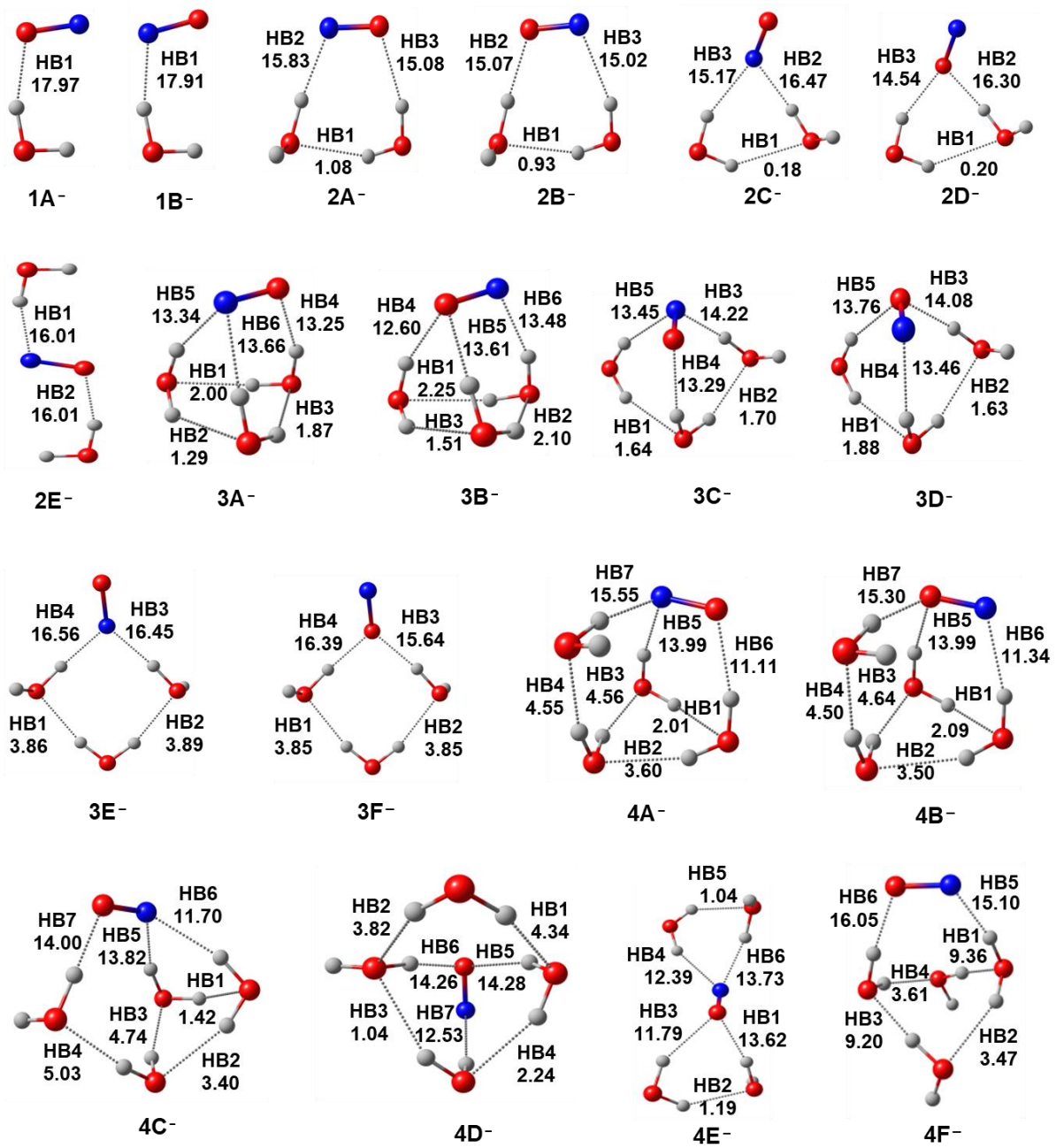

Figure 3.5 Values of all individual hydrogen bonding (HB) energies (in kcal/mol) estimated by MTA in $NO^{-}(H_2O)_{n=1\text{-}4}$ complexes.

The E_{BE} calculated for the most stable isomers, **1A**$^-$ and **1B**$^-$, are −17.25 and −17.17 kcal/mol, respectively. This shows that the strength of HB formed by NO^- through O- and N-atom with water is comparable. This is in line with the QTAIM results based on *ρ(r)* parameter. For $NO^-(H_2O)_2$ complexes, the E_{BE} values (range from −32.07 to −33.76 kcal/mol) are nearly twice that of E_{BE} determined for $NO^-(H_2O)$ complexes. The higher range of $\sum E_{NO^-\ldots H_2O}$ values (30.09 to 32.02 kcal/mol) may be the reason for the greater stabilization of $NO^-(H_2O)_2$ complexes. The corresponding $\sum E_{H_2O\ldots H_2O}$ values are below 2 kcal/mol.

In the case of $NO^-(H_2O)_3$ complexes (E_{BE} values range from −46.15 to −50.11 kcal/mol), the $\sum E_{NO^-\ldots H_2O}$ values are in the range between 32.03 and 41.30 kcal/mol, whereas, the $\sum E_{H_2O\ldots H_2O}$ values fall in the range of 3.34 to 7.75 kcal/mol. This higher range of $\sum E_{NO^-\ldots H_2O}$ values and moderate values of $\sum E_{H_2O\ldots H_2O}$ as compared to $NO^-(H_2O)_2$ complexes may be the reason for greater stabilization of $NO^-(H_2O)_3$ complexes.

For $NO^-(H_2O)_4$ complexes (E_{BE} values fall between −57.37 and −63.87 kcal/mol), the $\sum E_{NO^-\ldots H_2O}$ and $\sum E_{H_2O\ldots H_2O}$ values range from 31.15 to 51.53 kcal/mol and from 2.23 to 25.64 kcal/mol. Herein, the highest $\sum E_{NO^-\ldots H_2O}$ value (51.53 kcal/mol) obtained for **4E**$^-$ reveals strong NO^-…water interactions pertained in this complex, while the lowest $\sum E_{NO^-\ldots H_2O}$ (31.15 kcal/mol) is obtained for **4F**$^-$. Conversely, the lowest $\sum E_{H_2O\ldots H_2O}$ value (2.23 kcal/mol) is calculated for **4E**$^-$, wherein the water dimers stayed apart on each side of NO^- could explain the weaker water…water interactions observed in this complex. The higher $\sum E_{H_2O\ldots H_2O}$ value (25.64 kcal/mol) is attributed to the strong water…water interactions present in the cyclic water tetramer in **4F**$^-$. In comparison to the energetics of these less stable complexes, the more stable complexes **4A**$^-$ to **4D**$^-$ have moderate values of $\sum E_{NO^-\ldots H_2O}$ (range of 39.52 to 41.07 kcal/mol) and $\sum E_{H_2O\ldots H_2O}$ (range of 11.44 to 14.73 kcal/mol). It should be noted that $\sum E_{NO^-\ldots H_2O}$ values of more stable complexes of $NO^-(H_2O)_4$ complexes are in similar range of $\sum E_{NO^-\ldots H_2O}$ values obtained for more stable complexes of $NO^-(H_2O)_3$.

Overall, the individual energies of HBs formed via N- and O-atoms are comparable in $NO^-(H_2O)_n$ complexes, with energies ranging from 11.34 to 16.56 kcal/mol and from 11.11 to 16.39 kcal/mol, respectively. The strength of interactions between NO^- and H_2O increases (i.e., $\sum E_{NO^-\ldots H_2O}$ values) in $NO^-(H_2O)_n$ complexes with increasing n value. The water…water

interactions also strengthen when the water cluster size increases from two to four. The strong NO^-…water interactions produce cross-associated HB networks in $NO^-(H_2O)_n$ clusters. Thus, NO^- forms cyclic or cage-like structures with water clusters in stable complexes of $NO^-(H_2O)_{n=2-4}$. Similarly, microhydration of halides and OCS anions revealed cage-like HB networks with water clusters of size three and above.[191,219,220]

Table 3.1 Values of binding energies (E_{BE}) calculated by supermolecular approach, and the sum of energies of relevant individual interactions estimated by MTA in $NO^-(H_2O)_{n=1-4}$ complexes. All energy values are in kcal/mol.

Structure	E_{BE}	Sum of individual interaction energies from MTA calculations	
		$\sum E_{NO^-\ldots H_2O}$	$\sum E_{H_2O\ldots H_2O}$
1A$^-$	−17.25	17.97	-
1B$^-$	−17.17	17.91	-
2A$^-$	−33.76	30.91	1.08
2B$^-$	−33.30	30.09	0.93
2C$^-$	−32.81	31.64	0.18
2D$^-$	−32.25	30.84	0.20
2E$^-$	−32.07	32.02	-
3A$^-$	−50.11	40.25	5.16
3B$^-$	−49.71	39.69	5.86
3C$^-$	−48.16	40.96	3.34
3D$^-$	−47.95	41.30	3.51
3E$^-$	−47.23	33.01	7.75
3F$^-$	−46.15	32.03	7.70
4A$^-$	−63.87	40.65	14.72
4B$^-$	−63.65	40.63	14.73
4C$^-$	−62.08	39.52	14.59
4D$^-$	−61.98	41.07	11.44
4E$^-$	−58.04	51.53	2.23
4F$^-$	−57.37	31.15	25.64

The cooperativity contribution towards each of the HBs present in $NO^-(H_2O)_{n=2-4}$ complexes are reported in Table 3.2. As one can be seen from Figure 3.5 and Table 3.2, the energies of HBs formed between NO^- and water are in the range from 11.34 to 16.56 kcal/mol and from 11.11 to 16.39 kcal/mol for HBs formed via N- and O-atoms, respectively. The energies of HBs calculated for corresponding dimers isolated from complexes are found to be in the range from 15.18 to 17.60 kcal/mol and from 14.42 to 17.60 kcal/mol for HBs

formed via N- and O-atoms, respectively. Clearly, the range of energy values determined for HBs within the complexes is lower than the range of energy values calculated for corresponding HBs in isolated dimers. The difference in these two energy values of each HB is quantified as cooperativity contribution, which ranges from −0.99 to −4.33 kcal/mol and from −0.90 to −4.34 kcal/mol towards HBs formed through N- and O-atom, respectively.

The negative and positive cooperativity contributions are noted for HBs of water…water interactions in $NO^{-}(H_2O)_{n=2-4}$ complexes, i.e., lies in the range of −1.63 to 5.28 kcal/mol. It is worth mentioning that the complexes containing smaller water clusters (i.e., n = 2 – 3) have negative or close to zero values of cooperativity contributions towards water…water interactions. However, in the larger water clusters, i.e., $NO^{-}(H_2O)_{n=4}$, primarily positive cooperativity contributions are found toward water…water interactions.

Table 3.2 The relevant structural parameters *viz.* distance (in Å) and bond angle (in degree), energy in complex (E_{Int}^{MTA}), energy in dimer (E^{Dimer}), and cooperativity contribution (E^{Coop}) of all individual HBs in $NO^{-}(H_2O)_{n=1-4}$ complexes. All energy values are in kcal/mol.

Complex	Interaction Labels	Distance of interaction	Bond angle	E_{Int}^{MTA}	E^{Dimer}	E^{Coop}
1A⁻	HB1	1.761	167	-	17.97	-
1B⁻	HB1	1.825	162	-	17.91	-
2A⁻	HB1	2.113	153	1.08	2.53	−1.45
	HB2	1.741	171	15.83	17.27	−1.45
	HB3	1.965	163	15.08	16.53	−1.45
2B⁻	HB1	2.156	152	0.93	2.56	−1.63
	HB2	1.695	173	15.07	16.71	−1.63
	HB3	2.024	160	15.02	16.65	−1.63
2C⁻	HB1	2.265	140	0.18	1.30	−1.12
	HB2	1.765	169	16.47	17.59	−1.12
	HB3	2.009	156	15.17	16.29	−1.12
2D⁻	HB1	2.291	139	0.20	1.29	−1.09
	HB2	1.726	168	16.30	17.39	−1.09
	HB3	1.926	154	14.54	15.63	−1.09
2E⁻	HB1	1.883	161	16.01	17.60	−1.58
	HB2	1.815	166	16.01	17.60	−1.58
3A⁻	HB1	2.197	146	2.00	2.51	−0.51
	HB2	2.305	135	1.29	1.38	−0.09
	HB3	2.207	145	1.87	2.24	−0.38
	HB4	1.890	162	13.25	16.05	−2.80
	HB5	1.940	157	13.34	15.85	−2.51
	HB6	2.002	156	13.66	16.04	−2.38

3B^{-}	HB1	2.238	144	2.25	2.45	−0.21
	HB2	2.158	146	2.10	2.34	−0.24
	HB3	2.280	137	1.51	1.52	−0.01
	HB4	1.892	156	12.60	15.17	−2.58
	HB5	1.953	155	13.61	16.22	−2.61
	HB6	1.922	159	13.48	16.29	−2.80
3C^{-}	HB1	2.217	151	1.64	2.35	−0.71
	HB2	2.132	150	1.70	2.50	−0.80
	HB3	1.794	165	14.22	16.65	−2.43
	HB4	1.948	160	13.29	15.69	−2.40
	HB5	2.082	157	13.45	15.79	−2.34
3D^{-}	HB1	2.205	150	1.88	2.40	−0.52
	HB2	2.186	148	1.63	2.34	−0.70
	HB3	1.767	166	14.08	16.44	−2.36
	HB4	2.007	157	13.46	15.75	−2.29
	HB5	1.974	158	13.76	15.94	−2.17
3E^{-}	HB1	1.994	166	3.86	3.81	0.05
	HB2	1.992	167	3.89	3.83	0.06
	HB3	1.767	170	16.45	17.44	−0.99
	HB4	1.770	172	16.56	17.55	−0.99
3F^{-}	HB1	2.002	167	3.85	3.75	0.10
	HB2	2.003	167	3.85	3.79	0.07
	HB3	1.694	169	15.64	16.59	−0.95
	HB4	1.701	171	16.39	17.29	−0.90
4A^{-}	HB1	2.237	139	2.01	2.09	−0.09
	HB2	2.087	156	3.60	3.36	0.23
	HB3	2.032	154	4.56	3.56	1.00
	HB4	1.938	166	4.55	3.78	0.77
	HB5	1.933	160	13.99	16.61	−2.62
	HB6	1.929	167	11.11	15.45	−4.34
	HB7	1.764	168	15.55	17.30	−1.75
4B^{-}	HB1	2.199	141	2.09	2.16	−0.06
	HB2	2.117	155	3.50	3.31	0.19
	HB3	2.031	155	4.64	3.56	1.08
	HB4	1.952	166	4.50	3.74	0.76
	HB5	1.873	162	13.99	16.58	−2.60
	HB6	1.986	164	11.34	15.67	−4.33
	HB7	1.734	168	15.30	17.10	−1.80
4C^{-}	HB1	2.357	128	1.42	1.23	0.19
	HB2	2.125	154	3.40	3.14	0.26
	HB3	2.024	157	4.74	3.76	0.98
	HB4	1.917	169	5.03	4.06	0.97
	HB5	1.907	160	13.82	16.32	−2.50

	HB6	2.032	161	11.70	15.51	−3.81
	HB7	1.713	173	14.00	16.08	−2.08
4D⁻	HB1	1.992	161	4.34	3.67	0.67
	HB2	2.040	160	3.82	3.81	0.02
	HB3	2.197	147	1.04	2.50	−1.45
	HB4	2.139	148	2.24	2.47	−0.23
	HB5	1.934	156	14.28	15.99	−1.71
	HB6	1.676	172	14.26	16.19	−1.92
	HB7	1.997	157	12.53	15.58	−3.05
4E⁻	HB1	1.802	167	13.63	16.76	−3.13
	HB2	2.194	145	1.19	1.70	−0.51
	HB3	2.074	150	11.79	14.42	−2.63
	HB4	2.150	152	12.39	15.18	−2.79
	HB5	2.187	144	1.04	1.67	−0.63
	HB6	1.833	169	13.73	16.93	−3.20
4F⁻	HB1	1.732	171	9.36	4.08	5.28
	HB2	2.104	156	3.47	3.61	−0.15
	HB3	1.749	171	9.20	4.13	5.06
	HB4	2.064	155	3.61	3.71	−0.10
	HB5	1.769	169	15.10	16.40	−1.29
	HB6	1.732	171	16.05	17.11	−1.07

3.4.5 Energetics of individual HBs in $HNO(H_2O)_{n=1-4}$ complexes

The optimized structures of all $HNO(H_2O)_{n=1-4}$ complexes are displayed in Figure 3.6 and Figure 3.7. The $HNO(H_2O)_n$ complexes with n = 1, 2, and 3 are presented in Figure 3.6, and n = 4 is presented in Figure 3.7. The most stable isomers corresponding to different "n" values is consistent with the reported lowest energy structures in a previous study.[215] The individual HB energies of each isomer estimated from MTA are presented in Figure 3.6 and Figure 3.7. The sum of MTA-based energies of all HBs present between HNO and water (designated as $\sum E_{HNO\ldots H_2O}$) and the sum of energies of HBs between water molecules (designated as $\sum E_{H_2O\ldots H_2O}$) in $HNO(H_2O)_n$ complexes are provided in Table 3.3. Moreover, the structural parameters of HBs in $HNO(H_2O)_{n=1-4}$ complexes and cooperativity contributions (E^{Coop}) calculated for each HB in $HNO(H_2O)_{n=2-4}$ complexes are presented in Table 3.4. The HB distances in $HNO(H_2O)_{n=1-4}$ complexes are in the range of 1.743 – 2.796 Å.

For HNO monohydrate complexes, the binding energy (E_{BE}) value of the most stable isomer **1AH** is −5.10 kcal/mol, where the HB interaction is primarily due to the H-atom of HNO (HB donor) with water (HB distance is 2.171 Å). It should also be noted that the O-

atom of HNO (HB acceptor) has a secondary interaction with the H-atom of water (HB distance is 2.423 Å). The donor-acceptor orbitals involved in these two types of interactions with their stabilization energies are explained in the NBO section above. The HB energy in less stable dimeric complexes (**1BH** and **1CH**) is relatively smaller than the most stable isomer, the HB formed by N-atom (in **1BH**) and O-atom (in **1CH**) of HNO have E_{BE} values −3.91 and −2.93 kcal/mol, respectively (Table 3.3).

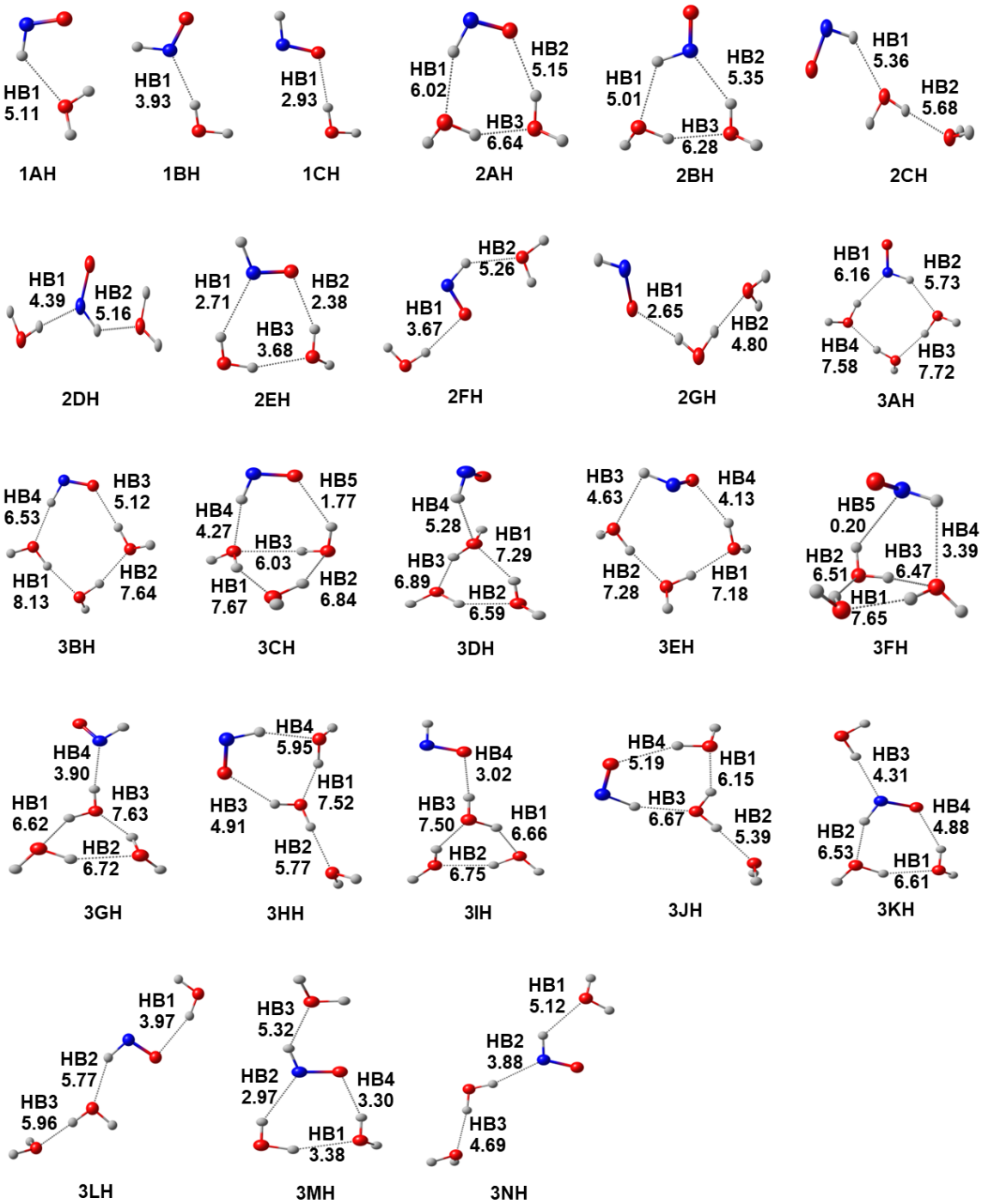

Figure 3.6 MTA-based energies of all individual HBs of various isomers in each category of $HNO(H_2O)_{n=1-3}$. All energy values are in kcal/mol.

Table 3.3 The binding energies (E_{BE}) and the sum of MTA-based energies (kcal/mol) of all HBs present between HNO and water ($\sum E_{HNO...H_2O}$) and HBs present between water molecules ($\sum E_{H_2O...H_2O}$) in HNO(H_2O)$_{n=1-4}$ complexes.

Structure	E_{BE}	$\sum E_{HNO...H_2O}$	$\sum E_{H_2O...H_2O}$	Structure	E_{BE}	$\sum E_{HNO...H_2O}$	$\sum E_{H_2O...H_2O}$
1AH	-5.10	5.11	-	**3KH**	-18.28	15.72	6.61
1BH	-3.91	3.93	-	**3LH**	-15.04	9.74	5.96
1CH	-2.93	2.93	-	**3MH**	-14.77	11.59	3.38
2AH	-14.06	11.17	6.64	**3NH**	-13.39	9.00	4.69
2BH	-13.52	10.36	6.28	**4AH**	-34.49	4.51	33.46
2CH	-10.80	5.36	5.68	**4BH**	-33.91	4.17	33.09
2DH	-9.27	9.55	-	**4CH**	-33.53	6.65	29.86
2EH	-9.03	5.09	3.68	**4DH**	-33.39	12.76	24.63
2FH	-8.66	8.93	-	**4EH**	-31.83	9.36	27.10
2GH	-7.45	2.65	4.80	**4FH**	-31.52	4.10	31.74
3AH	-24.02	11.89	15.30	**4GH**	-31.48	9.15	26.79
3BH	-23.43	11.65	15.77	**4HH**	-31.08	3.25	31.26
3CH	-22.08	6.04	20.54	**4IH**	-30.92	10.85	22.66
3DH	-21.25	5.28	20.77	**4JH**	-30.80	2.99	31.71
3EH	-21.25	8.76	14.46	**4KH**	-30.64	13.33	20.73
3FH	-21.01	3.59	20.63	**4LH**	-27.52	15.70	15.26
3GH	-20.16	3.90	20.97	**4MH**	-25.56	9.92	20.78
3HH	-20.09	10.86	13.29	**4NH**	-24.68	15.74	13.50
3IH	-19.41	3.02	20.91	**4OH**	-24.12	16.78	11.72
3JH	-19.35	11.86	11.54	**4PH**	-23.40	18.19	9.93

In the case of HNO(H_2O)$_2$ complexes, the calculated E_{BE} values are in a range from −7.45 to −14.06 kcal/mol. Out of the seven different isomers obtained, the more stable structures **2AH** and **2BH** (with E_{BE} values −14.06 and −13.52 kcal/mol, respectively) corresponds to a closed trimeric ring structure. Apart from the water…water HB interaction, the HBs formed by HNO are through H- and O-atoms in **2AH**, and H- and N-atoms in **2BH**. The $\sum E_{HNO...H_2O}$ and $\sum E_{H_2O...H_2O}$ values of these HBs are in the order of 10 – 11 kcal/mol and 6 – 7 kcal/mol, respectively, and the cooperativity contribution (E^{Coop}) towards these HBs is found to be in the order of 1 – 2 kcal/mol. The higher range of these energy values in comparison to the remaining isomers could explain the increased stability of **2AH** and **2BH**. The other trimeric ring configuration is present in **2EH**, wherein N- and O-atoms of HNO participated in HBs (HNO as HB acceptor) with water molecules. A lower $\sum E_{HNO...H_2O}$ value

(5.09 kcal/mol) calculated for these HBs, along with a lower $\sum E_{H_2O\ldots H_2O}$ value (3.68 kcal/mol), indicates that the HNO…water and water…water interactions are weaker in **2EH** than in **2AH**. This might account for the lesser stability of **2EH** (with E_{BE} = −9.03 kcal/mol) compared to **2AH**. The remaining complexes (from **2CH** to **2GH**) have acyclic structures and their lower $\sum E_{HNO\ldots H_2O}$ and $\sum E_{H_2O\ldots H_2O}$ values ranging from 2.65 to 9.55 kcal/mol and from 0.00 to 5.68 kcal/mol, respectively, explain the reduced stability of these complexes (E_{BE} values ranging from −7.45 to −10.80 kcal/mol) than **2AH** (E_{BE} = −14.06 kcal/mol). In addition, the lower E^{Coop} values noted in these complexes (range from −0.33 to 0.59 kcal/mol) also reveal the same. It should be noted that in **2CH** and **2GH**, only one atom of HNO is primarily involved in the HB interaction with water, which is H-atom in **2CH** (with an energy of 5.36 kcal/mol) and O-atom in **2GH** (with an energy of 2.65 kcal/mol). This suggests that the HB formed by the H-atom of HNO is stronger than the HB formed by the O-atom of HNO. Furthermore, the negative E^{Coop} values (−0.33 kcal/mol) found for all HBs in **2GH** show that they are anti-cooperative. These anti-cooperative HBs indicate that they are weakened by surrounding HBs, and as a result, **2GH** is the least stable isomer (with E_{BE} = −7.45 kcal/mol).

In various isomers of $HNO(H_2O)_3$ complexes, the E_{BE} values fall in the range from −13.39 to −24.02 kcal/mol. Of the 14 geometries obtained, the majority are four or three-membered rings except for the least stable **3LH** and **3NH** complexes. In the more stable configurations **3AH** and **3BH**, the HB energies fall between 5.12 and 8.13 kcal/mol with higher cooperativity contribution in the order of 2 – 3 kcal/mol towards these HBs. The small energy difference between **3AH** and **3BH** (with E_{BE} values −24.02 and −23.43 kcal/mol, respectively) is possibly due to the comparable $\sum E_{HNO\ldots H_2O}$ (~11 kcal/mol) and $\sum E_{H_2O\ldots H_2O}$ (~15 kcal/mol) values. It is to be noted that the HNO form HBs with water molecules via H- and N-atoms in **3AH**, while H- and O-atoms of HNO participated in HBs with water molecules in **3BH**. For the other optimized configurations **3CH** to **3NH**, the HNO forms HB with water via one, two, or three of its atoms. As a result, $\sum E_{HNO\ldots H_2O}$ and $\sum E_{H_2O\ldots H_2O}$ fall in a broader range (from 3.02 to 15.72 kcal/mol and 3.38 to 20.97 kcal/mol, respectively), with E^{Coop} values ranging from −0.43 to 2.96 kcal/mol. It should be noted that the highest $\sum E_{HNO\ldots H_2O}$ is obtained for **3KH**, where all the atoms of HNO participated in HBs with water molecules, whereas the highest $\sum E_{H_2O\ldots H_2O}$ is for **3GH** with a cyclic water trimer cluster. Similar water trimeric rings are found in **3CH**, **3DH**, **3FH**, **3GH**, and **3IH**; all of these

complexes have $\sum E_{H_2O\ldots H_2O}$ values above 20 kcal/mol, but these complexes have a lower range of $\sum E_{HNO\ldots H_2O}$ values (from 3.02 to 6.04 kcal/mol). This demonstrates that the self-association of water molecules weakens HNO…water interaction. Nonetheless, HNO alters the formation of cyclic water trimer in the most stable isomers of $HNO(H_2O)_3$ category (in **3AH** and **3BH**), indicating that cross-association of water clusters with HNO is the energetically preferred configuration in $HNO(H_2O)_3$ category.

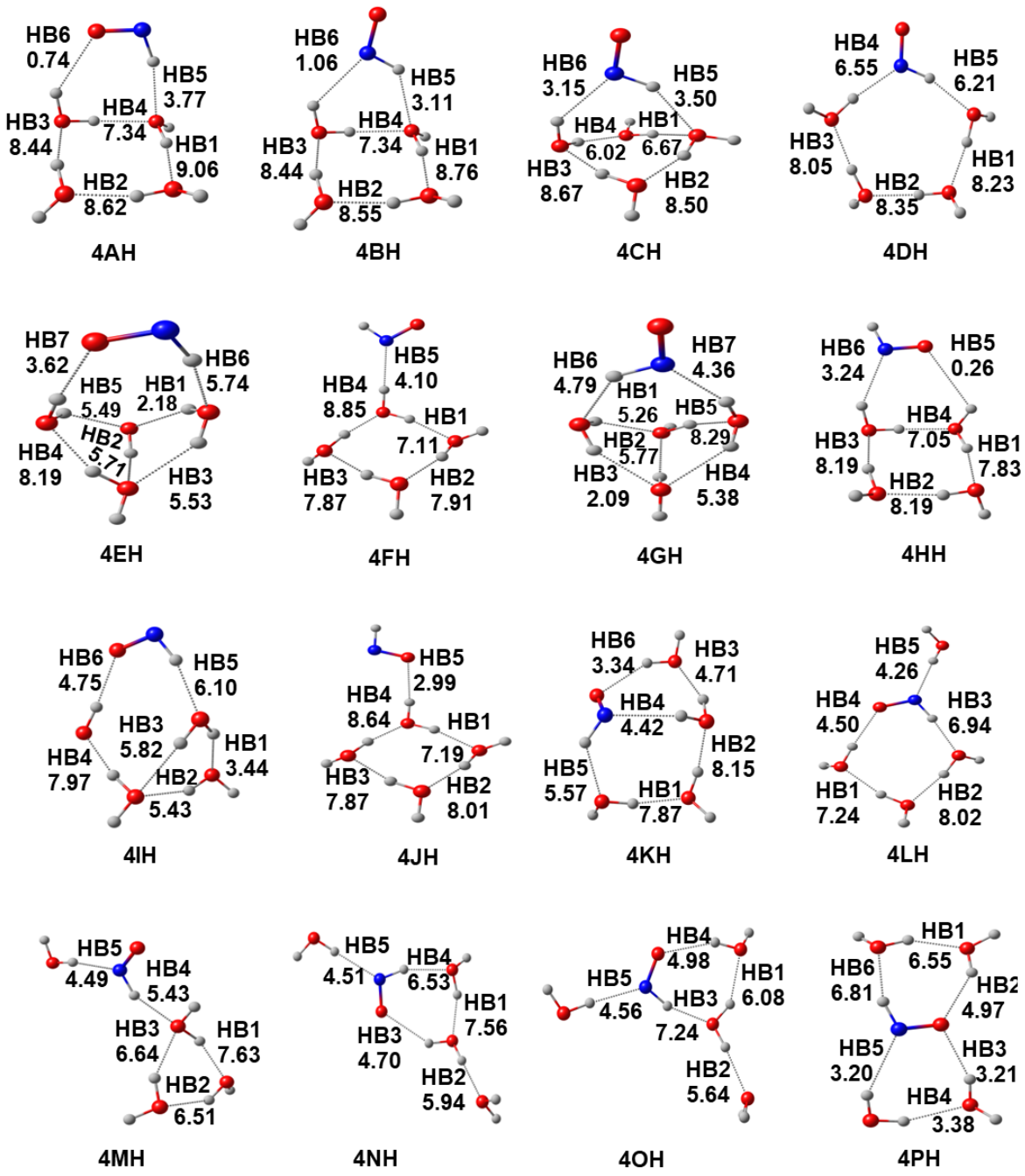

Figure 3.7 MTA-based energies of all individual HBs of $HNO(H_2O)_{n=4}$ complexes. All energy values are in kcal/mol.

Among the 16 optimized geometries of $HNO(H_2O)_4$ complexes, the water molecules form a tetrameric ring (self-association) and interact with HNO in **4AH**, **4BH**, **4CH**, **4EH**, **4FH**, **4GH**, **4HH**, and **4JH**. As a result, a higher range of $\sum E_{H_2O...H_2O}$ values (range from 26.79 to 33.46 kcal/mol) obtained for these complexes, whereas $\sum E_{HNO...H_2O}$ ranging from 2.99 to 9.36 kcal/mol. This indicates that the NO weakly interacted with water molecules due to the substantial strength of water...water interactions (with the self-association of water molecules). In other optimized configurations of the $HNO(H_2O)_4$ category, HNO disrupts the formation of water tetrameric rings, and cross-association of water clusters with HNO is observed. For **4DH**, a five-membered ring structure is formed by HNO and four water molecules. The remaining configurations of the $HNO(H_2O)_4$ category show fused tetrameric (composed of HNO and three water molecules) and trimeric rings (composed of HNO with two water molecules or three water molecules). These complexes have higher $\sum E_{HNO...H_2O}$ values (ranging from 9.92 to 18.19 kcal/mol) and lower $\sum E_{H_2O...H_2O}$ values (from 9.93 to 24.63 kcal/mol) than complexes with a water tetrameric ring. More importantly, all the atoms of HNO participate in HBs with water molecules in **4KH**, **4LH**, **4NH**, **4OH**, and **4PH** complexes, which account for their higher $\sum E_{HNO...H_2O}$ values (range from 13.33 to 18.19 kcal/mol). However, the E_{BE} values of these complexes varied significantly (from −23.40 to −30.64 kcal/mol), which may be due to a considerable drop in their $\sum E_{H_2O...H_2O}$ values (from 20.73 to 9.93 kcal/mol) because of weakened water…water interactions compared to other more stable isomers. Overall, the complexes with self-association of water clusters are the energetically preferred configuration in the $HNO(H_2O)_4$ category. The slightly higher E^{Coop} values (ranging between −0.31 and 4.38 kcal/mol) for water…water interactions than HNO…water interactions (range from −0.70 to 3.68 kcal/mol) also reveal the same.

As it is evident from the above discussions, the cyclic structures of HB networks in $HNO(H_2O)_n$ complexes are more stable than the noncyclic structures. In $HNO(H_2O)_{2\text{-}3}$ complexes, the strength and extent of both HNO…water and water…water HB interactions determine the most stable isomer. In $HNO(H_2O)_{n=4}$ complexes, the strength and extent of water…water HB interactions determine the most stable isomer. In HNO…water interactions, the individual energies of HBs formed by N- and O-atoms are in the range of 0.20 – 6.55 kcal/mol and 0.26 – 5.19 kcal/mol, respectively, which is lower than the individual energy values (ranging from 3.11 to 7.24 kcal/mol) obtained for HBs via H-atom of HNO. In general, both HBs of HNO…water and water…water interactions are cooperative in

$HNO(H_2O)_{n=2-4}$ complexes, and the negative cooperativity contributions towards HBs are not common.

Table 3.4 The relevant structural parameters *viz.* distance (in Å) and bond angle (in degree), energy in complex (E_{Int}^{MTA}), energy in dimer (E^{Dimer}), and cooperativity contribution (E^{Coop}) of all individual HBs in $HNO(H_2O)_{n=1-4}$ complexes. All energy values are in kcal/mol.

Complex	Interaction Labels	Distance of interaction	Bond angle	E_{Int}^{MTA}	E^{Dimer}	E^{Coop}
1AH	HB1	2.17	131	-	5.11	-
1BH	HB1	2.12	166	-	3.93	-
1CH	HB1	2.13	174	-	2.93	-
2AH	HB1	2.02	157	6.02	4.20	1.83
	HB2	2.07	155	5.15	3.32	1.83
	HB3	1.88	153	6.64	4.81	1.83
2BH	HB1	2.20	124	5.01	3.56	1.46
	HB2	2.10	144	5.35	3.89	1.46
	HB3	1.92	153	6.28	4.83	1.46
2CH	HB1	2.06	140	5.36	4.78	0.59
	HB2	1.91	178	5.68	5.10	0.59
2DH	HB1	2.09	173	4.39	3.86	0.53
	HB2	2.03	138	5.16	4.64	0.53
2EH	HB1	2.46	149	2.71	2.88	-0.17
	HB2	2.17	149	2.38	2.55	-0.17
	HB3	2.03	161	3.68	3.85	-0.17
2FH	HB1	2.10	136	3.67	3.20	0.48
	HB2	2.11	169	5.26	4.78	0.48
2GH	HB1	2.17	169	2.65	2.98	-0.33
	HB2	1.98	174	4.80	5.13	-0.33
3AH	HB1	1.97	162	6.16	3.85	2.31
	HB2	2.01	147	5.73	3.34	2.40
	HB3	1.82	168	7.72	4.96	2.76
	HB4	1.82	167	7.58	4.91	2.68
3BH	HB1	1.80	170	8.13	4.86	3.27
	HB2	1.81	165	7.64	4.85	2.79
	HB3	1.98	178	5.12	2.76	2.36
	HB4	1.95	172	6.53	3.69	2.84
3CH	HB1	1.84	154	7.67	4.71	2.96
	HB2	1.91	149	6.84	4.44	2.40
	HB3	2.19	134	6.03	4.10	1.92
	HB4	2.04	167	4.27	3.55	0.72
	HB5	2.23	144	1.77	1.62	0.16
3DH	HB1	1.87	153	7.29	4.81	2.47

	HB2	1.95	144	6.59	4.45	2.15
	HB3	1.96	147	6.89	4.87	2.02
	HB4	2.18	132	5.28	5.15	0.13
3EH	HB1	1.84	172	7.18	5.00	2.18
	HB2	1.84	172	7.28	5.10	2.18
	HB3	2.33	101	4.63	3.02	1.61
	HB4	2.03	152	4.13	2.53	1.61
3FH	HB1	1.85	154	7.65	4.83	2.82
	HB2	1.95	147	6.51	4.33	2.18
	HB3	2.05	144	6.47	4.68	1.79
	HB4	2.40	109	3.39	3.10	0.30
	HB5	2.80	105	0.20	0.55	-0.35
3GH	HB1	1.99	145	6.62	4.73	1.89
	HB2	1.94	148	6.72	4.50	2.22
	HB3	1.85	154	7.63	4.82	2.81
	HB4	2.11	171	3.90	3.68	0.21
3HH	HB1	1.80	161	7.52	4.79	2.73
	HB2	1.90	1.78	5.77	5.08	0.69
	HB3	2.17	148	4.91	3.27	1.64
	HB4	2.02	159	5.95	4.13	1.82
3IH	HB1	1.97	148	6.66	4.77	1.89
	HB2	1.94	148	6.75	4.49	2.26
	HB3	1.86	153	7.50	4.83	2.68
	HB4	2.09	175	3.02	2.92	0.10
3JH	HB1	1.95	149	6.15	4.83	1.33
	HB2	1.93	176	5.39	5.10	0.30
	HB3	1.95	159	6.67	4.01	2.66
	HB4	2.05	159	5.19	3.38	1.81
3KH	HB1	1.88	153	6.61	4.82	1.79
	HB2	1.96	157	6.53	3.99	2.53
	HB3	2.10	175	4.31	3.86	0.46
	HB4	2.15	150	4.88	3.31	1.57
3LH	HB1	2.11	162	3.97	3.18	0.79
	HB2	1.99	149	5.77	4.30	1.47
	HB3	1.89	179	5.96	5.03	0.93
3MH	HB1	2.04	158	3.38	3.61	-0.23
	HB2	2.39	151	2.97	2.74	0.23
	HB3	2.05	143	5.32	4.47	0.85
	HB4	2.09	156	3.30	3.02	0.27
3NH	HB1	2.11	135	5.12	4.81	0.31
	HB2	2.15	164	3.88	3.83	0.05
	HB3	1.99	173	4.69	5.13	-0.43
4AH	HB1	1.74	168	9.06	4.67	4.38

	HB2	1.77	165	8.62	4.76	3.85
	HB3	1.78	165	8.44	4.81	3.63
	HB4	1.89	161	7.34	4.86	2.48
	HB5	2.12	166	3.77	3.44	0.33
	HB6	2.27	141	0.74	1.17	-0.43
4BH	HB1	1.76	168	8.76	4.74	4.02
	HB2	1.77	166	8.55	4.77	3.78
	HB3	1.78	165	8.44	4.80	3.64
	HB4	1.91	161	7.34	4.85	2.48
	HB5	2.26	134	3.11	2.95	0.16
	HB6	2.34	129	1.06	1.33	-0.27
4CH	HB1	1.88	158	6.67	4.73	1.94
	HB2	1.75	161	8.50	4.32	4.19
	HB3	1.75	164	8.67	4.64	4.03
	HB4	1.90	157	6.02	4.19	1.82
	HB5	2.23	149	3.50	3.08	0.42
	HB6	2.26	137	3.15	2.67	0.48
4DH	HB1	1.77	175	8.23	4.83	3.40
	HB2	1.77	176	8.35	4.80	3.55
	HB3	1.78	174	8.05	4.82	3.22
	HB4	1.92	170	6.55	3.66	2.89
	HB5	1.92	163	6.21	3.09	3.12
4EH	HB1	2.10	145	2.18	2.42	-0.24
	HB2	1.98	140	5.71	4.21	1.50
	HB3	2.13	143	5.53	4.02	1.51
	HB4	1.80	155	8.19	4.71	3.48
	HB5	2.18	135	5.49	4.22	1.26
	HB6	1.99	164	5.74	3.64	2.10
	HB7	2.03	174	3.62	2.49	1.13
4FH	HB1	1.84	164	7.11	4.50	2.61
	HB2	1.81	166	7.91	4.89	3.02
	HB3	1.81	165	7.87	4.46	3.41
	HB4	1.75	169	8.85	4.73	4.12
	HB5	2.11	180	4.10	3.84	0.26
4GH	HB1	2.17	141	5.26	3.99	1.27
	HB2	1.96	142	5.77	4.23	1.53
	HB3	2.12	145	2.09	2.40	-0.31
	HB4	2.23	134	5.38	4.12	1.27
	HB5	1.79	156	8.29	4.74	3.55
	HB6	2.14	137	4.79	3.09	1.70
	HB7	2.06	159	4.36	3.01	1.35
4HH	HB1	1.81	164	7.83	4.90	2.93
	HB2	1.80	167	8.19	4.87	3.32

	HB3	1.79	164	8.19	4.35	3.84
	HB4	1.82	168	7.05	4.15	2.90
	HB5	2.78	118	0.26	0.97	-0.70
	HB6	2.27	147	3.24	3.01	0.23
4IH	HB1	1.96	152	3.44	2.64	0.80
	HB2	1.91	150	5.43	4.19	1.24
	HB3	2.23	136	5.82	3.81	2.01
	HB4	1.76	170	7.97	4.74	3.23
	HB5	1.94	164	6.10	3.45	2.65
	HB6	1.97	174	4.75	2.58	2.17
4JH	HB1	1.85	163	7.19	4.56	2.64
	HB2	1.80	167	8.01	4.91	3.10
	HB3	1.80	165	7.87	4.42	3.44
	HB4	1.76	168	8.64	4.73	3.91
	HB5	2.09	175	2.99	2.95	0.04
4KH	HB1	1.81	170	7.87	4.87	3.01
	HB2	1.79	168	8.15	4.79	3.36
	HB3	1.94	155	4.71	3.52	1.19
	HB4	2.31	134	4.42	2.78	1.64
	HB5	2.07	131	5.57	3.08	2.49
	HB6	2.09	149	3.34	2.60	0.74
4LH	HB1	1.82	165	7.24	4.88	2.36
	HB2	1.79	170	8.02	4.84	3.18
	HB3	1.89	173	6.94	3.37	3.57
	HB4	2.02	176	4.50	2.88	1.62
	HB5	2.09	172	4.26	3.80	0.46
4MH	HB1	1.84	156	7.63	4.74	2.89
	HB2	1.95	143	6.51	4.41	2.10
	HB3	2.02	144	6.64	4.78	1.86
	HB4	2.05	142	5.43	4.51	0.92
	HB5	2.08	170	4.49	3.86	0.62
4NH	HB1	1.80	161	7.56	4.79	2.77
	HB2	1.89	179	5.94	5.06	0.88
	HB3	2.29	142	4.70	3.09	1.60
	HB4	1.95	159	6.53	3.92	2.60
	HB5	2.08	179	4.51	3.82	0.69
4OH	HB1	1.95	148	6.08	4.82	1.26
	HB2	1.91	174	5.64	5.12	0.52
	HB3	1.88	162	7.24	3.56	3.68
	HB4	2.13	154	4.98	3.45	1.53
	HB5	2.08	174	4.56	3.85	0.72
4PH	HB1	1.87	154	6.55	4.82	1.74
	HB2	2.20	147	4.97	3.26	1.71

HB3	2.09	156	3.21	2.76	0.44
HB4	2.05	159	3.38	3.62	-0.24
HB5	2.42	149	3.20	2.94	0.26
HB6	1.94	159	6.81	3.94	2.87

3.4.6 Comparison between $NO^-(H_2O)_n$ and $HNO(H_2O)_n$ complexes

The most stable microhydrated complexes of NO^- are found as cyclic or cage-like structures, which might be due to the strong HBs present between NO^- and water. Thus cross-association is energetically preferred in $NO^-(H_2O)_n$ complexes. Microhydration frameworks of HNO show that the cyclic structure formed by HNO and water molecules (cross-association) is energetically more favorable for small clusters (n = 1–3), whereas self-association of water molecules is energetically preferred for larger clusters (n = 4) wherein HNO interact with a tetrameric water ring. The E_{BE} values obtained for $NO^-(H_2O)_n$ (in a range from −17.17 to −63.87 kcal/mol) and $HNO(H_2O)_n$ (ranging between −2.93 and −33.91 kcal/mol) complexes suggest that microhydrated complexes of NO^- are more stable than HNO. Figure 3.8 illustrates the higher E_{BE} values of the most stable isomers of $NO^-(H_2O)_n$ as compared to $HNO(H_2O)_n$ with various numbers (n = 1 – 4) of water molecules.

The free energy of the formation (ΔG) is a useful parameter for predicting the thermodynamic stability of microhydrated complexes. Table 3.5 provides the ΔG values (calculated at 298 K and 1 atm) of the most stable complexes of $NO^-(H_2O)_{n=1\text{-}4}$ and $HNO(H_2O)_n$. ΔG values of $NO^-(H_2O)_{n=1\text{-}4}$ complexes are ranging from −8.97 to −19.90 kcal/mol. The negative ΔG values indicate that the formation of microhydrated complexes of NO^- ions is favored at room temperature and pressure, but it does not mean that these clusters will be formed in the atmosphere regularly. If the concentrations of the species are considered, the concentrations of the clusters would be quite low. It is also to be noted that the ΔG values become more negative with the increase in cluster size, which is consistent with the generally observed trend of ΔG values of microhydrated complexes of charged species.[219,221] On the other hand, most stable complexes of $HNO(H_2O)_n$ have positive ΔG values ranging from 4.11 to 6.86 kcal/mol. This implies that neutral HNO water clusters are stable only at very low temperatures and pressure, and thus occur in the upper atmosphere. Previous studies have shown that the astronomically relevant molecules including HNO are adsorbed into dust grains coated with water ice in the interstellar medium at low temperature (10 K).[213]

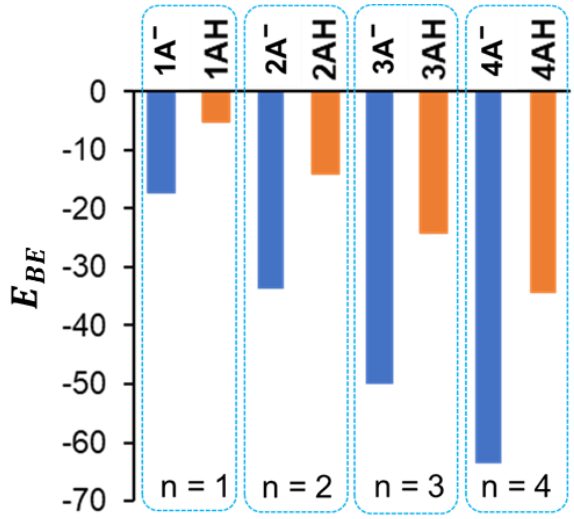

Figure 3.8 A comparison of E_{BE} (in kcal/mol) calculated by supermolecular approach of most stable isomers of $NO^{-}(H_2O)_{n=1-4}$ and $HNO(H_2O)_{n=1-4}$.

Table 3.5 ΔG values (in kcal/mol) at 298.15 K and 1 atm of most stable complexes of $NO^{-}(H_2O)_{n=1-4}$ (anionic) and $HNO(H_2O)_n$ (neutral).

$NO^{-}(H_2O)_n$ complex (anionic)	ΔG	$HNO(H_2O)_n$ complex (neutral)	ΔG
1A⁻	−8.97	**1AH**	4.11
2A⁻	−14.14	**2AH**	6.21
3A⁻	−17.44	**3AH**	6.35
4A⁻	−19.90	**4AH**	6.86

On comparing the HBs formed via N- and O-atoms ((NO)···H interactions) of NO^{-} and HNO with water, the topological parameter $\rho(r)$ obtained from QTAIM analysis (see Figure 3.2), as well as the $E^{(2)}$ energy estimated for orbitals overlap in NBO analysis suggest that the (NO)···H HBs in NO^{-}…water is much stronger than in the HNO…water interactions (see Figure 3.3 and Figure 3.4). Further, the MTA-based energies of the individual (NO)···H HBs present in $NO^{-}(H_2O)_{n=1-4}$ and $HNO(H_2O)_{n=1-4}$ complexes fall in the range of 11.11 – 16.56 kcal/mol and 0.20 – 6.55 kcal/mol, respectively (see Table 3.2 and Table 3.4). This also reveals that the (NO)···H HBs of NO^{-} are much stronger than those in HNO…water interactions. However, negative values of cooperativity contribution (E^{Coop}) are obtained for (NO)···H HBs of $NO^{-}(H_2O)_{n=2-4}$ complexes (ranging between −0.90 and −4.34 kcal/mol). This indicates that HBs in NO^{-}…water interactions are less stabilized in the complex than in their isolated dimer. For (NO)···H HBs of HNO in $HNO(H_2O)_{n=2-4}$ complexes, E^{Coop} values

ranging between −0.70 and 3.68 kcal/mol, this shows that the HBs in HNO…water interactions are more stabilized in the complex than in their isolated dimer.

3.5 Conclusions

In this study, we examined the HBs present in NO^-…water as well as in HNO…water interactions with the help of MESP, QTAIM, and NBO analyses. The electron donor (HB acceptor) sites on NO^- and HB donor as well as HB acceptor sites on HNO are identified with MESP analysis. QTAIM molecular graphs revealed that the HBs in NO^-…water interactions are much stronger than HBs in HNO…water interactions. The orbitals involved in different HBs in NO^-…water and HNO…water interactions are demonstrated by NBO analysis.

Further, we investigated the energies and cooperativity contributions of all HBs in the microhydrated networks of NO^- and HNO, i.e., $NO^-(H_2O)_{n=1-4}$ and $HNO(H_2O)_{n=1-4}$, respectively, with the help of MTA-based calculations. In $NO^-(H_2O)_{n=1-4}$ complexes, the individual energies of HBs formed via N- and O-atoms are comparable, with energies ranging from 11.34 to 16.56 kcal/mol and from 11.11 to 16.39 kcal/mol, respectively. The strength of NO^-…water interactions (total energies of individual HBs, i.e., $\sum E_{NO^-\ldots H_2O}$) show an increase in $NO^-(H_2O)_n$ complexes with an increase in cluster size from one to four ($\sum E_{NO^-\ldots H_2O}$ increased from 17.91 to 51.53 kcal/mol). These strong NO^-…water interactions result in cross-associated HB networks in $NO^-(H_2O)_{n=2-4}$ complexes. However, the negative E^{Coop} values (anti-cooperativity) obtained for HBs (range between −0.70 and −3.68 kcal/mol) in NO^-…water interactions of $NO^-(H_2O)_{n=2-4}$ complexes indicate that they are less stabilized in the complex than in their isolated dimer. Though HBs in the NO^-…water interactions are much stronger than that of HNO…water interactions. Further, the HBs in water…water interactions in $NO^-(H_2O)_n$ complexes show anti-cooperativity in complexes with smaller cluster sizes (n = 2 – 3), whereas they are primarily cooperative with larger water clusters (n = 4).

Among the three possible interactions of HNO (via H-, N-, and O-atoms) with a single water molecule, the HB energies are in the order of 2 – 5 kcal/mol. In $HNO(H_2O)_{n=2-4}$ complexes, the HBs via H-atom have an energy range of 3.11 – 7.24 kcal/mol, while the energies of HBs formed via N- and O-atoms are in the range of 0.20 – 6.55 kcal/mol and 0.26 – 5.19 kcal/mol, respectively. Herein, the highest HB energy values of 7.24 kcal/mol (via H-atom) and 6.55 kcal/mol (via N-atom) are obtained for $HNO(H_2O)_n$ complexes with cluster size four. The higher HB energies noted with increased water cluster size in $HNO(H_2O)_n$

complexes emphasize the strengthening of HNO…water interactions with increased cluster size. However, a significant $\sum E_{H_2O\ldots H_2O}$ value (33.46 kcal/mol) in comparison to $\sum E_{HNO\ldots H_2O}$ (4.51 kcal/mol) is obtained for the most stable isomer in $HNO(H_2O)_{n=4}$ category. Hence, the self-association of water molecules is energetically more favored for n = 4, whereas, cross-associated HB networks is energetically preferred for $HNO(H_2O)_n$ complexes with n = 2 and 3. In general, the strength of both HNO…water and water…water interactions increased with an increase in cluster size. The larger positive values of cooperativity contribution (range from −0.70 to 4.38 kcal/mol) obtained for HBs in $HNO(H_2O)_{n=2\text{-}4}$ complexes also reveal the same.

When comparing the HBs formed via N- and O-atoms (i.e., (NO)···H HBs) in $NO^-(H_2O)_n$ and $HNO(H_2O)_n$ complexes, the (NO)···H HBs of NO^- (with energies in the range of 11.11 – 16.56 kcal/mol) are much stronger than those in HNO…water interactions (energies ranging from 0.20 to 6.55 kcal/mol). This implies that NO^- is a stronger HB acceptor than HNO's -N=O functionality due to the additional charge on NO. Overall, it appears that the microhydrated complexes of NO^- are more stable than the HNO since the binding energy values of $NO^-(H_2O)_n$ complexes (which range from −17.17 to −63.87 kcal/mol) are higher than those of $HNO(H_2O)_n$ complexes (ranging between −2.93 and −33.91 kcal/mol). This is also attributed to the additional charge on NO in $NO^-(H_2O)_n$ complexes than neutral $HNO(H_2O)_n$ complexes.

Publications based on this chapter:

1. **Thufail M. Ismail**; Patkar, D.; Sajith, P. K.; Deshmukh, M. M. Interplay of Hydrogen, Pnicogen, and Chalcogen Bonding in $X(H_2O)_{n=1\text{-}5}$ (X = NO, NO^+, and NO^-) Complexes: Energetics Insights via Molecular Tailoring Approach. *The Journal of Physical Chemistry A* **2023**, 127, 10360–10374.

2. **Thufail M. Ismail**; Patkar, D.; Sajith, P. K.; Deshmukh, M. M. Hydrogen Bond Strengths in Microhydrated Clusters of HNO and HONO: Energetic Insights via Molecular Tailoring Approach. ***New Journal of Chemistry*** (communicated).

Chapter 4

Energetics of Hydrogen Bonding Interactions in $HONO(H_2O)_{n=1\text{-}4}$ Complexes

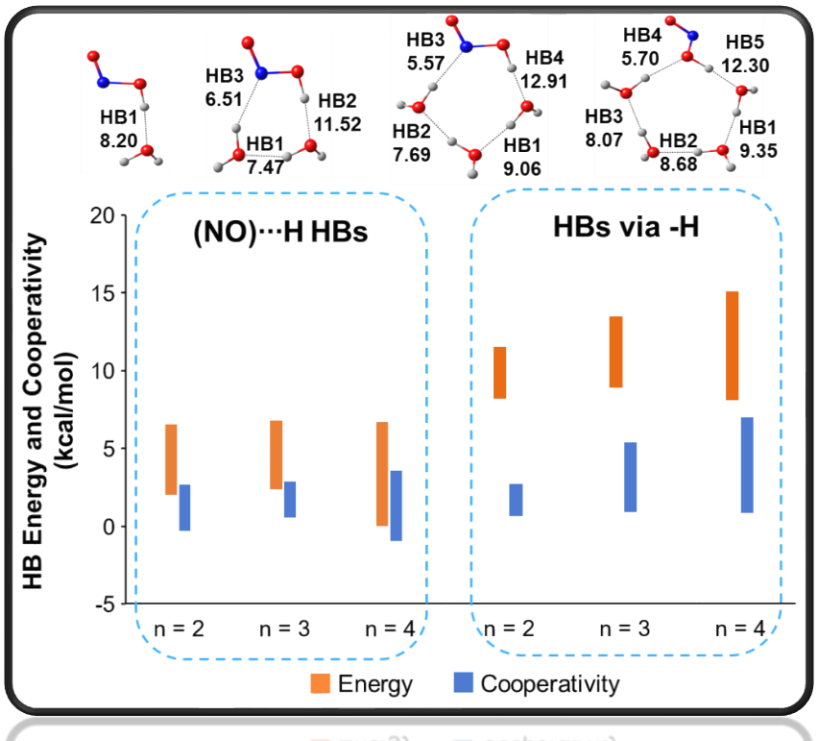

4.1 Abstract

Hydration of HONO plays important roles in various atmospheric events. The present study is an attempt to investigate the hydrogen bonding (HB) interactions in microhydrated networks (up to four water molecule) of HONO (i.e., $HONO(H_2O)_{n=1-4}$) at the MP2/6-311++G(d,p) level. The HBs are probed by molecular electrostatic potential (MESP), quantum theory of atoms in molecules (QTAIM), and natural bond orbital (NBO) analyses. Several HBs are possible between HONO and water due to four atoms and *cis-trans* isomerism in HONO, this includes (NO)···H HBs (formed via -N=O functionality) and other HBs (formed via -OH functionality). Further, the energies and cooperativity contribution of all individual HBs in $HONO(H_2O)_{n=1-4}$ complexes are examined with the help of molecular tailoring approach-based (MTA-based) method. The HBs formed via H-atom of HONO (energy varies in a range of 8.03 – 15.08 kcal/mol) are much stronger than the (NO)···H HBs of HONO (range from 0.01 to 6.77 kcal/mol). Among (NO)···H interactions, the HBs formed by N- and O-atoms have comparable strength (with energies ranging from 0.01 to 6.77 kcal/mol and from 1.09 to 6.25 kcal/mol, respectively). In addition, the greater positive values of cooperativity contribution (E^{Coop}; ranging from 0.61 to 7.01 kcal/mol) for HBs via H-atom of HONO than that of (NO)···H HB interactions (E^{Coop} in the range from −0.95 to 3.60 kcal/mol) in $HONO(H_2O)_{n=2-4}$ complexes also demonstrate the similar trend. The HB energies of water…water interactions are in a range of 2.71 – 9.75 kcal/mol. In general, the energies of all HBs in $HONO(H_2O)_{n=2-4}$ complexes increased with the increase in cluster size. Overall, the strong HONO…water interactions result in cross-associated HB networks in most stable complexes of $HONO(H_2O)_{n=2-4}$.

4.2 Introduction

Hydrated systems of oxidised species of NO (*viz.* NO^+ and HONO) have been studied in variety of atmospheric events. Formation of HONO from the reaction between NO^+ and a set of water molecules have been reported in many experimental as well as theoretical studies.[111–113,222] The size and shape of microhydrated networks have a pronounced influence on the formation of HONO. It has been reported that NO^+ interacts via N-atom with the O-atom of water molecule in their $NO^+(H_2O)$ complexes,[111,223] however the interaction between NO^+ and water is not well understood. On the other hand, studies on molecular clustering of HONO with other atmospheric species in the presence of water is well documented.[20,224] It is even predicted that molecular complexes of HONO with water clusters could be a site for

water condensation.[119] However, to the best of our knowledge, a systematic study on microhydration of HONO is not yet reported in the literature. It is evident from experimental as well as theoretical studies that hydrogen bond (HB) is formed between HONO and water in their dimer complexes.[22,225] In fact, energies and the cooperativity effect of individual HBs in microhydrated networks are beneficial for understanding the different reactions mediated by water.[79]

The objective of this work is to investigate (NO)···H HB (formed via N- and O-atoms in -N=O of HONO) interactions in the oxidised form of NO. For this purpose, HB interactions present in microhydrated complexes of HONO (up to four water molecules) are selected for this study. The energies and cooperativity of individual HB interactions in the microhydrated complexes of HONO are estimated with the help of molecular tailoring approach (MTA) based calculations. It was previously reported that NO^+ interacts with the O atom of water through the N atom and there is no HB interaction between NO^+ and water. This is further verified using MESP, QTAIM, and NBO analysis, and we compared the NO^+...water and HONO...water interactions.

4.3 Computational methods

The structures of all microhydrated complexes were simulated using MP2/6-311++G(d,p) level of theory with the Gaussian 16 program package.[192] For optimization, initial structures were modelled according to existing literature data of similar molecules and chemical intuitions. For larger clusters, a bottom-up approach is also applied, e.g. the $HONO(H_2O)_3$ is modelled by adding one H_2O to $HONO(H_2O)_2$ through different sides. Similarly, the top-down approach also aided to find any missed configurations of complexes. The optimized geometries were confirmed as local minima by frequency analysis due to the absence of imaginary frequencies. The Gibbs free energy change (ΔG) associated with the formation of the most stable structures of these complexes at 298 K and 1 atm is calculated.

For improved energetics, single-point calculations are carried out at the MP2 method by employing the aug-cc-pVTZ basis set for estimating the binding energy as well as MTA-based noncovalent interaction energies of all complexes. The MESP, QTAIM, and NBO analyses were also performed at the MP2/aug-cc-pVTZ//MP2/6-311++G(d,p) level of theory. AIMAll software is used for QTAIM analysis.[193] MESP analysis is carried out using Multiwfn software,[194] and visualized using VMD software.[195] NBO analysis is carried out using NBO version 3.1 implemented in Gaussian 16 software,[196] and the results are

visualized using Chemcraft software.[197] The binding energy (E_{BE}) of HONO(H_2O)$_n$ clusters is calculated by the supermolecular approach using Eq. 4.1.[202,216]

$$E_{BE} = E_{cluster} - (E_{HONO} + nE_{H_2O}) \quad \text{(Eq. 4.1)}$$

In the above equation, the terms $E_{cluster}$, E_{HONO}, and E_{H_2O} denote the total energy of the HONO(H_2O)$_n$ cluster, the energy of the HONO monomer, and the energy of a water monomer multiplied by n, which is the number of water molecules in a given cluster under consideration.

Further, the relative energies (represented by ΔE) are calculated for all the isomers with respect to the energy of the most stable one in their HONO(H_2O)$_n$ category (n = 1 – 4). For the sake of simplicity, the microhydrated complexes of HONO is written simply as **OH** and the number of water molecules (n) in the water cluster is denoted by **Wn**. Thus, the HONO(H_2O)$_n$ is abbreviated as **OHWn**. Additionally, the different isomers of **OHWn** are designated with natural numbers (**1**, **2**, **3**, etc.) based on their order of stability (ΔE values). For instance, the most stable isomer of HONO(H_2O)$_2$ complex is named **OHW2-1**, and other isomers are **OHW2-2**, **OHW2-3**, etc., depending on their decreasing stability (increasing ΔE values).

4.4 Results and discussion

The following sections discuss the findings of MESP, QTAIM, and NBO analyses on NO^+(H_2O) and HONO(H_2O) dimer complexes.

4.4.1 MESP analysis

MESP features can be employed to understand the interaction sites of molecules.[202,203] The electrostatic potential on molecular surfaces (at an isodensity value of 0.001 au) of NO^+ and water is shown in Figure 4.1(a). The V_{max} regions (195.5 kcal/mol) are located as a cylindrical belt around the N–O bond axis that is near the N-atom of NO^+. The V_{max} value on NO^+ is reduced to 176.1 kcal/mol in the interacted complex of NO^+ and H_2O. Herein, the interaction associated with the electron-deficient (V_{max}) region on the N-atom and electron-dense region of water can be called a pnicogen bond (PB).[207,208] Thus, NO^+…water interaction is a pnicogen bonding (PB) interaction.

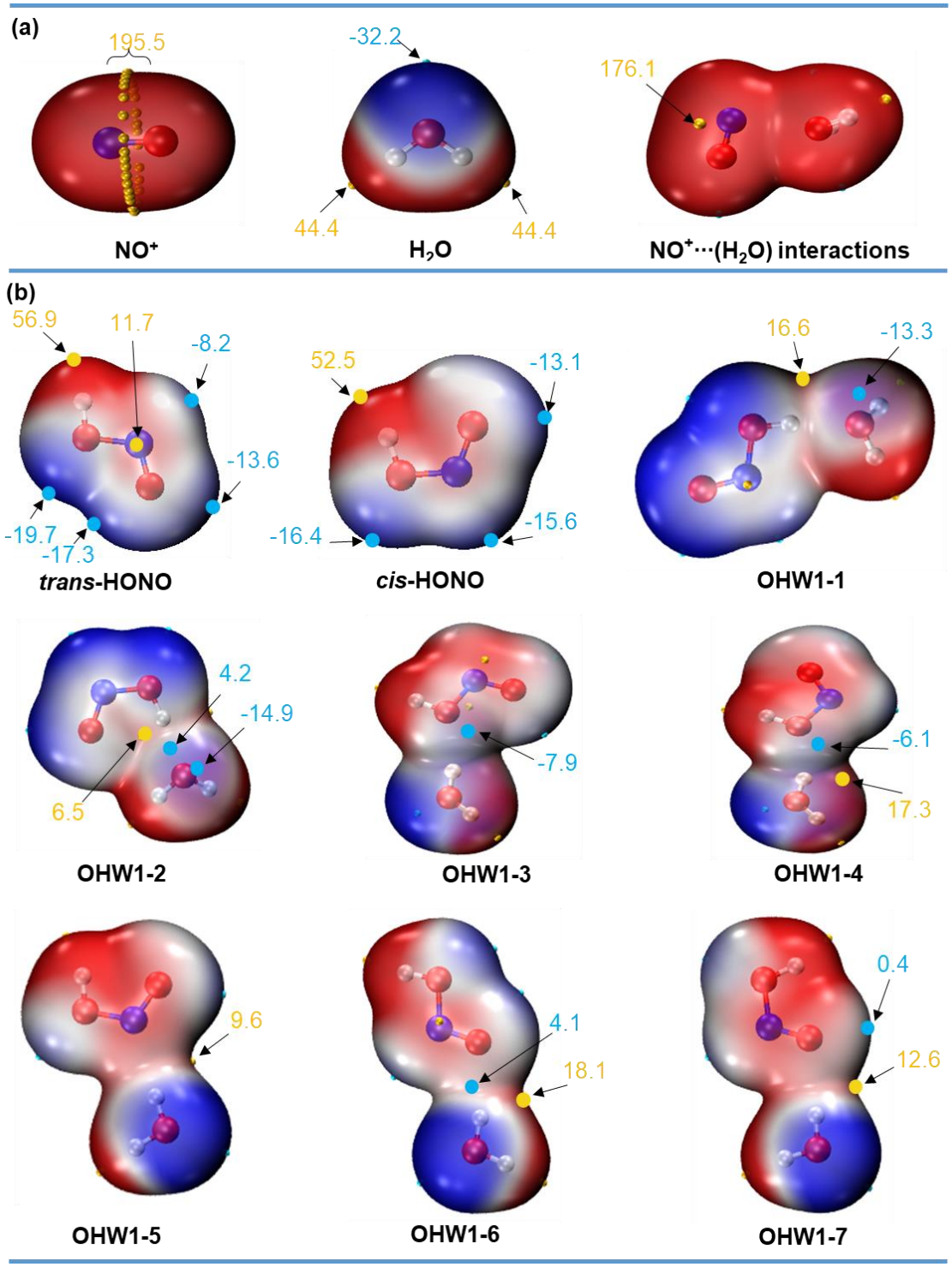

Figure 4.1 Electrostatic potential mapped on isodensity molecular surface (at 0.001 au) of monomers and dimers of (a) $NO^+(H_2O)$ complex (b) $HONO(H_2O)$ complexes. The positions of V_{min} and V_{max} at interacting sites are represented by cyan and golden spheres, respectively, and the corresponding values are shown in kcal/mol. The color ranges: blue for negative potential and red for positive potential.

For HONO(H_2O) dimer complexes (see Figure 4.1(b)), a reduction in V_{max} value near the H-atom of *trans*-HONO is observed (from 56.9 to 16.6 kcal/mol) due to HB interaction with water in **OHW1-1**, implying that HONO acts as HB acceptor in this interaction. Similarly, the H-atom of *cis*-HONO formed HB with water in **OHW1-2** with a reduction in V_{max} value from 52.5 to 6.5 kcal/mol. Hence, HONO acts as HB donor (electron acceptor) in the HB interactions of **OHW1-1** and **OHW1-2**. On the other hand, V_{min} sites near O-atom in -OH of HONO interact with water in **OHW1-3** and **OHW1-4**, a reduction in V_{min} value from −19.7 to −7.9 kcal/mol and from −16.4 to −6.1 kcal/mol, is observed for *trans*- (in **OHW1-3**) and *cis*-forms (in **OHW1-4**) of HONO, respectively. In **OHW1-5**, the V_{min} value of −15.6 near the N-atom of *cis*-HONO disappeared when HB formed via N-atom with water. In the case of **OHW1-6** and **OHW1-7**, V_{min} sites near O-atom in -N=O functionality of HONO interact with water, a change in V_{min} value from −13.6 to 4.1 kcal/mol and from −13.1 to −0.4 kcal/mol, is observed for *trans*- (in **OHW1-6**) and *cis*-forms (in **OHW1-7**) of HONO, respectively. The change in V_{min} values from more negative to less negative or positive values on HONO when interacting with water indicates that the HONO acts as HB acceptor (electron donor) in complexes of **OHW1-3**, **OHW1-4**, **OHW1-5**, **OHW1-6**, and **OHW1-7**.

4.4.2 QTAIM analysis

QTAIM plot of $NO^+(H_2O)$ dimer complex is displayed in Figure 4.2(a). The molecular graph of $NO^+(H_2O)$ complex shows that the N-atom of NO^+ interacts with O-atom water. Thus, this bond path confirms the PB interaction in NO^+ and water. The electron density ($\rho(r)$), Laplacian of electron density ($\nabla^2\rho(r)$), and the total electron energy density ($H(r)$) values at bcp on PB is 0.0309, 0.1233, and 0.0021 au, respectively. The positive $\nabla^2\rho(r)$ and $H(r)$ values suggest that the PB is a closed-shell interaction in the $NO^+(H_2O)$ complex.

For HONO(H_2O) dimer **OHW1-1** (see Figure 4.2(b)), the HB formed via H-atom of *trans*-HONO with O-atom of water has a $\rho(r)$ value (at bcp) of 0.0342 au. Similarly, in **OHW1-2**, the $\rho(r)$ value at HB formed via the H-atom of *cis*-HONO with the O-atom of water is 0.0339 au. In addition, the positive $\nabla^2\rho(r)$ and negative $H(r)$ values at bcp of these HBs suggest that they are a mix of closed-shell and shared-type HB interactions. On the other hand, HB formed via O-atom of -OH of HONO with water in **OHW1-3** (*trans*-HONO) and **OHW1-4** (*cis*-HONO), have $\rho(r)$ values of 0.0193 and 0.0182 au, respectively. In **OHW1-5**, the N-atom of *cis*-HONO participated in HB with a $\rho(r)$ value of 0.0141 au. In the case of **OHW1-6** (*trans*-HONO) and **OHW1-7**(*cis*-HONO), the HB formed via O-atom in -N=O

functionality of HONO with water have $\rho(r)$ values of 0.0136 and 0.0134 au, respectively. Based on the magnitudes of $\rho(r)$, the strength of HBs in HONO(H_2O) complexes are in the decreasing order of **OHW1-1**, **OHW1-2**, **OHW1-3**, **OHW1-4**, **OHW1-5**, **OHW1-6**, and **OHW1-7**. Further, the $\nabla^2\rho(r)$ and $H(r)$ values are positive for HBs in complexes **OHW1-3** to **OHW1-7**, indicating that these HBs are of closed-shell type interactions.

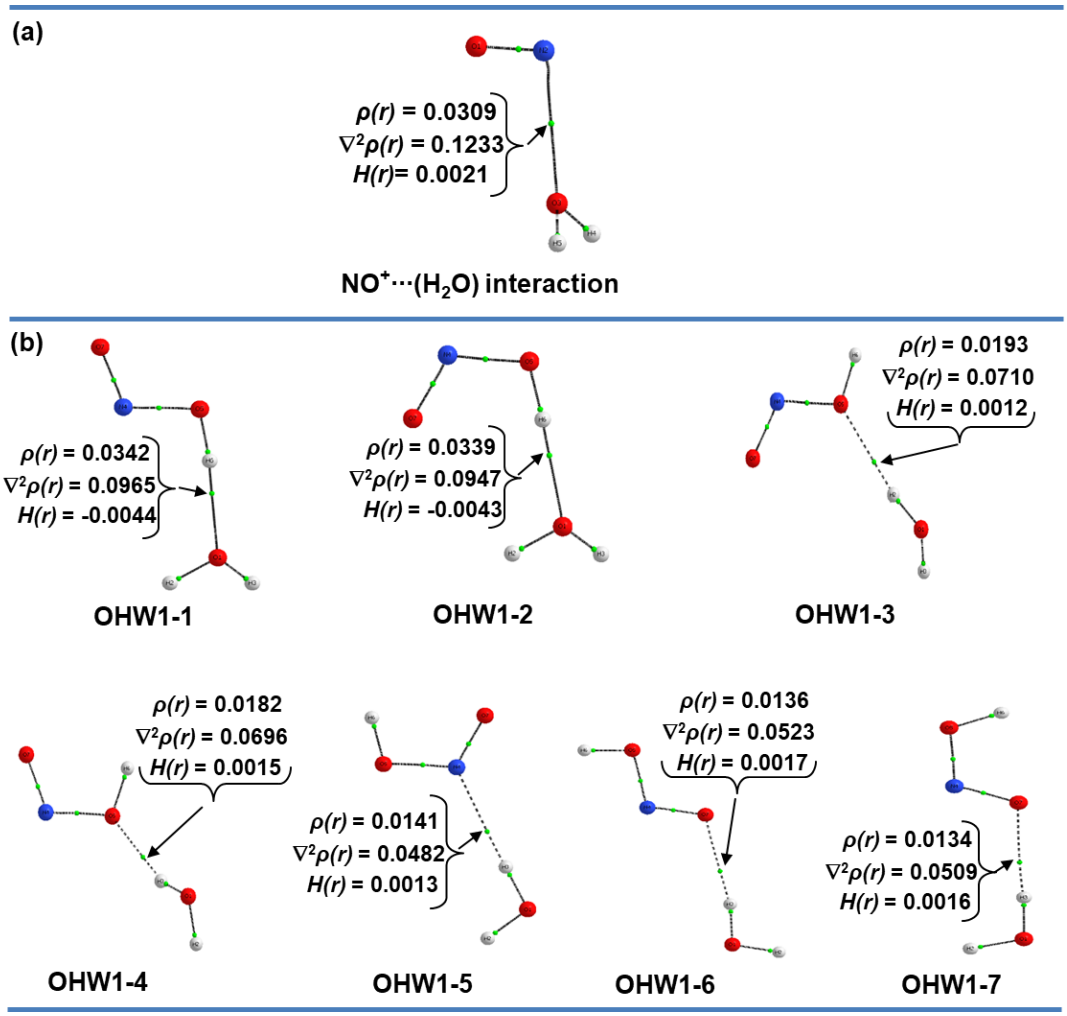

Figure 4.2 The QTAIM molecular graphs with values (in au) of QTAIM parameters at bcp (which is shown as small green spheres on each bond path) of relevant interaction in (a) $NO^+(H_2O)$ complex (b) HONO(H_2O) complexes.

4.4.3 NBO analysis

An NBO view of donor-acceptor orbitals involved in the PB interaction of $NO^+(H_2O)$ dimer and their stabilization energies ($E^{(2)}$; values greater than 0.1 kcal/mol are considered) are rendered in Figure 4.3(a). The interaction of lone pairs of water oxygen atom (lp(O)) with antibonding orbitals of N–O bond (π^*_{N-O}) confirms the PB interaction involved between NO^+

and water. The total stabilization ($E^{(2)}$) energy (sum of $E^{(2)}$ values of each orbital interaction) associated with the orbital interactions of PB is 6.45 kcal/mol.

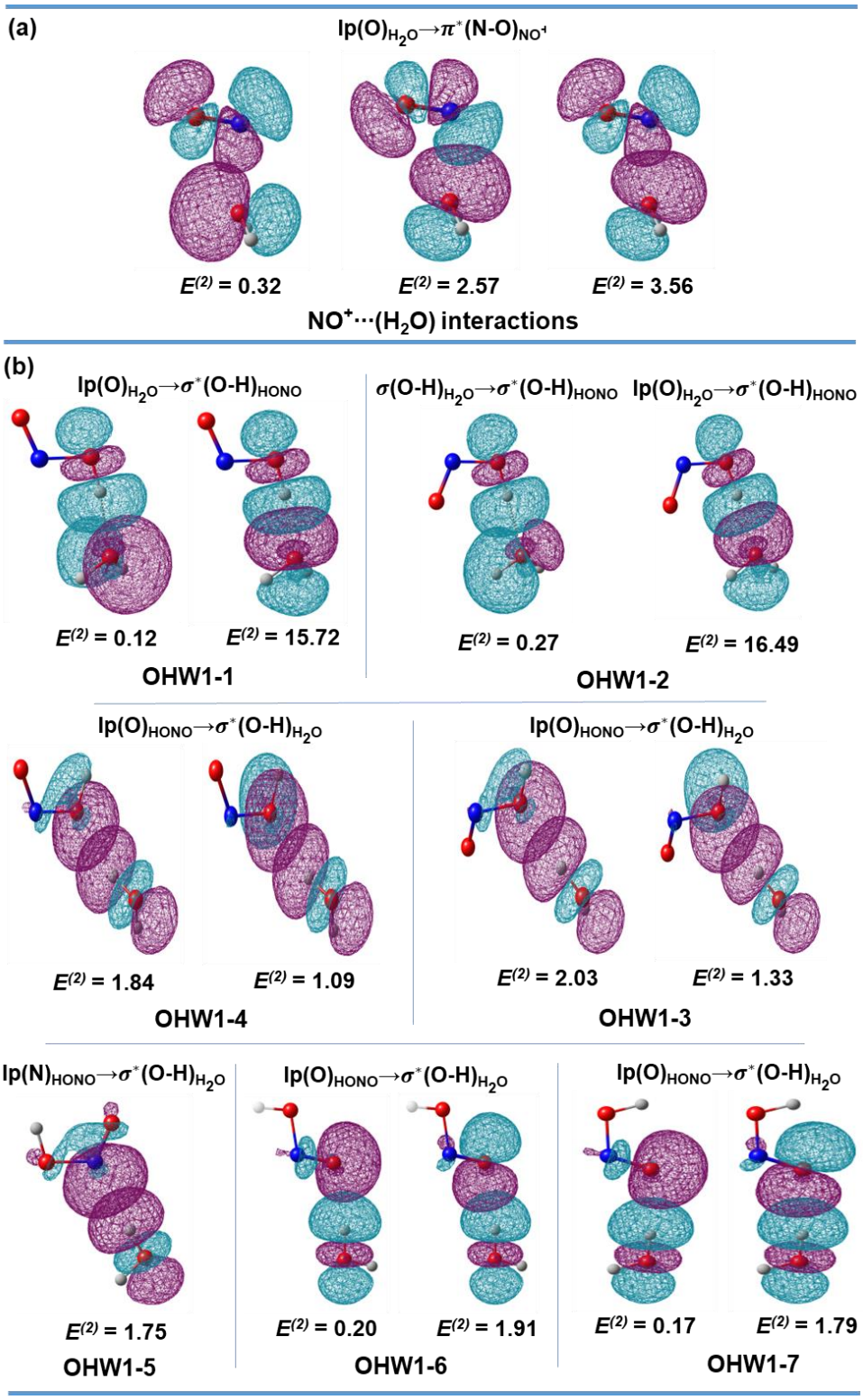

Figure 4.3 The donor-acceptor orbitals (isovalue = 0.03 au) with their stabilization energy ($E^{(2)}$; in kcal/mol) estimated based on second-order perturbation theory in NBO analysis for (a) PB interaction of $NO^{+}(H_2O)$ complex (b) HB interactions in $HONO(H_2O)$ complexes.

The donor-acceptor orbitals involved in the HBs of HONO(H_2O) dimers and their stabilization energies ($E^{(2)}$; values greater than 0.1 kcal/mol are considered) are displayed in Figure 4.3(b). For **OHW1-1**, the lone pairs of O-atom (lp(O)) of water interact with the antibonding orbital of the O–H bond (σ^*_{O-H}) of *trans*-HONO, with a total $E^{(2)}$ value of 15.84 kcal/mol. Similarly, the lone pairs of O-atom (lp(O)) of water interact with the antibonding orbital of O–H bond (σ^*_{O-H}) of *cis*-HONO in **OHW1-2**, in addition, to O–H bonding (σ_{O-H}) orbital of water also interacts with the antibonding orbital of O–H (σ^*_{O-H}) of *cis*-HONO. The total $E^{(2)}$ energy estimated for these orbitals interactions in **OHW1-2** is 16.76 kcal/mol. Based on orbital interactions, it can be said that the HONO acts as HB donor in the HB interactions of **OHW1-1** and **OHW1-2** complexes. On the other hand, the lone pairs of O-atom in -OH functionality of HONO interact with antibonding orbital (σ^*_{O-H}) of water in HBs of **OHW1-3** (*trans*-HONO) and **OHW1-4** (*cis*-HONO. The total $E^{(2)}$ values for these interactions are 3.36 and 2.93 kcal/mol, respectively. In **OHW1-5**, the lone pairs of N-atom of *cis*-HONO interacted with the antibonding orbital (σ^*_{O-H}) of water with a $E^{(2)}$ value of 1.75 kcal/mol. Similarly, the lone pairs of O-atom in N=O functionality of HONO interact with antibonding orbital (σ^*_{O-H}) of water in HBs of **OHW1-6** (*trans*-HONO) and **OHW1-7** (*cis*-HONO); the total $E^{(2)}$ values for these interactions are 2.11 and 1.96 kcal/mol, respectively. Therefore, the orbitals involved in the HBs of **OHW1-3** to **OHW1-7** complexes indicate that HONO is acting as HB acceptor (electron donor) when interacting with water.

Therefore, we found that PB interaction is only present between NO^+ and water in their $NO^+(H_2O)$ dimer, and hence the NO^+ is unable to form the HB interaction (via N- and O-atoms, i.e., (NO)···H) with water. On the other hand, (NO)···H and other HB interactions are present between HONO and water, hence the energies and cooperativity details of these HBs in the microhydrated networks of HONO are further discussed in the following section. Furthermore, a comparison between (NO)···H HBs and other HBs in HONO$(H_2O)_{n=1-4}$ complexes is also discussed in the final section.

4.4.4 Energetics of individual HBs in HONO$(H_2O)_{n=1-4}$ complexes

As mentioned, various HB interactions are present between HONO and water. This is due to the participation of four atoms of HONO in HBs and the *cis-trans* isomers of HONO. As a result, many isomers are possible for each category in HONO$(H_2O)_{n=1-4}$. The binding energy (E_{BE}) values of all HONO$(H_2O)_{n=1-4}$ complexes are listed in Table 4.1. The individual HB energies estimated by MTA and the ΔE values of optimized geometries of HONO$(H_2O)_n$

complexes with n = 1, 2, 3, 4 are presented in Figure 4.4, Figure 4.5, Figure 4.6, and Figure 4.7, respectively. The relevant structural parameters of HBs, along with their energetics, including cooperativity contribution (E^{Coop}) values, are listed in Table 4.2. The HB distances in HONO$(H_2O)_{n=1-4}$ complexes fall in a broader range of 1.541 – 2.745 Å. Furthermore, the sum of energies of individual HBs present between HONO and water (designated as $\sum E_{HONO...H_2O}$) and the sum of energies of HBs present between water molecules (designated as $\sum E_{H_2O...H_2O}$) are listed in Table 4.3.

For HONO(H_2O) dimer complexes (see Figure 4.4), the E_{BE} calculated for these complexes (see Table 4.1) falls in a range between −2.32 and −7.74 kcal/mol. The HB arising from the H-atom of *trans*-HONO is the most stable isomer **OHW1-1 (** E_{BE} = −7.74 kcal/mol), while the HB formed via the H-atom of *cis*-HONO is present in the **OHW1-2** (−7.57 kcal/mol). In other low-lying isomers, HONO is an HB acceptor when interacting with a water molecule. The O-atom in -OH functionality of *trans*-HONO engaged in HB in **OHW1-3** (E_B = −3.46 kcal/mol), whereas *cis*-HONO engaged in **OHW1-4** (E_B = −3.08 kcal/mol). For **OHW1-5**, O-atom of -N=O in *cis*-HONO participated in HB in **OHW1-5** (E_B = −2.52 kcal/mol). In the case of **OHW1-6** and **OHW1-7**, the HB formed via O-atom of -N=O in *trans*-HONO and *cis*-HONO, respectively; are found with E_{BE} values −2.41 and −2.32 kcal/mol, respectively. Overall, for HONO(H_2O) dimer complexes, the HB strength decreases in the order of **OHW1-1**, **OHW1-2**, **OHW1-3**, **OHW1-4**, **OHW1-5**, **OHW1-6**, and **OHW1-7**. This trend in HB strength of complexes is consistent with the trend observed by QTAIM analysis based on the *ρ(r)* parameter. Inferred from these results, the complexes in which HONO acts as an HB donor are more energetically favorable than the complexes in which HONO acts as an HB acceptor.

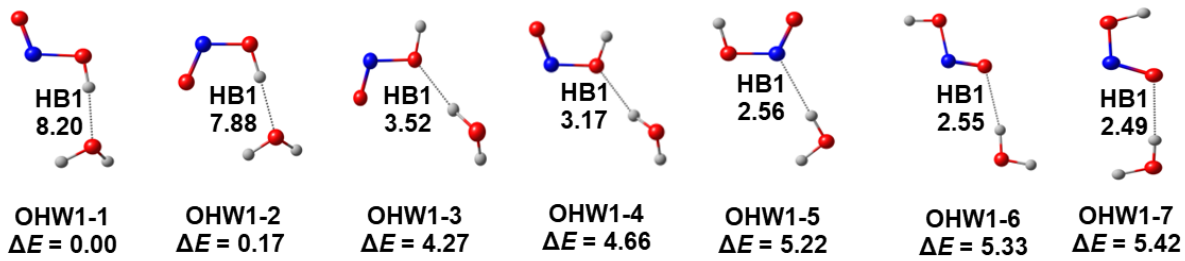

Figure 4.4 MTA-based energies of HBs present between HONO and water. Relative energies (Δ*E*) of HONO(H_2O) dimer complexes and HB energies are in kcal/mol.

Table 4.1 The binding energy (E_{BE}) values of $HONO(H_2O)_{n=1-4}$ complexes.

Structure	E_{BE}	Structure	E_{BE}
OHW1-1	−7.74	**OHW3-21**	−17.07
OHW1-2	−7.57	**OHW4-1**	−38.52
OHW1-3	−3.46	**OHW4-2**	−37.45
OHW1-4	−3.08	**OHW4-3**	−37.43
OHW1-5	−2.52	**OHW4-4**	−37.39
OHW1-6	−2.41	**OHW4-5**	−37.00
OHW1-7	−2.32	**OHW4-6**	−36.86
OHW2-1	−18.60	**OHW4-7**	−36.77
OHW2-2	−16.91	**OHW4-8**	−36.67
OHW2-3	−16.51	**OHW4-9**	−36.64
OHW2-4	−15.65	**OHW4-10**	−36.42
OHW2-5	−15.48	**OHW4-11**	−36.42
OHW2-6	−14.91	**OHW4-12**	−36.22
OHW2-7	−11.45	**OHW4-13**	−36.18
OHW2-8	−10.82	**OHW4-14**	−35.93
OHW2-9	−7.00	**OHW4-15**	−35.66
OHW2-10	−6.99	**OHW4-16**	−35.57
OHW2-11	−6.94	**OHW4-17**	−35.52
OHW3-1	−28.68	**OHW4-18**	−35.29
OHW3-2	−28.59	**OHW4-19**	−35.26
OHW3-3	−27.44	**OHW4-20**	−35.15
OHW3-4	−27.40	**OHW4-21**	−35.03
OHW3-5	−26.72	**OHW4-22**	−34.93
OHW3-6	−25.30	**OHW4-23**	−34.74
OHW3-7	−25.06	**OHW4-24**	−34.65
OHW3-8	−25.04	**OHW4-25**	−33.83
OHW3-9	−24.65	**OHW4-26**	−33.79
OHW3-10	−24.44	**OHW4-27**	−33.44
OHW3-11	−23.99	**OHW4-28**	−33.07
OHW3-12	−23.28	**OHW4-29**	−31.52
OHW3-13	−22.61	**OHW4-30**	−31.37
OHW3-14	−20.84	**OHW4-31**	−30.89
OHW3-15	−20.16	**OHW4-32**	−29.93
OHW3-16	−19.56	**OHW4-33**	−28.08
OHW3-17	−18.74	**OHW4-34**	−27.37
OHW3-18	−18.72	**OHW4-35**	−25.30
OHW3-19	−18.71	**OHW4-36**	−25.09
OHW3-20	−18.60		

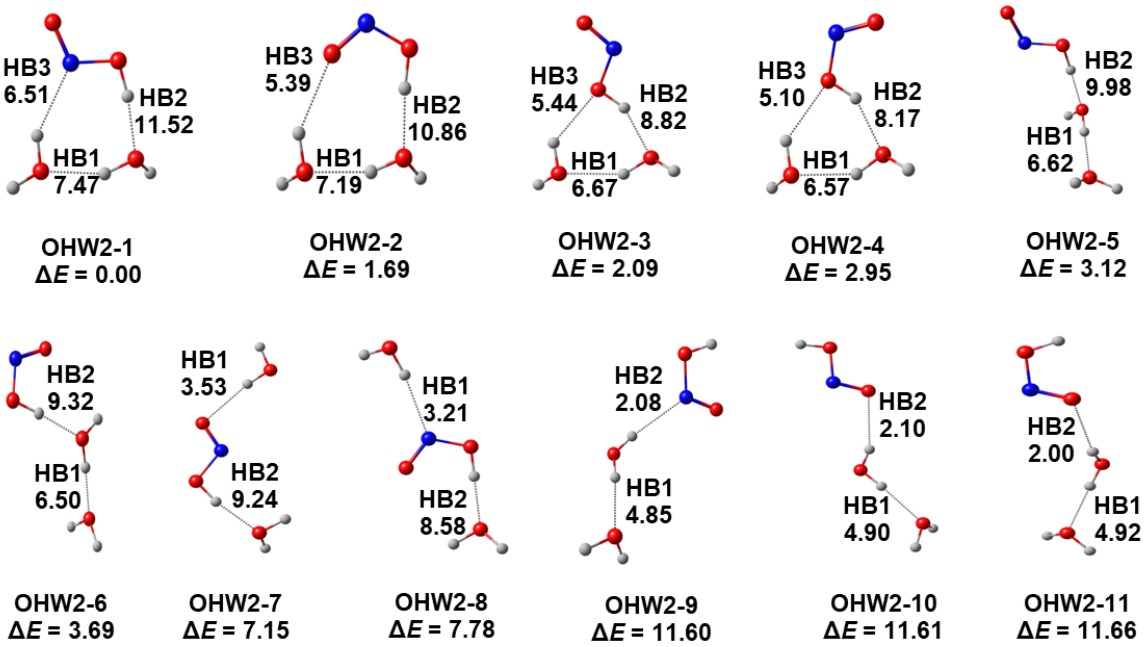

Figure 4.5 MTA-based energies of all individual HBs and relative energies (ΔE) of $HONO(H_2O)_n$ complexes with n = 2. All energy values are in kcal/mol.

In the case of $HONO(H_2O)_2$ complexes (see Figure 4.5), the E_{BE} values fall in a wide range from −6.94 to −18.60 kcal/mol. Among the 11 structures of optimized $HONO(H_2O)_2$ complexes, in the most stable isomer **OHW2-1**, the H- and N-atoms of *trans*-HONO participated in HB with water molecules and form a cyclic trimeric structure. Herein, the sum of energies of individual HBs ($\sum E_{HONO\ldots H_2O}$) is 18.03 kcal/mol, whereas $\sum E_{H_2O\ldots H_2O}$ is 7.47 kcal/mol. The **OHW2-2**, **OHW2-3**, and **OHW2-4** complexes also show a cyclic trimeric configuration. Lower values of $\sum E_{HONO\ldots H_2O}$ (range from 13.17 to 16.25 kcal/mol) determined in these complexes than **OHW2-1** could explain the lower stability of these complexes (ΔE values ranging between 1.69 and 2.95 kcal/mol). It is also to be noted that HBs (in HONO…water and water…water interactions) in **OHW2-1** have a larger E^{Coop} value (2.72 kcal/mol) than other low-lying isomers. The E^{Coop} values for HBs in other low-lying isomers range between −0.22 and 2.69 kcal/mol. In the other low-lying isomers (from **OHW2-5** to **OHW2-11**), an acyclic structure is observed. Herein, the $\sum E_{HONO\ldots H_2O}$ and $\sum E_{H_2O\ldots H_2O}$ values range from 2.00 to 12.77 kcal/mol and from 4.85 to 7.47 kcal/mol, respectively. The lowest $\sum E_{HONO\ldots H_2O}$ value (~ 2 kcal/mol) is obtained for **OHW2-9**, **OHW2-10,** and **OHW2-11** complexes, this could be the explanation for the lesser stability of these complexes (ΔE = ~12 kcal/mol). It should be noted that only atoms in the -N=O functionality of HONO are involved in the HBs of these lower stable complexes. Further,

anti-cooperative HBs are found in these complexes (with E^{Coop} values between −0.22 and −0.29 kcal/mol, respectively), which also account for their reduced stability. It is worth mentioning that the H-atom of HONO is primarily involved in HB formation in remaining more stable isomers. This again suggests that the HONO as HB donor when interacting with water has greater strength in comparison to HBs where HONO acts as HB acceptor.

For HONO trihydrates (see Figure 4.6), the E_{BE} values fall between −17.07 and −28.68 kcal/mol. Overall, there are 21 optimized geometries in this category. Of these, the tetrameric ring structure (composed of HONO and three water molecules) containing isomers from **OHW3-1** to **OHW3-5** shows greater stability (ΔE range from 0.00 to 1.98 kcal/mol). These complexes have a moderate value for both $\sum E_{HONO\ldots H_2O}$ and $\sum E_{H_2O\ldots H_2O}$, a range from 15.83 to 18.48 kcal/mol and from 16.17 to 16.75 kcal/mol, respectively. Isomers **OHW3-1** and **OHW3-2** are comparable in energy (ΔE = 0.09 kcal/mol for **OHW3-2**). It is to be noted that **OHW3-1**, **OHW3-2**, and **OHW3-3** contain *trans*-HONO and hence more stable than the *cis*-HONO orientation present in **OHW3-4** and **OHW3-5**. These complexes have a higher range of E^{Coop} values (in the order of 2 – 5 kcal/mol). In the case of other low-lying isomers from **OHW3-6** to **OHW3-21**, all have a trimeric ring composed of either one HONO and two water molecules or three water molecules except in **OHW3-18** and **OHW3-21**, which are noncyclic structures. The ΔE values of these complexes fall in a range from 3.38 to 11.61 kcal/mol. These complexes have a broader range of $\sum E_{HONO\ldots H_2O}$ (2.36 – 24.55 kcal/mol) and $\sum E_{H_2O\ldots H_2O}$ (5.75 – 21.07 kcal/mol) values, as well as a broad range of E^{Coop} values (from 0.26 to 5.39 kcal/mol). It is obvious that the complexes containing a trimeric ring of HONO with two water molecules exhibit higher $\sum E_{HONO\ldots H_2O}$ values than $\sum E_{H_2O\ldots H_2O}$. On the other hand, the complexes with trimeric water rings have higher $\sum E_{H_2O\ldots H_2O}$ values than $\sum E_{HONO\ldots H_2O}$. For instance, the maximum $\sum E_{HONO\ldots H_2O}$ value (24.55 kcal/mol) is obtained for complex **OHW3-12**, which contains two fused trimeric rings composed of HONO and two water molecules. In addition, the strongest HB (formed via the H-atom of HONO) with the highest cooperativity contribution in the HONO(H_2O)$_3$ category is also found in **OHW3-12**, the energy and E^{Coop} values for this HB are 13.49 and 5.39 kcal/mol, respectively. The highest $\sum E_{H_2O\ldots H_2O}$ value of 21.07 kcal/mol is found in **OHW3-10**, wherein a water trimer is present. Further, reduced number of HNO…water or water…water contacts in complexes from **OHW3-13** to **OHW3-21** validate the lesser stabilization of these complexes. The weakest HB in the HONO(H_2O)$_3$ category is formed by O-atom in -N=O functionality of

HONO in **OHW3-20**, with an energy of 2.36 kcal/mol. This also suggest that the HONO as HB donor when interacting with water have greater strength in comparison to HBs where HONO act as HB acceptor.

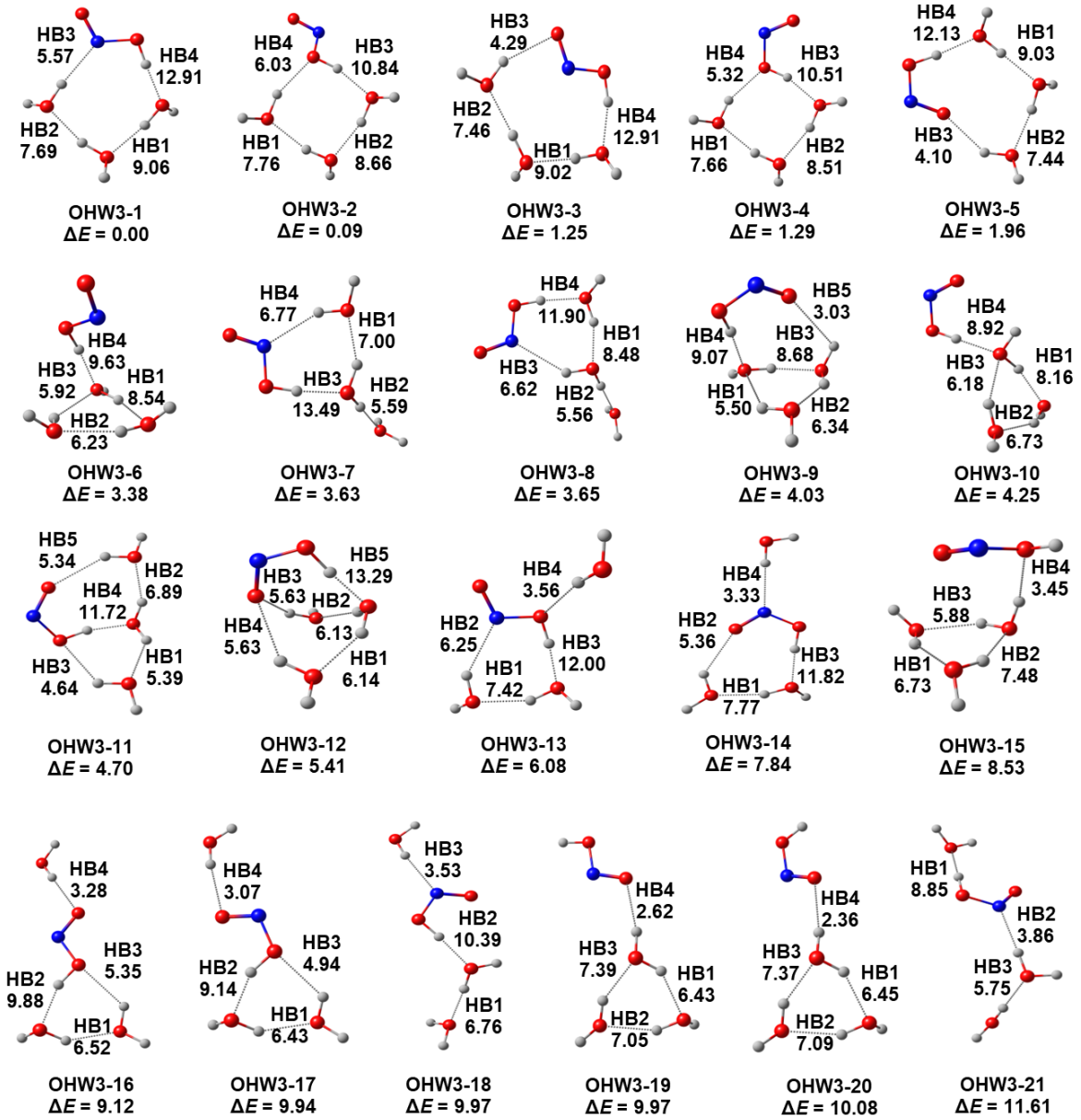

Figure 4.6 MTA-based energies of all individual HBs and relative energies (ΔE) of $HONO(H_2O)_n$ complexes with n = 3. All energy values are in kcal/mol.

In the case of $HONO(H_2O)_4$ complexes (see Figure 4.7), the E_{BE} values span in the range between −25.09 and −38.52 kcal/mol. Out of 36 optimized geometries, the most stable isomer **OHW4-1** is a pentameric ring of *trans*-HONO and four water molecules (cross-association). Similar cross-associated pentameric ring is found in **OHW4-2**, **OHW4-6**, **OHW4-12**, and **OHW4-24** complexes. The -OH functionality of *trans*-HONO is involved in

HBs with water molecules in **OHW4-1**. Further, the *cis*-HONO analogy of **OHW4-1** configuration is observed in **OHW4-2**. The lower stability of **OHW4-2** (ΔE = 1.07 kcal/mol) compared to **OHW4-1** is attributed to the lower stability of *cis*-HONO compared to *trans*-HONO. Among other cyclic pentameric ring complexes, the O-atom in -N=O functionality and H-atom of HONO form HBs with water molecules in **OHW4-6** (ΔE = 1.66 kcal/mol) and **OHW4-12** (ΔE = 2.30 kcal/mol). The *cis*-HONO in **OHW4-12** in contrast to *trans*-HONO in **OHW4-6** may account for their lower stability. Similarly, *cis*-HONO in **OHW4-24** with a ΔE value of 3.87 kcal/mol forms HBs via N-atom in -N=O functionality and H-atom with water molecules in their cyclic pentameric structure. These cross-associated complexes have moderate $\sum E_{HONO\ldots H_2O}$ and $\sum E_{H_2O\ldots H_2O}$ values in the order of 16 – 19 kcal/mol and 24 – 26 kcal/mol, respectively, compared to other isomers. In the other isomers, a cyclic water tetramer (self-association of water molecules) is present in isomers viz., **OHW4-3**, **OHW4-4**, **OHW4-5**, **OHW4-7**, **OHW4-9**, **OHW4-10**, **OHW4-13**, **OHW4-14**, **OHW4-15**, **OHW4-31**, **OHW4-32**, and **OHW4-35**. Obviously, the stronger water…water interactions in water tetrameric rings contribute to larger $\sum E_{H_2O\ldots H_2O}$ values (range of 20.34 – 33.24 kcal/mol), but a broader range of $\sum E_{HONO\ldots H_2O}$ values (2.26 – 20.75 kcal/mol) also be noted. The lowest $\sum E_{HONO\ldots H_2O}$ (2.26 kcal/mol) is due to the HB formed via O-atom in -N=O functionality of *cis*-HONO with water tetrameric ring in **OHW4-31**. Similar HB formed by *trans*-HONO in **OHW4-32** also have a lower energy value of 2.54 kcal/mol. In comparison to this, HB formed via O-atom in -OH functionality of *trans*-HONO with water tetrameric ring has a slightly higher energy value of 4.56 kcal/mol in **OHW4-35**. It should also be noted that the HB formed via O-atom in -OH functionality is slightly destabilized in **OHW4-3** and **OHW4-9** (with a negative HB energy value of −0.72 and −0.66 kcal/mol, respectively), and the negative E^{Coop} value (−0.64 kcal/mol) obtained for these HBs reveals that these HBs are less stabilized in the complex than in their isolated dimer. The remaining isomers in HONO(H_2O)$_4$ category contain either a tetrameric ring composed of HONO and three water molecules or trimeric rings (formed by HONO and two water molecules or three water molecules) or both except in **OHW4-36** (noncyclic structure). The $\sum E_{HONO\ldots H_2O}$ and $\sum E_{H_2O\ldots H_2O}$ values for these complexes span in a wide range of 12.30 – 26.42 kcal/mol and 12.67 – 29.14 kcal/mol, respectively. The highest $\sum E_{HONO\ldots H_2O}$ value (26.42 kcal/mol) is found in **OHW4-8**, in which HB via H-atom of *trans*-HONO with water have an energy of 14.88 kcal/mol is the major contributor. Similarly, the stronger HBs formed via H-atom of HONO are found in **OHW4-18** and **OHW4-27** complexes with energies of 14.54 and 15.08

respectively, as well as higher E^{Coop} values (in the order 4 – 7 kcal/mol) also calculated for these HBs. The large positive E^{Coop} values for these HBs indicate that they are situated in a strong cooperative network of HBs by other HONO…water and water…water interactions. In general, E^{Coop} values (ranging between −0.95 and 7.01 kcal/mol) obtained for HBs in HONO…water and water…water interactions in $HONO(H_2O)_4$ complexes are more positive than $HONO(H_2O)_{n=2-3}$ complexes. Furthermore, the least stable isomer **OHW4-36** in $HONO(H_2O)_{n=4}$ category has an acyclic structure with a lowest $\sum E_{H_2O\ldots H_2O}$ value (12.67 kcal/mol) compared to other isomers. This may be the reason for their lower stability (ΔE = 13.43 kcal/mol). Overall, the cross-associated HONO-water clusters with large cyclic structure is the energetically preferred configuration in $HONO(H_2O)_4$ category.

In short, the HONO can form HB interactions via four of their atoms in $HONO(H_2O)_{n=1-4}$ complexes. The most stable isomer in each cluster size of $HONO(H_2O)_{n=2-4}$ complexes is formed by a cyclic structure of *trans*-HONO and water molecules (cross-associated). This is in agreement with the previous studies, the *trans*-HONO is more stable than *cis*-HONO.[22,119] In general, the $\sum E_{HONO\ldots H_2O}$ values are increased when cluster size increases from one to four. The E^{Coop} values are also increased when cluster size increases from one to four. The cross-associated cyclic HB networks of HONO with water clusters are formed in the most stable complexes of $HONO(H_2O)_{n=2-4}$. Thus, the strength of both HONO…water and water…water interactions contribute to the overall stability of $HONO(H_2O)_{n=2-4}$ complexes. On comparing the strength of HBs in $HONO(H_2O)_{n=1-4}$ complexes, the HBs formed by -OH functionality of HONO have greater energy than HBs formed by -N=O functionality ((NO)···H interactions). A detailed comparison of the strength of HBs in $HONO(H_2O)_{n=1-4}$ complexes is given in the following sections.

Further, the free energy of the formation (ΔG) is a useful parameter for predicting the thermodynamic stability of microhydrated complexes. The ΔG values (calculated at 298.15 K and 1 atm) of the most stable complexes of $HONO(H_2O)_n$ are 1.01, 2.99, 3.18, and 1.90 kcal/mol for n = 1, 2, 3, and 4, respectively. The lower positive ΔG values indicate that $HONO(H_2O)_n$ complexes are not stable at room temperature and pressure; they may be stable at lower temperature and pressure.

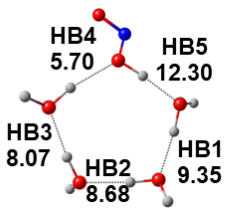

OHW4-1
ΔE = 0.00

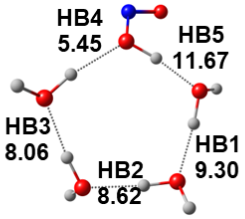

OHW4-2
ΔE = 1.07

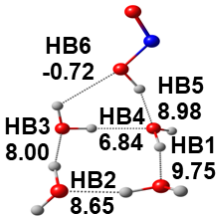

OHW4-3
ΔE = 1.09

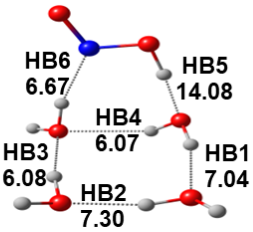

OHW4-4
ΔE = 1.13

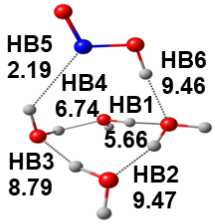

OHW4-5
ΔE = 1.52

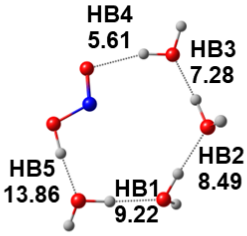

OHW4-6
ΔE = 1.66

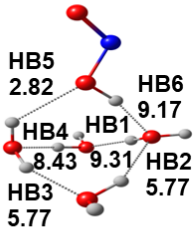

OHW4-7
ΔE = 1.75

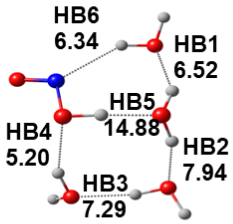

OHW4-8
ΔE = 1.85

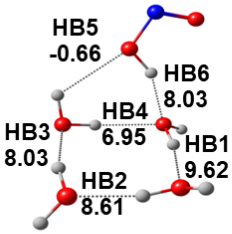

OHW4-9
ΔE = 1.89

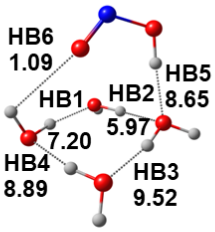

OHW4-10
ΔE = 2.10

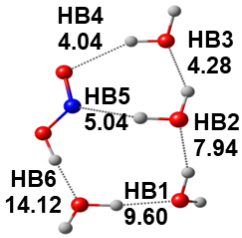

OHW4-11
ΔE = 2.11

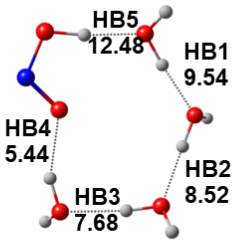

OHW4-12
ΔE = 2.30

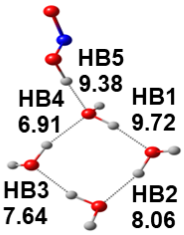

OHW4-13
ΔE = 2.34

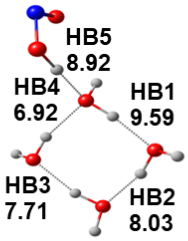

OHW4-14
ΔE = 2.59

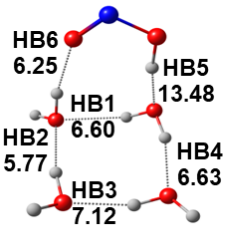

OHW4-15
ΔE = 2.86

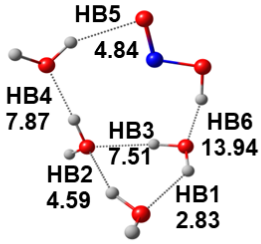

OHW4-16
ΔE = 2.95

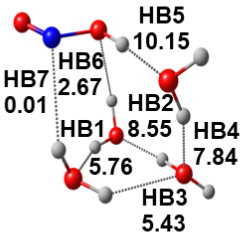

OHW4-17
ΔE = 3.00

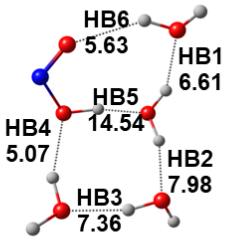

OHW4-18
ΔE = 3.23

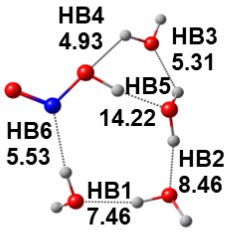

OHW4-19
ΔE = 3.26

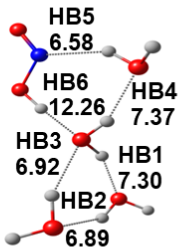

OHW4-20
ΔE = 3.38

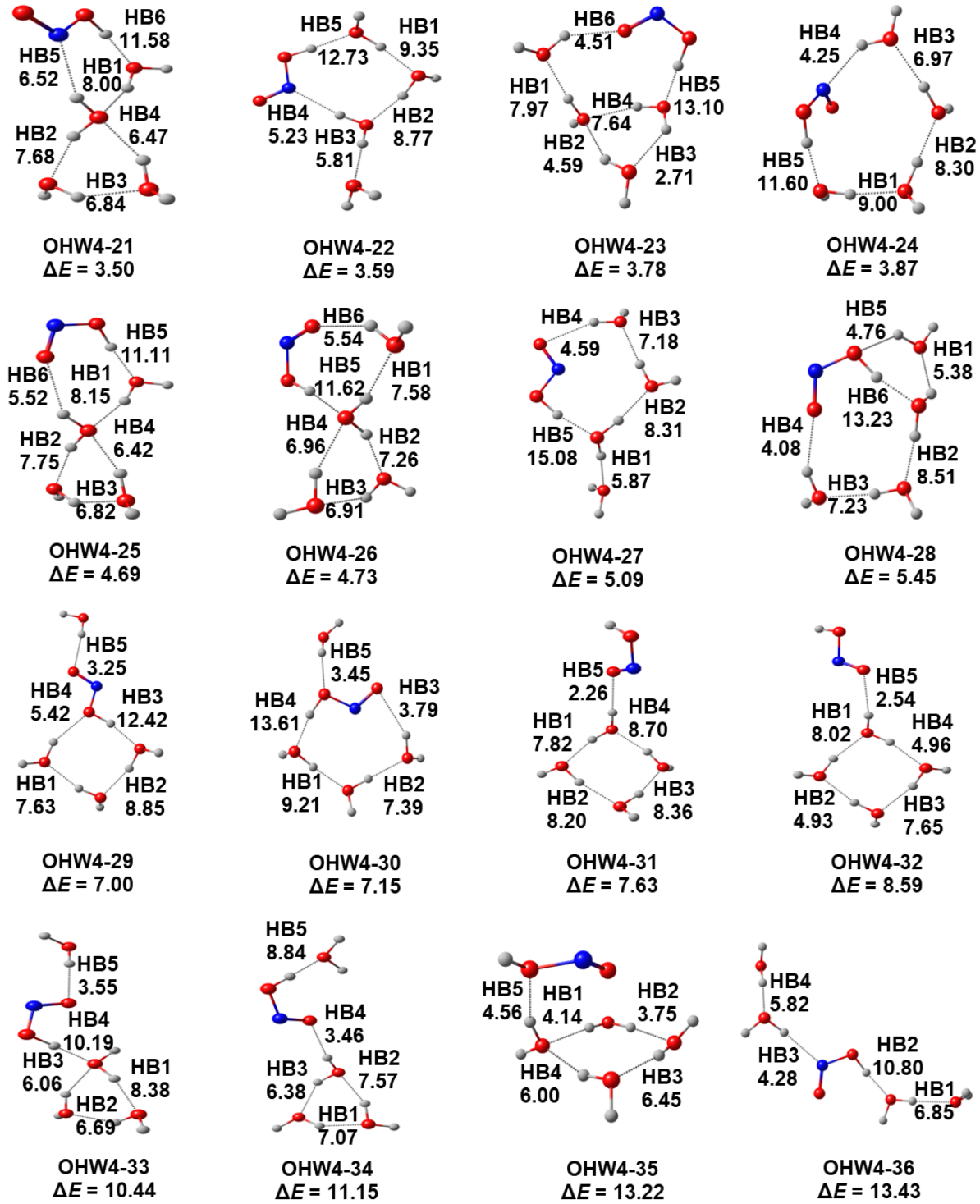

Figure 4.7 MTA-based energies of all individual HBs and relative energies (ΔE) of $HONO(H_2O)_n$ complexes with n = 4. All energy values are in kcal/mol.

Table 4.2 The relevant structural parameters *viz.* distance (in Å) and bond angle (in degree), energy in complex (E_{Int}^{MTA}), energy in the dimer (E^{Dimer}), and cooperativity contribution (E^{Coop}) of all HBs in HONO(H_2O)$_{n=1-4}$ complexes. All energy values are in kcal/mol.

Complex	Interaction Labels	Distance of interaction	Bond angle	E_{Int}^{MTA}	E^{Dimer}	E^{Coop}
OHW1-1	HB1	1.81	174	-	8.20	-
OHW1-2	HB1	1.81	178	-	7.88	-
OHW1-3	HB1	2.03	166	-	3.52	-
OHW1-4	HB1	2.05	160	-	3.17	-
OHW1-5	HB1	2.25	179	-	2.56	-
OHW1-6	HB1	2.18	170	-	2.55	-
OHW1-7	HB1	2.20	175	-	2.49	-
OHW2-1	HB1	1.83	154	7.47	4.75	2.72
	HB2	1.71	172	11.52	8.80	2.72
	HB3	2.18	148	6.51	3.79	2.72
OHW2-2	HB1	1.84	157	7.19	4.50	2.69
	HB2	1.71	173	10.86	8.17	2.69
	HB3	2.15	145	5.39	2.70	2.69
OHW2-3	HB1	1.92	148	6.67	4.73	1.94
	HB2	1.78	153	8.82	6.88	1.94
	HB3	2.17	132	5.44	3.50	1.94
OHW2-4	HB1	1.92	147	6.57	4.73	1.84
	HB2	1.80	149	8.17	6.33	1.84
	HB3	2.15	133	5.10	3.26	1.84
OHW2-5	HB1	1.85	176	6.62	5.04	1.58
	HB2	1.72	178	9.98	8.40	1.58
OHW2-6	HB1	1.86	177	6.50	5.06	1.44
	HB2	1.73	177	9.32	7.88	1.44
OHW2-7	HB1	2.11	170	3.53	2.86	0.67
	HB2	1.77	170	9.24	8.57	0.67
OHW2-8	HB1	2.20	172	3.21	2.60	0.61
	HB2	1.77	179	8.58	7.98	0.61
OHW2-9	HB1	1.97	176	4.85	5.13	-0.29
	HB2	2.30	169	2.08	2.37	-0.29
OHW2-10	HB1	1.96	175	4.90	5.14	-0.23
	HB2	2.26	155	2.10	2.33	-0.23
OHW2-11	HB1	1.96	175	4.92	5.13	-0.22
	HB2	2.23	154	2.00	2.22	-0.22
OHW3-1	HB1	1.74	172	9.06	4.65	4.42
	HB2	1.79	164	7.69	4.76	2.93
	HB3	2.03	173	5.57	2.99	2.59
	HB4	1.65	178	12.91	8.84	4.08

OHW3-2	HB1	1.81	165	7.76	4.62	3.13
	HB2	1.77	165	8.66	5.08	3.58
	HB3	1.67	165	10.84	7.45	3.39
	HB4	1.92	157	6.03	3.08	2.95
OHW3-3	HB1	1.76	172	9.02	4.83	4.20
	HB2	1.87	164	7.46	4.93	2.53
	HB3	2.18	173	4.29	2.15	2.13
	HB4	1.67	178	12.91	9.12	3.79
OHW3-4	HB1	1.82	165	7.66	4.89	2.77
	HB2	1.77	165	8.51	4.81	3.70
	HB3	1.68	162	10.51	7.02	3.49
	HB4	1.94	157	5.32	2.77	2.55
OHW3-5	HB1	1.76	179	9.03	4.77	4.26
	HB2	1.83	173	7.44	4.91	2.53
	HB3	2.03	142	4.10	1.84	2.27
	HB4	1.66	175	12.13	8.12	4.01
OHW3-6	HB1	1.77	157	8.54	4.64	3.89
	HB2	1.94	148	6.23	4.32	1.91
	HB3	2.23	133	5.92	4.24	1.68
	HB4	1.74	166	9.63	8.13	1.51
OHW3-7	HB1	1.90	151	7.00	4.81	2.19
	HB2	1.88	178	5.59	4.61	0.98
	HB3	1.63	173	13.49	8.96	4.54
	HB4	2.13	152	6.77	3.89	2.88
OHW3-8	HB1	1.76	160	8.48	4.59	3.88
	HB2	1.89	179	5.56	4.65	0.92
	HB3	2.31	142	6.62	3.72	2.89
	HB4	1.69	173	11.90	8.78	3.12
OHW3-9	HB1	2.16	130	5.50	4.19	1.31
	HB2	1.94	147	6.34	4.58	1.75
	HB3	1.79	158	8.68	4.68	4.00
	HB4	1.79	169	9.07	7.79	1.28
	HB5	2.75	109	3.03	1.31	1.72
OHW3-10	HB1	1.80	158	8.16	4.73	3.42
	HB2	1.92	144	6.73	4.62	2.11
	HB3	2.10	139	6.18	4.45	1.74
	HB4	1.76	178	8.92	8.08	0.84
OHW3-11	HB1	2.04	137	5.39	4.26	1.13
	HB2	1.88	154	6.89	4.84	2.05
	HB3	2.29	130	4.64	3.12	1.51
	HB4	1.62	164	11.72	7.30	4.42
	HB5	2.22	146	5.34	2.91	2.43
OHW3-12	HB1	1.92	151	6.14	4.19	1.95

	HB2	1.92	151	6.13	4.18	1.95
	HB3	2.32	137	5.63	2.85	2.78
	HB4	2.32	137	5.63	2.85	2.78
	HB5	1.59	176	13.29	7.89	5.39
OHW3-13	HB1	1.84	154	7.42	4.74	2.68
	HB2	2.26	143	6.25	3.78	2.47
	HB3	1.66	174	12.00	8.50	3.50
	HB4	2.01	165	3.56	2.99	0.57
OHW3-14	HB1	1.81	164	7.77	4.84	2.93
	HB2	2.25	137	5.36	2.61	2.75
	HB3	1.67	175	11.82	8.22	3.60
	HB4	2.17	179	3.33	2.67	0.65
OHW3-15	HB1	1.96	148	6.73	4.84	1.89
	HB2	1.85	152	7.48	4.76	2.71
	HB3	2.02	144	5.88	4.74	1.14
	HB4	2.14	148	3.45	3.19	0.26
OHW3-16	HB1	1.92	146	6.52	4.61	1.91
	HB2	1.72	158	9.88	7.32	2.55
	HB3	2.28	127	5.35	3.48	1.87
	HB4	2.12	177	3.28	2.74	0.54
OHW3-17	HB1	1.92	146	6.43	4.60	1.83
	HB2	1.73	154	9.14	6.67	2.47
	HB3	2.29	128	4.94	3.20	1.73
	HB4	2.15	171	3.07	2.52	0.55
OHW3-18	HB1	1.84	177	6.76	5.02	1.73
	HB2	1.68	175	10.39	8.00	2.39
	HB3	2.17	171	3.53	2.62	0.90
OHW3-19	HB1	1.98	144	6.43	4.81	1.61
	HB2	1.92	150	7.05	4.85	2.20
	HB3	1.87	152	7.39	4.81	2.58
	HB4	2.16	168	2.62	0.23	2.39
OHW3-20	HB1	1.98	145	6.45	4.80	1.65
	HB2	1.91	150	7.09	4.84	2.25
	HB3	1.88	151	7.37	4.81	2.56
	HB4	2.15	170	2.36	0.18	2.18
OHW3-21	HB1	1.76	178	8.85	7.98	0.87
	HB2	2.10	174	3.86	2.59	1.28
	HB3	1.91	180	5.75	5.12	0.64
OHW4-1	HB1	1.72	174	9.35	4.58	4.77
	HB2	1.75	176	8.68	4.73	3.96
	HB3	1.78	174	8.07	4.79	3.28
	HB4	1.88	168	5.70	2.74	2.96
	HB5	1.62	174	12.30	7.72	4.57

OHW4-2	HB1	1.72	174	9.30	4.62	4.68
	HB2	1.75	174	8.62	4.74	3.89
	HB3	1.78	174	8.06	4.83	3.23
	HB4	1.86	169	5.45	2.57	2.88
	HB5	1.62	171	11.67	7.26	4.40
OHW4-3	HB1	1.71	169	9.75	4.47	5.28
	HB2	1.76	166	8.65	4.72	3.93
	HB3	1.80	165	8.00	4.88	3.12
	HB4	2.03	153	6.84	4.69	2.15
	HB5	1.76	160	8.98	7.59	1.39
	HB6	2.45	120	-0.72	-0.08	-0.64
OHW4-4	HB1	1.78	166	7.04	3.66	3.38
	HB2	1.83	161	7.30	4.56	2.74
	HB3	1.86	169	6.08	4.51	1.57
	HB4	2.27	132	6.07	3.89	2.17
	HB5	1.61	175	14.08	8.99	5.09
	HB6	1.98	165	6.67	3.51	3.16
OHW4-5	HB1	1.94	150	5.66	4.35	1.31
	HB2	1.71	164	9.47	4.10	5.37
	HB3	1.75	164	8.79	4.56	4.23
	HB4	1.86	161	6.74	4.68	2.06
	HB5	2.50	133	2.19	1.59	0.59
	HB6	1.79	175	9.46	8.22	1.23
OHW4-6	HB1	1.73	176	9.22	4.11	5.11
	HB2	1.76	177	8.49	4.62	3.87
	HB3	1.82	176	7.28	4.49	2.79
	HB4	1.95	164	5.61	2.83	2.78
	HB5	1.62	173	13.86	8.99	4.86
OHW4-7	HB1	1.71	161	9.31	4.13	5.17
	HB2	1.99	153	5.77	4.56	1.21
	HB3	1.90	157	5.77	4.11	1.66
	HB4	1.77	162	8.43	4.48	3.95
	HB5	2.29	132	2.82	2.19	0.63
	HB6	1.76	166	9.17	7.72	1.45
OHW4-8	HB1	1.93	148	6.52	4.73	1.79
	HB2	1.81	160	7.94	4.89	3.05
	HB3	1.85	165	7.29	4.95	2.35
	HB4	1.99	154	5.20	2.85	2.34
	HB5	1.54	174	14.88	8.19	6.70
	HB6	2.26	145	6.34	4.03	2.31
OHW4-9	HB1	1.71	169	9.62	4.51	5.12
	HB2	1.76	166	8.61	4.74	3.88
	HB3	1.80	165	8.03	4.87	3.16

	HB4	1.99	155	6.95	4.75	2.20
	HB5	2.46	120	-0.66	-0.02	-0.64
	HB6	1.80	154	8.03	6.86	1.17
OHW4-10	HB1	1.84	164	7.20	4.90	2.29
	HB2	1.92	154	5.97	4.55	1.43
	HB3	1.71	167	9.52	4.07	5.45
	HB4	1.75	167	8.89	4.69	4.19
	HB5	1.81	171	8.65	7.59	1.06
	HB6	2.61	109	1.09	0.62	0.47
OHW4-11	HB1	1.72	172	9.60	4.54	5.06
	HB2	1.78	159	7.94	4.19	3.75
	HB3	1.99	150	4.28	3.13	1.15
	HB4	2.13	152	4.04	2.80	1.24
	HB5	2.19	153	5.04	2.56	2.48
	HB6	1.61	175	14.12	8.98	5.14
OHW4-12	HB1	1.73	176	9.54	4.49	5.05
	HB2	1.77	176	8.52	4.71	3.81
	HB3	1.80	172	7.68	4.86	2.83
	HB4	1.92	156	5.44	2.21	3.23
	HB5	1.63	174	12.48	8.06	4.41
OHW4-13	HB1	1.70	171	9.72	4.41	5.31
	HB2	1.79	163	8.06	4.37	3.68
	HB3	1.81	164	7.64	4.81	2.83
	HB4	1.90	161	6.91	4.74	2.17
	HB5	1.77	172	9.38	8.40	0.98
OHW4-14	HB1	1.71	170	9.59	4.47	5.12
	HB2	1.79	163	8.03	4.37	3.66
	HB3	1.81	164	7.71	4.82	2.89
	HB4	1.89	162	6.92	4.73	2.19
	HB5	1.77	178	8.92	8.11	0.81
OHW4-15	HB1	2.11	142	6.60	4.26	2.33
	HB2	1.88	169	5.77	4.52	1.25
	HB3	1.84	160	7.12	4.60	2.52
	HB4	1.80	164	6.63	3.62	3.01
	HB5	1.61	171	13.48	8.10	5.38
	HB6	1.94	167	6.25	2.66	3.60
OHW4-16	HB1	2.02	139	2.83	1.83	1.00
	HB2	1.95	152	4.59	4.03	0.56
	HB3	2.04	154	7.51	4.51	3.00
	HB4	1.84	177	7.87	4.80	3.07
	HB5	2.10	155	4.84	2.30	2.54
	HB6	1.63	165	13.94	9.11	4.83
OHW4-17	HB1	1.92	152	5.76	4.08	1.68

	HB2	1.77	159	8.55	4.62	3.93
	HB3	2.44	126	5.43	3.70	1.73
	HB4	1.77	159	7.84	4.27	3.58
	HB5	1.70	174	10.15	7.88	2.27
	HB6	2.52	125	2.67	1.65	1.02
	HB7	2.52	122	0.01	0.96	-0.95
OHW4-18	HB1	1.89	154	6.61	4.54	2.07
	HB2	1.81	162	7.98	4.97	3.01
	HB3	1.84	165	7.36	4.94	2.43
	HB4	1.96	156	5.07	2.65	2.42
	HB5	1.54	168	14.54	7.53	7.01
	HB6	2.21	146	5.63	2.97	2.66
OHW4-19	HB1	1.81	164	7.46	4.87	2.59
	HB2	1.77	169	8.46	4.86	3.60
	HB3	2.06	135	5.31	4.25	1.06
	HB4	2.31	128	4.93	3.36	1.58
	HB5	1.56	168	14.22	8.12	6.10
	HB6	2.05	173	5.53	3.16	2.36
OHW4-20	HB1	1.84	154	7.30	4.39	2.91
	HB2	1.93	144	6.89	4.74	2.15
	HB3	1.99	147	6.92	4.88	2.04
	HB4	1.84	155	7.37	4.77	2.60
	HB5	2.16	148	6.58	3.90	2.68
	HB6	1.68	174	12.26	8.87	3.39
OHW4-21	HB1	1.81	157	8.00	4.82	3.18
	HB2	1.84	155	7.68	4.80	2.87
	HB3	1.94	144	6.84	4.73	2.11
	HB4	2.00	145	6.47	4.51	1.96
	HB5	2.20	148	6.52	3.72	2.79
	HB6	1.70	171	11.58	8.78	2.80
OHW4-22	HB1	1.73	172	9.35	4.57	4.77
	HB2	1.73	166	8.77	4.57	4.20
	HB3	1.89	180	5.81	4.99	0.82
	HB4	2.09	171	5.23	3.03	2.20
	HB5	1.65	177	12.73	8.78	3.95
OHW4-23	HB1	1.79	173	7.97	4.81	3.16
	HB2	1.96	151	4.59	3.97	0.62
	HB3	2.01	141	2.71	1.86	0.84
	HB4	2.01	157	7.64	4.54	3.10
	HB5	1.62	177	13.10	8.10	5.01
	HB6	1.99	144	4.51	1.83	2.68
OHW4-24	HB1	1.74	171	9.00	4.54	4.46
	HB2	1.77	178	8.30	4.78	3.52

	HB3	1.83	174	6.97	4.50	2.47
	HB4	2.08	146	4.25	2.16	2.09
	HB5	1.63	165	11.60	7.44	4.16
OHW4-25	HB1	1.80	163	8.15	4.83	3.31
	HB2	1.83	155	7.75	4.80	2.95
	HB3	1.94	144	6.82	4.72	2.10
	HB4	2.01	144	6.42	4.51	1.91
	HB5	1.70	174	11.11	8.21	2.89
	HB6	2.18	145	5.52	2.66	2.87
OHW4-26	HB1	1.83	161	7.58	4.84	2.73
	HB2	1.85	153	7.26	4.43	2.84
	HB3	1.93	144	6.91	4.75	2.16
	HB4	1.98	148	6.96	4.88	2.08
	HB5	1.69	171	11.62	8.23	3.40
	HB6	2.14	145	5.54	2.77	2.77
OHW4-27	HB1	1.89	174	5.87	5.04	0.83
	HB2	1.81	173	8.31	5.01	3.30
	HB3	1.89	176	7.18	4.94	2.25
	HB4	2.17	155	4.59	2.18	2.40
	HB5	1.59	168	15.08	10.60	4.48
OHW4-28	HB1	2.07	135	5.38	4.29	1.09
	HB2	1.78	175	8.51	4.95	3.56
	HB3	1.83	172	7.23	4.98	2.25
	HB4	2.06	150	4.08	1.95	2.14
	HB5	2.25	131	4.76	3.14	1.61
	HB6	1.57	164	13.23	7.16	6.07
OHW4-29	HB1	1.82	165	7.63	4.92	2.71
	HB2	1.76	165	8.85	4.74	4.11
	HB3	1.62	167	12.42	7.73	4.69
	HB4	1.96	154	5.42	3.05	2.36
	HB5	2.13	175	3.25	2.75	0.50
OHW4-30	HB1	1.75	174	9.21	4.76	4.45
	HB2	1.86	176	7.39	4.95	2.44
	HB3	2.30	152	3.79	1.97	1.82
	HB4	1.62	167	13.61	8.83	4.79
	HB5	2.05	169	3.45	2.77	0.68
OHW4-31	HB1	1.81	165	7.82	4.93	2.89
	HB2	1.79	166	8.20	4.89	3.31
	HB3	1.78	166	8.36	4.84	3.52
	HB4	1.77	167	8.70	4.79	3.91
	HB5	2.15	177	2.26	2.22	0.04
OHW4-32	HB1	1.78	165	8.02	4.34	3.68
	HB2	1.79	167	4.93	1.72	3.21

	HB3	1.82	165	7.65	4.51	3.13
	HB4	1.81	165	4.96	1.72	3.24
	HB5	2.18	166	2.54	2.50	0.04
OHW4-33	HB1	1.77	160	8.38	4.66	3.72
	HB2	1.92	144	6.69	4.60	2.08
	HB3	2.15	137	6.06	4.37	1.69
	HB4	1.71	178	10.19	8.32	1.88
	HB5	2.09	178	3.55	2.66	0.88
OHW4-34	HB1	1.92	150	7.07	4.84	2.23
	HB2	1.86	153	7.57	4.77	2.80
	HB3	1.99	145	6.38	4.43	1.95
	HB4	2.05	171	3.46	2.55	0.92
	HB5	1.77	178	8.84	2.53	6.31
OHW4-35	HB1	2.11	175	4.14	4.78	-0.64
	HB2	2.01	162	3.75	3.72	0.04
	HB3	1.88	167	6.45	5.09	1.36
	HB4	1.87	158	6.00	4.53	1.47
	HB5	1.94	154	4.56	3.35	1.21
OHW4-36	HB1	1.83	177	6.85	5.01	1.84
	HB2	1.67	176	10.80	9.03	1.76
	HB3	2.08	176	4.28	3.63	0.65
	HB4	1.91	177	5.82	5.04	0.78

Table 4.3 The sum of MTA-based energies (kcal/mol) of all HBs present between HONO and water (designated as $\sum E_{HONO...H_2O}$) and all HBs present between water molecules (designated as $\sum E_{H_2O...H_2O}$) in HONO(H_2O)$_{n=1-4}$ complexes.

Structure	$\sum E_{HONO...H_2O}$	$\sum E_{H_2O...H_2O}$	Structure	$\sum E_{HONO...H_2O}$	$\sum E_{H_2O...H_2O}$
OHW1-1	8.20	-	**OHW3-21**	12.71	5.75
OHW1-2	7.88	-	**OHW4-1**	18.00	26.10
OHW1-3	3.52	-	**OHW4-2**	17.12	25.98
OHW1-4	3.17	-	**OHW4-3**	8.26	33.24
OHW1-5	2.56	-	**OHW4-4**	20.75	26.49
OHW1-6	2.55	-	**OHW4-5**	11.65	30.66
OHW1-7	2.49	-	**OHW4-6**	19.47	24.99
OHW2-1	18.03	7.47	**OHW4-7**	11.99	29.28
OHW2-2	16.25	7.19	**OHW4-8**	26.42	21.75
OHW2-3	14.26	6.67	**OHW4-9**	7.37	33.21
OHW2-4	13.17	6.57	**OHW4-10**	9.74	31.58
OHW2-5	9.98	6.62	**OHW4-11**	23.20	21.82
OHW2-6	9.32	6.50	**OHW4-12**	17.92	25.74
OHW2-7	12.77	-	**OHW4-13**	9.38	32.33
OHW2-8	11.79	-	**OHW4-14**	8.92	32.25

OHW2-9	2.08	4.85	**OHW4-15**	19.73	26.12
OHW2-10	2.10	4.90	**OHW4-16**	18.78	22.80
OHW2-11	2.00	4.92	**OHW4-17**	12.83	27.58
OHW3-1	18.48	16.75	**OHW4-18**	25.24	21.95
OHW3-2	16.87	16.42	**OHW4-19**	24.68	21.23
OHW3-3	17.20	16.48	**OHW4-20**	18.84	28.48
OHW3-4	15.83	16.17	**OHW4-21**	18.10	28.99
OHW3-5	16.23	16.47	**OHW4-22**	17.96	23.93
OHW3-6	9.63	20.69	**OHW4-23**	17.61	22.91
OHW3-7	20.26	12.59	**OHW4-24**	15.85	24.27
OHW3-8	18.52	14.04	**OHW4-25**	16.63	29.14
OHW3-9	12.10	20.52	**OHW4-26**	17.16	28.71
OHW3-10	8.92	21.07	**OHW4-27**	19.67	21.36
OHW3-11	21.70	12.28	**OHW4-28**	22.07	21.12
OHW3-12	24.55	12.27	**OHW4-29**	21.09	16.48
OHW3-13	21.81	7.42	**OHW4-30**	20.85	16.60
OHW3-14	20.51	7.77	**OHW4-31**	2.26	33.08
OHW3-15	3.45	20.09	**OHW4-32**	2.54	25.56
OHW3-16	18.51	6.52	**OHW4-33**	13.74	21.13
OHW3-17	17.15	6.43	**OHW4-34**	12.30	21.02
OHW3-18	13.92	6.76	**OHW4-35**	4.56	20.34
OHW3-19	2.62	20.87	**OHW4-36**	15.08	12.67
OHW3-20	2.36	20.91			

4.4.5 Comparison between (NO)···H HBs and other HBs in HONO$(H_2O)_{n=1-4}$ complexes

In HONO(H_2O) dimer, the HBs formed via N- and O-atoms in -N=O of HONO (i.e., (NO)···H HBs) have energy values around 2.50 kcal/mol in **OHW1-5**, **OHW1-6**, and **OHW1-7** complexes (see Figure 4.4). Whereas, the HBs formed via the H-atom of HONO (HONO as HB donor) in **OHW1-1** and **OHW1-2** have energy values in the order of 7 – 8 kcal/mol. The HBs formed via O-atom in -OH functionality of HONO (as HB acceptor) in **OHW1-3** and **OHW1-4** have energies in the order of 3 – 4 kcal/mol. This implies that the HONO forms stronger HBs with water when they act as HB donor than HB acceptor, which is attributed to the acidic nature of the H-atom of HONO and this effect is more pronounced in HONO$(H_2O)_{n=2-4}$ complexes as well. In HONO$(H_2O)_{n=2-4}$ complexes, the H-atom of HONO forms HBs with energies in the range of 8.03 – 15.08 kcal/mol, and the (NO)···H HBs have energies in the range from 0.01 to 6.77 kcal/mol. In Figure 4.8, it can be seen that the energies of HBs formed via H-atom increased with an increase in cluster size from 2 to 4, whereas, energies of (NO)···H HBs are comparable for varying cluster size from 2 to 4. However, the energies of (NO)···H HBs in HONO$(H_2O)_{n=2-4}$ complexes are greater than the

HONO(H_2O) dimer complexes. The positive cooperativity contribution (E^{Coop}) towards (NO)···H HBs (ranging from −0.95 to 3.60 kcal/mol) also indicate that the (NO)···H HBs are more stable in complexes than in dimer. For HBs via H-atom of HONO in HONO$(H_2O)_{n=2-4}$ complexes, significant positive E^{Coop} values ranging from 0.61 to 7.01 kcal/mol are obtained, supporting their higher HB energies. Thus, both the energies and cooperativity contribution of HBs in HONO$(H_2O)_{n=2-4}$ complexes manifest that the HBs formed via H-atom of HONO is much stronger than the (NO)···H HBs.

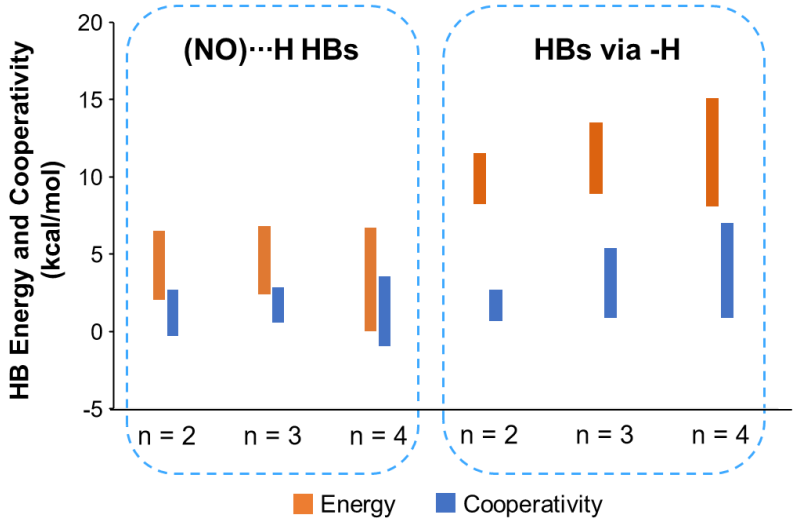

Figure 4.8 Comparison between energies and cooperativity contribution of HBs formed via -N=O functionality ((NO)···H interaction) and H-atom of HONO in HONO$(H_2O)_{n=2-4}$ complexes.

4.5 Conclusions

In this study, we investigated various noncovalent interactions present between NO^+ and water as well as HONO and water through various analyses such as MESP, QTAIM, and NBO. Only pnicogen bonding (PB) interaction is noted in $NO^+(H_2O)$ complex. On the other hand, four atoms of HONO can form hydrogen bonds (HBs) with water, hence (NO)···H HBs (formed via N- and O-atoms in -N=O of HONO) and other HBs are present between HONO and water. The interaction sites on monomers (NO^+, HONO, and H_2O) and dimers ($NO^+(H_2O)$ and HONO(H_2O)) are identified using MESP analysis. QTAIM molecular graphs confirmed the PB and HB interactions in $NO^+(H_2O)$ and HONO(H_2O) complexes, respectively. The orbitals involved in the PB and HB interactions are demonstrated by NBO analysis.

Further, in the microhydrated complexes of HONO (i.e., $HONO(H_2O)_{n=1-4}$), the energies and cooperativity contributions of all HBs are estimated with the help of MTA-based calculations. In $HONO(H_2O)$ dimer complexes, HBs formed via H-atom of HONO (HONO as HB donor) have the highest energy (in the order of 7 – 8 kcal/mol), whereas energies of HBs formed by remaining atoms of HONO (as HB acceptor) are in the order 2 – 4 kcal/mol. The stronger HBs by H-atom of HONO is attributed to its acidic nature, and this effect is more pronounced in $HONO(H_2O)_{n=2-4}$ complexes. For $HONO(H_2O)_{n=2-4}$ complexes, the H-atom of HONO forms HBs with energies ranging from 8.03 to 15.08 kcal/mol, and the HBs formed by -N=O functionality ((NO)···H) of HONO have energies in the range from 0.01 to 6.77 kcal/mol. In (NO)···H interactions, the energy range of HBs formed by N- and O-atoms are comparable (with energies ranging from 0.01 to 6.77 kcal/mol and from 1.09 to 6.25 kcal/mol, respectively). The strongest HB energy (15.08 kcal/mol) is found in **OHW4-27**, wherein the H-atom of *trans*-HONO forms HB with an acyclic water tetrameric cluster. A substantial positive cooperativity contribution (E^{Coop} ranging from 0.61 to 7.01 kcal/mol) are obtained for HBs formed via H-atom of HONO. The E^{Coop} values obtained for (NO)···H HBs (ranging from −0.95 to 3.60 kcal/mol) in $HONO(H_2O)_{n=2-4}$ complexes are lower than that of HBs via H-atom of HONO. This also explains the greater strength of HBs formed via H-atom than (NO)···H HBs.

Besides, the strength of water…water interactions are increased (HB energies up to 9.75 kcal/mol) for varying cluster size from 2 to 4. The E^{Coop} values toward HBs in water…water interactions are mostly positive (ranging from −064 to 5.45 kcal/mol), which could be a reason for increase in the strength of water…water interactions with increased cluster size. In general, both energies and E^{Coop} of HBs in HONO…water and water…water interactions increased when cluster size increases from 2 to 4. As a result, cross-associated HB networks formed by HONO and water clusters are found in most stable complexes in each categories of $HONO(H_2O)_{n=2-4}$.

Publication based on this chapter:

Thufail M. Ismail; Patkar, D.; Sajith, P. K.; Deshmukh, M. M. Hydrogen Bond Strengths in Microhydrated Clusters of HNO and HONO: Energetic Insights via Molecular Tailoring Approach. ***New Journal of Chemistry*** (communicated).

Chapter 5

Hydrogen Bonding Interactions of Substituted Nitroxide Radicals

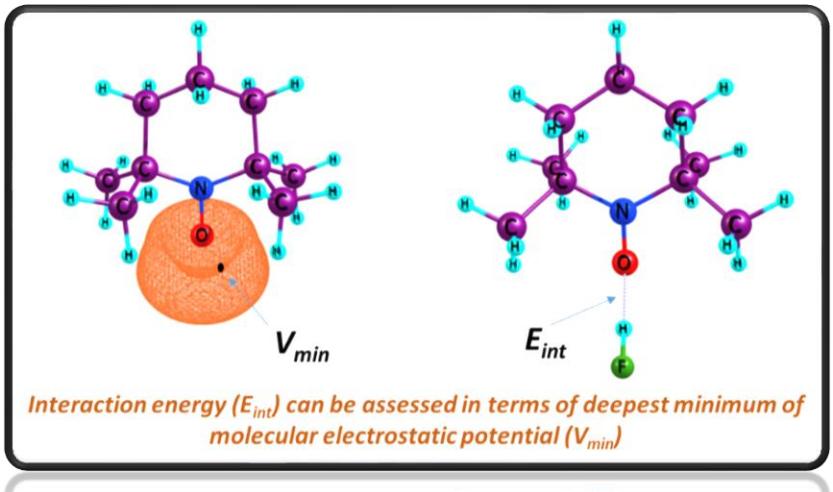

5.1 Abstract

Intermolecular hydrogen bonding (HB) interactions of nitroxide radicals (NO···H) with various electron acceptors accounts for their interesting properties and key applications. In this work we have performed a comprehensive and quantitative theoretical analysis of the NO···H HBs formed by nitroxide radicals with HF, H_2O, and CH_4 molecules as electron acceptors, employing DFT calculations at UM06L/6-311++G(d,p) level. The electronic effects of nitroxide radicals are assessed in terms of the molecular electrostatic potential minimum (V_{min}) around nitroxide oxygen atom. The observed V_{min} values reflect the electron donating and withdrawing features of the substituents present in the structural framework of nitroxide radicals. Similarly, the interaction energy (E_{int}) of hydrogen bonded complexes of nitroxides also reflects on electronic effects such as inductive and steric. Accordingly, a linear relationship has been established between V_{min} of nitroxides and interaction energy (E_{int}) values of their hydrogen bonded complexes. Further, quantum theory of atoms in molecules (QTAIM) analysis demonstrated that the nature of HB in complexes with electron donating substituent is a mix of closed shell and shared interaction while it is mostly closed shell in systems with electron withdrawing substituent. Besides, the symmetry adapted perturbation theory (SAPT) calculations show that the HBs are largely dependent on electrostatic component of the interaction energy in nitroxide-HF and nitroxide-H_2O complexes whereas the dominant contributor is dispersion in nitroxide-CH_4 complexes. The results herein suggest that, modifying the substituents in the structural motif of nitroxide radicals help to fine-tune the strength and nature of HBs in their complexes with electron acceptors. Moreover, quantification of the strength and nature of HB in nitroxide radicals can be effectively done with topological features of MESP and QTAIM parameters, and orbitals involved in the HBs are offered by NBO analysis. At the end of this chapter, a comparison of the HB strength of NO, HNO, HONO, and nitroxide molecules is provided.

5.2 Introduction

The significance of NO···H interactions of nitroxide radicals has been recognized by many experimental studies.[121,123–125] However, theoretical investigation on the strength and characteristics of NO···H interactions in nitroxides is less explored. In this regard, studies related to quantifying the hydrogen bond (HB) strength formed by various nitroxide radicals are discussed in Alkorta and Elguero's papers.[226,227] Alkorta and Elguero have determined the thermodynamics and hydrogen bond basicity of TEMPO and related nitroxides

theoretically and their studies have pointed out that in those nitroxides where other O-atoms (ketone, hydroxyl, and ether) are present the O-atom of the NO functionality is better HB acceptor than other O-atoms.[227] Recently, Alkorta *et al.* explored Cambridge Structural Database (CSD)[228] for intermolecular HBs formed by nitroxide radicals in crystals and reported a qualitative and quantitative analysis of such interactions.[226] However, a systematic theoretical study on HBs of nitroxide radicals and the factors influencing them has not been done so far. The present study focuses on exploring the HBs of a range of different substituted nitroxide radicals with hydrogen Fluoride (HF). The characteristics of HB in these complexes are further compared with iminoxyl radicals. In addition, other HB donors *viz.* H_2O and CH_4 were also incorporated in complexes of a few representative nitroxide radicals. Herein, results obtained from molecular electrostatic potential (MESP), quantum theory of atoms in molecules (QTAIM), symmetry-adapted perturbation theory (SAPT), and natural bond orbitals (NBO) analyses are also comprehended.

5.3 Computational methods

All the calculations were performed with the DFT method using UM06L[229] functional in conjunction with 6-311++G(d,p) basis set by using Gaussian 09 program packages.[230] It has been reported that M06L is the best performed functional in a benchmark study on noncovalent interactions of small organic molecules, its geometries and interaction energies are in close agreement with those derived from the higher *ab initio* level of theory (CCSD level).[231] The optimized geometries were confirmed as local minima by frequency analysis due to the absence of imaginary frequencies. The interaction energy (E_{int}) of all interacted systems of nitroxides with HF, H_2O, and CH_4 molecules were calculated by a supermolecular approach using Eq. 5.1, wherein $E_{complex}$, E_{NO}, and $E_{HF/H_2O/CH_4}$ are the energy of interacted system, energy of NO molecule, and energy of HF, H_2O or CH_4 molecules respectively.

$$E_{int} = E_{complex} - \left[E_{NO} + E_{HF/H_2O/CH_4}\right] \qquad \text{(Eq. 5.1)}$$

Symmetry-adapted perturbation theory (SAPT) analysis was performed at the zeroth-order SAPT[177] level with aug-cc-pVTZ basis set by using Psi4 suite of programs.[232] natural bond orbitals (NBO) analysis is carried out using NBO version 3.1 implemented in Gaussian 16 software.[196] NBO and MESP results are visualized using Chemcraft software.[197] QTAIM analysis is performed using the AIMAll software package.[193]

5.4 Results and discussion

A set of 23 nitroxide free radicals, mostly selected from the recent work by Alkorta *et al.*,[226] are used in this study. These are primarily retrieved from different structural moieties of X-ray structures in CSD.[228] In order to compare the hydrogen bonding (HB) ability of nitroxide radicals, four iminoxyl radicals were also selected in this study. Figure 5.1 presents the set of radicals considered in this study wherein **1–23** are nitroxide radicals and **24–27** are iminoxyl radicals.

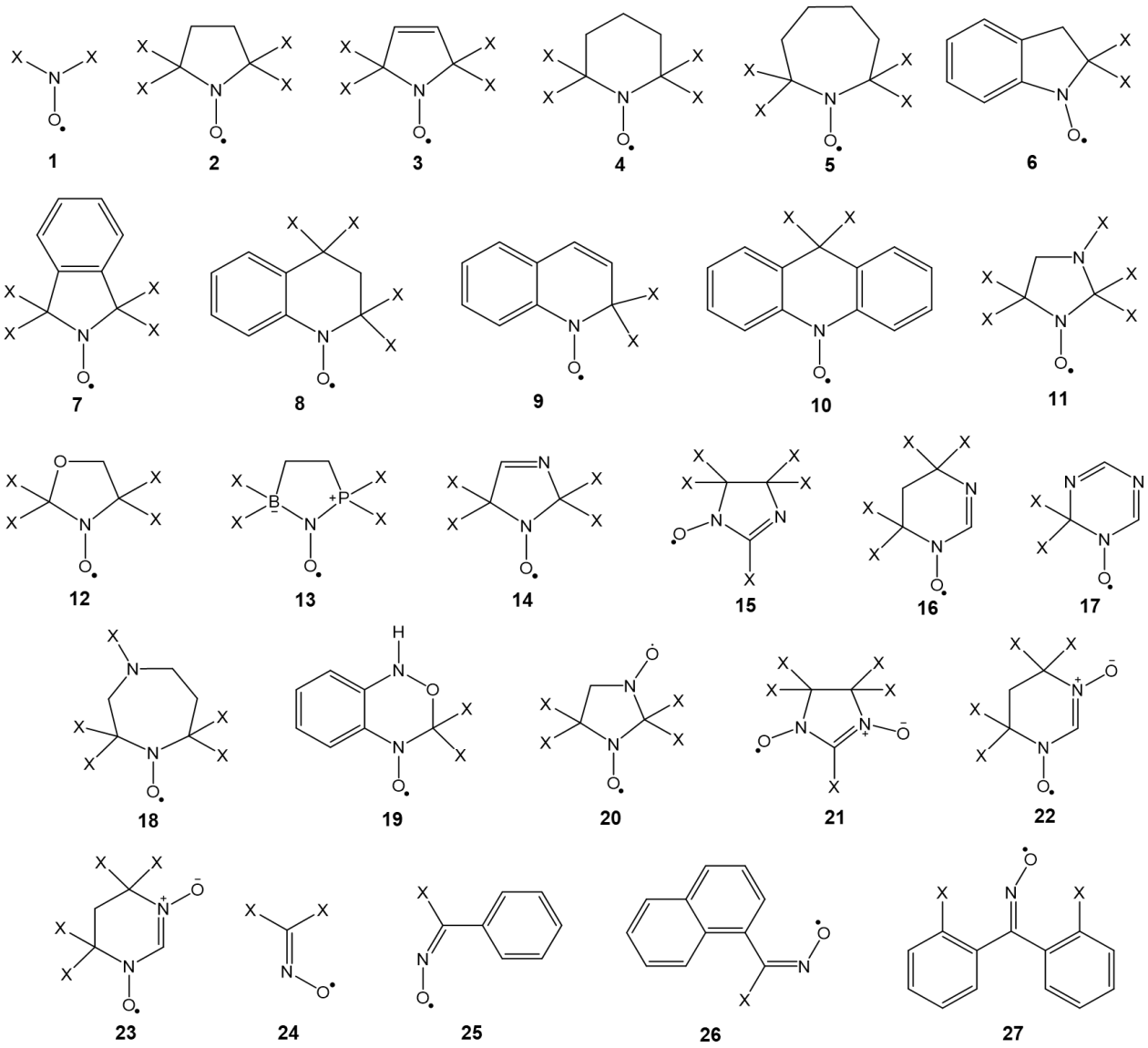

Figure 5.1 Structures of nitroxide and iminoxyl radicals considered in the study. The X represents substituents *viz.*, H, CH_3, or F.

The symbol X represents the substituent present in the nitroxide structural motifs. In order to understand the influence of substituent present in the structural framework on NO

moiety of nitroxide, we used unsubstituted reference H, electron-donating CH_3 and electron-withdrawing F (*i.e.*, X = H, CH_3, and F) substituents. Structures **1** and **24** are open chain radicals whereas the remaining are five, six, or seven-membered ring structures. The geometries of these radicals are first theoretically investigated to understand the influence of substituents on the structural framework of NO group before analysing their HB interactions. Systems **11–19** possess at least one heteroatom such as oxygen, nitrogen, boron, and phosphorus in the ring other than nitrogen atom of nitroxide radical. Structures **20–23** are dinitroxide radicals.

5.4.1 MESP analysis

Electronic features especially inductive effect due to differences in substituents, the presence of heteroatom, and the effect of ring size greatly influence the electron-rich region around oxygen atom of NO moiety in nitroxides, which can be easily monitored using MESP analysis.[161–165] The most negative potential value (V_{min}) of MESP is a crucial parameter to quantify the through-bond electronic effects in organic molecules.[165,233] The location of V_{min} most often reflects the electron-rich region of a molecule and hence V_{min} is expected at the lone pair region of O atom of NO moiety. Thus, the V_{min} value of the oxygen atom of NO moiety is used to assess the electronic effects of nitroxide radicals. The MESP topographical features for three representative radicals *viz.* **4**, **15**, and **24** with and without substituents are presented in Figure 5.2. A convenient as well as an arbitrarily chosen isopotential value −16.32 kcal/mol is adopted for MESP topography. MESP plots help to compare the regions of the negative electrostatic potential on molecular surfaces of nitroxide radicals. The isopotential surface is present around the lone pair regions of NO moiety in all cases and it is also visible around the lone pair of N atoms of the heterocyclic radical **15**. As depicted in Figure 5.2, V_{min} is marked as a black dot in the lone pair region on the O atom of NO moiety. MESP plots reveal a greater region of the negative electrostatic potential surface when electron-donating substituent CH_3 is present, whereas the comparatively smaller region of negative electrostatic potential for electron-withdrawing F substituent. V_{min} values also reflect the same fact and for the **15** series, the structure with electron-donating CH_3 substituent has shown the largest V_{min} value (−43.24 kcal/mol) while the electron-withdrawing F substituted species has shown the least negative V_{min} (−17.63 kcal/mol) with respect to the unsubstituted structure wherein the observed V_{min} is −41.60 kcal/mol. As expected from previous studies, V_{min} values reflect the substituent effects in nitroxide radicals.[165]

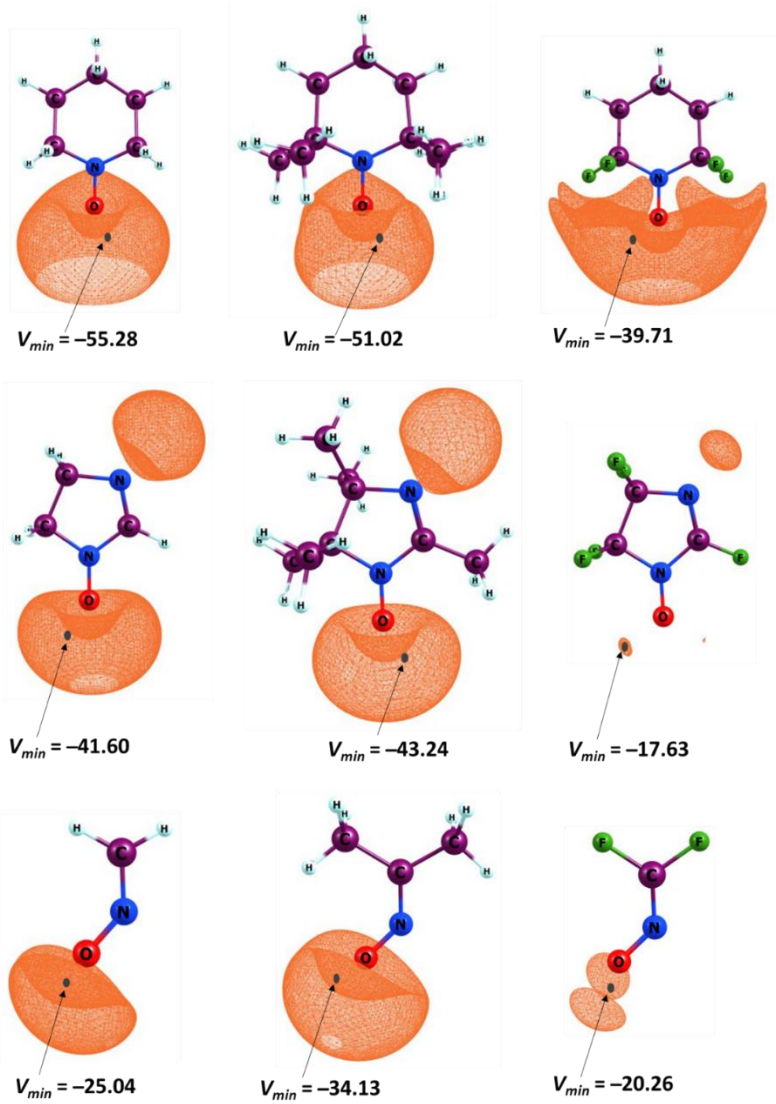

Figure 5.2 Molecular electrostatic potential mapped on isopotential surface value of −16.32 kcal/mol. The V_{min} values (in kcal/mol) of radicals **4**, **15,** and **24** with different substitutions (X = H, CH_3, and F) are marked as a black sphere.

A similar trend of substituent effects as in the case of **15** is noted for the iminoxyl radical **24**. In contrast to this, in the radical **4** series, the most negative V_{min} value of −55.28 kcal/mol was obtained for the unsubstituted species while the CH_3 substituted system has shown a V_{min} of −51.02 kcal/mol; apparently the fluorine substituted radical showed the least V_{min} (−39.71 kcal/mol). The observed difference in V_{min} noted for the CH_3 substituted species may be attributed to the steric effects of methyl groups which cause deformation of the ring moiety and result in lowering the electron density on the O-atom of NO functionality.[234]

Table 5.1 MESP (V_{min}) values of nitroxide radicals with substituents (X = H, CH_3, and F).

Structure	V_{min} (kcal/mol)		
	H	CH_3	F
1	−46.69	−53.59	2.51
2	−55.91	−53.46	−34.76
3	−53.28	−52.02	−32.99
4	−55.28	−51.02	−39.71
5	−55.85	−52.46	−41.09
6	−50.15	−49.01	−45.06
7	−51.95	−50.39	−35.14
8	−50.33	−46.81	−40.29
9	−48.93	−44.36	−43.86
10	−41.79	−41.48	−32.25
11	−53.15	−51.64	−24.45
12	−48.42	−48.63	−27.51
13	−54.91	−60.43	−39.78
14	−47.67	−48.41	−26.67
15	−41.60	−43.24	−17.63
16	−43.49	−44.18	−26.96
17	−32.32	−34.01	−25.38
18	−54.34	−51.52	−34.01
19	−45.15	−44.30	−42.17
20	−42.04	−43.32	−23.61
21	−44.79	−46.81	−26.79
22	−48.80	−50.81	−36.02
23	−40.47	−40.54	−39.53
24	−25.04	−34.13	−20.26
25	−26.02	−28.79	−23.45
26	−25.84	−31.17	−25.14
27	−27.67	−28.38	−30.06

Table 5.1 lists the V_{min} values of all the radicals considered in this study. The V_{min} value ranged from −25.04 to −55.91 kcal/mol for unsubstituted radicals, −28.38 to −60.43 kcal/mol for methyl-substituted, and 2.51 to −45.06 kcal/mol for fluorine substituted radicals. For the substituted systems, the electron-donating effect of the methyl group makes the nitroxide radical more electron-rich, whereas fluorine substitution withdraws electrons from the carbon chain thereby making the nitroxide radical electron poor. In general, when going from electron-withdrawing to electron donating group, an increase in the negative value of V_{min} is observed. Among all the radicals considered, methyl substituted **13** shows the deepest V_{min} value (−60.43 kcal/mol), indicating more electron donating ability of this radical. A

positive V_{min} value (2.51 kcal/mol) is obtained for fluorine substituted radical **1** which shows marked electron deficiency on the O-atom of NO moiety. In some cases, the unsubstituted radicals show more negative V_{min} values compared to methyl-substituted radical. This can be attributed to the steric effect caused by the methyl group resulting in decreased electron density on O on NO moiety as seen in the case of **4**. From Table 5.1 it can be noted that the V_{min} values of iminoxyl radicals are less negative compared to that of nitroxide radicals, these characteristics can be explained based on electron-donating character of alkyl residues present in nitroxide radicals.

5.4.2 Hydrogen bonding in nitroxide radicals

We analyzed the HBs in various complexes of nitroxide radicals with HF as the Lewis acid. Presented in Figure 5.3 are the optimized geometries of hydrogen-bonded complexes of radical **4** as a representative species. Table 5.2 presents the distance of NO···H interaction (d_2) for all the complexes along with the calculated interaction energy values (E_{int}).

Figure 5.3 Optimized geometries of hydrogen bonded complexes (with HF molecule) of radicals **4**, **15**, and **24** with different substitutions viz. H, CH_3, and F. The hydrogen bond distances are given in Å.

As postulated in earlier studies[226,235] herein we considered two conformations (*syn* and *anti*) about the nitroxide-HF unit for all complexes, however, the E_{int} values given in Table 5.2 correspond to the more stable conformer. The d_2 values fall in the range of 1.559 to 1.831Å for unsubstituted nitroxide complexes whereas the corresponding values in CH_3 and F substituted intermolecular complexes are respectively in the range of 1.562 to 1.797Å and 1.674 to 2.122Å. It is found that the lowest E_{int} (−0.23 kcal/mol) value which suggests a weak HB interaction (d_2 = 2.122Å) is observed in a complex formed by fluorine substituted radical **1**. The strongest HB interaction is obtained in a complex formed from the methyl-substituted radical **13** (E_{int} = −15.64 kcal/mol) wherein d_2 = 1.562 Å. It can be interpreted that shorter d_2 corresponds to greater E_{int} and hence stronger hydrogen-bonded complex. E_{int}

values of unsubstituted systems fall in the range from −5.42 to −14.99 kcal/mol while in CH_3 and F substituted systems E_{int} values respectively lie in the range from −6.62 to −15.64 kcal/mol and from −0.23 to −10.28 kcal/mol. Higher E_{int} values noted for complexes containing CH_3 substituted nitroxide radicals in comparison to their F substituted analogues can be explained based on electron-donating inductive effects of the CH_3 group. But in some cases, for instance, complexes involving radical **4** (see Figure 5.3), the unsubstituted species form stronger HBs than CH_3 substituted radicals on account of steric hindrance caused by CH_3 groups as discussed in the previous section.

Table 5.2 NO···H interaction distance (d_2) and interaction energy (E_{int}) of various hydrogen bonded complexes with and without substituents (X = H, CH_3, and F).

	d_2 (in Å)			E_{int} (in kcal/mol)		
Structure	H	CH_3	F	H	CH_3	F
1	1.714	1.659	2.122	−10.54	−12.23	−0.23
2	1.657	1.693	1.812	−12.70	−11.74	−7.09
3	1.664	1.697	1.809	−12.35	−11.46	−6.82
4	1.656	1.693	1.819	−12.51	−11.57	−7.58
5	1.647	1.677	1.782	−12.96	−12.26	−8.96
6	1.661	1.656	1.707	−12.16	−12.26	−9.87
7	1.666	1.700	1.802	−12.33	−11.21	−7.09
8	1.659	1.657	1.778	−12.20	−11.71	−7.99
9	1.662	1.655	1.781	−12.07	−11.47	−8.37
10	1.678	1.680	1.703	−10.42	−10.14	−8.84
11	1.665	1.656	1.834	−12.22	−12.68	−5.78
12	1.675	1.659	1.824	−11.69	−12.38	−6.18
13	1.559	1.562	1.674	−14.99	−15.64	−9.73
14	1.673	1.653	1.835	−11.77	−12.69	−6.14
15	1.693	1.680	1.848	−10.72	−11.25	−4.90
16	1.693	1.679	1.789	−10.65	−10.81	−7.04
17	1.723	1.710	1.807	−9.05	−9.39	−6.70
18	1.647	1.651	1.791	−12.85	−12.13	−8.93
19	1.667	1.655	1.723	−11.28	−11.64	−8.94
20	1.689	1.668	1.838	−12.41	−11.80	−5.85
21	1.661	1.635	1.782	−11.95	−12.99	−7.17
22	1.646	1.641	1.704	−12.39	−12.56	−9.79
23	1.675	1.671	1.691	−11.04	−11.08	−10.28
24	1.831	1.787	1.861	−5.42	−7.85	−5.12
25	1.816	1.797	1.817	−6.11	−6.62	−5.93
26	1.811	1.764	1.784	−6.01	−7.67	−6.52
27	1.809	1.786	1.829	−6.49	−7.27	−6.56

5.4.3 Relationship between E_{int} values and V_{min} values

It has been observed that both the E_{int} and V_{min} values reflect on electronic effects such as inductive and steric. In addition, it has been found that the highest V_{min} value is found for CH_3 substituted radical **13**, interestingly the same radical shows the strongest HB interaction with HF (see Table 5.1 and Table 5.2). Similarly, the lowest V_{min} value is obtained for F substituted radical **1**, for this radical has detected the least HB strength among other radicals. All these findings predict a relation between V_{min} values and E_{int} values, and Figure 5.4 illustrate the relationship between the V_{min} and E_{int} values for all radicals with different substitution. A strong correlation is obtained for unsubstituted radicals with a correlation coefficient of 0.944, whereas moderately good correlations are obtained for methyl and fluorine substituents with correlation coefficients 0.918 and 0.917 respectively. The factors such as steric effects, polarization, and the secondary interactions between the fluorine atom of HF and nearby atoms of the nitroxide radicals also contribute significantly to E_{int} values and hence some deviations from the linear plot shown by V_{min} are expected.[234,236] The correlation between V_{min} and E_{int} suggests that the V_{min} values reflect the electronic effect of nitroxide radicals and hence it can be used as a descriptor to assess the strength of HB interactions in such systems.

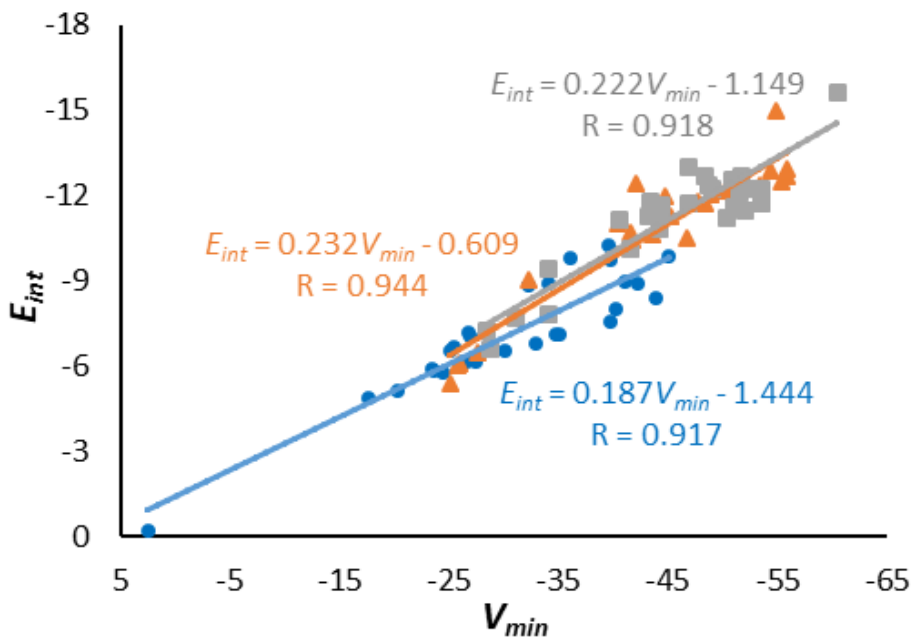

Figure 5.4 Correlation between V_{min} and E_{int} values of nitroxide-HF complexes (with substituents, X = H, CH_3, and F), orange triangles for X = H, gray squares for X = CH_3, and blue circles for X = F. The correlation coefficients is denoted by orange, gray and blue colours for X=H, CH_3, and F, respectively. All values are in kcal/mol.

5.4.4 Mulliken spin-density analysis

The Mulliken spin densities on nitrogen and oxygen atoms of NO moiety in nitroxide free radicals with different substituents are presented in Table 5.3. In general, the unpaired spin density is largely distributed on the NO moiety of the radical.[126] In the case of unsubstituted nitroxide radicals, a moderately lower spin density population is noted on the N atom compared to that of the O atom. The substituent present in the structural motif of nitroxide radical causes a fractional redistribution of unpaired spin density between N and O atoms. For instance, in the case of methyl-substituted nitroxide radicals, a slight increase in spin density value on the N atom at the expense of spin density on the O atom is observed in most of the cases, which is attributed to the partial shift of unpaired electron spin density population when an electron-donating substituent is present. A significant displacement of spin density from the N-atom towards the O-atom of NO moiety is noted in most of the cases when an electron-withdrawing substituent F is present in the structural motif of nitroxide radical. This is due to the greater contribution from the resonance structure >N–O• compared to the dipolar resonance structure > $N^{\bullet+}$–O^{-}, and hence a reduction in the spin density of N atom is noted.[125]

Table 5.3 Mulliken spin densities on N and O atoms of NO unit in nitroxide and iminoxyl radicals with and without substituents (X = H, CH_3, and F).

Structure	Spin density (in au)					
	X = H		X = CH_3		X = F	
	N	O	N	O	N	O
1	0.4351	0.5984	0.4191	0.5296	0.3650	0.2187
2	0.4327	0.5121	0.4532	0.5038	0.3223	0.6195
3	0.4273	0.5224	0.4687	0.5072	0.3315	0.6169
4	0.4501	0.5365	0.4407	0.5206	0.3268	0.6291
5	0.4038	0.5243	0.4491	0.5225	0.3597	0.5896
6	0.3231	0.4538	0.3424	0.4453	0.3016	0.5051
7	0.4206	0.5194	0.4793	0.5002	0.3197	0.6105
8	0.3403	0.4673	0.3565	0.4752	0.3159	0.5292
9	0.3110	0.4443	0.3386	0.4400	0.2774	0.5191
10	0.2948	0.4443	0.2957	0.4420	0.2825	0.4696
11	0.4344	0.5131	0.4789	0.4954	0.3096	0.6218
12	0.4347	0.5170	0.4701	0.5000	0.3254	0.6169
13	0.3254	0.5322	0.3406	0.5273	0.1828	0.6298
14	0.4235	0.5234	0.4721	0.5047	0.3237	0.6216
15	0.3150	0.4753	0.3482	0.4750	0.2688	0.5884
16	0.3208	0.5048	0.3290	0.4970	0.2805	0.5764

17	0.2426	0.4501	0.2706	0.4525	0.2132	0.5638
18	0.4005	0.5224	0.4588	0.5221	0.3817	0.5774
19	0.3343	0.4576	0.3444	0.4499	0.3195	0.5057
20	0.4144	0.5320	0.4486	0.5193	0.2989	0.6326
21	0.2487	0.3309	0.2780	0.3150	0.2079	0.3739
22	0.2447	0.3409	0.2545	0.3316	0.2201	0.3752
23	0.1687	0.3455	0.1797	0.3367	0.1654	0.3491
24	0.4731	0.5591	0.4401	0.5872	0.3448	0.6723
25	0.4458	0.5750	0.4523	0.5790	0.4130	0.6170
26	0.4449	0.5743	0.4633	0.5797	0.4156	0.6190
27	0.4619	0.5878	0.4532	0.5770	0.4663	0.5807

Table 5.4 Mulliken spin densities on atoms nitrogen, oxygen, hydrogen, and fluorine calculated for nitroxide-HF complexes of unsubstituted nitroxide radicals.

	Spin density (in au)			
Structure	N	O	H	F
1	0.4833	0.5596	−0.0076	−0.0004
2	0.4659	0.4839	−0.0142	0.0049
3	0.4599	0.4943	−0.0141	0.0050
4	0.4826	0.5023	−0.0127	0.0039
5	0.4542	0.4767	−0.0114	0.0076
6	0.3464	0.4203	−0.0128	0.0047
7	0.4464	0.4991	−0.0155	0.0060
8	0.3669	0.4303	−0.0137	0.0047
9	0.3368	0.4042	−0.0121	0.0057
10	0.3412	0.3698	−0.0025	0.0068
11	0.4684	0.4835	−0.0135	0.0046
12	0.4732	0.4826	−0.0122	0.0040
13	0.3864	0.4792	−0.0102	0.0016
14	0.4578	0.4949	−0.0127	0.0043
15	0.3442	0.4451	−0.0114	0.0043
16	0.3509	0.4761	−0.0125	0.0042
17	0.2782	0.4154	0.0005	0.0007
18	0.4401	0.4851	−0.0095	0.0032
19	0.3603	0.4164	−0.0114	0.0037
20	0.4460	0.4988	−0.0122	0.0044
21	0.2563	0.2907	−0.0076	0.0028
22	0.2520	0.2914	−0.0069	0.0026
23	0.1616	0.2897	−0.0069	0.0017
24	0.4953	0.5346	−0.0052	0.0023
25	0.4702	0.5469	−0.0064	0.0026
26	0.4686	0.5450	−0.0067	0.0027
27	0.4840	0.5573	−0.0090	0.0038

The HB-induced redistribution of spin densities of nitroxide radicals has been reported in earlier studies.[122] We further analyzed the redistribution of spin densities of NO moiety induced by the HB interaction in unsubstituted nitroxide-HF complexes (see Table 5.4 and Figure 5.5). In all complexes, nonzero values of spin densities on HF fragments is an evidence for the fractional spin transfer from nitroxide radical. Calculated electron spin density on the nitrogen atom is increased slightly in HF complexes, which indicates that there is a transfer of spin density from the O atom towards the N atom of NO moiety with HB.[237] This observation is in agreement with the previous findings of Ikryannikova et al. on a few nitroxides specifically used for spin probe applications.[125,126] Ikryannikova et al. investigated the effect of HB interactions on piperidine and imidazoline based nitroxides with water clusters. They concluded that spin density redistribution induced by hydration is significant for a spin label molecule. In spin-label applications, the changes in spin density distribution is very sensitive for a spin label molecule.

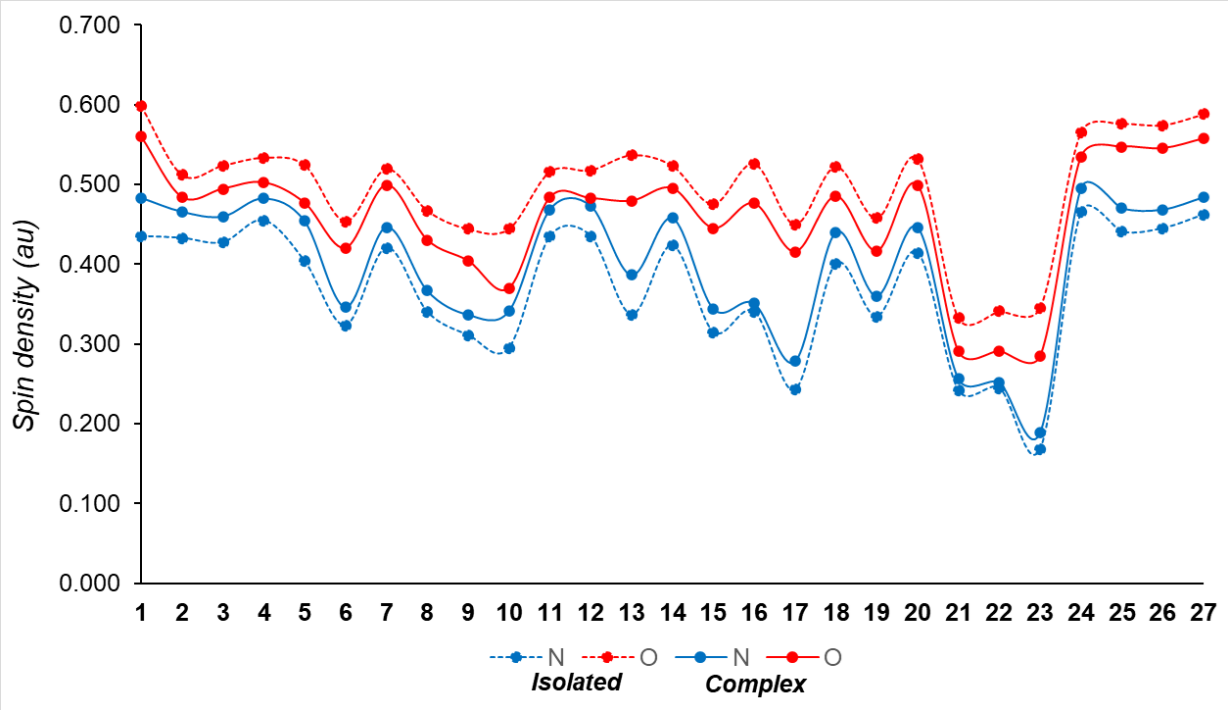

Figure 5.5 Plots of Mulliken spin densities on N- and O-atom of NO moiety of radicals in their isolated state (dotted line) and in complex with HF (bold line). The values of spin density on atoms are represented by blue and red color for N- and O-atoms of nitroxide radicals.

5.4.5 QTAIM analysis

The strength and nature of HBs in nitroxide-HF complexes are analysed using QTAIM parameters *viz.* electron density ($\rho(r)$), Laplacian of electron density ($\nabla^2\rho(r)$), and the total electron energy density ($H(r)$) at the bond critical point (bcp) of NO···H HB interaction. QTAIM topological plots of a representative complex with and without substituents are given in Figure 5.6. Table 5.5 presents the values of QTAIM parameters at the bcp for all complexes.

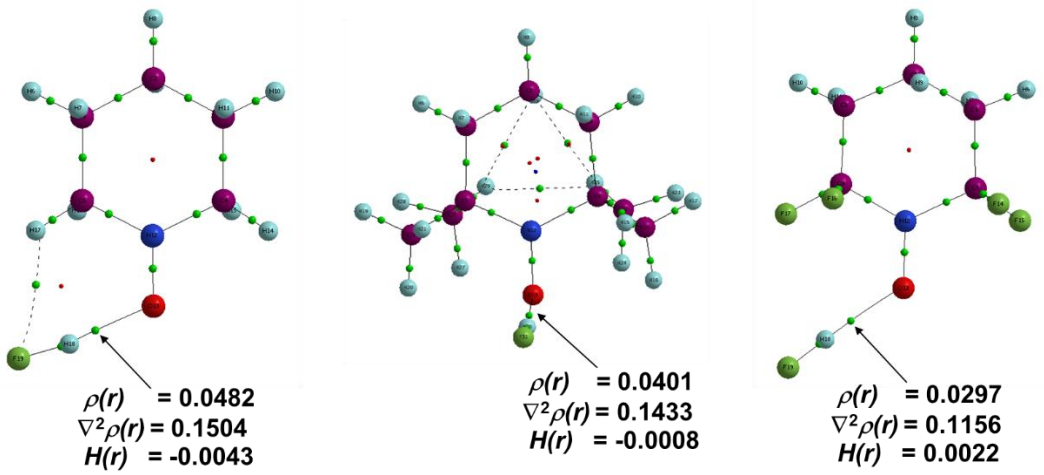

Figure 5.6 QTAIM plot of the complexes of **4** with substituents *viz.* H, CH_3 and F. Values of QTAIM parameters at the BCP (green spheres on bond path) on NO···H HB are given in au.

At first we consider the QTAIM parameters at the bcp of NO···H interaction of unsubstituted complexes of nitroxide radicals. The $\rho(r)$ value at the bcp is considered as an indicator of the strength of HB interaction.[76,238] The $\rho(r)$ values for all unsubstituted complexes fall in the range of 0.0405 − 0.0653 au; the minimum and maximum $\rho(r)$ value were noted for complexes formed by the radicals **17** and **13** respectively. The $\nabla^2\rho$ value, a measure of nature of a HB, fall within the range of 0.1376 – 0.1642 au. Generally it is considered that, for a typical HB, $\rho(r)$ and $\nabla^2\rho(r)$ should be lie respectively in the range of 0.002 − 0.035 au and 0.024 − 0.139 au.[167,168] High values of $\rho(r)$ and $\nabla^2\rho(r)$ are observed in all unsubstituted complexes, which indicates the presence of strong HB interactions in them. Apart from $\rho(r)$ and $\nabla^2\rho(r)$, $H(r)$ values at the bcp provide valuable information about the nature of a chemical bond. It can be seen that negative $H(r)$ values are observed for all nitroxide complexes, which fall in the range from −0.0013 to −0.0138 au. A positive $\nabla^2\rho$ along with a negative H value stand for a mix of closed-shell and shared NO···H HB interactions in complexes involving unsubstituted nitroxide radicals.[239]

Table 5.5 Values of QTAIM parameters (in au) at the bcp of NO···H HB in all complexes with and without substituents (X = H, CH_3, and F).

Structure	X= H			X = CH_3			X = F		
	$\rho(r)$	$\nabla^2\rho(r)$	$H(r)$	$\rho(r)$	$\nabla^2\rho(r)$	$H(r)$	$\rho(r)$	$\nabla^2\rho(r)$	$H(r)$
1	0.0434	0.1385	−0.0029	0.0478	0.1501	−0.0042	0.0125	0.0560	0.0029
2	0.0483	0.1501	−0.0044	0.0406	0.1425	−0.0010	0.0305	0.1175	0.0020
3	0.0474	0.1489	−0.0041	0.0401	0.1415	−0.0008	0.0308	0.1184	0.0020
4	0.0482	0.1504	−0.0043	0.0401	0.1433	−0.0008	0.0297	0.1156	0.0022
5	0.0489	0.1526	−0.0046	0.0431	0.1459	−0.0021	0.0323	0.1236	0.0013
6	0.0471	0.1493	−0.0043	0.0459	0.1498	−0.0029	0.0399	0.1414	−0.0007
7	0.0451	0.1480	−0.0036	0.0361	0.1404	−0.0006	0.0306	0.1187	0.0017
8	0.0469	0.1507	−0.0040	0.0453	0.1506	−0.0028	0.0325	0.1261	0.0016
9	0.0471	0.1502	−0.0037	0.0423	0.1438	−0.0017	0.0321	0.1194	0.0014
10	0.0424	0.1474	−0.0016	0.0418	0.1445	−0.0013	0.0387	0.1421	−0.0002
11	0.0473	0.1488	−0.0040	0.0467	0.1527	−0.0034	0.0290	0.1128	0.0023
12	0.0461	0.1472	−0.0035	0.0466	0.1518	−0.0034	0.0296	0.1149	0.0021
13	0.0653	0.1642	−0.0138	0.0631	0.1637	−0.0122	0.0488	0.1498	−0.0054
14	0.0464	0.1472	−0.0037	0.0475	0.1526	−0.0038	0.0295	0.1120	0.0019
15	0.0439	0.1428	−0.0027	0.0436	0.1478	−0.0021	0.0279	0.1097	0.0025
16	0.0427	0.1417	−0.0021	0.0432	0.1492	−0.0018	0.0342	0.1223	0.0005
17	0.0405	0.1376	−0.0013	0.0397	0.1426	−0.0005	0.0329	0.1180	0.0007
18	0.0490	0.1530	−0.0046	0.0459	0.1561	−0.0028	0.0320	0.1222	0.0013
19	0.0451	0.1503	−0.0032	0.0461	0.1535	−0.0031	0.0371	0.1387	0.0003
20	0.0475	0.1485	−0.0042	0.0463	0.1537	−0.0032	0.0285	0.1117	0.0024
21	0.0490	0.1499	−0.0049	0.0491	0.1577	−0.0044	0.0335	0.1260	0.0012
22	0.0503	0.1526	−0.0054	0.0480	0.1563	−0.0039	0.0430	0.1407	−0.0025
23	0.0467	0.1456	−0.0040	0.0438	0.1380	−0.0026	0.0406	0.1375	−0.0018
24	0.0279	0.1118	0.0026	0.0333	0.1221	0.0009	0.0285	0.1075	0.0017
25	0.0298	0.1031	0.0025	0.0318	0.1196	0.0016	0.0303	0.1157	0.0018
26	0.0297	0.1150	0.0021	0.0338	0.1236	0.0013	0.0330	0.1185	0.0011
27	0.0301	0.1152	0.0018	0.0306	0.1110	0.0015	0.0283	0.1108	0.0022

For CH_3 substituted nitroxide complexes, $\rho(r)$, $\nabla^2\rho(r)$, and $H(r)$ values at the bcp range from 0.0361 to 0.0631au, from 0.1380 to 0.1637 au, and from −0.0005 to −0.0122 au, respectively. Remarkably, high positive values of $\rho(r)$ and $\nabla^2\rho(r)$ along with negative values of $H(r)$ show stronger HB interaction with partial closed-shell and shared nature.[167,168,240] When the substituent X = F, the QTAIM parameters $\rho(r)$, $\nabla^2\rho(r)$, and $H(r)$ at the bcp are respectively fall in the range from 0.0125 to 0.0488 au, from 0.0560 to 0.1498 au, and from −0.0054 to 0.0029 au. Accordingly, $\rho(r)$ value decrease with F substitution which indicates the decrease in the strength of HB interaction as compared to X = H or CH_3 complexes. In addition, the positive $\nabla^2\rho(r)$ values and $H(r)$ values are either positive or close to zero in most of the cases (with X = F) suggesting ionic character of HB.[168,241]

5.4.6 Hydrogen bonded complexes with H_2O and CH_4

We used H_2O and CH_4 as Lewis acids for the purpose of assessment of HB interaction of unsubstituted nitroxide/iminoxyl radical with other HB donors. We have selected ten radicals *viz.* **3**, **4**, **11**, **12**, **13**, **16**, **17**, **21**, **24**, and **25** from the set of radicals depicted in Figure 5.1; among them **24** and **25** are iminoxyl radicals. We incorporated all categories of radicals in the ten representative systems from a total of 27 radicals.

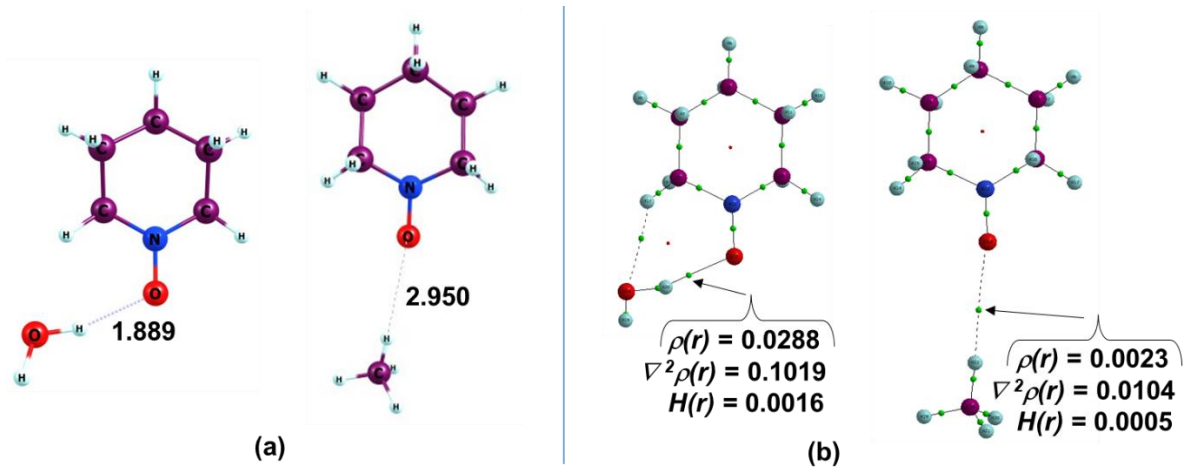

Figure 5.7 (a) Optimized geometries of complexes of unsubstituted nitroxide radical **4** with H_2O and CH_4. The distance of hydrogen bond is given in Å. (b) QTAIM topological plot with values of QTAIM parameters (in au) at NO···H interaction of the corresponding complexes.

The optimized geometries of hydrogen bonded complexes of unsubstituted radical **4** with H_2O and CH_4 are depicted in Figure 5.7(a). It should be noted that we have taken only the conformer of hydrogen bonded complexes in which a single H-atom of either H_2O or CH_4 is having HB with the O-atom of NO unit. The NO···H HB distance (d_2) and E_{int} values

computed for complexes are presented in Table 5.6. For complexes with H_2O, d_2 values range from 1.803Å to 2.146Å and E_{int} values range from −3.74 to −12.04 kcal/mol; the complex of **25** has the lowest E_{int} value (−3.74 kcal/mol) and complexes of **13** possess the highest E_{int} value (−12.04 kcal/mol). In the case of nitroxide-CH_4 complexes, d_2 values range from 2.440 to 3.257Å and E_{int} values range from −0.29 to −2.25 kcal/mol. It is clear that the HB interactions in nitroxide-CH_4 are very weak as compared to nitroxide-H_2O complexes. The complex formed between CH_4 and iminoxyl radical **25** has the lowest (−0.29 kcal/mol) and those formed by nitroxide radical **12** showed the highest (−2.25 kcal/mol) E_{int} values.

Table 5.6 Distance of hydrogen bond (HB; in Å) and interaction energy (E_{int}; in kcal/mol) values for hydrogen bonded complexes of unsubstituted nitroxide/iminoxyl radical with H_2O and CH_4.

Structure	Complexes with H_2O		Complexes with CH_4	
	HB distance	E_{int}	HB distance	E_{int}
3	1.894	−8.04	2.948	−0.52
4	1.889	−7.84	2.950	−0.59
11	1.890	−7.96	2.571	−2.00
12	1.901	−7.88	2.630	−2.25
13	1.803	−12.04	2.440	−1.81
16	1.925	−7.20	2.953	−0.47
17	1.954	−6.51	2.956	−0.42
21	1.913	−8.41	2.940	−0.46
24	2.146	−4.60	2.959	−0.34
25	2.086	−3.74	3.257	−0.29

The QTAIM topological plot along with QTAIM parameters of hydrogen bonded complexes of a representative radical with H_2O and CH_4 are sketched in Figure 5.7(b). The values of QTAIM parameters located at the bcp of NO···H bond paths of nitroxide-H_2O and nitroxide-CH_4 complexes are listed in Table 5.7. In nitroxide-H_2O complexes, values of $\rho(r)$ and $\nabla^2\rho(r)$ lie within the range of 0.0153 – 0.0369 au and 0.0582 – 0.1242 au, respectively, and $H(r)$ values ranging from −0.0002 to 0.0026 au. The positive $\nabla^2\rho(r)$ values and positive or close to zero values of $H(r)$ indicate typical closed-shell NO···H interactions in nitroxide-H_2O complexes. The calculated QTAIM parameters on NO···H HB for the nitroxide-CH_4 complexes have low $\rho(r)$ values (range from 0.0013 to 0.0106 au), positive $\nabla^2\rho(r)$ values (range from 0.0063 to 0.0303 au), and positive $H(r)$ values (ranging between 0.0004 and

0.0007 au). This suggests a weak and closed shell interaction in these hydrogen-bonded complexes.

Table 5.7 Values of QTAIM parameters (in au) on NO···H HB of nitroxide-H_2O and nitroxide-CH_4 complexes with radicals of **3**, **4**, **11**, **12**, **13**, **16**, **17**, **21**, **24**, and **25**.

Structure	Complexes with H_2O			Complexes with CH_4		
	$\rho(r)$	$\nabla^2\rho(r)$	$H(r)$	$\rho(r)$	$\nabla^2\rho(r)$	$H(r)$
3	0.0286	0.1013	0.0017	0.0023	0.0104	0.0005
4	0.0288	0.1019	0.0016	0.0023	0.0104	0.0005
11	0.0287	0.1021	0.0017	0.0074	0.0239	0.0006
12	0.0280	0.1004	0.0018	0.0067	0.0213	0.0005
13	0.0369	0.1242	−0.0002	0.0106	0.0303	0.0007
16	0.0264	0.0956	0.0020	0.0023	0.0104	0.0005
17	0.0248	0.0911	0.0021	0.0023	0.0103	0.0005
21	0.0277	0.0984	0.0017	0.0023	0.0105	0.0005
24	0.0153	0.0582	0.0020	0.0022	0.0102	0.0005
25	0.0160	0.0671	0.0026	0.0013	0.0063	0.0004

5.4.7 SAPT calculations

The contributions of different energy components *viz.* electrostatic, exchange, induction, and dispersion to the interaction energies are investigated at the SAPT0/aug-cc-pVTZ method on a selected number of hydrogen-bonded complexes formed by unsubstituted radicals namely, **3**, **4**, **11**, **12**, **13**, **16**, **17**, **21**, **24**, and **25**. All SAPT-derived components of the interaction energy of nitroxide-HF complexes are plotted in Figure 5.8(a) and corresponding values are listed in Table 5.8. The total SAPT interaction energy E_{int}^{SAPT} of the complexes range from −6.25 to −18.14 kcal/mol. The lower value of −6.25 kcal/mol corresponds to iminoxyl complex of **25** and a higher value of −18.14 kcal/mol is obtained for the complex formed by **13**. It can be seen that all values of exchange energy E_{exch} are positive; thereby it destabilizes the interacted complexes.[242,243] The sum of other energy components (*i.e.*, $E_{elst} + E_{ind} + E_{disp}$) imparts stabilization of the interacted complex.[243] As evident from Figure 5.8(a), the electrostatic component (E_{elst}) is the dominant contributor, about 52% to 58% to the overall stabilization energy. This is followed by the induction term (E_{ind}), which is 28% to 30% of the overall stabilizing energy. The dispersion component E_{disp} make comparatively modest contributions, ranging from −2.23 to −7.28 kcal/mol, in all complexes. The contribution of E_{disp} is about 14% to 19% to the total interaction energy. The magnitude of E_{elst} is comparable to that of E_{exch} except in a complex of **13**. In general, the E_{elst} is the most attractive term and plays a major role in the overall stabilization energy along with the induction term.

Table 5.8 The SAPT partitioning of interaction energy for unsubstituted complexes of **3**, **4**, **11**, **12**, **13**, **16**, **17**, **21**, **24**, and **25** radical with HF. All energy values are in kcal/mol.

Structure	E_{elst}	E_{exch}	E_{ind}	E_{disp}	E_{int}^{SAPT}
3	−17.62	16.78	−8.44	−4.32	−13.60
4	−18.31	18.08	−8.82	−4.47	−13.52
11	−17.73	16.96	−8.45	−4.35	−13.57
12	−16.96	16.48	−8.07	−4.29	−12.83
13	−27.53	31.60	−14.94	−7.28	−18.14
16	−15.21	15.82	−7.63	−4.20	−11.22
17	−13.04	13.94	−6.88	−3.94	−9.91
21	−19.06	17.96	−9.11	−4.70	−14.92
24	−7.59	7.22	−3.81	−2.23	−6.41
25	−7.58	8.34	−4.17	−2.84	−6.25

Table 5.9 The SAPT partitioning of interaction energy for unsubstituted complexes of **3**, **4**, **11**, **12**, **13**, **16**, **17**, **21**, **24**, and **25** radical with H_2O. All energy values are in kcal/mol.

Structure	E_{elst}	E_{exch}	E_{ind}	E_{disp}	E_{int}^{SAPT}
3	−11.33	11.04	−3.77	−4.22	−8.27
4	−11.89	12.18	−4.00	−4.21	−7.91
11	−11.74	11.70	−3.93	−4.26	−8.23
12	−11.60	11.60	−3.78	−4.28	−8.06
13	−21.51	22.57	−7.67	−6.92	−13.52
16	−10.34	10.79	−3.38	−4.05	−6.98
17	−9.52	10.37	−3.17	−4.10	−6.43
21	−14.10	13.66	−4.61	−4.70	−9.74
24	−5.98	6.38	−1.86	−3.14	−4.60
25	−5.33	5.79	−1.58	−3.03	−4.15

Table 5.10 The SAPT partitioning of interaction energy for unsubstituted complexes of **3**, **4**, **11**, **12**, **13**, **16**, **17**, **21**, **24**, and **25** radical with CH_4. All energy values are in kcal/mol.

Structure	E_{elst}	E_{exch}	E_{ind}	E_{disp}	E_{int}^{SAPT}
3	−0.26	0.21	−0.13	−0.48	−0.66
4	−0.27	0.22	−0.13	−0.49	−0.67
11	−1.24	2.74	−0.44	−2.99	−1.93
12	−1.43	3.19	−0.44	−3.39	−2.06
13	−2.21	4.22	−1.03	−3.05	−2.07
16	−0.22	0.21	−0.08	−0.49	−0.58
17	−0.21	0.21	−0.06	−0.48	−0.54
21	−0.26	0.21	−0.12	−0.51	−0.68
24	−0.17	0.20	−0.05	−0.43	−0.44
25	−0.09	0.08	−0.03	−0.32	−0.36

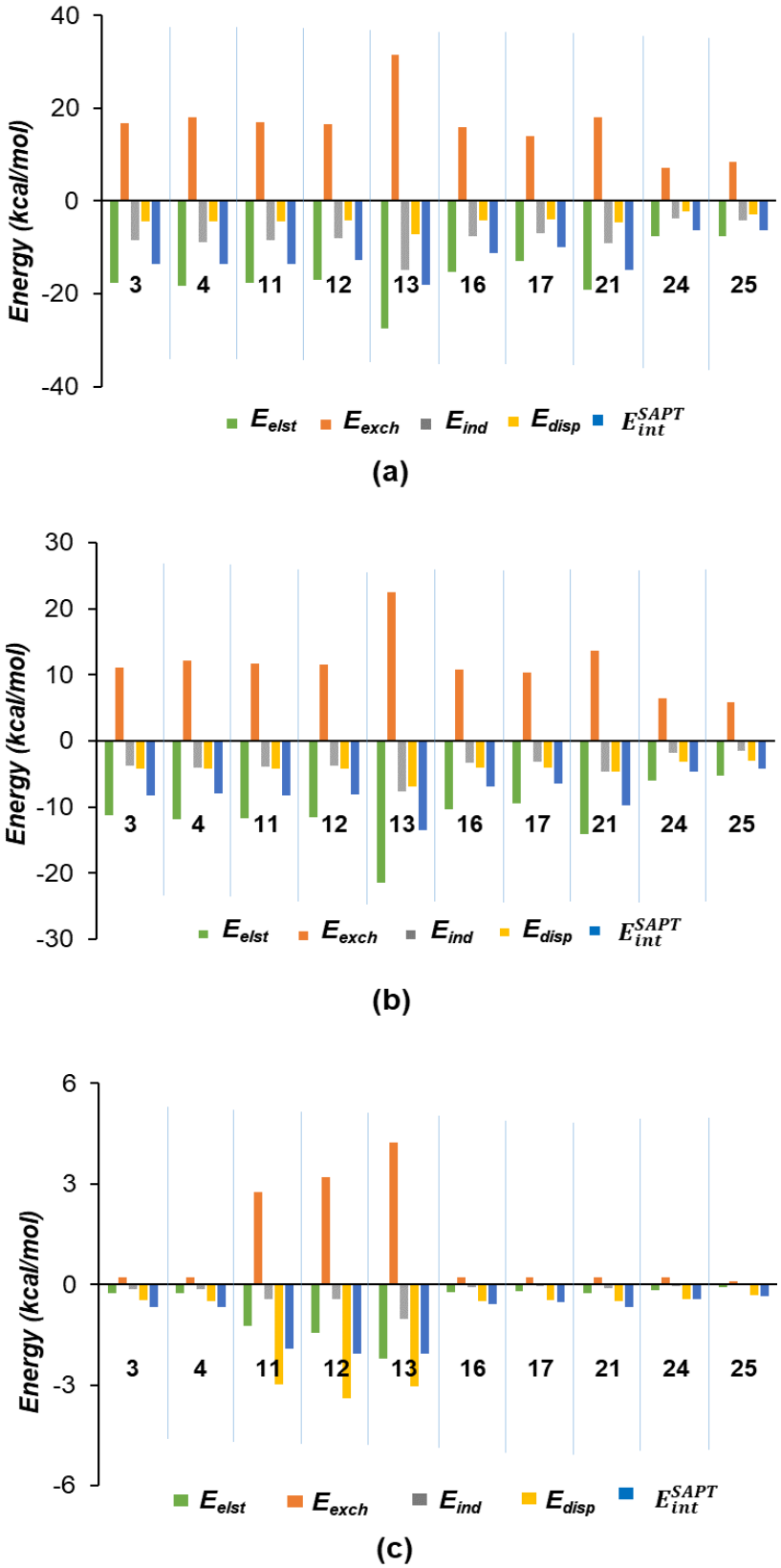

Figure 5.8 The SAPT partitioning of interaction energy for unsubstituted complexes of **3**, **4**, **11**, **12**, **13**, **16**, **17**, **21**, **24**, and **25** with (a) HF (b) H_2O, and (c) CH_4. The total SAPT interaction energy (blue) is the sum of all components *viz.* electrostatic (E_{elst}, green), exchange (E_{exch}, orange), dispersion (E_{disp}, yellow), and induction (E_{ind}, gray).

The SAPT0/aug-cc-pVTZ calculations were also performed on a series of complexes of unsubstituted radicals with H_2O and CH_4. The E_{int}^{SAPT} values and the components of various energy terms for all the complexes of nitroxide-H_2O and nitroxide-CH_4 are plotted in Figure 5.8(b) and Figure 5.8(c), respectively (corresponding values are listed in Table 5.9 and Table 5.10, respectively). For nitroxide-H_2O complexes, as given in Figure 5.8(b), the electrostatic term is the most prominent stabilizing component to overall SAPT energy like nitroxide-HF complexes. For methane interacted complexes, an analysis of SAPT result showed that the overall stabilization energy receives a contribution of about 21% to 35% from E_{elst}, 7% to 16% from E_{ind}, and 48% to 73% from E_{disp}. The energy components for nitroxide-CH_4 complexes are plotted in Figure 5.8(c). It is clear from Figure 5.8(c) that the overall stabilization energy is mainly composed of dispersion, resulting from the dipole - induced dipole interaction between nitroxide and CH_4. The next important attractive term is E_{elst} whereas E_{ind} plays comparatively least role in the overall stability of the hydrogen bonded complexes of CH_4.

5.4.8 NBO analysis

An NBO view of donor-acceptor orbitals (with $E^{(2)}$ energy larger than 0.1 kcal/mol) involved in the NO···H HBs of hydrogen-bonded complexes of **1** (**1-HF**) with various substituents is depicted in Figure 5.9. The lone pairs of oxygen atoms in NO moiety ($lp(O)_{NO}$) of radical **1** interact with the antibonding (σ_{H-F}^{*}) orbital of H−F bond in all **1-HF** complexes with various substituents. A total stabilization ($E^{(2)}$) energy of 17.99, 24.10, and 1.66 kcal/mol is calculated for complexes with unsubstituted, CH_3 substituted, and F substituted radical **1**, respectively. This again shows that CH_3 substituted radical **1** forms the strongest HB with HF, then it is followed by unsubstituted radical, and F substituted radical forms the weakest HB. Hence, NBO results are in agreement with the MESP and QTAIM results.

5.4.9 Comparison of strength of hydrogen bonding interactions of NO, HNO, HONO, and nitroxide

The hydrogen-bonded (with NO···H interaction) complexes of NO, HNO, HONO, and nitroxide radicals *viz.*, H_2NO and $(CH_3)_2NO$ with a water molecule is illustrated in Figure 5.10(a) along with their HB distances and interaction energy (E_{int}) values. The E_{int} values of $(CH_3)_2NO\ldots H_2O$, $H_2NO\ldots H_2O$, $HNO\ldots H_2O$, $HONO\ldots H_2O$, $NO\ldots H_2O$ interactions are −7.86, −8.25, −2.76, −2.14, and −0.77 kcal/mol, respectively. Therefore, the nitroxide-water

complexes is the most stable, and it is followed by HNO…H_2O, HONO…H_2O complexes, and the NO…H_2O is the least stable complex.

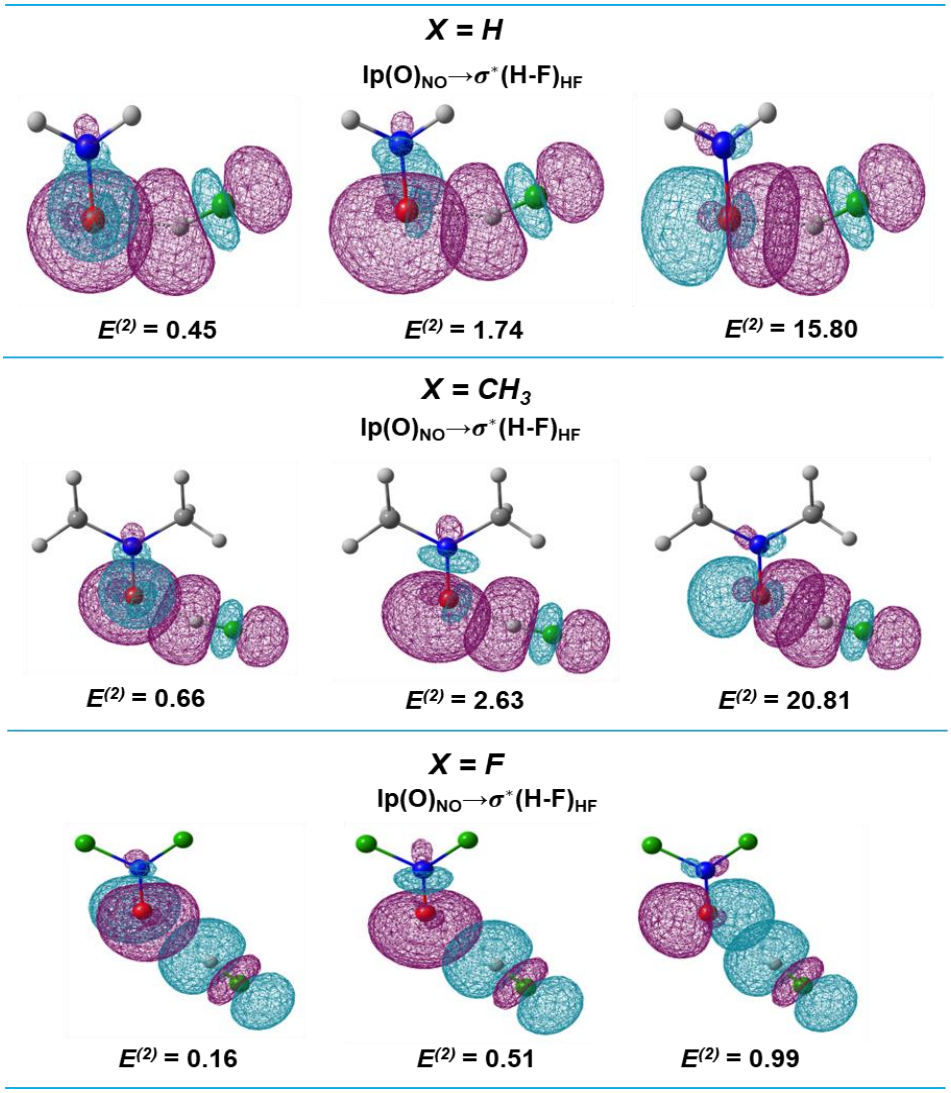

Figure 5.9 The donor-acceptor orbitals (isovalue = 0.03 au) involved in hydrogen-bonded complexes of **1** (**1-HF**) with various substituents (X = H, CH_3, and F). The $E^{(2)}$ energy for these interactions is estimated based on second-order perturbation theory in NBO analysis.

The distance of HB (NO···H) indicates that the strongest HB is present between $(CH_3)_2NO$ and H_2O (distance = 1.887 Å), then it is followed by H_2NO…H_2O (2.004 Å), HNO…H_2O (2.062 Å), HONO…H_2O (2.123 Å), and the weakest HB in NO…H_2O complex (2.249 Å). Hence, the nitroxide-water complexes have the strongest HB compared to other complexes, and the trend in HB strength corresponds to the trend in stability of these complexes based on E_{int} values. Furthermore, the HB strength in these complexes is also assessed using QTAIM parameters (see Figure 5.10(b)). Based on electron density ($\rho(r)$) values, the trend of NO···H HB strength followed by $(CH_3)_2NO$…H_2O ($\rho(r)$ = 0.0289 au),

$H_2NO\ldots H_2O$ (0.0238 au), $HNO\ldots H_2O$ (0.0189 au), $HONO\ldots H_2O$ (0.0158 au), $NO\ldots H_2O$ (0.0114 au) complexes is consistent with the trend found based on their HB distances.

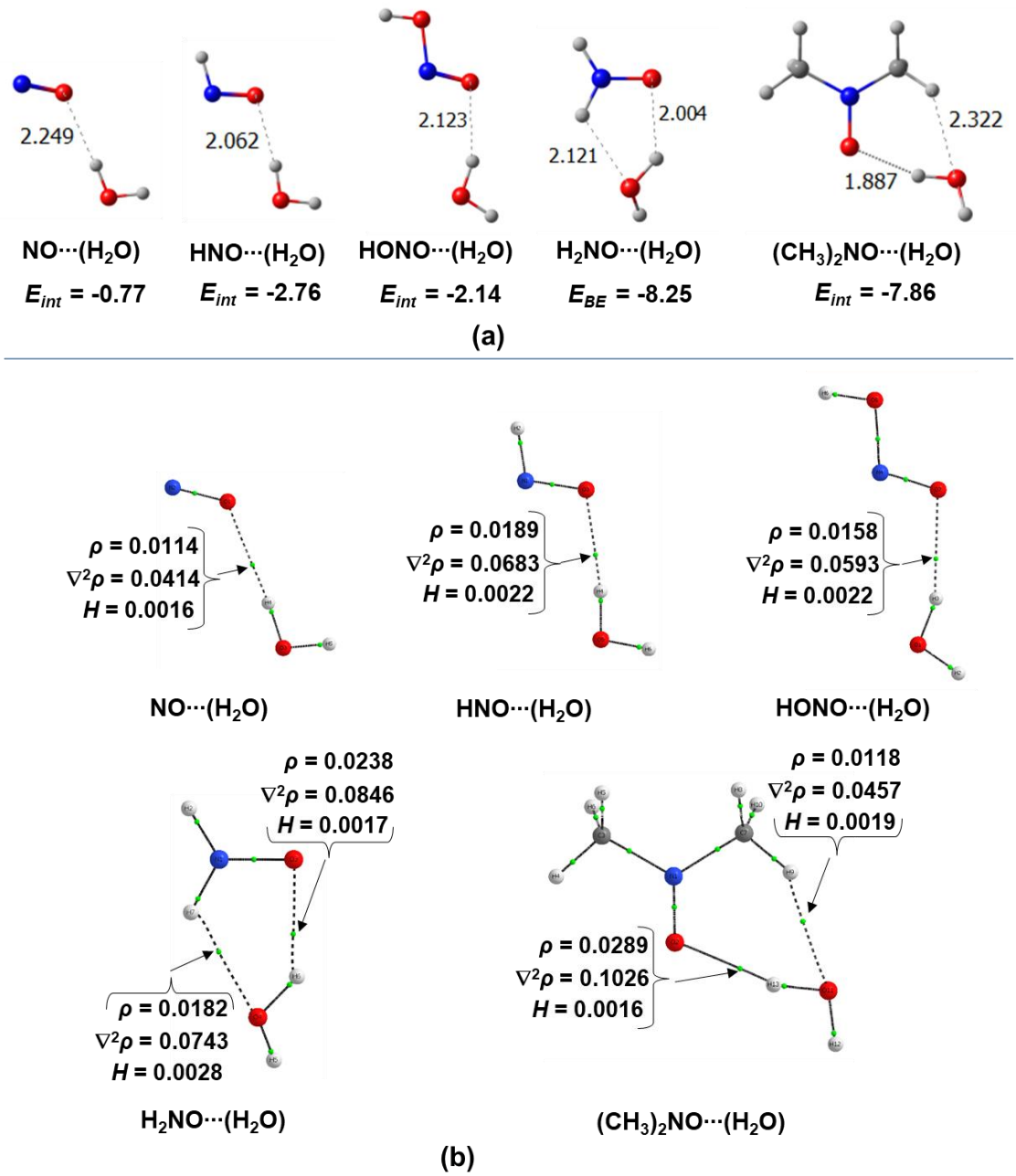

Figure 5.10 Hydrogen bonded (NO···H) complexes of NO, HNO, HONO, H_2NO, and $(CH_3)_2NO$ with water: (a) Optimized geometries with distance of hydrogen bond is given in Å and interaction energies (E_{int}) in kcal/mol, and (b) QTAIM topological plot with values of QTAIM parameters at hydrogen bonds in au.

It should also be noted that in nitroxide-water complexes, a weak HB is formed via CH_3 and H substituents of $(CH_3)_2NO$ and H_2NO nitroxides, respectively, with O-atom of

water (with a $\rho(r)$ value of 0.0118 and 0.0182 au, respectively). The higher $\rho(r)$ value of $H_2NO\ldots H_2O$ complex suggest a stronger secondary interaction in $H_2NO\ldots H_2O$ compared to that of $(CH_3)_2NO\ldots H_2O$. This may be the reason for greater stability of $H_2NO\ldots H_2O$ complex (E_{int} = −8.25 kcal/mol) than $(CH_3)_2NO\ldots H_2O$ (−7.86 kcal/mol).

5.5 Conclusions

In the present study, intermolecular hydrogen bond (HB) involving nitroxide radical has been investigated by using DFT calculations at the UM06L/6-311++G(d,p) level. The deepest minimum of MESP (V_{min}) around the O-atom of NO moiety is used to monitor the electronic effect of various substituted nitroxide radicals. The V_{min} values can be used as a good descriptor to measure the interaction energy of hydrogen-bonded complexes of nitroxide radicals. Further, the strength and nature of intermolecular HB interaction were characterized by QTAIM analysis. For all studied complexes of HF, the nature of HB is predicted to be partially closed-shell and shared-type interactions with electron-donating substituents whereas the HB is mostly closed-shell type interactions in systems with electron-withdrawing substituents. The SAPT calculations have revealed that the interaction energies of nitroxide complexes largely depend on the electrostatic term while the dispersion term is the major contributor to the interaction energy of nitroxide-CH_4 complexes. The NBO analysis rendered a picture of donor-acceptor orbitals involved in the HBs of a nitroxide hydrogen-bonded complex with various substituents. Furthermore, this chapter included a comparison of the HB interactions of NO, HNO, HONO, and nitroxide molecules. This shows that the strongest HB is formed by the nitroxide radical, followed by HNO and HONO, and the weakest HB is formed by NO. A fundamental understanding of the nature and strength of HB in nitroxide radicals is crucial since their chemical and biological applications rely largely on their ability to form intermolecular HB interactions. Insights on HB strength in nitroxide radicals revealed in this work could be beneficial in designing stable nitroxides for diverse applications *viz.* spin labeling, and hydrogen abstracter, amongst others.

Publication based on this chapter:

Thufail M. Ismail; Mohan, N.; Sajith, P. K. "Theoretical study of hydrogen bonding interactions in substituted nitroxide radicals". ***New Journal of Chemistry*** 2021, *45*, 3866-3875.

Chapter 6

Hydrogen Bond Assisted Adsorption of Nitric Oxide on Various Metal Loaded ZSM-5 Zeolites

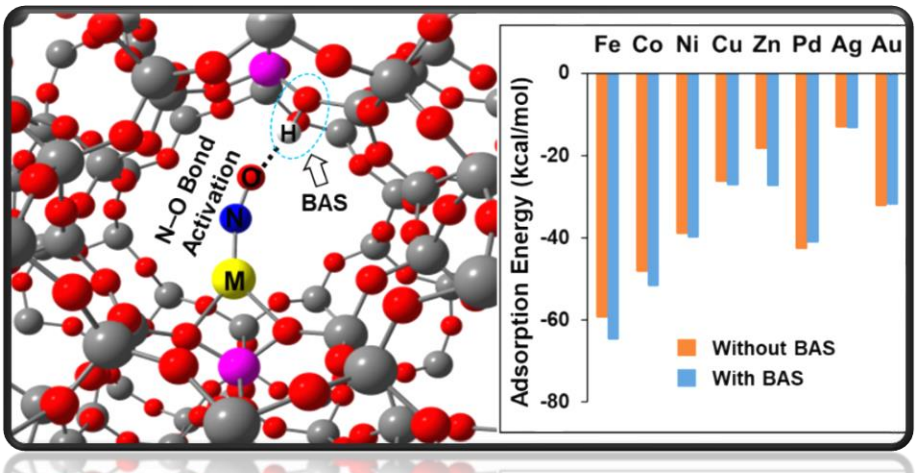

6.1 Abstract

Understanding the characteristics of nitric oxide (NO) adsorption on metal-loaded zeolites is a prerequisite for developing efficient catalysts for NO abatement reactions. In this study, we probed the effect of the hydrogen bond (NO···H interaction) that exists between adsorbed NO and Brønsted acid sites (BAS) in various metal-loaded ZSM-5 zeolites (M-ZSM-5, wherein M = Fe, Co, Ni, Cu, Zn, Pd, Ag, and Au) by using DFT calculations at B3LYP/def2-SVP level. The presence of NO···H hydrogen bond (HB) has altered the NO adsorption energies significantly; appreciable stabilization via HB is noted for NO complexes of Zn, Fe, and Co, and reasonable stabilization is obtained for Ni and Cu complexes, whereas an anomalous effect of a HB is identified in Ag, Pd, and Au species. Moderate weakening of N–O bond in all NO adsorbed complexes primarily due to a HB has been realized in terms of Mayer bond order and quantum theory of atoms in molecules (QTAIM) topological analyses; N–O bond activation follows the order, Ag < Pd < Au < Ni < Cu < Co < Fe < Zn. We obtained a good correlation between HB distance and molecular electrostatic potential (MESP) at the O-atom (V_O) of NO adsorbed on BAS-free M-ZSM-5; which suggests that V_O can be considered a key descriptor to infer the strength of a HB between the adsorbed NO and M-ZSM-5 with BAS. Finally, the energy decomposition analysis (EDA) in combination with natural orbitals for chemical valence (NOCV) has provided the qualitative aspects of electron back donation from the metal to the antibonding MO of NO; this back donation is quite impressive in HB-assisted NO adsorption. We expect that the findings of this study will open up the possibility of the design of BAS containing metal-loaded zeolites for the catalytic mitigation of NO.

6.2 Introduction

The metal-loaded ZSM-5 (denoted as M-ZSM-5) is extensively used as a catalyst for NO abatement reactions. The catalytic activity of different metals in M-ZSM-5 is reported in many experimental as well as theoretical studies.[40-44] Besides, studies have shown that Brønsted acid sites (BAS) have significant roles in the catalytic activity of ZSM-5 and other zeolites in many reactions.[135,244,245] It is evident from many experimental studies that hydrogen bond (HB) is formed between BAS and organic molecules.[134,137,246] However, to the best of our knowledge, a systematic experimental/theoretical exposition of the influence of BAS in M-ZSM-5 on the adsorption of NO has not been done so far. It is essential to address a cooperative effect of NO adsorption onto the metal atom, and the HB formed between the BAS and adsorbed NO. The HB formation can affect the N–O (or the M–NO)

bond in NO adsorbed on M-ZSM-5, which has an impact on the electronic structures and NO adsorption energy. Similarly, the extent of HB formation may differ with the type of metal atom being used in M-ZSM-5. Hence, we used different transition metals such as Fe, Co, Ni, Cu, Zn, Pd, Ag, and Au for the present study. Accordingly, the disparate metal atoms will produce differences in the adsorption of NO to M-ZSM-5. In the present work, we aim to delineate the characteristics of electronic interactions in NO adsorbed M-ZSM-5 using quantum computational calculations. In order to gain more insight into the energetics of adsorption, HB interactions, and electronic structures of the M–NO bond, various theoretical analyses such as Mulliken spin density analysis, bond order analysis, and energy decomposition analysis (EDA) combined with natural orbitals for chemical valence (NOCV) are carried out in addition to quantum theory of atoms in molecules (QTAIM) and molecular electrostatic potential (MESP) analyses.

6.3 Computational methods

A cluster model of ZSM-5 with 32 tetrahedra sites (T) obtained from the zeolite database was used for computational simulations.[247] The model contains terminal Si- or O-atoms; therefore, an adequate number of H-atoms were added to terminal Si/O-atoms to fulfil their valence. Standard single bond distances (*viz.* 1.47 Å for Si–H bond and 0.90 Å for O–H bond) were assigned to those capped H-atoms. The M-ZSM-5 structure is created by the replacement of a quadrivalent Si cation in the ten membered ring (10-MR) of the original cluster model of the ZSM-5 framework by a trivalent Al cation with the simultaneous insertion of a monovalent metal ion (M^+ = Fe^+, Co^+, Ni^+, Cu^+, Zn^+, Pd^+, Ag^+, and Au^+). The BAS containing M-ZSM-5 structure was obtained via substituting two vis-à-vis quadrivalent Si-cations in the 10-MR of the 32 tetrahedra cluster with two trivalent Al cations, separated by four SiO_4 tetrahedra units, and this model is designated as **4T**, accompanied by the incorporation of M and H ions. The structures with aluminium pairs separated by one, two, and three SiO_4 tetrahedra designated as **1T**, **2T**, and **3T,** respectively, were also modeled. In fact, we attempted various orientations of HBs by changing the position of BAS on the Cu-ZSM-5 cluster. We obtained that the **4T** model has the strongest HB with adsorbed NO and BAS with a distance of 1.904 Å, whereas the corresponding distances of **3T**, **2T,** and **1T** are 2.090 Å, 2.466 Å, and 4.372 Å respectively; the optimized geometries are depicted in Figure 6.1. Thus, the orientation in which the strongest HB interaction is present, i.e., the **4T** model, is selected for the present study. The cluster models of M-ZSM-5 with and without BAS are depicted in Figure 6.2. The complexations of NO to M-ZSM-5 with and without BAS are

conveniently represented in the text as H···(ON)–M-ZSM-5 (or M–NO···H) and (ON)–M-ZSM-5 (or, M–NO), respectively.

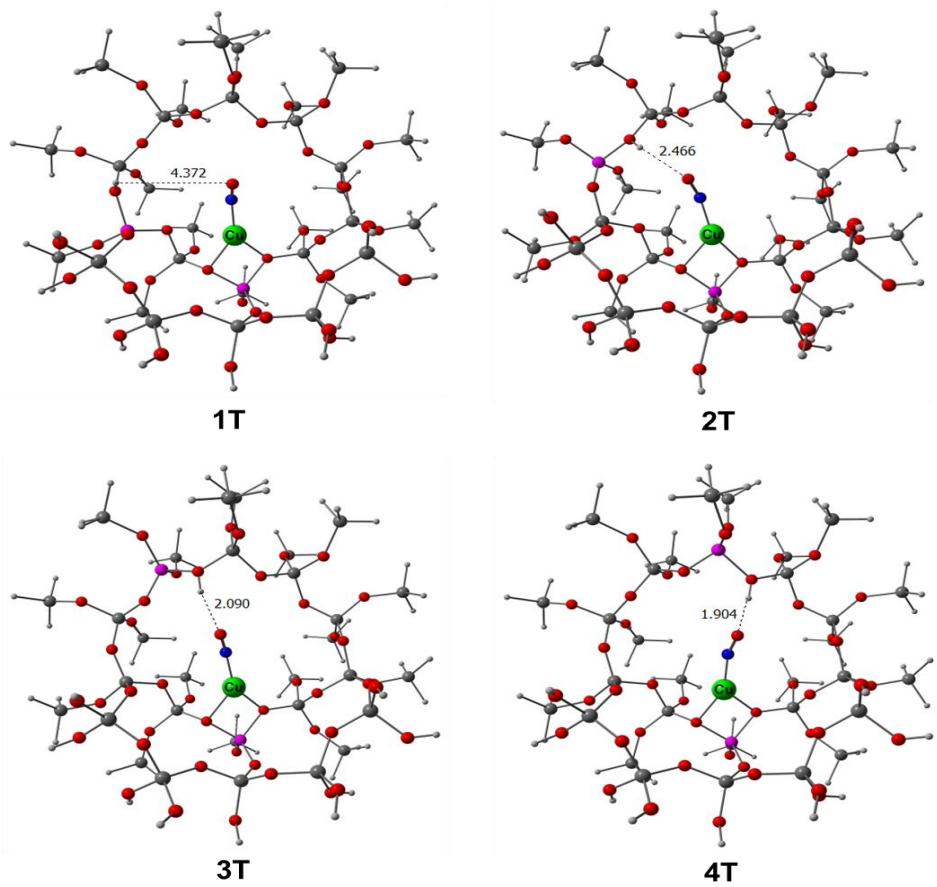

Figure 6.1 Optimized geometries of H···(ON)–Cu-ZSM-5 complexes (**1T**, **2T**, **3T,** and **4T**) with different positioning of BAS. The relevant bond distance is given in Å.

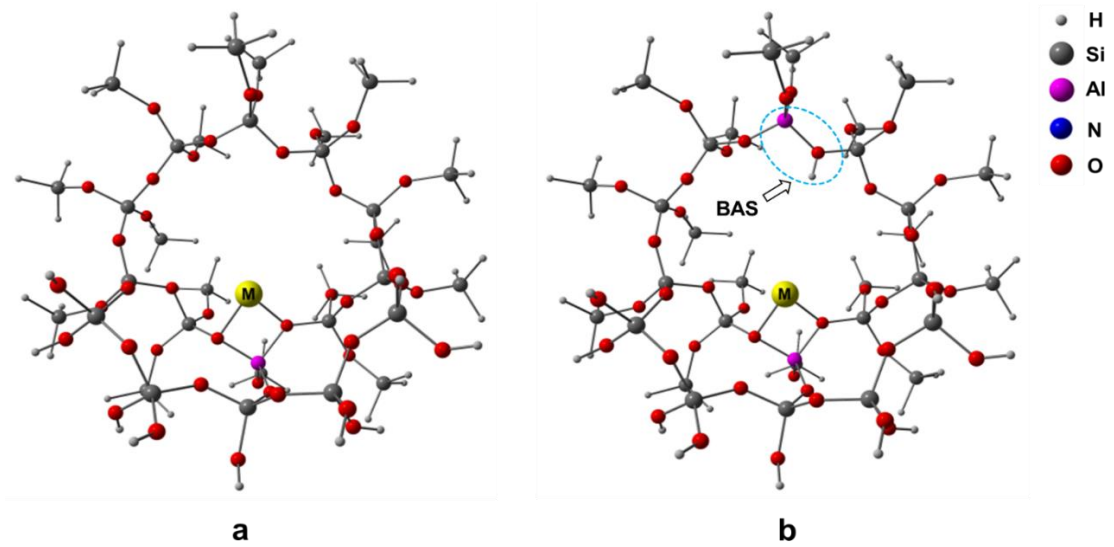

Figure 6.2 The cluster model of M-ZSM-5 used in this study. (**a**) System without BAS. (**b**) System with BAS (**4T** model). In the structures, M denotes (Yellow spheres) the monovalent transition metal ions (M = Fe, Co, Ni, Cu, Zn, Pd, Ag, and Au).

Density functional theory (DFT) within the formalism of B3LYP[157] level with def2-SVP[147] basis set was used for geometry optimization and subsequent frequency calculations of all the structures simulated by employing the Gaussian 16 program package.[192] During geometry optimizations, the Si-atoms and the terminal H-atoms capped to Si/O-atoms in the cluster model of M-ZSM-5 were kept fixed to maintain the confinement of the ZSM-5 framework. For better energy estimates, single-point calculations were additionally performed at B3LYP and the dispersion-corrected B3LYP-D3 methods using the def2-TZVP basis set.[147,159]

Adsorption energy (E_{ads}) was calculated using equation (Eq. 6.1), wherein $E_{complex}$, E_{NO}, and $E_{M-ZSM-5}$ are the energies of (ON)–M-ZSM-5 (or H···(ON)–M-ZSM-5), NO, and M-ZSM-5 (or M-ZSM-5 with BAS) species respectively.

$$E_{ads} = E_{complex} - (E_{NO} + E_{M-ZSM-5}) \qquad \text{(Eq. 6.1)}$$

The optimized geometries were further utilized for quantum theory of atoms in molecules (QTAIM) and molecular electrostatic potential (MESP) and energy decomposition (EDA) analyses. QTAIM analysis is carried out in AIMAll software.[193] EDA is performed using Amsterdam Density Functional (ADF) package introduced by Morokuma[78] and subsequently improved by Ziegler et al.[248] Relativistic adjustments based on Zero Order Regular Approximation (ZORA)[249] are employed during the EDA as encoded in ADF 2019.105 software.[250] The generalized gradient approximation functional BP86 composed of Becke exchange and Perdew correlation functional is utilized for EDA.[157,251] The spin-unrestricted EDA is carried out assuming spin-unrestricted fragments (NO and M-ZSM-5) form a spin-unrestricted complex.[252] As discussed in the chapter 1 based on EDA, the total interaction energy (E_{int}^{EDA}) or total binding energy (*TBE*) is the sum of energies of electrostatic term E_{elst}, Pauli's term E_{pauli}, and the orbital contribution term E_{orb} (see Eq. 6.2).[252]

$$TBE = E_{Pauli} + E_{ES} + E_{Orb} \qquad \text{(Eq. 6.2)}$$

Ultimately, the extended transition state (ETS) approach[253], in combination with the natural orbitals for chemical valence (NOCV) theory[254], has been used to get insights into the nature of charge transfer in these complexes.

6.4 Results & discussion

6.4.1 Electronic-structural features and N–O stretching frequencies of M–NO and M–NO···H complexes

It has been noted that NO binding to a metal atom can occur either via end-on (through N-terminal or O-terminal) or side-on mode.[255] Herein, we obtained that N-terminal end-on adsorption to M-ZSM-5 is the most favorable mode of NO adsorption, which agrees with previous reports.[138] Therefore, further discussions are based on the optimized geometries of the N-terminal mode of NO adsorption over M-ZSM-5 structures. It should be noted that except for Cu, Ag, and Au species, more than one spin multiplicities is possible for the NO adsorbed complexes. For instance, the Fe(I) complex can have singlet, triplet, quintet, and septet spin multiplicities. The optimized geometries of NO-adsorbed complexes with different spin multiplicities were determined for each M^+ species at the B3LYP/def2-SVP level of theory. The correct multiplicity of the complex in each case is then assigned as the species with the lowest energy in accordance with the strategy employed by Fellah.[256] In the case of (ON)–Fe-ZSM-5, the complex with triplet multiplicity was found to be the most stable species; the singlet, quintet, and septet spin multiplicity structures are found to be 45.88, 18.81, and 38.18 kcal/mol higher in energy than the triplet species. The energetics of M-ZSM-5 and (ON)–M-ZSM-5 complexes with different spin multiplicities are given in Table 6.1. The correct spin state obtained for (ON)–M-ZSM-5 complexes is also applicable to H···(ON)–M-ZSM-5 complexes, which is verified from single point calculation performed for different spin states at B3LYP/def2-SVP level of theory using optimized geometry of most stable spin state. The most stable spin states obtained in this study are consistent with the previous theoretical studies on NO adsorption to various metal-loaded zeolites.[50,256,257] For instance, triplet spin state for (ON)–Fe-ZSM-5 using DFT method,[256] doublets for NO adsorbed M-ZSM-5 complexes of Ag and Au using DFT method,[50] and also the well-studied NO adsorbed Cu loaded zeolites have doublet spin state.[257] Similarly, the most stable spin state obtained in this study for Co–NO, Ni–NO, Pd–NO, and Zn–NO complexes are doublet, singlet, singlet, and triplet, respectively.

The optimized geometries of (ON)–M-ZSM-5 and H···(ON)–M-ZSM-5 complexes with M = Fe, Co, Ni, Cu, Zn, Pd, Ag, and Au ions in their most stable spin multiplicity state are depicted in Figure 6.3. The important geometrical parameters at the complexation sites of the various complexes are listed in Table 6.2. It can be noted from Table 6.2 that the M–N distances for the (ON)–M-ZSM-5 complexes range from 1.601 to 2.166 Å while the N–O

bond distances range from 1.140 to 1.212 Å. The bond distances predicted herein reasonably agree with the values computed earlier.[50,256,258] The calculated M–N–O bond angle (∠MNO) for the Fe, Co, and Ni complexes are roughly (~4º to 6º) close to 180º; while the ∠MNO for the Cu, Zn, Pd, Ag, and Au complexes are about 50º to 30º lower than 180º indicating the bent nature of the M–N–O moiety. The ∠MNO values obtained herein are consistent with those estimated in earlier studies for NO adsorbed metal complexes.[50,256,257,259,260] The end-on linear M–NO species (as in M = Fe, Co, and Ni, vide supra) in the metal nitrosyls might have a NO^+ state; while the end-on bent (angle ~ 120º) M–NO segment indicates the presence of NO^- state.[261] Moreover, the half-bent M–N–O with a bond angle of ~ 140 – 150º (as in M = Cu, and Pd, noted above) is expected to be a NO radical state, while an angle between 130 – 140º is shown by Zn, Ag, and Au suggests an intermediate state between NO^- and NO radical states.[262]

Table 6.1 The relative energies of M-ZSM-5 and (ON)–M-ZSM-5 complexes in their different spin states (M = Fe, Co, Ni, Zn, and Pd).

M-ZSM-5	Spin Multiplicity	Relative Energy (kcal/mol)	(ON)–M-ZSM-5	Spin Multiplicity	Relative Energy (kcal/mol)
Fe	2	29.74	Fe–NO	1	45.88
	4	0.00		3	0.00
	6	3.69		5	18.81
				7	38.18
Co	1	39.81	Co–NO	2	0.00
	3	0.00		4	14.03
	5	12.72		6	49.79
Ni	2	0.00	Ni–NO	1	0.00
	4	26.68		3	10.44
Zn	2	0.00	Zn–NO	1	7.04
	4	120.15		3	0.00
Pd	2	0.00	Pd–NO	1	0.00
	4	68.23		3	21.03

The computed stretching frequencies of the N–O bond (ν_{NO}) in various (ON)–M-ZSM-5 complexes are also given in Table 6.2. The lowest ν_{NO} was observed for the Zn complex (1672 cm^{-1}), while the highest value was obtained for the Ni complex (2081 cm^{-1}). The experimental ν_{NO} reported for Fe–NO, Cu–NO, Ag–NO, and Au–NO complexes are 1786 cm^{-1}, 1813 cm^{-1}, 1884 cm^{-1}, and 1817 cm^{-1} respectively;[48,263–265] the corresponding calculated values are respectively 1930 cm^{-1}, 1986 cm^{-1}, 2019 cm^{-1}, and 1981 cm^{-1}.

Obviously, the calculated ν_{NO} values are overestimated compared to experimental values. Previous studies have shown that most popular DFT methods cannot exactly reproduce the experimental ν_{NO} values; thus, scaling factors were used therein.[266,267] Thus, it is quite obvious from the calculated N–O bond distances and stretching frequencies that considerable N–O bond elongation occurs upon adsorption of NO to various M-ZSM-5 structures.

Table 6.2 Important structural parameters[a], N–O stretching frequencies[a], adsorption energies[b], and ΔE_{ads} of various (ON)–M-ZSM-5 and H···(ON)–M-ZSM-5 complexes.

Complex	Bond distance (Å)			∠MNO (°)	ν_{NO} (cm^{-1})	E_{ads} (kcal/mol)	ΔE_{ads} (kcal/mol)
	M–N	N–O	NO···H				
Fe–NO	1.721	1.172	--	176.26	1930	–59.22	–5.27
Fe–NO···H	1.734	1.183	1.748	177.50	1887	–64.49	
Co–NO	1.689	1.163	--	173.79	1969	–47.94	–3.59
Co–NO···H	1.703	1.175	1.802	169.21	1914	–51.53	
Ni–NO	1.601	1.144	--	175.61	2081	–38.89	–0.79
Ni–NO···H	1.598	1.153	1.922	177.31	2036	–39.68	
Cu–NO	1.835	1.153	--	148.16	1986	–26.09	–0.87
Cu–NO···H	1.802	1.160	1.904	156.02	1944	–26.96	
Zn–NO	1.891	1.212	--	131.27	1672	–18.23	–8.87
Zn–NO···H	1.891	1.215	1.645	138.67	1700	–27.10	
Pd–NO	1.777	1.140	--	145.57	2007	–42.46	1.64
Pd–NO···H	1.770	1.151	2.006	144.21	1946	–40.82	
Ag–NO	2.166	1.144	--	134.23	2019	–13.01	–0.11
Ag–NO···H	2.145	1.147	2.223	136.96	1997	–13.12	
Au–NO	1.977	1.147	--	133.28	1981	–31.97	0.21
Au–NO···H	1.959	1.152	2.176	135.83	1952	–31.76	

[a] From the B3LYP/def2-SVP level of theory.

[b] From the B3LYP/def2-TZVP//B3LYP/def2-SVP level of theory.

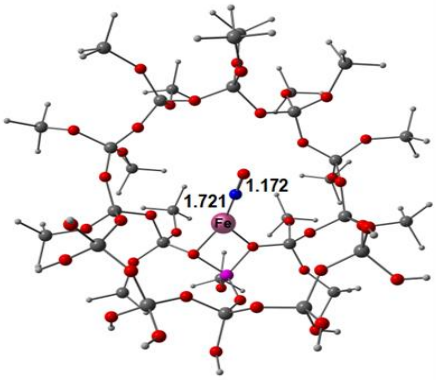

Fe–NO

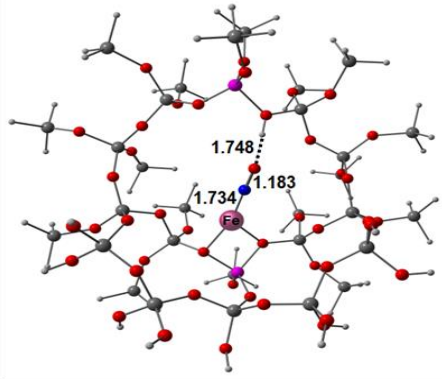

Fe–NO···H

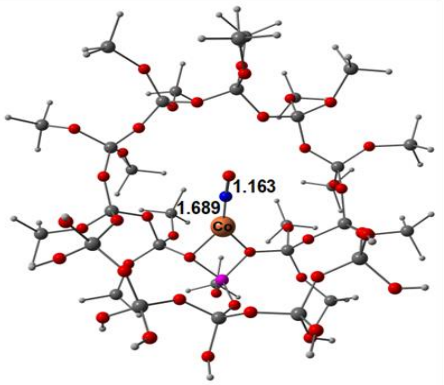

Co–NO

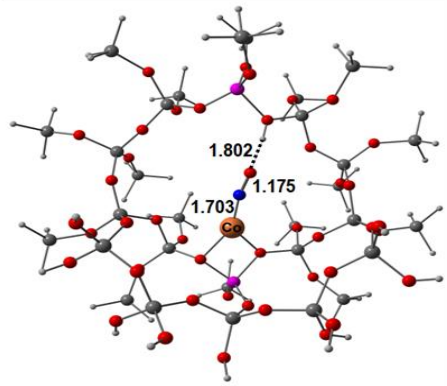

Co–NO···H

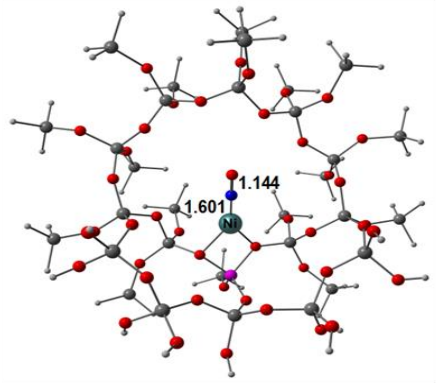

Ni–NO

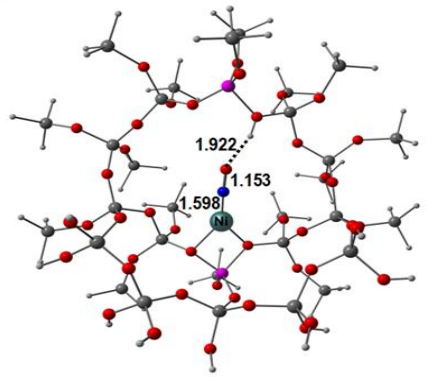

Ni–NO···H

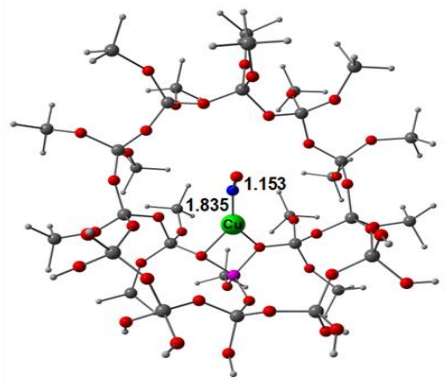

Cu–NO

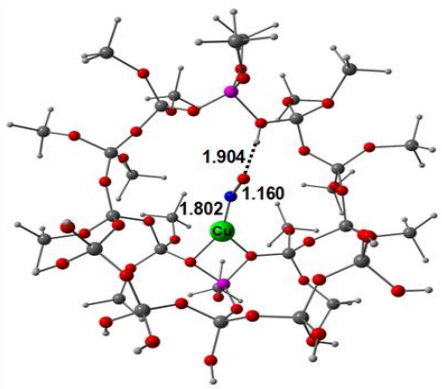

Cu–NO···H

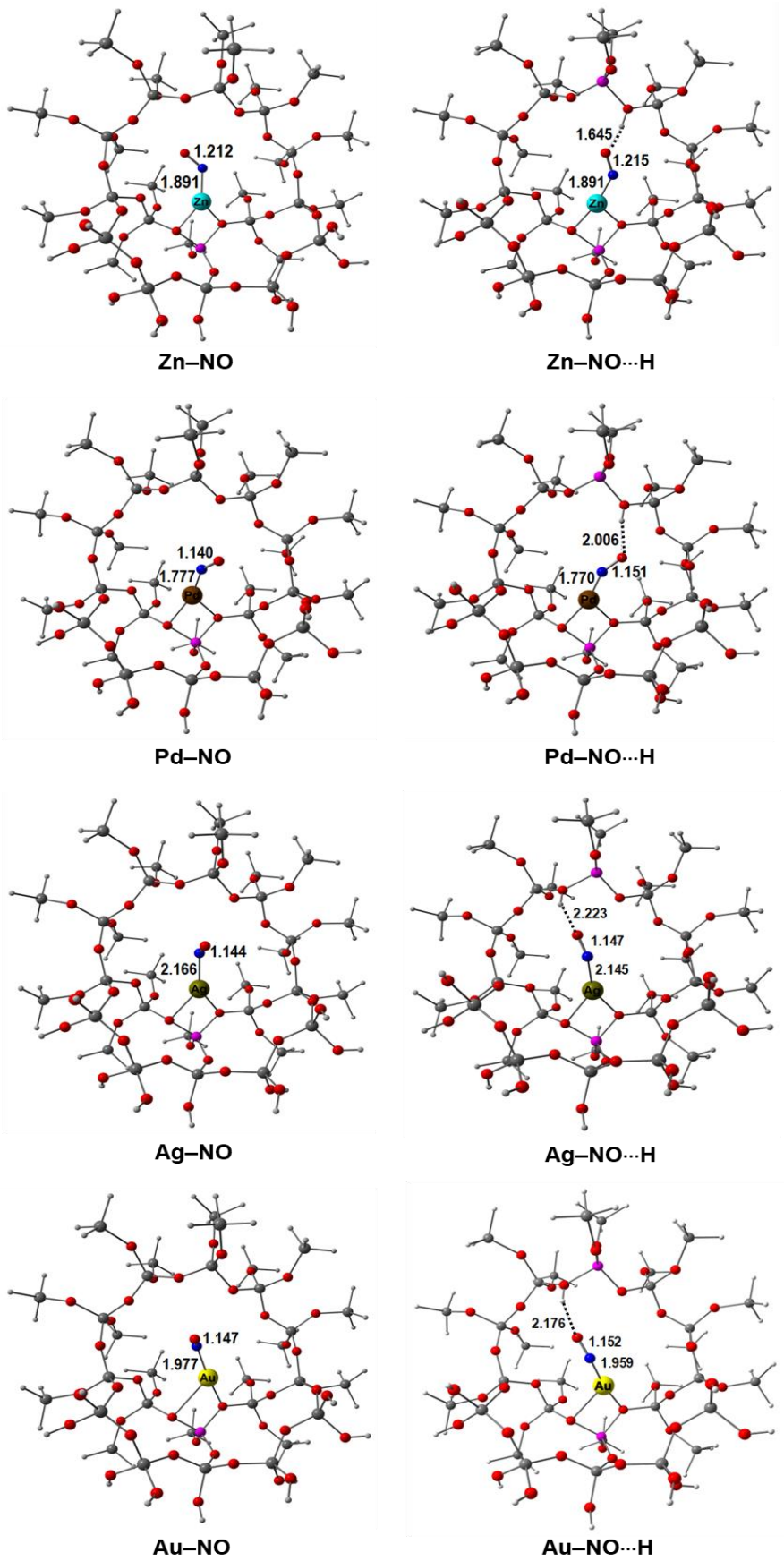

Figure 6.3 Optimized geometries of (ON)–M-ZSM-5 and H···(ON)–M-ZSM-5 complexes. The M–N, N–O, and HB distances are in Å unit.

The M–N bond distances listed in Table 6.2 for the H···(ON)–M-ZSM-5 complexes range from 1.598 Å to 2.145 Å. It may be noted that the M–N distance remains the same in both H···(ON)–M-ZSM-5 and (ON)–M-ZSM-5 complexes of Zn metal. Table 6.2 also depicts that the N–O bond is elongated in all H···(ON)–M-ZSM-5 complexes compared to their (ON)–M-ZSM-5 counterparts. Moreover, a considerable decrease in N–O bond stretching frequencies (except for the Zn complex) has been noticed in the H···(ON)–M-ZSM-5 complexes. Clearly, additional elongation of the N–O bond in H···(ON)–M-ZSM-5 complexes as compared to (ON)–M-ZSM-5 systems can be attributed due to the HB formation between the BAS and NO. A similar weakening of the N–O bond is observed in BAS-assisted NO adsorption on Cu-SAPO-34 studied by Uzunova using DFT methods.[268] The HB distances estimated herein fall in the range of 1.645 to 2.223 Å. Further, from the HB distances, it can be assumed that the weak HB formation occurs in H···(ON)–M-ZSM-5 for Pd (HB distance = 2.006 Å), Ag (2.223 Å), and Au (2.176 Å) while all other metals have strong HBs (with HB distances below 2.000 Å). Based on the HB distances, the HB strength follows the order for different metal species as Ag < Au < Pd < Ni < Cu < Co < Fe < Zn.

6.4.2 Adsorption energies (E_{ads})

The E_{ads} values obtained for NO adsorption on various M-ZSM-5 without BAS at the B3LYP/def2-TZVP//B3LYP/def2-SVP level of theory are listed in Table 6.2; apparently, the E_{ads} fall within –13.01 to –59.22 kcal/mol. The E_{ads} obtained herein are comparable with the E_{ads} for adsorption of NO on various metal-loaded zeolites reported earlier.[51,269] For instance, the E_{ads} calculated using the periodic DFT method (PW91) and higher level *ab initio* for NO adsorption on Cu-loaded zeolite clusters are about –27.00 kcal/mol.[257,269] Similarly, an E_{ads} of –41.8 kcal/mol for NO adsorption on Pd-SSZ-13 (using the HSE06 method) reasonably agrees with our predictions herein.[51] The E_{ads} obtained with different metals in this study follow the order: Ag < Zn < Cu < Au < Ni < Pd < Co < Fe.

With a few exceptions, the E_{ads} for NO adsorption on M-ZSM-5 with BAS computed at B3LYP/def2-TZVP//B3LYP/def2-SVP level of theory are more negative than systems without BAS (see Table 6.2). A comparison of E_{ads} for NO adsorptions on M-ZSM-5 with and without BAS at the B3LYP/def2-TZVP//B3LYP/def2-SVP level is shown in Figure 6.4. Also, we computed the difference in adsorption energy (ΔE_{ads} = E_{ads} (complex with BAS) - E_{ads} (complex without BAS)) and given in Table 6.2. The E_{ads} values calculated at the B3LYP-D3/def2-TZVP//B3LYP/def2-SVP level for both systems are also depicted in Figure

6.4; the corresponding values are listed in Table 6.3. Although Grimme's dispersion corrected (GD3) B3LYP method gives higher E_{ads} values, the relative ordering and trends obtained in E_{ads} from both levels of theories are the same. It is clear from Figure 6.4 that except for Pd and Au metals, the NO adsorbed M-ZSM-5 with BAS possesses more stabilization than M-ZSM-5 without BAS (hence negative ΔE_{ads} values). In fact, this stabilization effect is minimal for Ag metal, characterized by a weak HB (2.223 Å) and a low negative value for ΔE_{ads} (–0.12 kcal/mol). The weak HB formation (HB length > 2.000 Å) obtained for Pd and Au in H···(ON)–MZSM-5 complexes can rationalize the slight destabilization reflected in their positive ΔE_{ads} values. It can be recognized that the strength of the HB (NO···H) in the H···(ON)–M-ZSM-5 complexes influence the stabilization of NO complexes of M-ZSM-5 with BAS. Thus, it is important to assess the strength of the NO···H HB on the stabilization of NO complexes with a simultaneous slight weakening of the N–O bond.

For completeness, we present an excerpt of the results (E_{ads} values) obtained from modeling the end-on (through O-atom) and side-on adsorptions of NO to M-ZSM-5. The obtained E_{ads} for O-terminal attachment of NO to M-ZSM-5 without BAS lies within a range of –5.89 to –41.39 kcal/mol at the B3LYP/def2-SVP level of theory. The E_{ads} values for Fe, Co, Ni, Cu, Zn, Pd, Ag, and Au are –41.39, –33.18, –6.36, –16.83, –11.83, –5.89, –8.54, and –15.56 kcal/mol, respectively. We obtained the optimized structures of complexes with the side-on attachment of NO to the M-atom of M-ZSM-5 for only Fe, Co, Ni, Cu, and Au. The adsorption energies obtained at the B3LYP/def2-SVP level for Fe, Co, Ni, Cu, and Au systems are –50.69, –39.55, –35.67, –17.32, and –11.34 kcal/mol, respectively. Thus, in agreement with previous studies, the NO's O-terminal and side-on binding possess fewer stabilizations than its N-terminal adsorption to M-ZSM-5.[138]

Table 6.3 The E_{ads} for various NO complexes of M-ZSM-5 in their most stable spin state (without and with BAS) calculated at B3LYP-D3/def2-TZVP//B3LYP/def2-SVP, and B3LYP/def2-SVP levels of theories.

Metal	E_{ads} (in kcal/mol)	
	B3LYP-D3/def2-TZVP// B3LYP/def2-SVP	B3LYP/def2-SVP
Fe–NO	–63.40	–64.89
Fe–NO···H	–68.05	–72.42
Co–NO	–51.37	–58.72
Co–NO···H	–55.90	–63.72
Ni–NO	–43.15	–49.06

Ni–NO···H	–44.40	–51.51
Cu–NO	–30.14	–30.94
Cu–NO···H	–31.38	–32.75
Zn–NO	–24.69	–24.39
Zn–NO···H	–32.44	–34.24
Pd–NO	–47.00	–43.92
Pd–NO···H	–45.95	–42.67
Ag–NO	–17.37	–15.98
Ag–NO···H	–17.65	–16.68
Au–NO	–37.49	–33.56
Au–NO···H	–36.90	–33.86

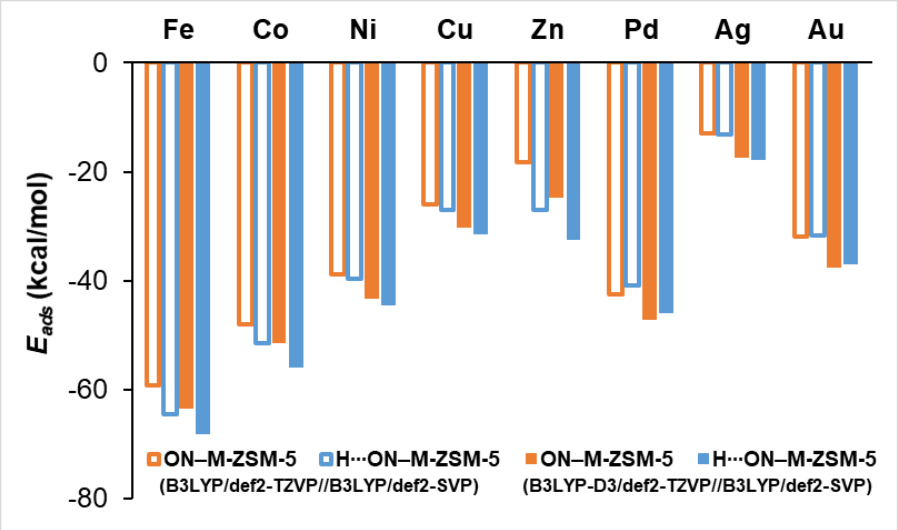

Figure 6.4 Comparison of adsorption energy (E_{ads}) for NO adsorption on M-ZSM-5 with and without BAS calculated at the B3LYP/def2-TZVP//B3LYP/def2-SVP and B3LYP-D3/def2-TZVP//B3LYP/def2-SVP levels of theory.

6.4.3 Mulliken spin density analysis

Mulliken spin densities on metal atom (M) and O- & N- atoms of NO for (ON)–M-ZSM-5 and H···(ON)–M-ZSM-5 complexes obtained at the B3LYP/def2-TZVP//B3LYP/def2-SVP level of theory are given in Table 6.4. It has been reported that variation in the Mulliken spin densities on M can be used as an indicator of change in the oxidation state of the metal atom in the zeolite framework upon adsorption of adsorbate like NO molecule.[52,53] It can be noted from Table 6.4 that the Mulliken spin densities on Fe, Co, Cu, Ag, and Au have increased from bare M-ZSM-5 to (ON)–M-ZSM-5 complex. On the other hand, lower spin densities are noted on Ni, Zn, and Pd in their (ON)–M-ZSM-5 complexes than their bare metal counterparts. The spin densities on M atoms have exhibited similar trends while moving from BAS containing M-ZSM-5 to H···(ON)–M-ZSM-5 complexes.

The spin densities on N-atoms of adsorbed NO in all (ON)–M-ZSM-5 and H···(ON)–M-ZSM-5 complexes are higher than that on O-atoms; concomitantly, the spin densities on N-atoms in H···(ON)–M-ZSM-5 complexes are greater than that in (ON)–M-ZSM-5 complexes. In contrast to this, the spin densities on O-atoms in H···(ON)–M-ZSM-5 complexes are lower than that in (ON)–M-ZSM-5 complexes; this is probably due to the HB formations in H···(ON)–M-ZSM-5 complexes. It may be considered that the transfer of spin density from O-atom to N-atom occurred during the NO···H HB formations in all these H···(ON)–M-ZSM-5 complexes. A moderate amount of spin accumulation on N-atom has been noticed in H···(ON)–M-ZSM-5 complexes with M as Fe, Co, and Zn. Interestingly, the strong NO···H HB formations can account for substantial stabilization of these complexes as estimated in terms of E_{ads}.

Table 6.4 Mulliken spin densities on metal atom (M) of M-ZSM-5 (with and without BAS), and M, N, and O atoms of NO adsorbed complexes (with and without BAS) calculated at the B3LYP/def2-TZVP//B3LYP/def2-SVP level of theory.

Metal	Without BAS				With BAS			
	M-ZSM-5	(ON)–M-ZSM-5			M-ZSM-5	H···(ON)–M-ZSM-5		
	M	**M**	**N**	**O**	**M**	**M**	**N**	**O**
Fe	2.958	3.257	–0.696	–0.608	2.949	3.348	–0.842	–0.564
Co	1.964	2.139	–0.620	–0.567	1.961	2.253	–0.762	–0.549
Ni	0.943	0	0	0	0.940	0	0	0
Cu	0	0.043	0.585	0.373	0	0.002	0.659	0.339
Zn	0.906	0.244	0.981	0.763	0.903	0.175	1.111	0.689
Pd	0.850	0	0	0	0.845	0	0	0
Ag	0	0.085	0.574	0.343	0	0.073	0.600	0.325
Au	0	0.147	0.495	0.356	0	0.143	0.521	0.331

6.4.4 NBO charges

Basically, charge redistribution can be considered an impetus of charge transfer between atoms (or groups) in a molecule; herein, the charge delocalization in NO complexes has been traced using NBO analysis.[170] A comparison of NBO charges on M-, N-, and O-atoms of NO complexes of M-ZSM-5 with and without BAS is shown in Figure 6.5 (the NBO results are collected in Table 6.5). It is evident from Table 6.5 that charges on Fe, Co, and Zn in bare M-ZSM-5 have increased upon NO adsorption, while charges have dropped for Ni, Cu, Ag, Pd and Au-atoms in (ON)–M-ZSM-5 with respect to bare M-ZSM-5. A similar trend for changes in NBO charges on M-atoms has been noticed while moving from BAS containing M-ZSM-5

to H···(ON)–M-ZSM-5. Nevertheless, the change in charge on Fe, Co, and Zn upon NO adsorption is more pronounced in NO complexes with BAS than in their BAS-free counterparts, whereas the change in charge on Ni, Cu, Pd, Ag, and Au induced by NO adsorption in BAS containing NO complexes are slighter than their BAS-free equivalents. It may be a reason for significant stabilization noted in the E_{ads} values of H···(ON)–M-ZSM-5 complexes for Fe, Co, and Zn metals.[270]

Additionally, we compared the charges on N- and O-atoms of both (ON)–M-ZSM-5 and H···(ON)–M-ZSM-5 complexes. We found that the charge on N-atoms (except for the Pd system) became more positive, whereas the charge on O-atoms turned out to be more negative on moving from (ON)–M-ZSM-5 to H···(ON)–M-ZSM-5. Further, the negative charge change on O-atoms is more prominent than the development of positive charge on N-atoms. An appreciable increase in negative charge on O-atoms in H···(ON)–M-ZSM-5 can be considered a result of partial charge transfer from N to O due to the HB interaction of the O atom with BAS. It can be noted from Figure 6.5 and Table 6.5 that the net charge on NO moiety is more negative in H···(ON)–M-ZSM-5 complexes with Fe, Co, Ni, Cu, and Zn metals than their corresponding (ON)–M-ZSM-5 complexes, while the charge on NO is positive for metals Pd, Ag and Au in H···(ON)–M-ZSM-5 complexes. This is again a point of the reason for higher E_{ads} values observed for Fe, Co, Ni, Cu, and Zn metals in H···(ON)–M-ZSM-5 complexes, and similar or lower E_{ads} values found for Ag, Au, and Pd in H···(ON)–M-ZSM-5 complexes as compared to their corresponding (ON)–M-ZSM-5 complexes.

Table 6.5 NBO charges on metal atom (M) of bare M-ZSM-5 (with and without BAS) & on M, N, and O of (ON)–M-ZSM-5 complexes (with and without BAS).

Metal	Without BAS				With BAS			
	M-ZSM-5	(ON)–M-ZSM-5			M-ZSM-5	H···(ON)–M-ZSM-5		
	M	M	N	O	M	M	N	O
Fe	0.853	1.002	–0.109	–0.169	0.838	1.071	–0.086	–0.255
Co	0.865	0.890	–0.042	–0.137	0.853	0.971	–0.038	–0.226
Ni	0.846	0.676	0.136	–0.117	0.836	0.719	0.142	–0.187
Cu	0.896	0.805	0.053	–0.090	0.890	0.843	0.076	–0.166
Zn	0.829	1.280	–0.320	–0.228	0.819	1.330	–0.270	–0.286
Pd	0.721	0.564	0.203	–0.082	0.709	0.625	0.198	–0.163
Ag	0.844	0.726	0.124	–0.070	0.838	0.742	0.139	–0.112
Au	0.743	0.606	0.145	–0.043	0.737	0.652	0.148	–0.107

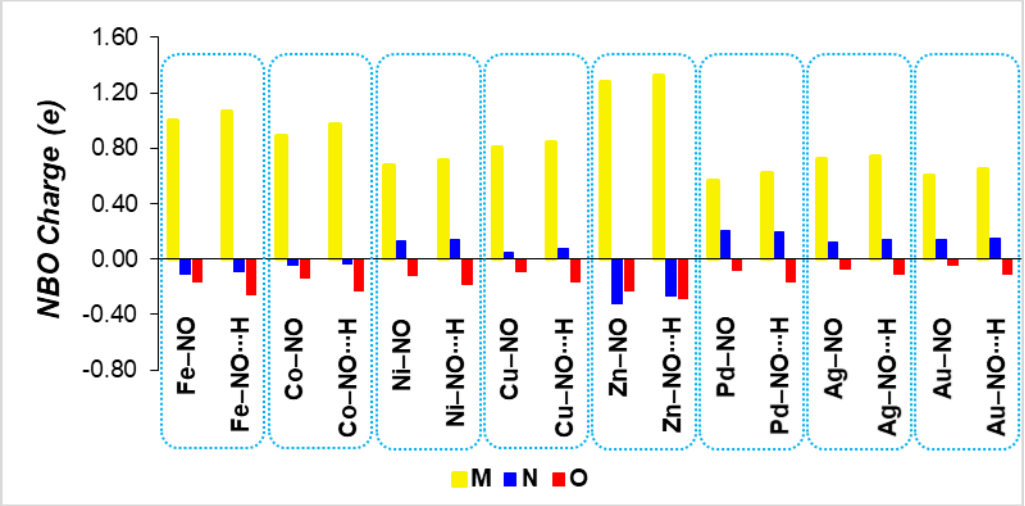

Figure 6.5 NBO charges on metal (M), N-, and O- atoms of NO in (ON)–M-ZSM-5 and H···(ON)–M-ZSM-5 systems. Rectangular bars filled with yellow, blue, and red colors represent M, N, and O atoms, respectively.

6.4.5 Bond order

The appraisal of N–O bond strength in (ON)–M-ZSM-5 and H···(ON)–M-ZSM-5 complexes is beneficial for understanding the N–O bond activation upon adsorption. The Mayer bond order index has been successfully used to evaluate the strength of N–O bonds in many (ON)–M complexes and (ON)–M-zeolites.[271,272] Table 6.6 reports the Mayer bond orders obtained for M–N and N–O of NO-complexes at the B3LYP/def2-SVP level of theory.

Table 6.6 Mayer Bond Order for M–N and N–O Bonds in (ON)–M-ZSM-5 and H···(ON)–M-ZSM-5 Complexes.

Metal	Mayer bond order index			
	(ON)–M-ZSM-5		H···(ON)–M-ZSM-5	
	M–N	N–O	M–N	N–O
Fe	1.004	1.673	0.961	1.599
Co	1.072	1.736	1.042	1.646
Ni	1.405	1.861	1.443	1.796
Cu	0.704	1.903	0.736	1.823
Zn	0.760	1.450	0.705	1.399
Pd	1.343	1.922	1.403	1.837
Ag	0.431	1.973	0.453	1.953
Au	0.697	1.926	0.744	1.883

It can be seen that reasonable changes (either increase or decrease) in the M–N bond order have occurred while moving from (ON)–M-ZSM-5 to H···(ON)–M-ZSM-5. However, the N–O bond order has reduced in all H···(ON)–M-ZSM-5 complexes compared to (ON)–M-

ZSM-5 complexes. Thus, the BAS (in H···(ON)–M-ZSM-5) has a marked effect on the N–O bond weakening, symbolizing the hydrogen bond-assisted N–O bond activation expected in the present study.

6.4.6 MESP analysis

The MESP of atoms or molecular entities is a valuable parameter to express a variety of chemical behavior of a molecule, such as electronegativity, reactive sites, ability to participate in noncovalent interactions, and so on.[75,201] Herein, we calculated the MESP on the O-atom (the HB acceptor) of NO in BAS free (ON)–M-ZSM-5 complex, and the results are given in Table 6.7. The electron-rich character of the O-atom is reflected in the potential at its nucleus (denoted as V_O). It is well-known that the more the negative potential value on the HB acceptor, the stronger the ability of that atom to interact with a proton.[164,202] It can be noted that the most negative V_O value (–22.288 au) is obtained for Zn–NO while the lower negative (–22.156 au) V_O is possessed by Ag–NO complex. Interestingly, the Zn–NO···H complex has the shortest HB distance (1.645 Å), while the longest HB distance (2.223 Å) is shown by Ag–NO···H. This noteworthy relation between V_O in (ON)–M-ZSM-5 and HB distance in H···(ON)–M-ZSM-5 complexes for Zn and Ag metals can also be extended to other structures, and the correlation is depicted in Figure 6.6. We obtained a decent correlation (correlation coefficient = 0.937) between V_O of (ON)–M-ZSM-5 complexes and HB distances in H···(ON)–M-ZSM-5 complexes.

Table 6.7 Molecular electrostatic potential value on oxygen atom (V_O) of NO in (ON)–M-ZSM-5 and H-bond (NO···H) distance in H···(ON)–M-ZSM-5 complexes.

Complex	V_O (in au)	NO···H (in Å)
Fe	–22.252	1.748
Co	–22.228	1.802
Ni	–22.194	1.922
Cu	–22.184	1.904
Zn	–22.288	1.645
Pd	–22.164	2.006
Ag	–22.156	2.223
Au	–22.151	2.176

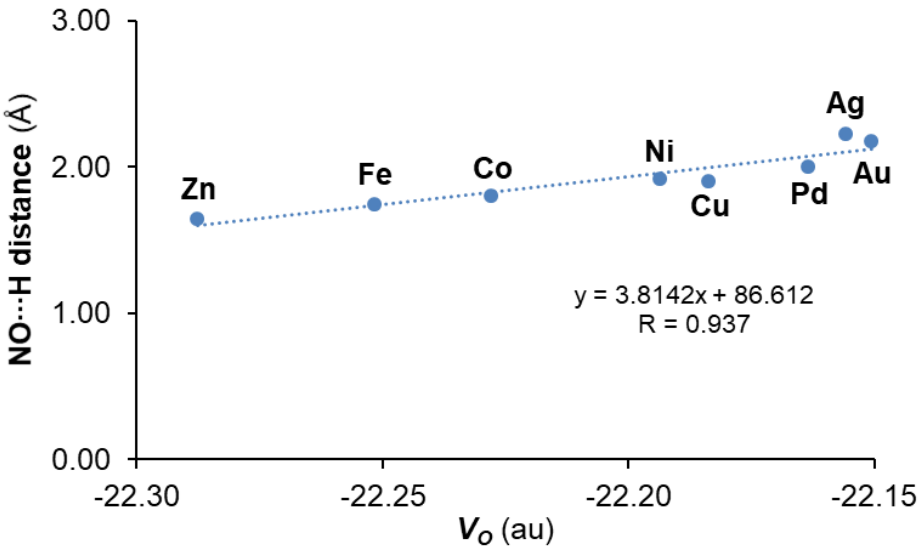

Figure 6.6 Correlation between the V_O of the (ON)–M-ZSM-5 complexes and NO···H hydrogen bond distances in the H···(ON)–M-ZSM-5 complexes.

6.4.7 QTAIM analysis

The values of QTAIM parameters *viz.* electron density ($\rho(r)$), $\nabla^2\rho(r)$, and total electron energy density ($H(r)$) at the bond critical point (bcp) of N–O bond in (ON)–M-ZSM-5 and H···(ON)–M-ZSM-5 complexes are listed in Table 6.8. The $\rho(r)$ values range from 0.5017 to 0.6104 au in (ON)–M-ZSM-5 complexes, while it typically falls in the range from 0.4955 to 0.5927 au in H···(ON)–M-ZSM-5 complexes. Intuitively, the low range of $\rho(r)$ noted for the H···(ON)–M-ZSM-5 complexes suggest that N–O bond weakening has occurred due to NO···H HB, which further confirms our notion that N–O bond weakening can be possible upon NO binding to M-ZSM-5 with BAS. The QTAIM parameters of a representative system (H···(ON)–Fe-ZSM-5) are shown in Figure 6.7.

The QTAIM parameters at the BCP of NO···H HB in H···(ON)–M-ZSM-5 complexes are also given in Table 6.8. In these structures, the computed $\rho(r)$ range from 0.0106 to 0.0465 au, the $\nabla^2\rho(r)$ values are between 0.0374 and 0.1532 au. Their corresponding $H(r)$ values lie between –0.0002 and 0.0040 au. The positive $\nabla^2\rho(r)$ value and negative $H(r)$ value noted in Zn–NO···H complex indicate partial covalent character for the HB, and also this HB is characterized by the highest $\rho(r)$ value (0.0465 au). On the contrary, the positive values of $\nabla^2\rho(r)$ and $H(r)$ for HB in all other complexes indicate typical closed-shell interactions. The successors of Zn in terms of high $\rho(r)$ values are Fe (0.0344 au), Co (0.0294 au), Cu (0.0241 au), and Ni (0.0218 au); this array is in line with the decreasing order of ΔE_{ads} values obtained for these complexes (H···(ON)–M-ZSM-5). Moreover, low $\rho(r)$ values found for Pd

(0.0177 au), Ag (0.0106 au), and Au (0.0113 au) in H···(ON)–M-ZSM-5 complexes reveal a relatively weaker HB interaction, corroborating with their anomalous ΔE_{ads} values.

Table 6.8 QTAIM parameters (in au) at the BCP of N–O bond in (ON)–M-ZSM-5 and H···(ON)–M-ZSM-5 complexes, as well as at the BCP of NO···H hydrogen bond of H···(ON)–M-ZSM-5 complexes.

Metal	N–O bond			NO···H bond		
	$\rho(r)$	$\nabla^2\rho(r)$	$H(r)$	$\rho(r)$	$\nabla^2\rho(r)$	$H(r)$
Fe–NO	0.5569	–1.7312	–0.9043	---	---	---
Fe–NO···H	0.5401	–1.6429	–0.8573	0.0344	0.1290	0.0035
Co–NO	0.5715	–1.8511	–0.9608	---	---	---
Co–NO···H	0.5519	–1.7360	–0.9012	0.0294	0.1142	0.0040
Ni–NO	0.6027	–2.0857	–1.0628	---	---	---
Ni–NO···H	0.5882	–1.9985	–1.0140	0.0218	0.0832	0.0032
Cu–NO	0.5857	–2.0004	–1.0488	---	---	---
Cu–NO···H	0.5735	–1.9122	–1.0003	0.0241	0.0855	0.0029
Zn–NO	0.5017	–1.3723	–0.7468	---	---	---
Zn–NO···H	0.4955	–1.3461	–0.7319	0.0465	0.1532	–0.0002
Pd–NO	0.6104	–2.1870	–1.1097	---	---	---
Pd–NO···H	0.5927	–2.0623	–1.0425	0.0177	0.0648	0.0023
Ag–NO	0.5994	–2.1701	–1.1317	---	---	---
Ag–NO···H	0.5926	–2.1226	–1.1099	0.0106	0.0374	0.0009
Au–NO	0.5970	–2.0908	–1.0878	---	---	---
Au–NO···H	0.5863	–2.0162	–1.0515	0.0113	0.0420	0.0013

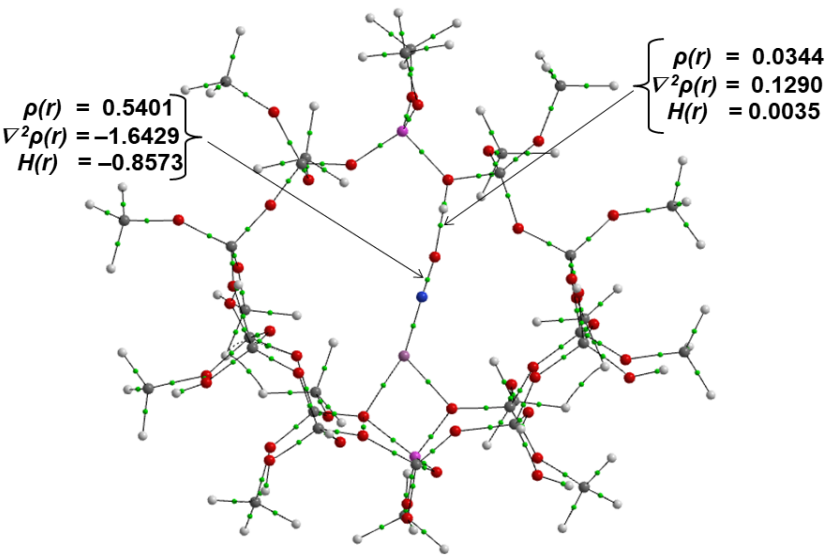

Figure 6.7 The QTAIM molecular graph of Fe–NO···H complex. The values of QTAIM parameters at the BCP (which is shown as small green spheres on each bond path) of the N–O bond and NO···H bond are in au.

6.4.8 Energy decomposition analysis

Energy decomposition analysis (EDA) is an indispensable method to quantify the intermolecular interactions and is thus used to predict the nature of interactions in the complexes of NO and M-ZSM-5 (with and without BAS). In the EDA calculations, NO, M-ZSM-5, and their complexes have been treated as neutral entities. The total binding energy (*TBE*) predicted via EDA has contributions from Pauli's repulsion (E_{Pauli}), electrostatic (E_{ES}), and orbital interactions (E_{Orb}).[252] Results of EDA are conveniently represented in Figure 6.8, and corresponding values are given in Table 6.9.

Table 6.9 Contribution of energy components (in eV) towards *TBE* for (ON)–M-ZSM-5 and H···(ON)–M-ZSM-5 complexes from EDA.

Metal	Pauli's Repulsion, E_{Pauli}	Electrostatic Interactions, E_{ES}	Orbital Interactions, E_{Orb}	Total Binding Energy, *TBE*
Fe–NO	6.44	–3.45	–8.81	–5.82
Fe–NO···H	6.71	–3.45	–9.28	–6.01
Co–NO	7.80	–4.32	–10.24	–6.76
Co–NO···H	8.96	–4.98	–10.87	–6.88
Ni–NO	9.01	–5.24	–8.66	–4.89
Ni–NO···H	10.25	–5.63	–9.57	–4.95
Cu–NO	3.24	–1.93	–3.28	–1.97
Cu–NO···H	4.40	–2.77	–3.69	–2.06
Zn–NO	9.36	–4.09	–6.95	–1.69
Zn–NO···H	9.72	–3.94	–7.89	–2.12
Pd–NO	10.00	–5.81	–7.40	–3.21
Pd–NO···H	10.43	–5.85	–7.70	–3.12
Ag–NO	1.77	–0.91	–2.03	–1.17
Ag–NO···H	2.19	–1.31	–2.05	–1.17
Au–NO	5.12	–3.28	–4.10	–2.26
Au–NO···H	5.30	–3.16	–4.39	–2.25

It can be seen that the H···(ON)–Co-ZSM-5 complex has the highest *TBE* (–6.88 eV); whereas the complex(es) with Ag has the lowest *TBE* (–1.17 eV). In all the complexes, it is observed that the E_{Pauli} component of *TBE* is greater than E_{ES}. Moreover, it is interesting to note that, in the Ni, Zn, Pd, and Au complexes (with and without BAS), the estimated E_{Pauli} is greater than E_{Orb}. Therefore, Pauli's repulsion plays a significant role in lowering the *TBE* in these complexes. In line with the E_{ads} values, the *TBE* is greater in H···(ON)–M-ZSM-5 complexes (except in the case of Pd and Au complexes) than in (ON)–M-ZSM-5 complexes. For instance, the *TBE* obtained for (ON)–Fe-ZSM-5 and H···(ON)–Fe-ZSM-5 complexes are

–5.82 eV and –6.01 eV, respectively; however, *TBE* for the (ON)–Pd-ZSM-5 and H···(ON)–Pd-ZSM-5 complexes are –3.21 eV and –3.12 eV, respectively. Consequently, this supports our earlier perception that HB helps stabilize the NO complexes in most of the cases.

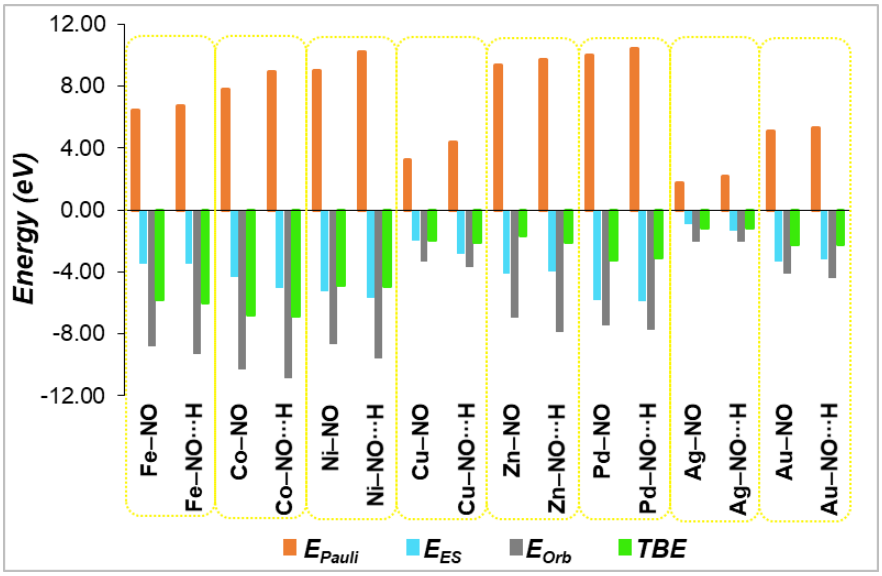

Figure 6.8 Contributions of energy components E_{Pauli}, E_{ES}, and E_{Orb} towards *TBE* for (ON)–M-ZSM-5 and H···(ON)–M-ZSM-5 complexes. Rectangular bars filled with orange, blue, gray, and green colors represent E_{Pauli}, E_{ES}, E_{Orb}, and *TBE*, respectively.

The NOCV analysis[254] permits one to draw quantitative details of the intra-fragment charge transfer profile along the interaction axis of the fragments in a complex as well as the orbital energy contributions. Three NOCV contours (denoted as **1**, **2,** and **3**) with the largest eigenvalues along the bond region of M and NO derived from NOCV analysis for (ON)–M-ZSM-5 and H···(ON)–M-ZSM-5 complexes with M = Fe, Co, Ni, Cu, Zn, Pd, Ag, and Au are given in Figure 6.9. In the contours, the color code of CT is from red → blue (i.e., red denotes loss of electrons while blue signifies gain of electrons). The orbital energy contributions corresponding to **1**, **2**, and **3** for all complexes are consolidated in Table 6.10 along with their eigenvalues. From the data in Table 6.10, it can be noted that the orbital binding energy values are negative for **1**, **2**, and **3** of all the complexes, and eigenvalues are higher than 0.1. The highest contribution (–101.39 kcal/mol) for type **1** is associated with the H···(ON)–Zn-ZSM-5 species. Type **1** contours shown in Figure 6.9 illustrate that electrons are shifted from M towards NO. However, contour types **2** and **3** for the H···(ON)–Cu-ZSM-5 complex demonstrate that an outflow of charge from antibonding orbital of NO to the empty s-orbital on copper as demonstrated previously by Kozyra et al.[273] The outflow of charge from antibonding orbital of NO to vacant s-orbital on M-atom have also been noticed for

contour type **2** of Zn and Au as well as contour type **3** of Co in their (ON)–M-ZSM-5 and H···(ON)–M-ZSM-5 complexes. Inspection of all the remaining NOCV contours points at the back-donation of charge from the metal d-orbital to the antibonding orbital of NO.

A close inspection of the NOCV contours of H···(ON)–M-ZSM-5 complexes reveals the fact that the BAS of the zeolite (i.e., the host fragment) plays a significant role in the intra-fragment charge transfer processes. For instance, in the type **1** contour of H···(ON)–Fe-ZSM-5 complex, there is charge flow from the hydrogen of BAS to the NO species; a similar trend can be noticed BAS containing systems. This charge flow from the hydrogen implies that the HB helps the NO adsorption on the M atom of the zeolite. In brief, the EDA and NOCV analyses have shown that systems stabilized by a HB (i.e., H···(ON)–M-ZSM-5) show an additional N–O bond weakening and a predominant charge transfer character than (ON)–M-ZSM-5 systems.

Table 6.10 Orbital Energy Contributions of three major NOCVs of (ON)–M-ZSM-5 and H···(ON)–M-ZSM-5 complexes and their eigenvalues.

Complexes	Orbital Energy Contributions (in kcal/mol)			Eigenvalues		
	1	**2**	**3**	**1**	**2**	**3**
Fe–NO	–78.42	–48.38	–6.30	0.98	0.54	0.24
Fe–NO···H	–77.14	–49.31	–4.18	1.00	0.54	0.24
Co–NO	–84.51	–28.64	–12.32	1.00	0.38	0.21
Co–NO···H	–93.40	–20.85	–22.77	1.00	0.36	0.25
Ni–NO	–19.33	–29.01	–36.90	0.51	0.45	0.25
Ni–NO···H	–23.39	–23.28	–42.96	0.53	0.44	0.28
Cu–NO	–71.21	–7.10	–15.62	0.99	0.16	0.13
Cu–NO···H	–67.26	–20.52	–15.34	0.81	0.21	0.16
Zn–NO	–90.07	–56.11	---	0.87	0.54	---
Zn–NO···H	–101.39	–66.57	---	0.93	0.52	---
Pd–NO	–45.73	–18.54	–10.31	0.57	0.33	0.17
Pd–NO···H	–42.93	–25.01	–9.27	0.52	0.39	0.17
Ag–NO	–40.45	–20.38	---	0.55	0.22	---
Ag–NO···H	–69.41	–4.16	---	0.90	0.14	---
Au–NO	–76.70	–11.45	–19.76	0.91	0.23	0.12
Au–NO···H	–72.64	–15.69	–24.79	0.83	0.25	0.15

Fe–NO

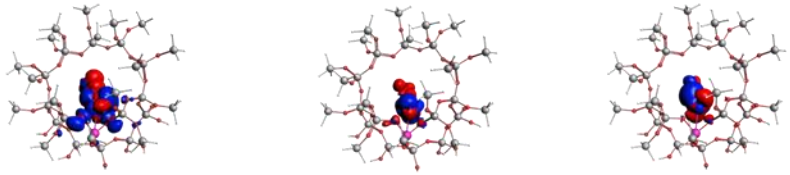

Fe–NO···H

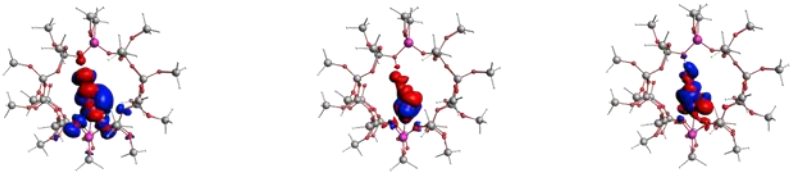

Co–NO

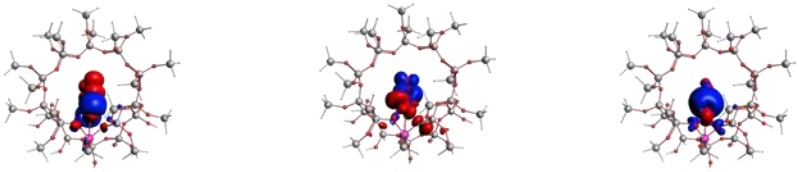

Co–NO···H

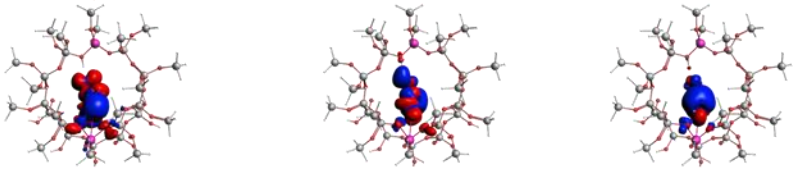

Ni–NO

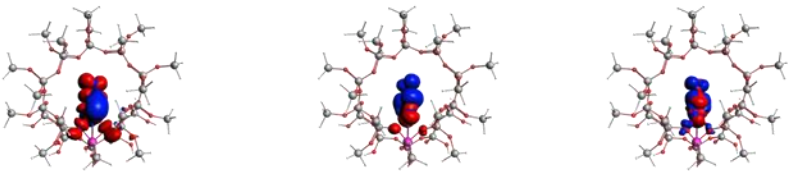

Ni–NO···H

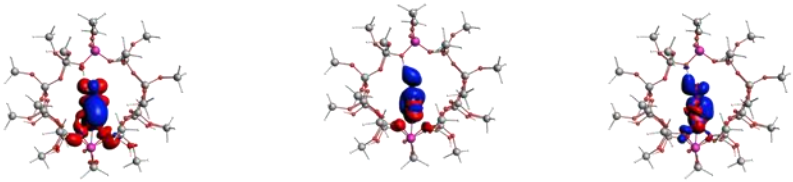

Cu–NO

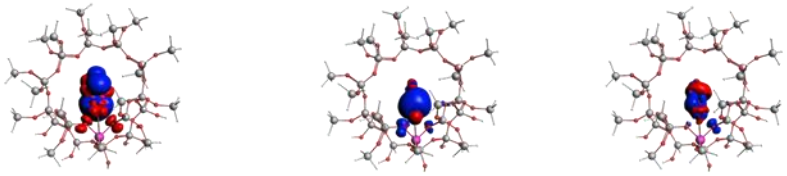

Cu–NO···H

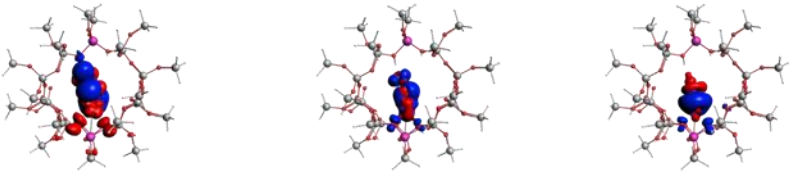

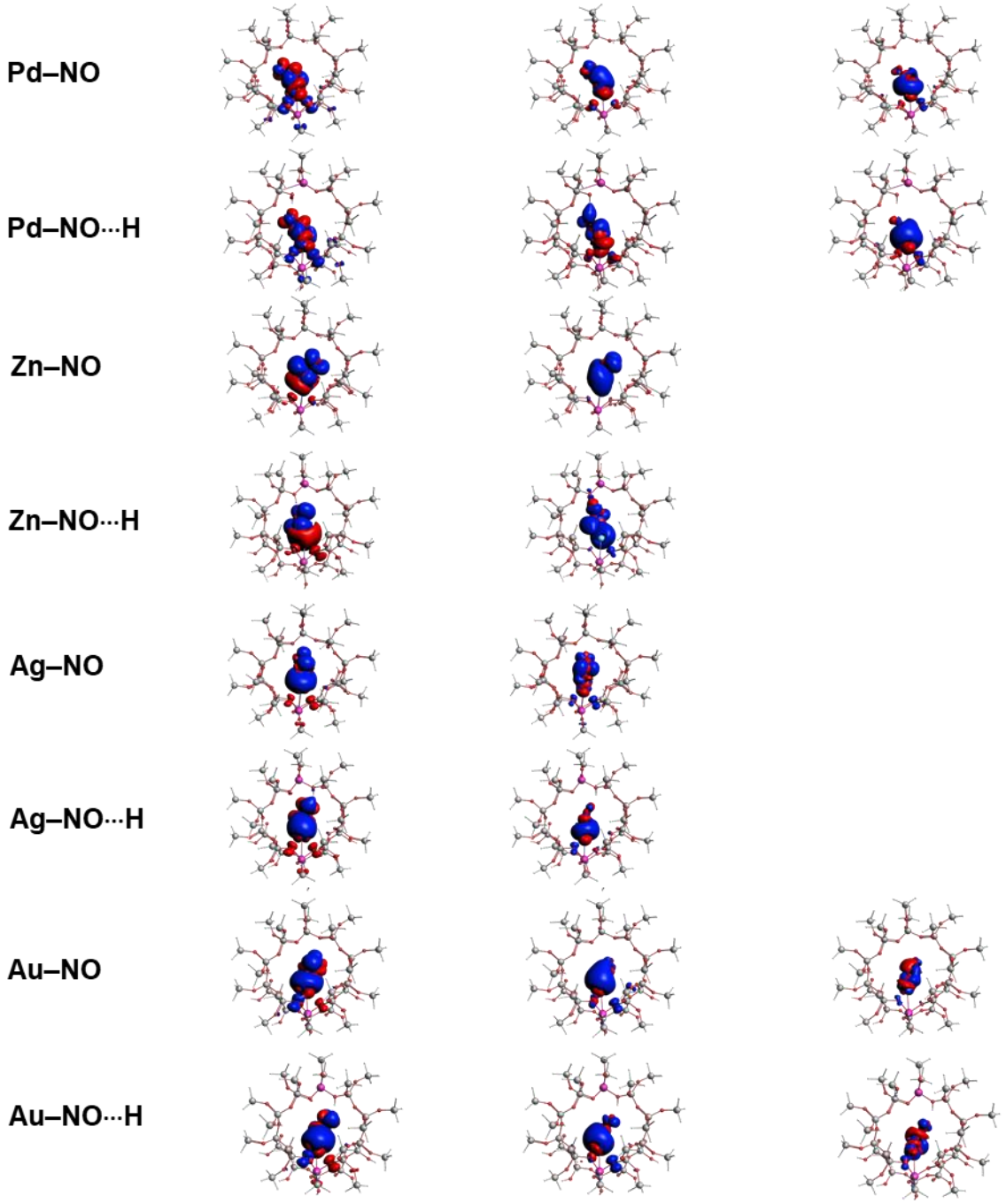

Figure 6.9 Contours of major NOCV's of (ON)–M-ZSM-5 and H···(ON)–M-ZSM-5 complexes.

6.5 Conclusions

Effective NO adsorption to the metal species and synergic N–O bond activation are prime aspects of the metal-loaded zeolite mediated NO abatement approach. In this DFT-based theoretical study, we found that the incorporation of Brønsted acid sites (BAS) in several transition metal-loaded ZSM-5 zeolites has a marked effect on NO adsorption. It was obtained that the HB (NO···H) in BAS containing NO complex (*viz.* H···(ON)–M-ZSM-5,

with M as Fe, Co, Ni, Cu, and Zn) significantly improves the NO adsorption energy (E_{ads}) in comparison with NO adsorption to BAS free M-ZSM-5. The calculated E_{ads} values in both BAS assisted and free complexes follow the order: Ag < Zn < Cu < Au < Ni < Pd < Co < Fe. The NBO analyses on M-, N-, and O-atoms have established that charge redistribution is more profound in H···(ON)–M-ZSM-5 complexes than (ON)–M-ZSM-5 complexes. It is noteworthy that the MESP on the O-atom (V_O) of BAS free (ON)–M-ZSM-5 is a valid theoretical descriptor of NO···H HB strength in H···(ON)–M-ZSM-5 complexes as we have obtained a good correlation between V_O and HB distance. The QTAIM-based parameter $\rho(r)$ at the bond critical point of the NO···H bond path in H···(ON)–M-ZSM-5 complexes corroborated the differences in HB strengths associated with different metal species. The Mayer bond order and QTAIM analyses have shown noticeable N–O bond weakening in all BAS-containing complexes. The N–O bond weakening follows the order: Ag < Pd < Au < Ni < Cu < Co < Fe < Zn. The EDA-NOCV analysis reveals that the back-donation plays a crucial role in activating the N–O bond by increasing the electrons in the antibonding orbital of NO. We hope that the BAS-assisted NO adsorption/N–O bond activation can be extended to further model zeolite compounds.

Publication based on this chapter:

Thufail M. Ismail; Prasanthkumar, K. P.; Ebenezer, C.; Anjali, B. A.; Solomon, R. V.; Sajith, P. K. Hydrogen-Bond-Assisted Adsorption of Nitric Oxide on Various Metal-Loaded ZSM-5 Zeolites. *Langmuir* **2022**, 38, 10492–10502.

Chapter 8

Recommendations

The detrimental impact of increasing emission of nitric oxide in the environment urges its effective mitigation strategies. Studies have shown several techniques for the adsorption and decomposition of NO on noble metals, metal oxides, and perovskite surfaces.[41] Over the past three decades, porous materials such as metal-loaded zeolites have been explored for long-lasting impact on applications of adsorption, diffusion, separation, catalysis, etc.[44,274] In this regard, these materials have shown immense potential in nitric oxide (NO) adsorption and decomposition processes. The combination of specific metals and the features of the porous framework are vital factors to the superior catalytic activity of these materials.

The role of Brønsted acid site (BAS) present nearby adsorbed NO on various metal-loaded ZSM-5 has been investigated in Chapter 6. The weakening of the N–O bond due to the hydrogen bonding interaction (NO···H) of adsorbed NO with BAS is observed therein. Thus, this intends to investigate the role of BAS in NO decomposition reaction. The mechanistic pathways of NO decomposition reaction over Cu-loaded zeolites are well explored.[257,275] Accordingly, it is anticipated to design a Cu-ZSM-5 catalyst with the proper positioning of BAS in the proximity of adsorbed NO on the Cu-center and investigate the role of BAS in the NO decomposition. The mechanism shown in Scheme 7.1 is generally observed for catalytic direct decomposition of NO over Cu-loaded zeolites;[275] based on this scheme, the mechanistic pathway for the NO decomposition reaction over BAS-presented metal-loaded zeolites can be proposed.

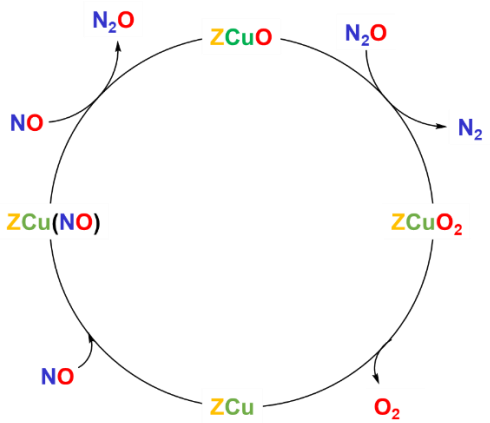

Scheme 7.1 Proposed mechanism for catalytic direct decomposition of NO over Cu-loaded zeolite.[275]

References

(1) Richter-Addo, G. B.; Legzdins, P.; Burstyn, J. Introduction: Nitric Oxide Chemistry. *Chem. Rev.* **2002**, *102* (4), 857–859.

(2) McCleverty, J. A. Chemistry of Nitric Oxide Relevant to Biology. *Chem. Rev.* **2004**, *104* (2), 403–418.

(3) Ford, P. C.; Shiro, Y.; van Eldik, R. Renaissance in NO Chemistry. *Inorg. Chem.* **2021**, *60* (21), 15831–15834.

(4) Crutzen, P. J. The Role of NO and NO_2 in the Chemistry of the Troposphere and Stratosphere. *Annu. Rev. Earth Planet. Sci.* **1979**, *7* (1), 443–472.

(5) Wang, P. G.; Xian, M.; Tang, X.; Wu, X.; Wen, Z.; Cai, T.; Janczuk, A. J. Nitric Oxide Donors: Chemical Activities and Biological Applications. *Chem. Rev.* **2002**, *102* (4), 1091–1134.

(6) Bruckdorfer, R. The Basics about Nitric Oxide. *Mol. Aspects Med.* **2005**, *26* (1), 3–31.

(7) Koshland, D. E. The Molecule of the Year. *Science* **1992**, *258* (5090), 1861.

(8) *Press release. NobelPrize.org*. https://www.nobelprize.org/prizes/medicine/1998/press-release/.

(9) Ford, P. C.; Miranda, K. M. The Solution Chemistry of Nitric Oxide and Other Reactive Nitrogen Species. *Nitric Oxide* **2020**, *103*, 31–46.

(10) Suarez, S. A.; Vargas, P.; Doctorovich, F. A. Updating NO•/HNO Interconversion under Physiological Conditions: A Biological Implication Overview. *J. Inorg. Biochem.* **2021**, *216*, 111333.

(11) Gallego, C. M.; Mazzeo, A.; Vargas, P.; Suárez, S.; Pellegrino, J.; Doctorovich, F. Azanone (HNO): Generation, Stabilization and Detection. *Chem. Sci.* **2021**, *12* (31), 10410–10425.

(12) Harrison, R. M.; Peak, J. D.; Collins, G. M. Tropospheric Cycle of Nitrous Acid. *J. Geophys. Res. Atmos.* **1996**, *101* (D9), 14429–14439.

(13) Anglada, J. M.; Martins-Costa, M. T. C.; Francisco, J. S.; Ruiz-López, M. F. Photoinduced Oxidation Reactions at the Air–Water Interface. *J. Am. Chem. Soc.* **2020**, *142* (38), 16140–16155.

(14) Hughes, M. N. Relationships between Nitric Oxide, Nitroxyl Ion, Nitrosonium Cation and Peroxynitrite. *Biochim. Biophys. Acta - Bioenerg.* **1999**, *1411* (2), 263–272.

(15) Flores-Santana, W.; Switzer, C.; Ridnour, L. A.; Basudhar, D.; Mancardi, D.; Donzelli, S.; Thomas, D. D.; Miranda, K. M.; Fukuto, J. M.; Wink, D. A. Comparing the Chemical Biology of NO and HNO. *Arch. Pharm. Res.* **2009**, *32* (8), 1139–1153.

(16) Paolocci, N.; Jackson, M. I.; Lopez, B. E.; Miranda, K.; Tocchetti, C. G.; Wink, D. A.; Hobbs, A. J.; Fukuto, J. M. The Pharmacology of Nitroxyl (HNO) and Its Therapeutic Potential: Not Just the Janus Face of NO. *Pharmacol. Ther.* **2007**, *113* (2), 442–458.

(17) Feelisch, M. Nitroxyl Gets to the Heart of the Matter. *Proc. Natl. Acad. Sci.* **2003**, *100* (9), 4978–4980.

(18) Miranda, K. M. The Chemistry of Nitroxyl (HNO) and Implications in Biology. *Coord. Chem. Rev.* **2005**, *249* (3), 433–455.

(19) Sherman, M. P.; Grither, W. R.; McCulla, R. D. Computational Investigation of the Reaction Mechanisms of Nitroxyl and Thiols. *J. Org. Chem.* **2010**, *75* (12), 4014–4024.

(20) Harrison, R. M.; Kitto, A.-M. N. Evidence for a Surface Source of Atmospheric Nitrous Acid. *Atmos. Environ.* **1994**, *28* (6), 1089–1094.

(21) Su, H.; Cheng, Y.; Oswald, R.; Behrendt, T.; Trebs, I.; Meixner, F. X.; Andreae, M. O.; Cheng, P.; Zhang, Y.; Pöschl, U. Soil Nitrite as a Source of Atmospheric HONO and OH Radicals. *Science.* **2011**, *333* (6049), 1616–1618.

(22) Zhao, H.; Du, L. Atmospheric Implication of the Hydrogen Bonding Interaction in Hydrated Clusters of HONO and Dimethylamine in the Nighttime. *Environ. Sci. Process. Impacts* **2017**, *19* (1), 65–77.

(23) Karoui, H.; Moigne, F. Le; Ouari, O.; Tordo, P. Nitroxide Radicals: Properties, Synthesis and Applications. In *Stable Radicals*; John Wiley & Sons, Ltd, 2010; pp 173–229.

(24) Sumathi, R.; Sengupta, D.; Nguyen, M. T. Theoretical Study of the H_2 + NO and Related Reactions of [H_2NO] Isomers. *J. Phys. Chem. A* **1998**, *102* (18), 3175–3183.

(25) Dean, A. M.; Bozzelli, J. W. Combustion Chemistry of Nitrogen BT - Gas-Phase Combustion Chemistry; Gardiner, W. C., Ed.; Springer New York: New York, NY, 2000; pp 125–341.

(26) Bertin, D.; Gigmes, D.; Marque, S. R. A.; Tordo, P. Kinetic Subtleties of Nitroxide Mediated Polymerization. *Chem. Soc. Rev.* **2011**, *40* (5), 2189–2198.

(27) Zottler, E.; Gescheidt, G. Nitroxides: Versatile Reporters and Reactants. *J. Chem. Res.* **2011**, *35* (5), 257–267.

(28) Tamura, M.; Nakazawa, Y.; Shiomi, D.; Nozawa, K.; Hosokoshi, Y.; Ishikawa, M.; Takahashi, M.; Kinoshita, M. Bulk Ferromagnetism in the β-Phase Crystal of the p-Nitrophenyl Nitronyl Nitroxide Radical. *Chem. Phys. Lett.* **1991**, *186* (4), 401–404.

(29) Galli, C.; Gentili, P.; Lanzalunga, O. Hydrogen Abstraction and Electron Transfer with Aminoxyl Radicals: Synthetic and Mechanistic Issues. *Angew. Chemie Int. Ed.* **2008**, *47* (26), 4790–4796.

(30) Popova, A. M.; Kálai, T.; Hideg, K.; Qin, P. Z. Site-Specific DNA Structural and Dynamic Features

Revealed by Nucleotide-Independent Nitroxide Probes. *Biochemistry* **2009**, *48* (36), 8540–8550.
(31) Gast, P.; Herbonnet, R. T. L.; Klare, J.; Nalepa, A.; Rickert, C.; Stellinga, D.; Urban, L.; Möbius, K.; Savitsky, A.; Steinhoff, H.-J.; Groenen, E. J. J. Hydrogen Bonding of Nitroxide Spin Labels in Membrane Proteins. *Phys. Chem. Chem. Phys.* **2014**, *16* (30), 15910–15916.
(32) Lietzow, M. A.; Hubbell, W. L. Motion of Spin Label Side Chains in Cellular Retinol-Binding Protein: Correlation with Structure and Nearest-Neighbor Interactions in An Antiparallel β-Sheet. *Biochemistry* **2004**, *43* (11), 3137–3151.
(33) Hubbell, W. L.; Altenbach, C. Investigation of Structure and Dynamics in Membrane Proteins Using Site-Directed Spin Labeling. *Curr. Opin. Struct. Biol.* **1994**, *4* (4), 566–573.
(34) Griffith, O. H.; Waggoner, A. S. Nitroxide Free Radicals: Spin Labels for Probing Biomolecular Structure. *Acc. Chem. Res.* **1969**, *2* (1), 17–24.
(35) Lewandowski, M.; Gwozdzinski, K. Nitroxides as Antioxidants and Anticancer Drugs. *Int. J. Mol. Sci.* **2017**, *18* (11), 2490.
(36) Soule, B. P.; Hyodo, F.; Matsumoto, K.; Simone, N. L.; Cook, J. A.; Krishna, M. C.; Mitchell, J. B. The Chemistry and Biology of Nitroxide Compounds. *Free Radic. Biol. Med.* **2007**, *42* (11), 1632–1650.
(37) Rybarczyk-Pirek, A. J.; Łukomska-Rogala, M.; Wojtulewski, S.; Palusiak, M. N-Oxide as a Proton Accepting Group in Multicomponent Crystals - X-Ray and Theoretical Studies on New p-Nitropyridine-N-Oxide Co-Crystals. *Cryst. Growth Des.* **2015**, *15* (12), 5802–5815.
(38) Amorati, R.; Pedulli, G. F.; Pratt, D. A.; Valgimigli, L. TEMPO Reacts with Oxygen-Centered Radicals under Acidic Conditions. *Chem. Commun.* **2010**, *46* (28), 5139–5141.
(39) Jones, C.; Rose, R. P. Synthesis and Characterisation of Tetramethylpiperidinyloxide (TEMPO) Complexes of Group 13 Metal Hydrides. *New J. Chem.* **2007**, *31* (8), 1484–1487.
(40) Zhang, R.; Liu, N.; Lei, Z.; Chen, B. Selective Transformation of Various Nitrogen-Containing Exhaust Gases toward N_2 over Zeolite Catalysts. *Chem. Rev.* **2016**, *116*, 3658–3721.
(41) Xie, P.; Ji, W.; Li, Y.; Zhang, C. NO Direct Decomposition: Progress, Challenges and Opportunities. *Catal. Sci. Technol.* **2021**, *11*, 374–391.
(42) Zhang, L.; Wu, Q.; Meng, X.; Müller, U.; Feyen, M.; Dai, D.; Maurer, S.; McGuire, R.; Moini, A.; Parvulescu, A. N.; Zhang, W.; Shi, C.; Yokoi, T.; Pan, X.; Bao, X.; Gies, H.; Marler, B.; De Vos, D. E.; Kolb, U.; Xiao, F. S. Recent Advances in the Preparation of Zeolites for the Selective Catalytic Reduction of NO_x in Diesel Engines. *React. Chem. Eng.* **2019**, *4*, 975–985.
(43) Pu, Y.; Xie, X.; Jiang, W.; Yang, L.; Jiang, X.; Yao, L. Low-Temperature Selective Catalytic Reduction of NO_x with NH_3 over Zeolite Catalysts: A Review. *Chinese Chem. Lett.* **2020**, *31*, 2549–2555.
(44) Van Speybroeck, V.; Hemelsoet, K.; Joos, L.; Waroquier, M.; Bell, R. G.; Catlow, C. R. A. Advances in Theory and Their Application within the Field of Zeolite Chemistry. *Chem. Soc. Rev.* **2015**, *44*, 7044–7111.
(45) Rhodes, C. J. Zeolites: Physical Aspects and Environmental Applications. *Annu. Reports Prog. Chem. - Sect. C* **2007**, *103*, 287–325.
(46) Sachtler, W. M. H.; Zhang, Z. Zeolite-Supported Transition Metal Catalysts; Eley, D. D., Pines, H., Weisz, P. B. B. T.-A. in C., Eds.; Academic Press, 1993; Vol. 39, pp 129–220.
(47) Shamzhy, M.; Opanasenko, M.; Concepción, P.; Martínez, A. New Trends in Tailoring Active Sites in Zeolite-Based Catalysts. *Chem. Soc. Rev.* **2019**, *48*, 1095–1149.
(48) Joyner, R.; Stockenhuber, M. Preparation, Characterization, and Performance of Fe-ZSM-5 Catalysts. *J. Phys. Chem. B* **1999**, 5963–5976.
(49) Zhang, S.; Zhang, C.; Wang, Q.; Ahn, W. S. Co and Mn Co-Impregnated ZSM-5 Prepared from Recycled Industrial Solid Wastes for Low-Temperature NH_3-SCR. *Ind. Eng. Chem. Res.* **2019**, *58*, 22857–22865.
(50) Sierraalta, A.; Hernandez-Andara, R.; Ehrmann, E. Theoretical Study on Silver- and Gold-Loaded Zeolite Catalysts: Thermodynamics and IR Spectroscopy. *J. Phys. Chem. B* **2006**, *110*, 17912–17917.
(51) Mandal, K.; Gu, Y.; Westendorff, K. S.; Li, S.; Pihl, J. A.; Grabow, L. C.; Epling, W. S.; Paolucci, C. Condition-Dependent Pd Speciation and NO Adsorption in Pd/Zeolites. *ACS Catal.* **2020**, *10*, 12801–12818.
(52) Pietrzyk, P.; Góra-Marek, K.; Mazur, T.; Mozgawa, B.; Radoń, M.; Chiesa, M.; Zhao, Z.; Sojka, Z. Structure and Mechanistic Relevance of Ni^{2+}–NO Adduct in Model HC SCR Reaction over NiZSM-5 Catalyst – Insights from Standard and Correlation EPR and IR Spectroscopic Studies Corroborated by Molecular Modeling. *J. Catal.* **2021**, *394*, 206–219.
(53) Morpurgo, S. A DFT Study on the Mechanism of NO Decomposition Catalyzed by Short-Distance Cu(I) Pairs in Cu-ZSM-5. *Mol. Catal.* **2017**, *434*, 96–105.
(54) Iwamoto, M.; Furukawa, H.; Mine, Y.; Uemura, F.; Mikuriya, S. I.; Kagawa, S. Copper(II) Ion-Exchanged ZSM-5 Zeolites as Highly Active Catalysts for Direct and Continuous Decomposition of Nitrogen Monoxide. *J. Chem. Soc. Chem. Commun.* **1986**, 1272–1273.

(55) Groothaert, M. H.; Van Bokhoven, J. A.; Battiston, A. A.; Weckhuysen, B. M.; Schoonheydt, R. A. Bis(μ-Oxo)Dicopper in Cu-ZSM-5 and Its Role in the Decomposition of NO: A Combined in Situ XAFS, UV-Vis-Near-IR, and Kinetic Study. *J. Am. Chem. Soc.* **2003**, *125*, 7629–7640.
(56) Kumashiro, R.; Kuroda, Y.; Nagao, M. New Analysis of Oxidation State and Coordination Environment of Copper Ion-Exchanged in ZSM-5 Zeolite. *J. Phys. Chem. B* **1999**, *103*, 89–96.
(57) Smeets, P. J.; Groothaert, M. H.; van Teeffelen, R. M.; Leeman, H.; Hensen, E. J. M.; Schoonheydt, R. A. Direct NO and N_2O Decomposition and NO-Assisted N_2O Decomposition over Cu-Zeolites: Elucidating the Influence of the CuCu Distance on Oxygen Migration. *J. Catal.* **2007**, *245*, 358–368.
(58) Ruggiero, C. E.; Carrier, S. M.; Cramer, C. J.; Tolman, W. B.; Antholine, W. E.; Whittaker, J. W. Synthesis and Structural and Spectroscopic Characterization of Mononuclear Copper Nitrosyl Complexes: Models for Nitric Oxide Adducts of Copper Proteins and Copper-Exchanged Zeolites. *J. Am. Chem. Soc.* **1993**, *115*, 11285–11298.
(59) Schneider, W. F.; Hass, K. C.; Ramprasad, R.; Adams, J. B. Density Functional Theory Study of Transformations of Nitrogen Oxides Catalyzed by Cu-Exchanged Zeolites. *J. Phys. Chem. B* **1998**, *102*, 3692–3705.
(60) Sojka, Z.; Che, M.; Giamello, E. EPR Investigation of the Electronic Structure of Mononuclear Copper (I) Nitric Oxide Adduct Formed upon Low-Pressure Adsorption of NO onto Cu/ZSM-5 Zeolite. *J. Phys. Chem. B* **1997**, *101*, 4831–4838.
(61) Rudolph, J.; Jacob, C. R. Computational Insights into the Mechanism of the Selective Catalytic Reduction of NO_x: Fe- versus Cu-Exchanged Zeolite Catalysts. *ACS Omega* **2019**, *4* (5), 7987–7993.
(62) Stępniewski, A.; Radoń, M.; Góra-Marek, K.; Broclawik, E. Ammonia-Modified Co(II) Sites in Zeolites: Spin and Electron Density Redistribution through the Co^{II}-NO Bond. *Phys. Chem. Chem. Phys.* **2016**, *18*, 3716–3729.
(63) Lanzafame, P.; Papanikolaou, G.; Perathoner, S.; Centi, G.; Giordano, G.; Migliori, M. Weakly Acidic Zeolites: A Review on Uses and Relationship between Nature of the Active Sites and Catalytic Behaviour. *Microporous Mesoporous Mater.* **2020**, *300*, 110157.
(64) Chizallet, C.; Bouchy, C.; Larmier, K.; Pirngruber, G. Molecular Views on Mechanisms of Brønsted Acid-Catalyzed Reactions in Zeolites. *Chem. Rev.* **2023**, *123* (9), 6107–6196.
(65) Barone, G.; Casella, G.; Giuffrida, S.; Duca, D. H−ZSM-5 Modified Zeolite: Quantum Chemical Models of Acidic Sites. *J. Phys. Chem. C* **2007**, *111* (35), 13033–13043.
(66) Liang, T.; Chen, J.; Qin, Z.; Li, J.; Wang, P.; Wang, S.; Wang, G.; Dong, M.; Fan, W.; Wang, J. Conversion of Methanol to Olefins over H-ZSM-5 Zeolite: Reaction Pathway Is Related to the Framework Aluminum Siting. *ACS Catal.* **2016**, *6* (11), 7311–7325.
(67) Lin, B.; Zhang, Q.; Wang, Y. Catalytic Conversion of Ethylene to Propylene and Butenes over H−ZSM-5. *Ind. Eng. Chem. Res.* **2009**, *48* (24), 10788–10795.
(68) Liu, C.; Malta, G.; Kubota, H.; Kon, K.; Toyao, T.; Maeno, Z.; Shimizu, K. I. In Situ/Operando IR and Theoretical Studies on the Mechanism of NH_3-SCR of NO/NO_2 over H-CHA Zeolites. *J. Phys. Chem. C* **2021**, *125*, 13889–13899.
(69) Yokoi, T.; Mochizuki, H.; Namba, S.; Kondo, J. N.; Tatsumi, T. Control of the Al Distribution in the Framework of ZSM-5 Zeolite and Its Evaluation by Solid-State NMR Technique and Catalytic Properties. *J. Phys. Chem. C* **2015**, *119*, 15303–15315.
(70) Nash, M. J.; Shough, A. M.; Fickel, D. W.; Doren, D. J.; Lobo, R. F. High-Temperature Dehydrogenation of Brønsted Acid Sites in Zeolites. *J. Am. Chem. Soc.* **2008**, *130* (8), 2460–2462.
(71) Liu, F.; Huang, K.; Zheng, A.; Xiao, F. S.; Dai, S. Hydrophobic Solid Acids and Their Catalytic Applications in Green and Sustainable Chemistry. *ACS Catal.* **2018**, *8* (1), 372–391.
(72) Grabowski, S. J. *Understanding Hydrogen Bonds*; Theoretical and Computational Chemistry Series; The Royal Society of Chemistry, 2021.
(73) Arunan, E.; Desiraju, G. R.; Klein, R. A.; Sadlej, J.; Scheiner, S.; Alkorta, I.; Clary, D. C.; Crabtree, R. H.; Dannenberg, J. J.; Hobza, P.; Kjaergaard, H. G.; Legon, A. C.; Mennucci, B.; Nesbitt, D. J. Definition of the Hydrogen Bond (IUPAC Recommendations 2011). *Pure Appl. Chem.* **2011**, *83* (8), 1637–1641.
(74) Grabowski, S.J. *Understanding Hydrogen Bonds, Theoretical and Experimental Views*; The Royal Society of Chemistry: Cambridge, UK, 2021.
(75) Politzer, P.; Truhlar, D. G. *Chemical Applications of Atomic and Molecular Electrostatic Potentials*; Plenum Press: New York, 1981.
(76) Bader, R. F. W. A Quantum Theory of Molecular Structure and Its Applications. *Chem. Rev.* **1991**, *91* (5), 893–928.
(77) Reed, A. E.; Curtiss, L. A.; Weinhold, F. Intermolecular Interactions from a Natural Bond Orbital, Donor-Acceptor Viewpoint. *Chem. Rev.* **1988**, *88* (6), 899–926.
(78) Kitaura, K.; Morokuma, K. A New Energy Decomposition Scheme for Molecular Interactions within

the Hartree-Fock Approximation. *Int. J. Quantum Chem.* **1976**, *X*, 325–340.
(79) Gadre, S. R.; Yeole, S. D.; Sahu, N. Quantum Chemical Investigations on Molecular Clusters. *Chem. Rev.* **2014**, *114* (24), 12132–12173.
(80) Rosenfeld, D.; Sherwood, S.; Wood, R.; Donner, L. Climate Effects of Aerosol-Cloud Interactions. *Science.* **2014**, *343* (6169), 379–380.
(81) Calvert, J. G.; Lazrus, A.; Kok, G. L.; Heikes, B. G.; Walega, J. G.; Lind, J.; Cantrell, C. A. Chemical Mechanisms of Acid Generation in the Troposphere. *Nature* **1985**, *317* (6032), 27–35.
(82) Vaida, V. Perspective: Water Cluster Mediated Atmospheric Chemistry. *J. Chem. Phys.* **2011**, *135* (2), 20901.
(83) De Laurentiis, E.; Minella, M.; Berto, S.; Maurino, V.; Minero, C.; Vione, D. The Fate of Nitrogen upon Nitrite Irradiation: Formation of Dissolved vs. Gas-Phase Species. *J. Photochem. Photobiol. A Chem.* **2015**, *307–308*, 30–34.
(84) Olasehinde, E. F.; Takeda, K.; Sakugawa, H. Development of an Analytical Method for Nitric Oxide Radical Determination in Natural Waters. *Anal. Chem.* **2009**, *81*, 6843–6850.
(85) Anglada, J. M.; Martins-Costa, M. T. C.; Francisco, J. S.; Ruiz-López, M. F. Photoinduced Oxidation Reactions at the Air-Water Interface. *J. Am. Chem. Soc.* **2020**, *142* (38), 16140–16155.
(86) Anifowose, A. J.; Takeda, K.; Sakugawa, H. Photoformation Rate, Steady-State Concentration and Lifetime of Nitric Oxide Radical (NO) in a Eutrophic River in Higashi-Hiroshima, Japan. *Chemosphere* **2015**, *119*, 302–309.
(87) Mack, J.; Bolton, J. R. Photochemistry of Nitrite and Nitrate in Aqueous Solution: A Review. *J. Photochem. Photobiol. A Chem.* **1999**, *128*, 1–13.
(88) Tian, Y.; Wang, K. K.; Yang, G. P.; Li, P. F.; Liu, C. Y.; Ingeniero, R. C. O.; Bange, H. W. Continuous Chemiluminescence Measurements of Dissolved Nitric Oxide (NO) and Nitrogen Dioxide (NO_2) in the Ocean Surface Layer of the East China Sea. *Environ. Sci. Technol.* **2021**, *55* (6), 3668–3675.
(89) Adesina, A. O.; Sakugawa, H. Photochemically Generated Nitric Oxide in Seawater: The Peroxynitrite Sink and Its Implications for Daytime Air Quality. *Sci. Total Environ.* **2021**, *781*, 146683.
(90) Tian, Y.; Yang, G. P.; Liu, C. Y.; Li, P. F.; Chen, H. T.; Bange, H. W. Photoproduction of Nitric Oxide in Seawater. *Ocean Sci.* **2020**, *16*, 135–148.
(91) Tian, Y.; Xue, C.; Liu, C. Y.; Yang, G. P.; Li, P. F.; Feng, W. H.; Bange, H. H. Nitric Oxide (NO) in the Bohai Sea and the Yellow Sea. *Biogeosciences* **2019**, *16*, 4485–4496.
(92) Olasehinde, E. F.; Takeda, K.; Sakugawa, H. Photochemical Production and Consumption Mechanisms of Nitric Oxide in Seawater. *Environ. Sci. Technol.* **2010**, *44* (22), 8403–8408.
(93) Zafiriou, O. C.; McFarland, M.; Bromund, R. H. Nitric Oxide in Seawater. *Science.* **1980**, *207* (4431), 637–639.
(94) Crespo-Otero, R.; Suardiaz, R.; Montero, L. A.; García De La Vega, J. M. Potential Energy Surfaces and Jahn-Teller Effect on CH_4...NO Complexes. *J. Chem. Phys.* **2007**, *127* (10).
(95) Cybulski, H.; Zuchowski, P. S.; Fernández, B.; Sadlej, J. The Water-Nitric Oxide Intermolecular Potential-Energy Surface Revisited. *J. Chem. Phys.* **2009**, *130* (10), 104303.
(96) Kalai, C.; Alikhani, M. E.; Zins, E. L. The Molecular Electrostatic Potential Analysis of Solutes and Water Clusters: A Straightforward Tool to Predict the Geometry of the Most Stable Micro-Hydrated Complexes of β-Propiolactone and Formamide. *Theor. Chem. Acc.* **2018**, *137* (11).
(97) Kalai, C.; Zins, E. L.; Alikhani, M. E. A Theoretical Investigation of Water–Solute Interactions: From Facial Parallel to Guest–Host Structures. *Theor. Chem. Acc.* **2017**, *136* (4).
(98) Gillan, M. J.; Alfè, D.; Michaelides, A. Perspective: How Good Is DFT for Water? *J. Chem. Phys.* **2016**, *144* (13).
(99) Gerber, R. B.; Varner, M. E.; Hammerich, A. D.; Riikonen, S.; Murdachaew, G.; Shemesh, D.; Finlayson-Pitts, B. J. Computational Studies of Atmospherically-Relevant Chemical Reactions in Water Clusters and on Liquid Water and Ice Surfaces. *Acc. Chem. Res.* **2015**, *48* (2), 399–406.
(100) Lalitha, M.; Senthilkumar, L. DFT Study on $X^{-}\cdot(H_2O)_n$=1-10 (X = OH, NO_2, NO_3, CO_3) Anionic Water Cluster. *J. Mol. Graph. Model.* **2014**, *54* (2), 148–163.
(101) Desai, S. R.; Feigerle, C. S.; Miller, J. C. Laser Ionization Mass Spectrometry of Homogeneous and Binary Molecular Clusters of Nitric Oxide. *J. Chem. Phys.* **1994**, *101*, 4526–4535.
(102) Dozova, N.; Krim, L.; Alikhani, M. E.; Lacome, N. Vibrational Spectra and Structures of H_2O-NO, HDO-NO, and D_2O-NO Complexes. An IR Matrix Isolation and DFT Study. *J. Phys. Chem. A* **2006**, *110*, 11617–11626.
(103) Šmídová, D.; Lengyel, J.; Kočišek, J.; Pysanenko, A.; Fárník, M. Analysis of Mixed Nitric Oxide–Water Clusters by Complementary Ionization Methods. *Int. J. Mass Spectrom.* **2017**, *421*, 144–149.
(104) Myszkiewicz, G.; Sadlej, J. Ab Initio Study for the Intermolecular Potential of the Water-Nitric Oxide Complex. *Chem. Phys. Lett.* **2000**, *318*, 232–239.
(105) Martinez Gonzalez, M.; Bravo-Rodriguez, K.; Suardiaz, R.; Garcia de la Vega, J. M.; Montero, L. A.;

Sanchez-Garcia, E.; Crespo-Otero, R. Complexes of Nitric Oxide with Water and Imidazole. *Theor. Chem. Acc.* **2015**, *134*, 88.
(106) Orenha, R. P.; San Gregorio, L. R.; Galembeck, S. E. Computational Study of the Interaction between NO, NO^+, and NO^- with H_2O. *J. Mol. Model.* **2016**, *22*, 276.
(107) Eaton, J. G.; Arnold, S. T.; Bowen, K. H. The Negative Ion Photoelectron (Photodetachment) Spectra of $NO^-(H_2O)_{n=1,2}$. *Int. J. Mass Spectrom. Ion Process.* **1990**, *102*, 303–312.
(108) Myshakin, E. M.; Jordan, K. D.; Robertson, W. H.; Weddle, G. H.; Johnson, M. A. Dominant Structural Motifs of $NO^-\cdot(H_2O)_n$ Complexes: Infrared Spectroscopic and Ab Initio Studies. *J. Chem. Phys.* **2003**, *118*, 4945–4953.
(109) Relph, R. A.; Guasco, T. L.; Elliott, B. M.; Kamrath, M. Z.; McCoy, A. B.; Steele, R. P.; Schofield, D. P.; Jordan, K. D.; Viggiano, A. A.; Ferguson, E. E.; Johnson, M. A. How the Shape of an H-Bonded Network Controls Proton-Coupled Water Activation in HONO Formation. *Science* **2010**, *327*, 308–312.
(110) Shafirovich, V.; Lymar, S. V. Spin-Forbidden Deprotonation of Aqueous Nitroxyl (HNO). *J. Am. Chem. Soc.* **2003**, *125*, 6547–6552.
(111) Hammam, E.; Lee, E. P. F.; Dyke, J. M. Ab Initio Molecular Orbital Calculations on $NO^+\cdot(H_2O)_n$ Cluster Ions. Part I: Minimum-Energy Structures and Possible Routes to Nitrous Acid Formation. *J. Phys. Chem. A* **2000**, *104*, 4571–4580.
(112) Asada, T.; Nagaoka, M.; Koseki, S. Ab Initio Electron Correlated Studies on the Intracluster Reaction of $NO+(H_2O)_n \rightarrow H_3O^+(H_2O)_{n-2}$ (HONO) (n = 4 and 5). *Phys. Chem. Chem. Phys.* **2011**, *13*, 1590–1596.
(113) Linton, K. A.; Wright, T. G.; Besley, N. A. Quantum Chemical Study of the Structure, Spectroscopy and Reactivity of $NO^+.(H_2O)_{N=1-5}$ Clusters. *Philos. Trans. R. Soc. A Math. Phys. Eng. Sci.* **2018**, *376*, 20170152.
(114) Bartberger, M. D.; Fukuto, J. M.; Houk, K. N. On the Acidity and Reactivity of HNO in Aqueous Solution and Biological Systems. *Proc. Natl. Acad. Sci. U. S. A.* **2001**, *98*, 2194–2198.
(115) Shafirovich, V.; Lymar, S. V. Nitroxyl and Its Anion in Aqueous Solutions: Spin States, Protic Equilibria, and Reactivities toward Oxygen and Nitric Oxide. *Proc. Natl. Acad. Sci. U. S. A.* **2002**, *99*, 7340–7345.
(116) Zhang, K.; Thynell, S. T. Examination of the Mechanism of the Yield of N_2O from Nitroxyl (HNO) in the Solution Phase by Theoretical Calculations. *J. Phys. Chem. A* **2017**, *121*, 4505–4516.
(117) Fehling, C.; Friedrichs, G. Dimerization of HNO in Aqueous Solution: An Interplay of Solvation Effects, Fast Acid–Base Equilibria, and Intramolecular Hydrogen Bonding? *J. Am. Chem. Soc.* **2011**, *133*, 17912–17922.
(118) Zhao, X.; Liu, Z.; Zhao, R.; Xu, T. The Effect of $(H_2O)_{n\ (n = 1–3)}$ Clusters on the Reaction of HONO with HCl: A Mechanistic and Kinetic Study. *Phys. Chem. Chem. Phys.* **2022**, *24*, 10011–10024.
(119) Bulychev, V. P.; Buturlimova, M. V; Tokhadze, K. G. Quantum-Mechanical Prediction of the Averaged Structure, Anharmonic Vibrational Frequencies, and Intensities of the $H_2O\cdots$trans-HONO Complex and Comparison with the Experiment. *J. Phys. Chem. A* **2017**, *121*, 7255–7260.
(120) Franchi, P.; Lucarini, M.; Pedrielli, P.; Pedulli, G. F. Nitroxide Radicals as Hydrogen Bonding Acceptors. An Infrared and EPR Study. *ChemPhysChem* **2002**, *3*, 789–793.
(121) Karoui, H.; Moigne, F. Le; Ouari, O.; Tordo, P. *Nitroxide Radicals: Properties, Synthesis and Applications*; 2010.
(122) Houriez, C.; Ferré, N.; Siri, D.; Masella, M. Further Insights into the Environmental Effects on the Computed Hyperfine Coupling Constants of Nitroxides in Aqueous Solution. *J. Phys. Chem. B* **2009**, *113*, 15047–15056.
(123) Owenius, R.; Engström, M.; Lindgren, M.; Huber, M. Influence of Solvent Polarity and Hydrogen Bonding on the EPR Parameters of a Nitroxide Spin Label Studied by 9-GHz and 95-GHz EPR Spectroscopy and DFT Calculations. *J. Phys. Chem. A* **2001**, *105*, 10967–10977.
(124) Nalepa, A.; Möbius, K.; Plato, M.; Lubitz, W.; Savitsky, A. Nitroxide Spin Labels—Magnetic Parameters and Hydrogen-Bond Formation: A High-Field EPR and EDNMR Study. *Appl. Magn. Reson.* **2019**, *50*, 1–16.
(125) Ikryannikova, L. N.; Ustynyuk, L. Y.; Tikhonov, A. N. DFT Study of Nitroxide Radicals: Explicit Modeling of Solvent Effects on the Structural and Electronic Characteristics of 4-Amino-2,2,6,6-Tetramethyl-Piperidine-N-Oxyl. *Magn. Reson. Chem.* **2010**, *48*, 337–349.
(126) Ikryannikova, L. N.; Ustynyuk, L. Y.; Tikhonov, A. N. DFT Study of Nitroxide Radicals. 1. Effects of Solvent on Structural and Electronic Characteristics of 4-Amino-2,2,5,5-Tetramethyl-3-Imidazoline-N-Oxyl. *J. Phys. Chem. A* **2004**, *108*, 4759–4768.
(127) Smirnova, T. I.; Smirnov, A. I.; Paschenko, S. V; Poluektov, O. G. Geometry of Hydrogen Bonds Formed by Lipid Bilayer Nitroxide Probes: A High-Frequency Pulsed ENDOR/EPR Study. *J. Am. Chem. Soc.* **2007**, *129*, 3476–3477.
(128) Chestnut, M. M.; Milikisiyants, S.; Voinov, M. A.; Koolivand, A.; Smirnova, T. I.; Smirnov, A. I.

Profiling Water Concentration across Lipid Bilayer Membranes by Hyscore Spectroscopy of Nitroxides. *Biophys. J.* **2022**, *121*, 214a.
(129) Bagryanskaya, E. G.; Marque, S. R. A. Scavenging of Organic C-Centered Radicals by Nitroxides. *Chem. Rev.* **2014**, *114*, 5011–5056.
(130) Romero, F. M.; Ziessel, R.; Bonnet, M.; Pontillon, Y.; Ressouche, E.; Schweizer, J.; Delley, B.; Grand, A.; Paulsen, C. Evidence for Transmission of Ferromagnetic Interactions through Hydrogen Bonds in Alkyne-Substituted Nitroxide Radicals: Magnetostructural Correlations and Polarized Neutron Diffraction Studies. *J. Am. Chem. Soc.* **2000**, *122*, 1298–1309.
(131) Palčić, A.; Valtchev, V. Analysis and Control of Acid Sites in Zeolites. *Appl. Catal. A Gen.* **2020**, *606*, 117795.
(132) Abdelrahman, O. A.; Vinter, K. P.; Ren, L.; Xu, D.; Gorte, R. J.; Tsapatsis, M.; Dauenhauer, P. J. Simple Quantification of Zeolite Acid Site Density by Reactive Gas Chromatography. *Catal. Sci. Technol.* **2017**, *7*, 3831–3841.
(133) Vlasenko, N. V.; Kochkin, Y. N.; Telbiz, G. M.; Shvets, O. V.; Strizhak, P. E. Insight into the Active Site Nature of Zeolite H-BEA for Liquid Phase Etherification of Isobutylene with Ethanol. *RSC Adv.* **2019**, *9*, 35957–35968.
(134) Wang, Y.; Lei, Z.; Chen, B.; Guo, Q.; Liu, N. Adsorption of NO and N2O on Fe-BEA and H-BEA Zeolites. *Appl. Surf. Sci.* **2010**, *256*, 4042–4047.
(135) Goncalves, T. J.; Plessow, P. N.; Studt, F. Theoretical Study on the NO_x Selective Catalytic Reduction on Single-Cu Sites and Brønsted Acid Sites in Cu-SSZ-13. *J. Phys. Chem. C* **2021**, *125*, 12594–12602.
(136) Liu, C.; Malta, G.; Kubota, H.; Toyao, T.; Maeno, Z.; Shimizu, K. I. Mechanism of NH_3-Selective Catalytic Reduction (SCR) of NO/NO_2 (Fast SCR) over Cu-CHA Zeolites Studied by In Situ/Operando Infrared Spectroscopy and Density Functional Theory. *J. Phys. Chem. C* **2021**, *125*, 21975–21987.
(137) Rivallan, M.; Ricchiardi, G.; Bordiga, S.; Zecchina, A. Adsorption and Reactivity of Nitrogen Oxides (NO_2, NO, N_2O) on Fe-Zeolites. *J. Catal.* **2009**, *264*, 104–116.
(138) Anggara, T.; Paolucci, C.; Schneider, W. F. Periodic DFT Characterization of NO_x Adsorption in Cu-Exchanged SSZ-13 Zeolite Catalysts. *J. Phys. Chem. C* **2016**, *120*, 27934–27943.
(139) Sajith, P. K.; Shiota, Y.; Yoshizawa, K. Role of Acidic Proton in the Decomposition of NO over Dimeric Cu(I) Active Sites in Cu-ZSM-5 Catalyst: A QM/MM Study. *ACS Catal.* **2014**, *4*, 2075−2085.
(140) Kawakami, K.; Ogura, M. Theoretical Investigation of Novel Two-Step Decomposition of Nitric Oxide over Fe(II) Ion-Exchanged Zeolites Using DFT Calculations. *Catal. Today* **2015**, *242*, 343–350.
(141) Gorelsky, S. I.; Ghosh, S.; Solomon, E. I. Mechanism of N_2O Reduction by the M_4-S Tetranuclear CuZ Cluster of Nitrous Oxide Reductase. *J. Am. Chem. Soc.* **2006**, *128*, 278–290.
(142) Lu, J.; Bi, B.; Lai, W.; Chen, H. Origin of Nitric Oxide Reduction Activity in Flavo–Diiron NO Reductase: Key Roles of the Second Coordination Sphere. *Angew. Chemie* **2019**, *131*, 3835–3839.
(143) Ferousi, C.; Majer, S. H.; Dimucci, I. M.; Lancaster, K. M. Biological and Bioinspired Inorganic N-N Bond-Forming Reactions. *Chem. Rev.* **2020**, *120*, 5252–5307.
(144) Lin, Y. W.; Yeung, N.; Gao, Y. G.; Miner, K. D.; Tian, S.; Robinson, H.; Lu, Y. Roles of Glutamates and Metal Ions in a Rationally Designed Nitric Oxide Reductase Based on Myoglobin. *Proc. Natl. Acad. Sci. U. S. A.* **2010**, *107*, 8581–8586.
(145) Wijeratne, G. B.; Bhadra, M.; Siegler, M. A.; Karlin, K. D. Copper(I) Complex Mediated Nitric Oxide Reductive Coupling: Ligand Hydrogen Bonding Derived Proton Transfer Promotes $N_2O_{(g)}$ Release. *J. Am. Chem. Soc.* **2019**, *141*, 17962–17967.
(146) Dunning Jr., T. H. Gaussian Basis Sets for Use in Correlated Molecular Calculations. I. The Atoms Boron through Neon and Hydrogen. *J. Chem. Phys.* **1989**, *90*, 1007–1023.
(147) Weigend, F. Accurate Coulomb-Fitting Basis Sets for H to Rn. *Phys. Chem. Chem. Phys.* **2006**, *8*, 1057–1065.
(148) Hay, P. J.; Wadt, W. R. Ab Initio Effective Core Potentials for Molecular Calculations. Potentials for K to Au Including the Outermost Core Orbitals. *J. Chem. Phys.* **1985**, *82*, 299–310.
(149) Jansen, H. B.; Ros, P. Non-Empirical Molecular Orbital Calculations on the Protonation of Carbon Monoxide. *Chem. Phys. Lett.* **1969**, *3*, 140–143.
(150) Liu, B.; McLean, A. D. Accurate Calculation of the Attractive Interaction of Two Ground State Helium Atoms. *J. Chem. Phys.* **1973**, *59*, 4557–4558.
(151) Boys, S. F.; Bernardi, F. The Calculation of Small Molecular Interactions by the Differences of Separate Total Energies. Some Procedures with Reduced Errors. *Mol. Phys.* **1970**, *19*, 553–566.
(152) Perdew, J. P.; Wang, Y. Accurate and Simple Analytic Representation of the Electron-Gas Correlation Energy. *Phys. Rev. B* **1992**, *45*, 13244–13249.
(153) Becke, A. D. Density-Functional Exchange-Energy Approximation with Correct Asymptotic Behavior. *Phys. Rev. A* **1988**, *38*, 3098–3100.
(154) Lee, C.; Yang, W.; Parr, R. G. Development of the Colle-Salvetti Correlation-Energy Formula into a

Functional of the Electron Density. *Phys. Rev. B* **1988**, *37*, 785–789.
(155) Zhao, Y.; Truhlar, D. G. The M06 Suite of Density Functionals for Main Group Thermochemistry, Thermochemical Kinetics, Noncovalent Interactions, Excited States, and Transition Elements: Two New Functionals and Systematic Testing of Four M06-Class Functionals and 12 Other Function. *Theor. Chem. Acc.* **2008**, *120*, 215–241.
(156) Tao, J.; Perdew, J. P.; Staroverov, V. N.; Scuseria, G. E. Climbing the Density Functional Ladder: Nonempirical Meta--Generalized Gradient Approximation Designed for Molecules and Solids. *Phys. Rev. Lett.* **2003**, *91*, 146401.
(157) Becke, A. D. Density-functional Thermochemistry. III. The Role of Exact Exchange. *J. Chem. Phys.* **1993**, *98*, 5648–5652.
(158) Wu, X.; Vargas, M. C.; Nayak, S.; Lotrich, V.; Scoles, G. Towards Extending the Applicability of Density Functional Theory to Weakly Bound Systems. *J. Chem. Phys.* **2001**, *115*, 8748–8757.
(159) Grimme, S.; Ehrlich, S.; Goerigk, L. Effect of the Damping Function in Dispersion Corrected Density Functional Theory. *J. Comput. Chem.* **2011**, *32*, 1456–1465.
(160) Politzer, P.; Murray, J. S. The Fundamental Nature and Role of the Electrostatic Potential in Atoms and Molecules. *Theor. Chem. Acc.* **2002**, *108*, 134–142.
(161) Suresh, C. H.; Koga, N. Quantifying the Electronic Effect of Substituted Phosphine Ligands via Molecular Electrostatic Potential. *Inorg. Chem.* **2002**, *41*, 1573–1578.
(162) Kumar, A.; Gadre, S. R.; Mohan, N.; Suresh, C. H. Lone Pairs: An Electrostatic Viewpoint. *J. Phys. Chem. A* **2014**, *118*, 526–532.
(163) Mohan, N.; Suresh, C. H.; Kumar, A.; Gadre, S. R. Molecular Electrostatics for Probing Lone Pair-π Interactions. *Phys. Chem. Chem. Phys.* **2013**, *15*, 18401–18409.
(164) Mohan, N.; Suresh, C. H. A Molecular Electrostatic Potential Analysis of Hydrogen, Halogen, and Dihydrogen Bonds. *J. Phys. Chem. A* **2014**, *118*, 1697–1705.
(165) Suresh, C. H.; Alexander, P.; Vijayalakshmi, K. P.; Sajith, P. K.; Gadre, S. R. Use of Molecular Electrostatic Potential for Quantitative Assessment of Inductive Effect. *Phys. Chem. Chem. Phys.* **2008**, *10*, 6492–6499.
(166) Matta, C. F.; Boyd, R. J. *An Introduction to the Quantum Theory of Atoms in Molecules*; 2007.
(167) Koch, U.; Popelier, P. L. A. Characterization of C-H-O Hydrogen Bonds on the Basis of the Charge Density. *J. Phys. Chem.* **1995**, *99*, 9747–9754.
(168) Cremer, D.; Kraka, E. A Description of the Chemical Bond in Terms of Electron Density and Energy. *Croat. Chem. Acta* **1984**, *57*, 1259–1281.
(169) Reed, A. E.; Weinstock, R. B.; Weinhold, F. Natural Population Analysis. *J. Chem. Phys.* **1985**, *83*, 735–746.
(170) Weinhold, F.; Landis, C. R.; Glendening, E. D. What Is NBO Analysis and How Is It Useful? *Int. Rev. Phys. Chem.* **2016**, *35*, 399–440.
(171) Stasyuk, O. A.; Sedlak, R.; Guerra, C. F.; Hobza, P. Comparison of the DFT-SAPT and Canonical EDA Schemes for the Energy Decomposition of Various Types of Noncovalent Interactions. *J. Chem. Theory Comput.* **2018**, *14*, 3440–3450.
(172) Zhao, L.; von Hopffgarten, M.; Andrada, D. M.; Frenking, G. Energy Decomposition Analysis. *WIREs Comput. Mol. Sci.* **2018**, *8*, e1345.
(173) Jeziorski, B.; Moszynski, R.; Szalewicz, K. Perturbation Theory Approach to Intermolecular Potential Energy Surfaces of van Der Waals Complexes. *Chem. Rev.* **1994**, *94*, 1887–1930.
(174) Patkowski, K. Recent Developments in Symmetry-Adapted Perturbation Theory. *WIREs Comput. Mol. Sci.* **2020**, *10*, e1452.
(175) Gonthier, J. F.; Sherrill, C. D. Density-Fitted Open-Shell Symmetry-Adapted Perturbation Theory and Application to π-Stacking in Benzene Dimer Cation and Ionized DNA Base Pair Steps. *J. Chem. Phys.* **2016**, *145*, 134106.
(176) Frenking, G.; Fröhlich, N. The Nature of the Bonding in Transition-Metal Compounds. *Chem. Rev.* **2000**, *100*, 717–774.
(177) Hohenstein, E. G.; Sherrill, C. D. Density Fitting of Intramonomer Correlation Effects in Symmetry-Adapted Perturbation Theory. *J. Chem. Phys.* **2010**, *133*, 0–12.
(178) Deshmukh, M. M.; Gadre, S. R. Molecular Tailoring Approach for the Estimation of Intramolecular Hydrogen Bond Energy. *Molecules*. 2021, *26*, 2928.
(179) Deshmukh, M. M.; Suresh, C. H.; Gadre, S. R. Intramolecular Hydrogen Bond Energy in Polyhydroxy Systems: A Critical Comparison of Molecular Tailoring and Isodesmic Approaches. *J. Phys. Chem. A* **2007**, *111*, 6472–6480.
(180) Deshmukh, M. M.; Gadre, S. R.; Bartolotti, L. J. Estimation of Intramolecular Hydrogen Bond Energy via Molecular Tailoring Approach. *J. Phys. Chem. A* **2006**, *110*, 12519–12523.
(181) Ahirwar, M. B.; Gurav, N. D.; Gadre, S. R.; Deshmukh, M. M. Molecular Tailoring Approach for

Estimating Individual Intermolecular Interaction Energies in Benzene Clusters. *J. Phys. Chem. A* **2021**, *125*, 6131–6140.
(182) Ahirwar, M. B.; Gadre, S. R.; Deshmukh, M. M. Direct and Reliable Method for Estimating the Hydrogen Bond Energies and Cooperativity in Water Clusters, W_n, n = 3 to 8. *J. Phys. Chem. A* **2020**, *124*, 6699–6706.
(183) Ahirwar, M. B.; Patkar, D.; Yadav, I.; Deshmukh, M. M. Appraisal of Individual Hydrogen Bond Strengths and Cooperativity in Ammonia Clusters via a Molecular Tailoring Approach. *Phys. Chem. Chem. Phys.* **2021**, *23*, 17224–17231.
(184) Patkar, D.; Ahirwar, M. B.; Gadre, S. R.; Deshmukh, M. M. Unusually Large Hydrogen-Bond Cooperativity in Hydrogen Fluoride Clusters, $(HF)_n$, n = 3 to 8, Revealed by the Molecular Tailoring Approach. *J. Phys. Chem. A* **2021**, *125*, 8836–8845.
(185) Patkar, D.; Ahirwar, M. B.; Deshmukh, M. M. Energetic Ordering of Hydrogen Bond Strengths in Methanol-Water Clusters: Insights via Molecular Tailoring Approach. *ChemPhysChem* **2022**, *23*, e202200143.
(186) Patkar, D.; Bharati Ahirwar, M.; Deshmukh, M. M. A Tug of War between the Self- and Cross-Associating Hydrogen Bonds in Neutral Ammonia-Water Clusters: Energetic Insights by Molecular Tailoring Approach. *ChemPhysChem* **2022**, *23*, e202200476.
(187) Arildii, D.; Matsumoto, Y.; Dopfer, O. Microhydration of the Pyrrole Cation (Py^+) Revealed by IR Spectroscopy: Ionization-Induced Rearrangement of the Hydrogen-Bonded Network of $Py^+(H_2O)_2$. *J. Phys. Chem. A* **2023**, *127*, 2523–2535.
(188) Chatterjee, K.; Dopfer, O. Microhydration Structures of Protonated Oxazole. *J. Phys. Chem. A* **2019**, *123*, 7637–7650.
(189) Kim, Y.; Meyer, H. Multiphoton Spectroscopy of NO?Rg (Rg = Rare Gas) van Der Waals Systems. *Int. Rev. Phys. Chem.* **2001**, *20*, 219–282.
(190) Salmi, T.; Runeberg, N.; Halonen, L.; Lane, J. R.; Kjaergaard, H. G. Computational Vibrational and Electronic Spectroscopy of the Water Nitric Oxide Complex. *J. Phys. Chem. A* **2010**, *114*, 4835–4842.
(191) Mondal, S.; Teja, A. U.; Singh, P. C. Theoretical Study on the Microhydration of Atmospherically Important Carbonyl Sulfide in Its Neutral and Anionic Forms: Bridging the Gap between the Bulk and Finite Size Microhydrated Cluster. *J. Phys. Chem. A* **2015**, *119*, 3644–3652.
(192) Frisch, M. J.; Trucks, G. W.; Schlegel, H. B.; Scuseria, G. E.; Robb, M. A.; Cheeseman, J. R.; Scalmani, G.; Barone, V.; Petersson, G. A.; Nakatsuji, H. et al. Gaussian 16, Revision B.01; Gaussian, Inc.: Wallingford, CT, 2016.
(193) Keith, T. A. AIMAll Program, Version 17.11.14; TK Gristmill Software: Overland Park, KS, 2017.
(194) Lu, T.; Chen, F. Multiwfn: A Multifunctional Wavefunction Analyzer. J. Comput. Chem. 2012, 33, 580−592.
(195) Humphrey, W.; Dalke, A.; Schulten, K. VMD: Visual Molecular Dynamics. J. Mol. Graph. 1996, 14, 33−38.
(196) Glendening, E. D.; Reed, A. E.; Carpenter, J. E.; Weinhold, F. *NBO Version 3.1*.
(197) Zhurko, G. Chemcraft 1.8 program; Ivanovo, Russia, 2005. https://chemcraftprog.com (accessed 2023-04-09).
(198) Pathak, R. K.; Gadre, S. R. Maximal and Minimal Characteristics of Molecular Electrostatic Potentials. *J. Chem. Phys.* **1990**, *93*, 1770–1773.
(199) Murray, J. S.; Politzer, P. The Electrostatic Potential: An Overview. *WIREs Comput. Mol. Sci.* **2011**, *1*, 153–163.
(200) Sajith, P. K.; Suresh, C. H. Trans and Cis Influences in Hypervalent Iodine(III) Complexes: A DFT Study. *Inorg. Chem.* **2013**, *52*, 6046–6054.
(201) Sajith, P. K.; Suresh, C. H. Quantification of the Trans Influence in Hypervalent Iodine Complexes. *Inorg. Chem.* **2012**, *51*, 967–977.
(202) Ismail, T. M.; Mohan, N.; Sajith, P. K. Theoretical Study of Hydrogen Bonding Interactions in Substituted Nitroxide Radicals. *New J. Chem.* **2021**, *45*, 3866–3875.
(203) Ismail, T. M.; Prasanthkumar, K. P.; Ebenezer, C.; Anjali, B. A.; Solomon, R. V.; Sajith, P. K. Hydrogen-Bond-Assisted Adsorption of Nitric Oxide on Various Metal-Loaded ZSM-5 Zeolites. *Langmuir* **2022**, *38*, 10492–10502.
(204) Suresh, C. H.; Remya, G. S.; Anjalikrishna, P. K. Molecular Electrostatic Potential Analysis: A Powerful Tool to Interpret and Predict Chemical Reactivity. *WIREs Comput. Mol. Sci.* **2022**, *12* (5), e1601.
(205) Krishnapriya, V. U.; Suresh, C. H. The Use of Electrostatic Potential at Nuclei in the Analysis of Halogen Bonding. *New J. Chem.* **2022**, *46*, 6158–6164.
(206) Chandra, S.; Suryaprasad, B.; Ramanathan, N.; Sundararajan, K. Nitrogen as a Pnicogen?: Evidence for π-Hole Driven Novel Pnicogen Bonding Interactions in Nitromethane–Ammonia Aggregates Using

Matrix Isolation Infrared Spectroscopy and Ab Initio Computations. *Phys. Chem. Chem. Phys.* **2021**, *23*, 6286–6297.
(207) Politzer, P.; Murray, J. S.; Clark, T. The π-Hole Revisited. *Phys. Chem. Chem. Phys.* **2021**, *23*, 16458–16468.
(208) Varadwaj, A.; Varadwaj, P. R.; Marques, H. M.; Yamashita, K. Definition of the Pnictogen Bond: A Perspective. *Inorganics* **2022**, *10*, 149, 1–15.
(209) Ramachandran, C. N.; Ruckenstein, E. Water Clustering in the Presence of a CO_2 Molecule. *Comput. Theor. Chem.* **2011**, *966*, 84–90.
(210) Hartt, G. M.; Shields, G. C.; Kirschner, K. N. Hydration of OCS with One to Four Water Molecules in Atmospheric and Laboratory Conditions. *J. Phys. Chem. A* **2008**, *112*, 4490–4495.
(211) Korchagina, K. A.; Spiegelman, F.; Cuny, J. Molecular Dynamics Study of the Collision-Induced Reaction of H with CO on Small Water Clusters. *J. Phys. Chem. A* **2017**, *121*, 9485–9494.
(212) Patel, C. K. N.; Burkhardt, E. G.; Lambert, C. A. Spectroscopic Measurements of Stratospheric Nitric Oxide and Water Vapor. *Science* **1974**, *184*, 1173–1176.
(213) McIntyre, S. M.; Ennis, C.; Garden, A. L. A Computational Investigation into the Hydrogenation of NO on Water Ice Surfaces to Rationalize the NO:HNO:NOH Disparity in Space. *ACS Earth Sp. Chem.* **2023**, *7*, 1195–1206.
(214) Li, W.; Pérez, C.; Steber, A. L.; Schnell, M.; Lv, D.; Wang, G.; Zeng, X.; Zhou, M. Evolution of Solute–Water Interactions in the Benzaldehyde-$(H_2O)_{1–6}$ Clusters by Rotational Spectroscopy. *J. Am. Chem. Soc.* **2023**, *145*, 4119–4128.
(215) Solimannejad, M.; Nassirinia, N.; Amani, S. $HNO(H_2O)_n$ (n = 1–4) Clusters: A Theoretical Study. *Struct. Chem.* **2011**, *22*, 865–871.
(216) Chalasinski, G.; Szczesniak, M. M. Origins of Structure and Energetics of van Der Waals Clusters from Ab Initio Calculations. *Chem. Rev.* **1994**, *94*, 1723–1765.
(217) Wick, C. R.; Clark, T. On Bond-Critical Points in QTAIM and Weak Interactions. *J. Mol. Model.* **2018**, *24*, 142.
(218) Jabłoński, M. Bond Paths between Distant Atoms Do Not Necessarily Indicate Dominant Interactions. *J. Comput. Chem.* **2018**, *39*, 2183–2195.
(219) Kim, J.; Lee, H. M.; Suh, S. B.; Majumdar, D.; Kim, K. S. Comparative Ab Initio Study of the Structures, Energetics and Spectra of $X^-\cdot(H_2O)_{n=1–4}$ [X=F,Cl,Br,I] Clusters. *J. Chem. Phys.* **2000**, *113*, 5259–5272.
(220) Lee, H. M.; Kim, K. S. Structures and Spectra of Iodide–Water Clusters $I^-(H_2O)_{n=1–6}$: An Ab Initio Study. *J. Chem. Phys.* **2001**, *114*, 4461–4471.
(221) Krishnakumar, P.; Maity, D. K. Microhydration of Neutral and Charged Acetic Acid. *J. Phys. Chem. A* **2017**, *121*, 493–504.
(222) Yu, F.; Xu, G. Noncovalent Interactions in Hydrated Nitrosonium Ion Clusters Mediated by Hydrogen-Bonded Water Networks. *J. Phys. Chem. A* **2023**, *127*, 4787–4792.
(223) Ismail, T. M.; Patkar, D.; Sajith, P. K.; Deshmukh, M. M. Interplay of Hydrogen, Pnicogen, and Chalcogen Bonding in $X(H_2O)_{n=1–5}$ (X = NO, NO^+, and NO^-) Complexes: Energetics Insights via a Molecular Tailoring Approach. *J. Phys. Chem. A* **2023**.
(224) Ni, S.; Meng, T.-T.; Huang, G.-Q.; Tang, Y.-Z.; Bai, F.-Y.; Zhao, Z. Roles of Amides on the Formation of Atmospheric HONO and the Nucleation of Nitric Acid Hydrates. *J. Phys. Chem. A* **2023**.
(225) Tang, S.; Tsona, N. T.; Du, L. Elucidating the Mechanism and Kinetics of the Water-Assisted Reaction of Nitrous Acid with Hydroxyl Radical. *Phys. Chem. Chem. Phys.* **2019**, *21*, 18071–18081.
(226) Alkorta, I.; Elguero, J.; Elguero, E. Nitroxide Stable Radicals Interacting as Lewis Bases in Hydrogen Bonds: A Search in the Cambridge Structural Data Base for Intermolecular Contacts. *J. Mol. Struct.* **2017**, *1148*, 150–161.
(227) Alkorta, I.; Elguero, J. A Theoretical Study of the Thermodynamic and Hydrogen-Bond Basicity of TEMPO Radical and Related Nitroxides. *Struct. Chem.* **2014**, *25*, 1873–1880.
(228) Groom, C. R.; Bruno, I. J.; Lightfoot, M. P.; Ward, S. C. The Cambridge Structural Database. *Acta Crystallogr. Sect. B Struct. Sci. Cryst. Eng. Mater.* **2016**, *72*, 171–179.
(229) Zhao, Y.; Truhlar, D. G. A New Local Density Functional for Main-Group Thermochemistry, Transition Metal Bonding, Thermochemical Kinetics, and Noncovalent Interactions. *J. Chem. Phys.* **2006**, *125*, 194101.
(230) Frisch, M. J.; Trucks, G. W.; Schlegel, H. B.; Scuseria, G. E.; Robb, M. A.; Cheeseman, J. R.; Scalmani, G.; Barone, V.; Mennucci, B.; Petersson, G. A.; et al. Gaussian 09, Revision B.01. Gaussian, Inc.,: Wallingford CT 2009.
(231) Remya, K.; Suresh, C. H. Which Density Functional Is Close to CCSD Accuracy to Describe Geometry and Interaction Energy of Small Noncovalent Dimers? A Benchmark Study Using Gaussian09. *J. Comput. Chem.* **2013**, *34*, 1341–1353.

(232) Parrish, R. M.; Burns, L. A.; Smith, D. G. A.; Simmonett, A. C.; DePrince, A. E.; Hohenstein, E. G.; Bozkaya, U.; Sokolov, A. Y.; Di Remigio, R.; Richard, R. M.; Gonthier, J. F.; James, A. M.; McAlexander, H. R.; Kumar, A.; Saitow, M.; Wang, X.; Pritchard, B. P.; Verma, P.; Schaefer, H. F.; Patkowski, K.; King, R. A.; Valeev, E. F.; Evangelista, F. A.; Turney, J. M.; Crawford, T. D.; Sherrill, C. D. Psi4 1.1: An Open-Source Electronic Structure Program Emphasizing Automation, Advanced Libraries, and Interoperability. *J. Chem. Theory Comput.* **2017**, *13*, 3185–3197.
(233) Sayyed, F. B.; Suresh, C. H. Quantification of Substituent Effects Using Molecular Electrostatic Potentials : Additive Nature and Proximity Effects. *New J. Chem.* **2009**, *33*, 2465–2471.
(234) Mathew, J.; Thomas, T.; Suresh, C. H. Quantitative Assessment of the Stereoelectronic Profile of Phosphine Ligands. *Inorg. Chem.* **2007**, *46*, 10800–10809.
(235) Alkorta, I.; Elguero, J. A Theoretical Study of the Thermodynamic and Hydrogen-Bond Basicity of TEMPO Radical and Related Nitroxides. *Struct. Chem.* **2014**, *25*, 1873–1880.
(236) Politzer, P.; Murray, J. S. σ-Hole Interactions: Perspectives and Misconceptions. *Crystals* **2017**, *7*, 212.
(237) Zhao, C.; Lu, Y.; Zhu, Z.; Liu, H. Theoretical Exploration of Halogen Bonding Interactions in the Complexes of Novel Nitroxide Radical Probes and Comparison with Hydrogen Bonds. *J. Phys. Chem. A* **2018**, *122*, 5058–5068.
(238) Grabowski, S. J. What Is the Covalency of Hydrogen Bonding? *Chem. Rev.* **2011**, *111*, 2597–2625.
(239) Zhang, S.; Wang, G.; Lu, Y.; Zhu, W.; Peng, C.; Liu, H. The Interactions Between Imidazolium-Based Ionic Liquids and Stable Nitroxide Radical Species : A Theoretical Study. *J. Phys. Chem. A* **2016**, *120*, 6089–6102.
(240) Sahoo, D. K.; Jena, S.; Dutta, J.; Rana, A.; Biswal, H. S. Nature and Strength of M−H⋯S and M−H⋯Se (M = Mn, Fe, & Co) Hydrogen Bond. *J. Phys. Chem. A* **2019**, *123*, 2227–2236.
(241) Rozas, I.; Alkorta, I.; Elguero, J. Behavior of Ylides Containing N, O, and C Atoms as Hydrogen Bond Acceptors. *J. Am. Chem. Soc.* **2000**, *122*, 11154–11161.
(242) Bankiewicz, B.; Matczak, P.; Palusiak, M. Electron Density Characteristics in Bond Critical Point (QTAIM) versus Interaction Energy Components (SAPT): The Case of Charge-Assisted Hydrogen Bonding. *J. Phys. Chem. A* **2012**, *116*, 452–459.
(243) Hoja, J.; Sax, A. F.; Szalewicz, K. Is Electrostatics Sufficient to Describe Hydrogen-Bonding Interactions? *Chem. Eur. J.* **2014**, *20*, 2292–2300.
(244) Zalazar, M. F.; Paredes, E. N.; Romero Ojeda, G. D.; Cabral, N. D.; Peruchena, N. M. Study of Confinement and Catalysis Effects of the Reaction of Methylation of Benzene by Methanol in H-Beta and H-ZSM-5 Zeolites by Topological Analysis of Electron Density. *J. Phys. Chem. C* **2018**, *122*, 3350–3362.
(245) Zalazar, M. F.; Peruchena, N. M. Topological Description of the Bond-Breaking and Bond-Forming Processes of the Alkene Protonation Reaction in Zeolite Chemistry: An AIM Study. *J. Mol. Model.* **2011**, *17*, 2501–2511.
(246) Roohi, H.; Akbari, F. Adsorption of Parent Nitrosamine on the Nanocrystaline H-Zeolite: A Theoretical Study. *Appl. Surf. Sci.* **2010**, *256*, 7575–7582.
(247) *Database of Zeolite Structures.* http://www.iza-structure.org/databases/.
(248) Ziegler, T.; Rauk, A. On the Calculation of Bonding Energies by the Hartree Fock Slater Method. *Theor. Chim. Acta* **1977**, *46*, 1–10.
(249) Van Lenthe, E.; Ehlers, A.; Baerends, E.-J. Geometry Optimizations in the Zero Order Regular Approximation for Relativistic Effects. *J. Chem. Phys.* **1999**, *110*, 8943–8953.
(250) Te Velde, G.; Bickelhaupt, F. M.; Baerends, E. J.; Fonseca Guerra, C.; Van Gisbergen, S. J. A.; Snijders, J. G.; Ziegler, T. Chemistry with ADF. *J. Comput. Chem.* **2001**, *22*, 931–967.
(251) Perdew, J. P. Density-Functional Approximation for the Correlation Energy of the Inhomogeneous Electron Gas. *Phys. Rev. B* **1986**, *33*, 8822–8824.
(252) Ebenezer, C.; Solomon, R. V. Impact of Coordination Modes of N-Donor Ligands on Am(III)/Eu(III) Separation in Nuclear Waste Water Treatment – A DFT Study. *ChemistrySelect* **2021**, *6*, 11876–11886.
(253) Mitoraj, M. P.; Parafiniuk, M.; Srebro, M.; Handzlik, M.; Buczek, A.; Michalak, A. Applications of the ETS-NOCV Method in Descriptions of Chemical Reactions. *J. Mol. Model.* **2011**, *17*, 2337–2352.
(254) Mitoraj, M.; Michalak, A. Natural Orbitals for Chemical Valence as Descriptors of Chemical Bonding in Transition Metal Complexes. *J. Mol. Model.* **2007**, *13*, 347–355.
(255) Thomas, J. L. C.; Bauschlicher, C. W.; Hall, M. B. Binding of Nitric Oxide to First-Transition-Row Metal Cations: An Ab Initio Study. *J. Phys. Chem. A* **1997**, *101*, 8530–8539.
(256) Fellah, M. F. CO and NO Adsorptions on Different Iron Sites of Fe-ZSM-5 Clusters : A Density Functional Theory Study. *J. Phys. Chem. C* **2011**, *115*, 1940–1951.
(257) Pulido, A.; Nachtigall, P. Theoretical Investigation of Dinitrosyl Complexes in Cu-Zeolites as Intermediates in $DeNO_x$ Process. *Phys. Chem. Chem. Phys.* **2009**, *11*, 1447–1458.
(258) Davidová, M.; Nachtigallová, D.; Nachtigall, P.; Sauer, J. Nature of the Cu^+-NO Bond in the Gas Phase

and at Different Types of Cu^+ Sites in Zeolite Catalysts. *J. Phys. Chem. B* **2004**, *108*, 13674–13682.
(259) Fujisawa, K.; Soma, S.; Kurihara, H.; Dong, H. T.; Bilodeau, M.; Lehnert, N. A Cobalt-Nitrosyl Complex with a Hindered Hydrotris(Pyrazolyl)Borate Coligand: Detailed Electronic Structure, and Reactivity towards Dioxygen. *Dalt. Trans.* **2017**, *46*, 13273–13289.
(260) Landry, V. K.; Pang, K.; Quan, S. M.; Parkin, G. Tetrahedral Nickel Nitrosyl Complexes with Tripodal $[N_3]$ and $[Se_3]$ Donor Ancillary Ligands: Structural and Computational Evidence That a Linear Nitrosyl Is a Trivalent Ligand. *Dalt. Trans.* **2007**, 820–824.
(261) Ampßler, T.; Monsch, G.; Popp, J.; Riggenmann, T.; Salvador, P.; Schröder, D.; Klüfers, P. Not Guilty on Every Count: The "Non-Innocent" Nitrosyl Ligand in the Framework of IUPAC′s Oxidation-State Formalism. *Angew. Chem., Int. Ed.* **2020**, *59*, 12381–12386.
(262) Gallego, C. M.; Mazzeo, A.; Gaviglio, C.; Pellegrino, J.; Doctorovich, F. Structure and Reactivity of $NO/NO^+/NO^-$ Pincer and Porphyrin Complexes. *Eur. J. Inorg. Chem.* **2021**, *2021*, 4712–4730.
(263) Qiu, S.; Ohnish, R.; Ichikawa, M. Formation and Interaction of Carbonyls and Nitrosyls on Gold(I) in ZSM-5 Zeolite Catalytically Active in NO Reduction with CO. *J. Phys. Chem.* **1994**, *98*, 2719–2721.
(264) Chao, C. C.; Lunsford, J. H. An Infrared and Electron Paramagnetic Resonance Study of Some Silver-Nitric Oxide Complexes in Y Type Zeolites. *J. Phys. Chem.* **1974**, *78*, 1174–1177.
(265) Iwamoto, M.; Yahiro, H.; Mizuno, N.; Zhang, W. X.; Mine, Y.; Furakawa, H.; Kagawa, S. Removal of Nitrogen Monoxide through a Novel Catalytic Process. 2. Infrared Study on Surface Reaction of Nitrogen Monoxide Adsorbed on Copper Ion-Exchanged ZSM-5 Zeolites. *J. Phys. Chem.* **1992**, *96*, 9360–9366.
(266) Wong, M. W. Vibrational Frequency Prediction Using Density Functional Theory. *Chem. Phys. Lett.* **1996**, *256*, 391–399.
(267) Uzunova, E. L.; Göltl, F.; Kresse, G.; Hafner, J. Application of Hybrid Functionals to the Modeling of NO Adsorption on Cu - SAPO-34 and Co - SAPO-34 : A Periodic DFT Study. *J. Phys. Chem. C* **2009**, *113*, 5274–5291.
(268) Uzunova, E. L. Theoretical Study of Nitrogen Dioxide and Nitric Oxide Co-Adsorption and $DeNO_x$ Reaction on Cu-SAPO−34 and Cu-SSZ−13 in Presence of Brønsted Acid Sites. *Mol. Catal.* **2018**, *447*, 47–55.
(269) Moreno-González, M.; Millán, R.; Concepción, P.; Blasco, T.; Boronat, M. Spectroscopic Evidence and Density Functional Theory (DFT) Analysis of Low-Temperature Oxidation of Cu^+ to $Cu^{2+}NO_x$ in Cu-CHA Catalysts: Implications for the SCR-NO_x Reaction Mechanism. *ACS Catal.* **2019**, *9*, 2725−2738.
(270) Tang, Y.; Chen, W.; Shi, J.; Wang, Z.; Cui, Y.; Teng, D.; Li, Y.; Feng, Z.; Dai, X. Nitrogen and Boron Coordinated Single-Atom Catalysts for Low-Temperature CO/NO Oxidations. *J. Mater. Chem. A* **2021**, *9*, 15329–15345.
(271) Suzuki, T.; Tanaka, H.; Shiota, Y.; Sajith, P. K.; Arikawa, Y.; Yoshizawa, K. Proton-Assisted Mechanism of NO Reduction on a Dinuclear Ruthenium Complex. *Inorg. Chem.* **2015**, *54*, 7181–7191.
(272) Pietrzyk, P.; Zasada, F.; Piskorz, W.; Kotarba, A.; Sojka, Z. Computational Spectroscopy and DFT Investigations into Nitrogen and Oxygen Bond Breaking and Bond Making Processes in Model $DeNO_x$ and DeN_2O Reactions. *Catal. Today* **2007**, *119*, 219–227.
(273) Kozyra, P.; Radon, M.; Datka, J.; Broclawik, E. On the Nature of Spin-and Orbital-Resolved Cu^+-NO Charge Transfer in the Gas Phase and at Cu(I) Sites in Zeolites. *Struct. Chem.* **2012**, *23*, 1349–1356.
(274) Yang, D.; Gates, B. C. Catalysis by Metal Organic Frameworks: Perspective and Suggestions for Future Research. *ACS Catal.* **2019**, *9*, 1779–1798.
(275) Schneider, W. F.; Hass, K. C.; Ramprasad, R.; Adams, J. B. First-Principles Analysis of Elementary Steps in the Catalytic Decomposition of NO by Cu-Exchanged Zeolites. *J. Phys. Chem. B* **1997**, *101*, 4353–4357.

LIST OF PUBLICATIONS

Based on Thesis work:

1. **Thufail M. Ismail**; Mohan, N.; Sajith, P. K. "Theoretical study of hydrogen bonding interactions in substituted nitroxide radicals". ***New Journal of Chemistry*** 2021, *45*, 3866-3875. https://doi.org/10.1039/D0NJ05362G.

2. **Thufail M. Ismail**; Prasanthkumar, K. P.; Ebenezer, C.; Anjali, B. A.; Solomon, R. V.; Sajith, P. K. Hydrogen-Bond-Assisted Adsorption of Nitric Oxide on Various Metal-Loaded ZSM-5 Zeolites. ***Langmuir*** 2022, 38, 10492–10502. https://doi.org/10.1021/acs.langmuir.2c01270.

3. **Thufail M. Ismail**; Patkar, D.; Sajith, P. K.; Deshmukh, M. M. Interplay of Hydrogen, Pnicogen, and Chalcogen Bonding in $X(H_2O)_{n=1-5}$ (X = NO, NO^+, and NO^-) Complexes: Energetics Insights via Molecular Tailoring Approach. ***The Journal of Physical Chemistry A***. (https://doi.org/10.1021/acs.jpca.3c04181).

4. **Thufail M. Ismail**; Patkar, D.; Sajith, P. K.; Deshmukh, M. M. Hydrogen Bond Strengths in Microhydrated Clusters of HNO and HONO: Energetic Insights via Molecular Tailoring Approach. ***New Journal of Chemistry*** (communicated).

Other works:

5. Ganie, A. A.; **Thufail M. Ismail**; Sajith, P. K.; Dar, A. A. Validation of the supramolecular synthon preference through DFT and physicochemical property investigations of pyridyl salts of organo-sulfonates. ***New Journal of Chemistry*** 2021, *45*, 4780-4790. https://doi.org/10.1039/D0NJ05485B.

6. Farhan, K. M.; Thabassum, A. N. K.; **Thufail M. Ismail**; Sajith, P. K. Theoretical investigation into the effect of water on the N_2O decomposition reaction over the Cu-ZSM-5 catalyst. ***Catalysis Science & Technology*** 2022, *12*, 1466-1475. https://doi.org/10.1039/D1CY01883C.

7. Ganie, A. A.; Rashid, S.; Ahangar, A. A.; **Thufail M. Ismail**; Sajith, P. K.; Dar, A. A. Expanding the Scope of Hydroxyl-pyridine Supramolecular Synthon to Design Molecular Solids. ***Crystal Growth & Design*** 2022, *22*, 1972–1983. https://doi.org/10.1021/acs.cgd.2c00006.

8. Saranya, K. P.; **Thufail M. Ismail**; Kavya, P.; Shanthil, M.; Sajith, P. K. Decoding the Interplay between Inter and Intramolecular Hydrogen Bonding in Fluorescence of Salicylidene 2- anthryl amine. ***Chemistry Select*** (Under revision).